ADAM MICKIEWICZ UNIVERSITY IN POZNAŃ

FACULTY OF PHYSICS AND ASTRONOMY

INSTITUTE OF SPINTRONICS AND QUANTUM INFORMATION

DEPARTMENT OF MESOSCOPIC PHYSICS

PhD dissertation

Spin-orbit driven transport effects in a two-dimensional electron gas with selected forms of Rashba and Dresselhaus spin-orbit interaction

ANNA KRZYŻEWSKA

Supervisor
dr hab. ANNA DYRDAŁ, prof. UAM

Poznań, 2024

Contents

Serce rozumnego zdobywa wiedzę,
a ucho mądrych szuka wiedzy

Prz 18,15

Abbreviations

2DEG/2DHG   two-dimensional electron gas / two-dimensional hole gas

AHE   anomalous Hall effect

AHC   anomalous Hall conductivity

ANE   anomalous Nernst effect

ANC   anomalous Nernst conductivity

BIA   bulk inversion asymmetry

BCD   Berry curvature dipole

BMR   bilinear magnetoresistance

CISP   current-induced spin polarization

NLHE   non-linear Hall effect

SHA   spin Hall angle

SHC   spin Hall conductivity

SHE   spin Hall effect

SIA   structure inversion asymmetry

SOC/SOI   spin-orbit coupling / spin orbit interaction

TISP   thermally-induced spin polarization

Streszczenie

Postęp technologiczny w dziedzinie miniaturyzacji urządzeń elektronicznych w ostatnich dziesięcioleciach stwarza potrzebę głębszego zrozumienia zjawisk fizycznych zachodzących na poziomie mikroskopowym. W rezultacie zaczęto badać układy o niskiej wymiarowości, takie jak cienkie warstwy, które można traktować jako struktury dwuwymiarowe.

Obiecującym obszarem w tej dziedzinie jest spintronika, która uwzględnia nie tylko ładunek elektronu, jak konwencjonalna elektronika, ale także jego spin. Jednym z kluczowych zagadnień spintroniki jest oddziaływanie typu spin-orbita, które wpływa na zjawiska transportowe, takie jak efekty Halla czy polaryzacja spinowa w układzie.

W ramach niniejszej pracy doktorskiej badano właściwości transportowe układów dwuwymiarowych z oddziaływaniem spinowo-orbitalnym (SO), wykorzystując metody teorii pola w fizyce ciała stałego, w szczególności formalizm funkcji Greena z podejściem diagramowym. W pracy analizowane są oddziaływania SO typu Rashby i Dresselhausa, ze szczególnym uwzględnieniem ich form kubicznych. Badany układ, dwuwymiarowy gaz elektronowy (2DEG), jest wykorzystywany do modelowania heterostruktur półprzewodnikowych oraz interfejsów i powierzchni tlenków perowskitowych.

Przedłożona dysertacja doktorska składa się z cyklu sześciu artykułów naukowych, poprzedzonych wstępem teoretycznym, uporządkowanych w kolejności ich publikacji.

W ramach rozprawy rozważana jest nierównowagowa polaryzacja spinowa wywołana zewnętrznym polem elektrycznym (CISP) w dwuwymiarowym gazie elektronowym z liniową i kubiczną formą oddziaływania SO typu Dresselhausa. Wykazano, że w takim układzie obecność członu kubicznego zmniejsza polaryzację spinową. Z kolei, w przypadku magnetycznego 2DEG, przykładowo, gdy próbka jest umieszczona na podłożu magnetycznym, pojawia się dodatkowa, odporna na domieszkowanie w układzie składowa polaryzacji spinowej.

W pracy analizowany jest także anomalny efekt Halla (AHE), charakteryzujący się przepływem prądu ładunkowego w kierunku prostopadłym do zewnętrznego pola elektrycznego, w magnetycznym 2DEG z izotropową i anizotropową formą kubicznego oddziaływania SO typu Rashby.

Wyniki, jakościowo podobne w obu modelach, wskazują na dominującą rolę wkładu do AHE od stanów poniżej poziomu Fermiego.

Ponadto zbadano spinowy efekt Halla (SHE), czyli przepływ prądu spinowego w kierunku prostopadłym do zewnętrznego pola elektrycznego, w 2DEG z izotropową formą kubicznego oddziaływania SO typu Rashby. Wykazano, że obecność magnetyzacji w kierunku prostopadłym do płaszczyzny układu zmniejsza SHE, zwłaszcza gdy magnetyzacja dominuje nad oddziaływaniem SO.

Część rozprawy poświęcona jest analizie nieliniowych zjawisk transportowych. Pokazano, że w magnetycznym 2DEG z kubiczną formą oddziaływania SO typu Rashby, nieliniowy efekt Halla można kontrolować za pomocą pola magnetycznego w płaszczyźnie, przy czym wkład od stanów z morza Fermiego jest największy, gdy pole magnetyczne i elektryczne są przyłożone prostopadle względem siebie. Z kolei biliniowy magnetoopór, wywołany nierównowagową polaryzacją spinową w układzie, jest proporcjonalny do wartości zarówno pola elektrycznego, jak i magnetycznego.

Praca obejmuje także analizę efektów termoelektrycznych. Poprzeczna odpowiedź ładunkowa wywołana gradientem temperatury, znana jako anomalny efekt Nernsta, nie różni się znacząco zarówno w układzie z izotropową jak i anizotropową formą oddziaływania SO typu Rashby. Zaobserwowana zmiana znaku anomalnego przewodnictwa Nernsta w funkcji potencjału chemicznego odzwierciedla współzawodnictwo pomiędzy oddziaływaniem SO a magnetyzacją w układzie. Z kolei składowa polaryzacji spinowej wywołanej gradientem temperatury (TISP) równoległa do kierunku siły wymuszającej, w 2DEG z oddziaływaniem SO typu Dresselhausa, jest związana z CISP poprzez relację Motta. TISP przyjmuje większe wartości przy niższej gęstości nośników i może być sterowana za pomocą magnetyzacji i wartości oddziaływania SO, tj. poprzez napięcie bramkujące.

Podsumowując, niniejsza dysertacja stanowi wkład do zrozumienia własności transportowych indukowanych oddziaływaniem spinowo-orbitalnym, które odgrywa kluczową rolę w projektowaniu urządzeń spintronicznych, umożliwiając tym samym rozwój technologii przetwarzania i przechowywania danych.

Struktura niniejszego opracowania jest następująca. W rozdziale pierwszym (Chapter 1) przedstawiono cel oraz motywację badań, a także wprowadzono pojęcia charakteryzujące badane układy dwuwymiarowe, w tym rozważane formy oddziaływania spinowo-orbitalnego. Rozdział drugi (Chapter 2) został poświęcony opisowi metody, tj. formalizmowi funkcji Matsubary-Green'a w reżimie liniowej odpowiedzi w podejściu diagramowym. W rozdziale trzecim (Chapter 3) opisano analizowane w pracy efekty transportowe. Z kolei rozdział czwarty (Chapter 4) zawiera przedruki artykułów wchodzących w skład dysertacji, wraz z komentarzem. Opracowanie

jest zakończone podsumowaniem (s.), gdzie zebrano najistotniejsze rezultaty badań.

Abstract

Technological advances in electronic miniaturization have driven the need for a deeper insight into microscopic physical phenomena. This has led to the emergence of low-dimensional systems, e.g., thin layers that can be considered as two-dimensional structures.

A promising field in this regard is spintronics, which explores both electron charge and spin. One of the fundamental concepts in spintronics is the spin-orbit interaction impacting transport phenomena such as the anomalous Hall effect, spin Hall effect or spin polarization in the system.

The dissertation investigates transport properties in two-dimensional systems with spin-orbit interaction (SOI), utilizing advanced field theory methods in solid-state physics, particularly Green's functions formalism with a diagrammatic approach. The author focuses on cubic SOI forms, Rashba and Dresselhaus types, intrinsically related to the band structure describing properties of the system itself. The investigated system, a two-dimensional electron gas (2DEG), is used to model semiconductor heterostructures and interfaces or surfaces of perovskite oxides.

The doctoral dissertation includes a theoretical introduction followed by six articles published in peer-reviewed journals arranged in chronological order.

Firstly, the dissertation considers non-equilibrium spin polarization induced by an external electric field in a 2DEG with both linear and cubic forms of Dresselhaus SOI. It shows that, in such a system, the cubic term of the Dresselhaus SOI reduces the spin polarization. In turn, in a magnetized 2DEG, e.g., when the sample is placed on a magnetic substrate, an additional non-dissipative component of spin polarization appears, which is robust against impurities in the system.

Secondly, the thesis examines an anomalous Hall effect (AHE), which is characterized by a charge current appearing perpendicular to an applied external electric field, in a magnetized 2D system with isotropic or anisotropic forms of cubic Rashba SOI. In both models, the results exhibit qualitatively similar behavior, highlighting the dominant contribution to the AHE from the states

below the Fermi level.

Moreover, the spin Hall effect (SHE), i.e., a spin current that flows perpendicular to an applied external electric field, is investigated in a 2D system with an isotropic form of cubic Rashba SOI. Additionally, the research demonstrates that out-of-plane magnetization in the system suppresses the effect, particularly when the magnetization dominates over the Rashba SOI.

A significant part of the dissertation is devoted to the analysis of nonlinear transport phenomena. In a magnetized 2DEG with cubic Rashba SOI, the nonlinear Hall effect can be controlled *via* an in-plane magnetic field. The contribution from the states in the Fermi sea reaches its maximum when the magnetic field is aligned perpendicular to the external electric field. In turn, the bilinear magnetoresistace, induced by the non-equilibrium spin polarization in the system, exhibits linear scaling with both the electric and magnetic field.

Additionally, this thesis covers the analysis of thermoelectric effects, such as an anomalous Nernst effect (ANE) and thermally-induced spin polarization (TISP). ANE, i.e., transverse charge response evoked by a temperature gradient, exhibits no qualitative difference between isotropic and anisotropic Rashba models. The anomalous Nernst conductivity reverses with changes in the chemical potential, indicating the interplay between spin-orbit interaction and magnetization in the system. In turn, the longitudinal component of TISP in a 2DEG with Dresselhaus SOI correlates with current-induced spin polarization *via* a Mott relation. TISP is stronger at lower carriers densities and can be tuned with a strength of the magnetization and spin-orbit interaction which is adjusted through the gate voltage.

In summary, this research contributes to understanding spin-related phenomena, crucial for building the foundation of spintronic devices that drive modern electronic systems, advancing in data processing and storage technologies.

The structure of the following work is as follows. In Chapter 1, the aim and motivation of the research are presented, and basic concepts utilized in the thesis, such as cubic forms of spin orbit-interaction, are introduced. Chapter 2 is devoted to the Matsubara-Green's functions formalism in the linear response regime, which constitutes the basic method of the conducted research. In Chapter 3 the investigated transport effects are introduced. Chapter 4 includes reprints of the articles comprising the dissertation, each with preface, and the summary is provided at page 109, where the main outcomes are emphasized.

List of the articles constituting the thesis

A-1: A. Krzyżewska, A. Dyrdał, J. Berakdar, *Temperature Dependence of Spin Hall Effect in k–Cubed Rashba Model*, Acta Physica Polonica A **133**, 558 (2018)

A-2: A. Krzyżewska, A. Dyrdał, J. Barnaś, J. Berakdar, *Anomalous Hall and Nernst Effects in 2D Systems: Role of Cubic Rashba Spin–Orbit Coupling*, Phys. Status Solidi RRL **12**, 1800232 (2018)

A-3: A. Krzyżewska, A. Dyrdał, *Anomalous Hall and Nernst effects in a two-dimensional electron gas with an anisotropic cubic Rashba spin-orbit interaction*, J. Magn. Magn. Mater. **497**, 165919 (2020)

A-4: A. Krzyżewska, A. Dyrdał, *Non-equilibrium spin polarization in magnetic two-dimensional electron gas with k-linear and k-cubed Dresselhaus spin-orbit interaction*, Physica E **135**, 114961 (2022)

A-5: A. Krzyżewska, A. Dyrdał, *Bilinear magnetoresistance in 2DEG with isotropic cubic Rashba spin-orbit interaction*, J. Magn. Magn. Mater. **589**, 171615 (2024)

A-6: A. Krzyżewska, A. Dyrdał, *Nonlinear Hall Effect in Isotropic k-Cubed Rashba Model: Berry-Curvature-Dipole Engineering by In-Plane Magnetic Field*, Phys. Status Solidi RRL **n/a**, 2400123 (2024)

1

Introduction

1.1 Motivation

Undoubtedly, technological progress in the miniaturization of electronic devices over the last few decades creates the necessity for deeper insight into the physical phenomena at the microscopic level. An important aspect regarding miniaturization is the size of the system, which inevitably moves toward *low-dimensionality*. Furthermore, low-dimensional systems offer an intriguing platform for physicists, as the quantum mechanical laws governing these systems manifest in macroscopic behaviors, such as the quantization of the Hall effects in two-dimensional system. On the other hand, the physical mechanisms standing behind the Hall phenomena such as anomalous or spin Hall effects, are govern by the *spin-orbit interaction*. Spin-orbit interaction in solid-state physics can have an extrinsic origin, related to spin-dependent scattering events on impurities, or an intrinsic one, related to the breaking of inversion symmetry in the host crystal.

Furthermore, *transport properties*, including Hall effects, are among the most powerful tools for characterizing materials. Resistivity measurements, for instance, allow one to extract not only conductivity information but also, with the aid of theoretical analysis, data on carriers concentration, scattering processes, and band structure, as well as the identification of phase transitions. Moreover, applying external forces such as a magnetic field, strain, or a temperature gradient offers deeper insights into the material, enhancing its potential for application in electronic devices.

On the other hand, transport effects themselves hold significant potential for practical applications. *Exempli gratia*, the intrinsic nonlinear Hall effect, due to its sensitivity to spatial-symmetry breaking, creates possibilities for its use in piezoelectric devices. Furthermore, nonlinear effects that result in a unidirectional response could be utilized in spin-logic devices.

Two-dimensional systems can be realized in semiconductor heterostructures, which are well-known materials in solid-state physics with established fabrication methods and electronic properties that can be externally tuned through gating or doping. Additionally, the two-dimensional electron gas that forms at their interfaces is characterized by spin-orbit coupling, which arises due to the breaking of inversion symmetry in the underlying material. In recent years, scientists have been particularly interested in the high-mobility two-dimensional electron gas found at the interfaces and surfaces of perovskite oxides, such as $LaAlO_3$/$SrTiO_3$, which exhibits intriguing physical properties such as metallic conductivity, ferromagnetism, and low-temperature superconductivity. Moreover, the inversion symmetry breaking at the interface leads to strong Rashba spin-orbit coupling in the two-dimensional electron gas, making it an excellent platform for investigating spin-to-charge interconversion effects.

Therefore, the aim of this dissertation is to investigate selected transport effects, such as the linear and nonlinear anomalous Hall effects, the spin Hall effect, bilinear magnetoresistance, and non-equilibrium spin polarization in two-dimensional systems (e.g., semiconductor heterostructures and perovskite oxide interfaces) with different forms of spin-orbit interaction induced by the breaking of inversion symmetry in the system.

1.2 Two-dimensional electron gas

The observed world around us on the macroscale is undoubtedly three-dimensional (3D). Nevertheless, one can imagine a system with reduced dimensionality, where the motion of particles is spatially confined in at least one direction. *Exempli gratia*, in a two-dimensional (2D) system[1], carriers are free to move in the xy-plane while being confined in the z-direction. Strictly speaking, the length of the system along the z-axis is smaller than the *elastic mean free path* of the electron. In such a scenario, carriers trapped in a potential quantum well (QW) grown in the z-direction, form a *two-dimensional electron gas* (2DEG) [1–3].

To mathematically describe the electronic states in a QW, one can solve the eigenvalue problem by assuming an infinite xy-plane and employing an envelope function with the effective-mass approximation [4]. The Schrödinger equation then takes the form [1, 5]:

$$\left[-\frac{\hbar^2}{2} \left(\frac{1}{m_x} \frac{\partial^2}{\partial x^2} + \frac{1}{m_y} \frac{\partial^2}{\partial y^2} + \frac{1}{m_z} \frac{\partial^2}{\partial z^2} \right) + V(z) \right] \Psi(x, y, z) = E \Psi(x, y, z). \quad (1.1)$$

---

[1]In the case of thin-layer structures with a finite spatial extent in the growth direction, one has in mind a *quasi-2D* system.

m_i, where $i = \{x, y, z\}$, represents the components of the effective mass of the electrons in the conduction band, while $V(z)$ denotes the potential that forms the QW. The electrons are confined in the z-direction and move freely in the xy-plane. Thus, the solution can be postulated in the form:

$$\Psi(x, y, z) = \phi_n(z)e^{\mathrm{i}k_x x + \mathrm{i}k_y y} \tag{1.2}$$

and the Schrödinger, eq. (1.1), can be separated into two independent differential equations:

$$-\frac{\hbar^2}{2}\left(\frac{1}{m_x}\frac{\partial^2}{\partial x^2} + \frac{1}{m_y}\frac{\partial^2}{\partial y^2}\right)e^{\mathrm{i}k_x x + \mathrm{i}k_y y} = E_{xy}e^{\mathrm{i}k_x x + \mathrm{i}k_y y} \tag{1.3a}$$

$$\left[-\frac{\hbar^2}{m_z}\frac{\partial^2}{\partial z^2} + V(z)\right]\phi_n(z) = E_{z,n}\phi_n(z). \tag{1.3b}$$

The solutions are:

$$E_{xy} = \frac{\hbar^2}{2m_{\parallel}}\left(k_x^2 + k_y^2\right) \tag{1.4a}$$

$$E_{z,n} \cong \frac{\hbar^2\pi^2}{2m_z}\frac{n^2}{L^2}, \tag{1.4b}$$

where $n = 1, 2, 3, ...$ and, for simplicity, $m_x = m_y = m_{\parallel}$. With infinite square-well approximation, the solutions are standing waves in the QW growing along the z-direction. Thus, the eigenvalues of the electron states in a 2DEG are given by [1, 5]:

$$E_n = \frac{\hbar^2}{2m_{\parallel}}\left(k_x^2 + k_y^2\right) + E_{z,n}. \tag{1.5}$$

For low carriers concentration, only the lowest band is relevant ($n = 1$), while the contributions from higher bands can be neglected.

A 2DEG typically forms at the interface between two different materials, such as semiconductor heterostructures, which are discussed in section 1.2.1. Additionally, a 2DEG has also been observed at the interfaces and surfaces of perovskite oxides, briefly described in section 1.2.2.

1.2.1 Semiconductor heterostructures

In retrospect, Wolfgang Pauli's 1931 remark[2] to Rudolf Peierls, stating, "*One shouldn't work on semiconductors, that is a filthy mess; who knows whether any semiconductors exist*", has proven to be less accurate. The field of semiconductor electronics has since emerged as a groundbreaking area of study with extensive device applications. For instance, the *metal–oxide–semiconductor field-effect transistor* (MOSFET) catalyzed a revolution in electronics during the latter half of the 20th century.

---

[2]Letter to Peierls, 29 September 1931; *Wolfgang Pauli – Wissenschaftlicher Briefwechsel mit Bohr, Einstein, Heisenberg u.a. Band II: 1930–1939*, Springer, 1985, p. 94.

Advancements in thin-film fabrication technology enable the deposition of multilayered structures through growth techniques such as *molecular beam epitaxy* (MBE) or *metallorganic vapor phase epitaxy* (MOVPE) [1, 6]. The semiconductor heterostructure consists of alternating layers of different semiconductors deposited on top of each other using the epitaxial method, e.g., 'layer A' and 'layer B' as depicted in Fig. 1.1a.

In thermodynamic equilibrium, the differing energy gaps in semiconductor building layers 'A' and 'B' lead to a band offset (band gap alignment), causing band bending at the intra-atomic distance and ultimately resulting in the formation of a quantum well. In an n-doped semiconductor (a crystal lattice doped with atoms that have one additional valence electron), electrons from the donors move from the valence band to the conduction band, accumulating in the energetically more favorable quantum well and forming a two-dimensional electron gas (2DEG). Conversely, in a p-doped semiconductor (a structure doped with atoms possessing fewer valence electrons than the atoms constituting the crystal lattice), holes emerge due to the presence of acceptors in the structure, leading to the formation of a two-dimensional hole gas (2DHG) in the quantum well created in the valence band [5]. Additionally, in a superlattice, a series of quantum wells is created, as illustrated in Fig. 1.1a.

The shape of QW can be controlled by applying a front gate bias (an external electric field perpendicular to the 2D sample plane) [7] or through doping [1, 5, 8]. For instance, in a $GaAs/Ga_{1-x}Al_xAs$ heterostructure, varying the parameter x allows tuning between a symmetric quantum well (for $x = 0$) and an asymmetric quantum well (for $x \neq 0$), see Fig. 1.1b [8].
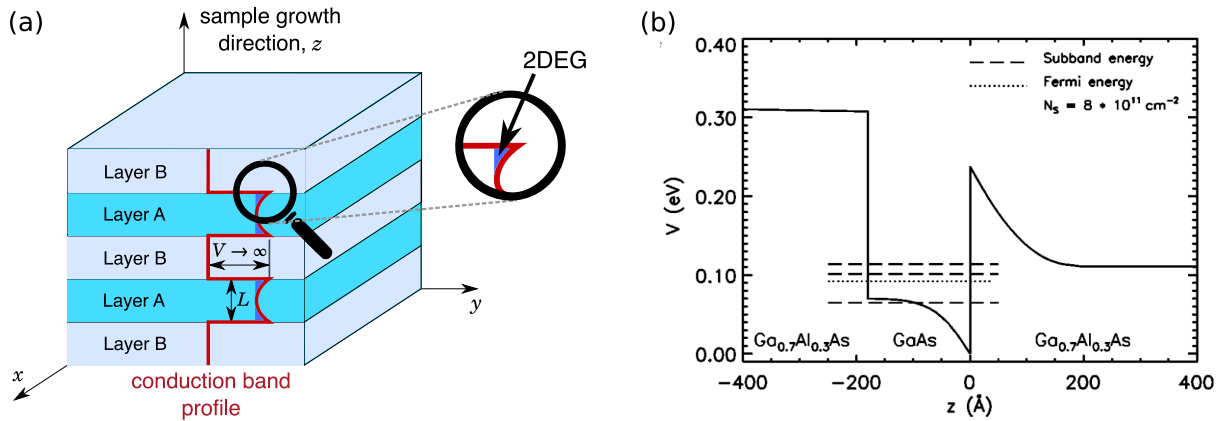
Figure 1.1: (a) Conduction band profile of a symmetric quantum well (QW) formed by a potential difference at the interfaces; in xy-plane a 2DEG forms in the QW; L is the quantum well width and V stands for QW potential. (b) Conduction band profile of an asymmetrically doped $GaAs/Ga_{0.7}Al_{0.3}As$ quantum well. For the sake of clarity, the valence band is not drawn on the sketch. Figure (b) is taken from [8] © (1998) by the American Physical Society

Quantum wells can be realized using semiconductor alloys containing elements from groups III (e.g., B, Al, Ga, In) and V (e.g., N, P, As, Sb) of the periodic table, such as GaAs, InSb, and InAs,

collectively known as III-V semiconductor heterostructures. Another group, characterized by generally wider energy gap, includes II-VI semiconductor heterostructures, such as ZnO, ZnS, CdS, CdTe, and HgTe[3]. Semiconductor heterostructures from both groups exhibit sp^3-orbital hybridization, resulting in either a zinc-blende or wurtzite structure [5].

1.2.2 Perovskite oxides interfaces (LAO/STO)

Besides semiconductor heterostructures, another promising materials where 2DEG forms are the surfaces and interfaces of perovskite oxides, which have garnered significant scientific attention in recent years [11–15].

Perovskite oxides are insulators in their bulk form, but at the surface and interface of oxide heterostructures, high-mobility 2DEG emerges, exhibiting intriguing physical properties such as metallic conductivity[4], ferromagnetism, and large spin-charge interconversion effect [13, 17, 18]. Additionally, phenomena such as low-temperature superconductivity and ferroelectricity have been observed at perovskite oxide interfaces, which are not typically seen in semiconductor heterostructures [13].

Bulk perovskite oxides have an empirical formula ABO_3, where 'B' represents a transition-metal atom (an atom with partially filled d-orbital), e.g., Ti, Al, or Ta. The electronic properties of these materials are influenced by material-dependent interfacial band bending [19]. More precisely, at the microscopic level, the system's properties are determined by the balance between transition-metal d-orbitals, hybridized oxygen p-orbitals, and electronics correlations [15].

It turns out that in order to induce a 2DEG at the interface of perovskite composite, at least one of the two insulating perovskites must be polar or ferroelectric [19, 20]. One of the most extensively studied perovskite oxide heterostructures is $LaAlO_3/SrTiO_3$ (LAO/STO). Here, the mechanism behind the formation of the 2DEG is as follows [12, 17, 21, 22]: the polar discontinuity at the LAO/STO interface, i.e., $(LaO)^{1+}/(TiO_2)^0$, causes a divergence in the electrostatic potential. To counterbalance this divergence, a compensating charge $\pm 0.5e$ is transferred from the charged layer of LAO to the charge-neutral layer of STO. These transferred electrons partially occupy Ti $3d$-orbitals near the interfacial region, leading to the formation of the 2DEG.

---

[3]HgTe is characterized by a zero-energy gap and exhibits a topologically non-trivial phase. In turn, CdTe/HgTe semiconductor heterostructure provides an excellent platform for studying the properties of topological insulators [9, 10].

[4]It has been established that LAO/STO interfaces become conductive when the thickness of the polar layer (LAO) exceeds 3-4 unit cells [16].

1.3 Spin-orbit interaction (SOI)

In this dissertation, spin-orbit interaction (SOI) plays the leading role. Therefore, a deep understanding of its nature and physical background is crucial for accurately comprehending the phenomena discussed. Section 1.3.1 introduces the concept of intrinsic angular momentum, i.e., *spin*. Section 1.3.2 discusses spin-orbit interaction in an atom, and section 1.3.3 provides a brief review of different types of spin-orbit interaction (SOI) in the solid state. Sections 1.3.4 and 1.3.5 are dedicated to the Rashba and Dresselhaus types of SOI, respectively, focusing on their cubic forms.

1.3.1 The concept of orbital and spin angular momenta – historical background

The orbital and spin angular momenta were introduced in the early 20th century, benefiting from developments in quantum mechanics that allowed for a microscopic description of magnetism.

Starting from Faraday's law, which states that a time-varying electric field, $\mathbf{E}$, induces a magnetic field, $\mathbf{B}$ [23, 24]:

$$\nabla \times \mathbf{E} = -\frac{\partial \mathbf{B}}{\partial t}, \tag{1.6}$$

one concludes that an electric current circulating in a loop creates a magnetic field. In classical mechanics, it is known that a rotating object possesses a mechanical moment. Combining these two statements, one can associate a magnetic moment, $\boldsymbol{\mu}$, with a rotating charge, e.

According to the Bohr model of the hydrogen atom, part of the "old quantum theory" proposed by Bohr and Sommerfeld in the early 1920s (referred to as a "semi-classical approach"), an electron is treated as a charged particle orbiting the nucleus, and possessing an orbital magnetic moment, $\boldsymbol{\mu}_{orb}$, related to the *orbital angular momentum*, $\mathbf{l}$ [23, 24]:

$$\boldsymbol{\mu}_{orb} = -\frac{e}{2}r^2\boldsymbol{\omega} = -\frac{e}{2}\mathbf{r} \times \mathbf{v} = -\frac{e}{2m_e}\mathbf{l} \tag{1.7}$$

with m_e representing the electron mass. Quantum mechanics asserts that angular momentum, $\mathbf{l}$, is quantized, as demonstrated by the Stern-Gerlach experiment in 1922 [25]. (e.g., for a hydrogen atom $\mathbf{l} = \hbar$). Furthermore, to explain the small splitting observed in the hydrogen atom spectrum, Goldsmith and Uhlenbeck, building on Compton's idea, introduced a new quantum number known as *spin angular momentum*, or simply *spin*, $\mathbf{s}$, an intrinsic property of the electron[5] with a spin magnetic moment, $\boldsymbol{\mu}_{spin}$ [26, 27]:

$$\boldsymbol{\mu}_{spin} = -\frac{e}{m}\mathbf{s} = g\mu_B\mathbf{s}, \tag{1.8}$$

---

[5]By analogy to classical physics, spin is often depicted as a spinning particle. However, it has no connection to any spatial movement; therefore, to avoid misunderstanding, the spin should be regarded as an intrinsic feature of the particle itself.

where g is the g-factor, $\mu_B = -\frac{e\hbar}{2m}$ denotes the Bohr magneton, and the spin $\mathbf{s} = \hbar/2$ for an electron.

As a consequence of the existence of orbital and spin angular momenta, $\boldsymbol{\mu}_{orb}$ and $\boldsymbol{\mu}_{spin}$, the magnetic properties of a material are generally determined by three main effects: (i) electron-electron interaction, which describes how the electron spins are oriented with respect to each other, (ii) chemical environment, which specifies how the bonding between neighboring atoms influences the orbital contribution to the magnetic moment, (iii) *spin-orbit coupling*, which refers to the interaction (coupling) between spin and orbital angular momenta, describing the tendency of these momenta to align with each other. These three effects collectively contribute to the magnetic properties of materials, determining their magnetic behavior and characteristics [24].

1.3.2   Spin-orbit interaction in atom

If an electron moves in an electric field – whether orbiting the nucleus in atomic physics or traveling through a periodic potential as an itinerant particle in solid-state physics – it experiences a magnetic field in its rest frame, according to Faraday's law, eq. (1.6). Since the electron carries a magnetic moment that interacts with the magnetic field, it implies a direct coupling between the electron's spin and momentum, known as *spin-orbit coupling* (SOC) [4, 28].

The behavior of spin-1/2 fermions in relativistic quantum theory is accurately described by Dirac's theory [29, 30]. By taking the nonrelativistic approximation of the Dirac equation, which is justified by the relatively low velocities of electrons in solids ($v \approx 10^6$ m/s) compared to the speed of light, $v \ll c$, one obtains the Hamiltonian that describes the spin-orbit interaction [28, 31, 32]:

$$H_{so,atom} = -\frac{1}{2m_0^2 c^2} \mathbf{s} \cdot \left(\mathbf{p} \times \nabla V_{at} \right), \tag{1.9}$$

where m_0 stands for the free electron mass, c is the speed of light, and V_{at} represents the Coulomb potential of the atomic core. The spin angular momentum of an electron can be described with a vector of Pauli matrices $\mathbf{s} = \hbar\boldsymbol{\sigma}/2$ acting on the spinor wave function of the electron, while $\mathbf{p} = \hbar\mathbf{k}$ denotes the electron momentum. Thus, the Hamiltonian (1.9) can be expressed in a different form as [28, 33]:

$$H_{so,atom} = -\frac{\hbar}{4m^2 c^2} \boldsymbol{\sigma} \cdot \left(\mathbf{p} \times \nabla V \right) = -\frac{\lambda_C^2}{4} \boldsymbol{\sigma} \cdot \left(\mathbf{k} \times \nabla V \right), \tag{1.10}$$

where $\lambda_0 = \hbar/(mc)$, while $\lambda_C = 2\pi\lambda_0$ corresponds to the Compton wavelength of a free electron, and $\lambda = -\lambda_C^2/4$ represents the strength of the atomic SOC.

1.3.3   Spin-orbit interaction in solid state

In crystals, Bloch electrons experience an external potential in their rest frame, $\tilde{V} = V_{lat} + V(\mathbf{r})$. Here, V_{lat} represents the periodic potential of the crystal lattice, while $V(\mathbf{r})$ denotes an aperi-
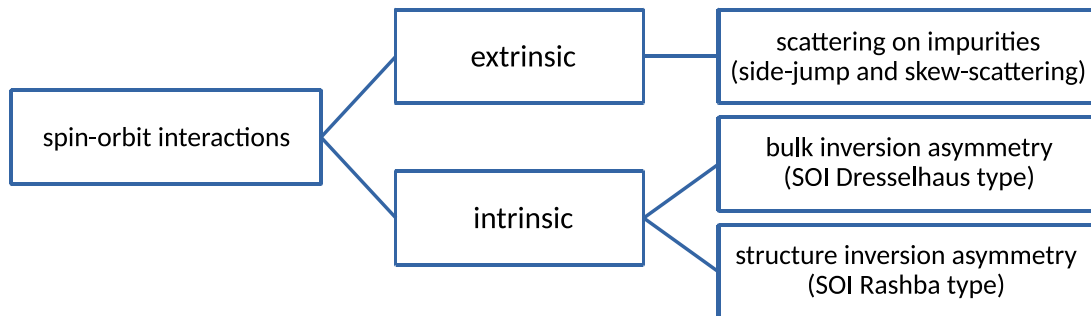
odic component that varies slowly on the scale of the lattice constant, and includes contributions from impurities, boundaries, confinement, and external electric field. In solid-state physics, the behavior of carriers is described in terms of the band structure. For semiconductors, the minimum of the energy spectrum typically occurs at a high-symmetry point, allowing the transport properties of the material to be analyzed using an effective Hamiltonian that describes the system near this point. The general form of the effective single-particle Hamiltonian that describes spin-orbit coupling is given by [34]:

$$H_{so,lat} = \lambda \boldsymbol{\sigma} \cdot \left(\mathbf{k} \times \nabla \tilde{V} \right).$$ (1.11)

Since the impurities are considered to be the source of (extrinsic) spin-orbit interaction (SOI), then λ depends on the crystal lattice, and $\tilde{V}$ is the potential due to the impurities.

In turn, when SOI arises due to inversion symmetry breaking in the host crystal, the effective Hamiltonian (1.11) can be expressed in terms of an intrinsic spin-orbital field, $\mathbf{b}(\mathbf{k})$, around which electron's spin precesses [34, 35]:

$$H_{so,lat}^{int} = \frac{1}{2} \mathbf{b}(\mathbf{k}) \cdot \boldsymbol{\sigma}.$$ (1.12)

```
                            ┌──────────────────────────────────┐
              ┌──────────┐  │    scattering on impurities       │
              │ extrinsic│──│ (side-jump and skew-scattering)   │
              └──────────┘  └──────────────────────────────────┘
┌─────────────────┐
│ spin-orbit      │        ┌──────────────────────────────────┐
│ interactions    │        │   bulk inversion asymmetry        │
└─────────────────┘        │    (SOI Dresselhaus type)         │
              ┌──────────┐ └──────────────────────────────────┘
              │ intrinsic│
              └──────────┘ ┌──────────────────────────────────┐
                           │ structure inversion asymmetry     │
                           │      (SOI Rashba type)            │
                           └──────────────────────────────────┘
```

Figure 1.2: Different types of spin-orbit interaction

Thus, the origin of spin-orbit coupling can be classified into extrinsic and intrinsic types, as shown in Figure 1.2. Below, the physical background behind different types of SOI is discussed.

The extrinsic type is associated with scattering processes on the impurities, i.e., side-jump and skew scattering [32]. In both extrinsic processes, carriers with opposite spins scatter in opposite directions.

In the *side-jump scattering* process, depicted in Figure 1.3(a), the electron deflects under the influence of the field created by an impurity. As it leaves the impurity field, it deflects back, resulting in a transverse displacement (side step). However, the electron continues to move in its original direction. The semiclassical interpretation of side-jump processes was first proposed by Berger [37] in the context of the anomalous Hall effect. In contrast, the *skew-scattering* process,
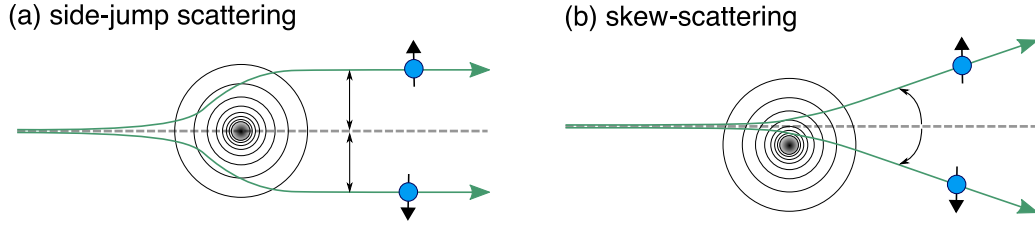
Figure 1.3: Extrinsic types of spin-orbit interaction include (a) side-jump scattering process and (b) skew scattering process. Adapted from [36]

introduced by Smith [38], and shown in Figure 1.3(b), has an asymmetric character and leads to a change in the electron's direction of motion.

Intrinsic SOC is related to the internal properties of the system and requires the breaking of inversion symmetry in the host crystal. In structures such as zinc blende or hexagonal wurtzite, inversion symmetry is broken within the unit cell, leading to *bulk inversion asymmetry* (BIA), which gives rise to the Dresselhaus type of SOC, discussed in Section 1.3.5. On the other hand, in two-dimensional systems, if the confinement potential along the growth direction is asymmetric – such as at the interfaces or surfaces of the sample – *structure inversion asymmetry* (SIA) occurs, resulting in Rashba-type SOC, see Section 1.3.4.

Asymmetric 2D quantum wells (QWs), where inversion symmetry is broken due to the growth process, provide a prominent platform for studying spin-orbit interaction (SOI) [39]. Such conditions are observed at surfaces or interfaces of III-V semiconductor heterostructures with narrow band gaps, like GaAs and InSb, II-VI semiconductor heterostructures with wide band gaps, like ZnS and CdTe, (Sec. 1.2.1), or at interfaces of perovskite oxides (Sec. 1.2.2), where a 2DEG forms.

Controlling the strength of spin-orbit interactions is essential for the development of spin-based devices. The strength of Rashba-type interaction can be manipulated – or even switched off – using a gate voltage [40–42], or by tuning the doping concentration ratio between the two sides of the quantum well [43–45]. Modulation doping [1] enhances carriers mobility in 2D systems. In this technique, the outer layers of a "QW sandwich" are doped, while the central layer remains undoped. Carriers then diffuse from the adjacent layers into the well, where they remain and can move freely. This approach contrasts with scenarios where the central layer itself acts as a donor or acceptor, which reduces carrier mobility due to ionized-impurity scattering [1, 44–46].

On the other hand, the particular form of Dresselhaus SOC in a two-dimensional system depends on the crystallographic grown direction of the quantum well [35, 47] (see Section 1.3.5). Moreover, the strength of Dresselhaus SOC can be adjusted by selecting different materials or altering the sample thickness, which correlates with the quantum well width[6] [48].

---

[6]Assuming a quantum well with infinitely high potential, the quantum well width, L, is related to the size quantization of the electron wavevector along the growth direction, z, see Fig. 1.1(a).

The Rashba or Dresselhaus SOC strength parameter can be experimentally determined through various techniques, such as angle-resolved photoemission spectroscopy (ARPES) [49, 50], or quantum transport measurements, i.e., analysis of Shubnikov-de Haas oscillations [40, 51] or through magnetoconductance measurements using weak antilocalization phenomena [52, 53]. For example, in InAs quantum well sandwiched by $In_{0.52}Al_{0.48}As/In_{0.53}Ga_{0.47}As$, a large linear Rashba coefficient tuned by the gate voltage in the range of $\approx 4 - 10 \cdot 10^{-12}$ eV m has been found [40, 51], while for perovskite oxides interfaces like LAO/STO, a comparable value of approximately $\approx 0.5 \cdot 10^{-11}$ eV m has been reported [42, 54]. In particular, when both types of intrinsic SOC are present in the system, i.e., Rashba and Dresselhuas SOC, Ho Park et al. [51] showed that by measuring and analyzing Shubnikov-de Haas oscillations for various crystallographic directions, Rashba and Dresselhaus strength parameters can be extracted separately.

1.3.4 Rashba-type SOI

If a 2DEG forms in xy-plane and the inversion symmetry is broken in the z-direction, the Rashba-type SOC occurs. The effective Hamiltonian describing the k-linear spin splitting of the bands at the high-symmetry point Γ in the 2DEG, where the quantum well grows along the z-direction, takes the well-known form [31, 55]:

$$\hat{H} = \hat{H}_{kin} + \hat{H}_{LR}, \tag{1.13}$$

where the kinetic energy of the quasiparticels in the 2DEG is described by $\hat{H}_{kin} = \frac{\hbar^2 k^2}{2m}\sigma_0$, and the k-linear SOI term reads as:

$$\hat{H}_{LR} = \lambda \left(k_x \sigma_y - k_y \sigma_x\right) \tag{1.14}$$

with λ standing for the Rashba strength parameter, $\mathbf{k} = (k_x, k_y, 0)$ is the wavevector, σ_0 is the identity matrix, and $\sigma_{x,y}$ are the Pauli matrices acting in the spin space. Eigenvalues of the Hamiltonian (1.13) are given by $E_\pm = \frac{\hbar^2 k^2}{2m} \pm \lambda k$.

The expectation value of the spin operator for the n-th band is given by:

$$\langle \hat{\mathbf{S}} \rangle_n = \frac{1}{\langle \Psi_n \mid \Psi_n \rangle} \left(\left\langle \Psi_n \left| \hat{S}_x \right| \Psi_n \right\rangle, \left\langle \Psi_n \left| \hat{S}_y \right| \Psi_n \right\rangle, \left\langle \Psi_n \left| \hat{S}_z \right| \Psi_n \right\rangle \right),$$

with Ψ_n standing for the eigenfunction for the n-th band, and for the two-band k-linear Rashba model described by Hamintonian (1.14), $\langle \hat{\mathbf{S}} \rangle_\pm^{LR}$ takes the following form:

$$\langle \hat{\mathbf{S}} \rangle_\pm^{LR} = \frac{\hbar}{2} \left(\pm \sin\phi, \pm \cos\phi, 0\right), \tag{1.15}$$

where ϕ is the angle in k-space, i.e., $\mathbf{k} = k(\cos(\phi), \sin(\phi), 0)$, and $n = \pm$ corresponds to the band.
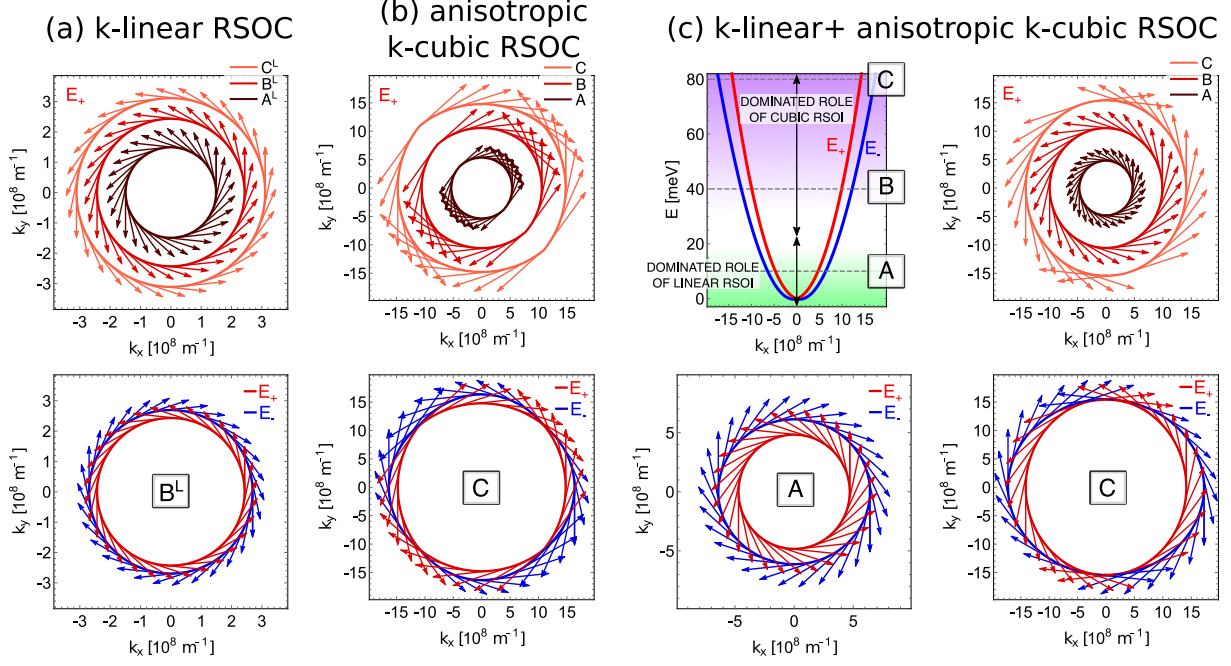
Figure 1.4: (a) Fermi contours for the k-linear Rashba system, described by Hamiltonian (1.13): (top) E_+ subband for three different Fermi levels, and (bottom) E_+ and E_- for a fixed Fermi level. (b) Fermi contours for anisotropic k-cubic Rashba system, described by Hamiltonian (1.17): (top) E_+ subband for three different Fermi levels, and (bottom) E_+ and E_- for a fixed Fermi level. (c) k-linear and anisotropic k-cubed Rashba system: (top left) dispersion relation and indicated Fermi levels 'A', 'B', 'C', which correspond to (top right) Fermi contours for E_+, (bottom left) Fermi contours for both subbands $E_\pm$ for Fermi level 'A', and (bottom right) $E_\pm$ for Fermi level 'C'. The arrows on the Fermi contours indicate the expectation value of the spin. The parameters are: $A^L = 20$ meV, $B^L = 50$ meV, $C^L = 80$ meV, $A = 10$ meV, $B = 40$ meV, $C = 80$ meV, linear Rashba SOC parameter for (a) $\lambda = 2 \cdot 10^{-11}$ eV m, for (c) $\lambda = 0.5 \cdot 10^{-11}$ eV m, $\alpha = 2.14 \cdot 10^{-30}$ eV m^3, and an effective mass for (a) $m = 0.05 m_0$, for (b) and (c) $m = 1.14 m_0$

Figure 1.4(a) presents the expectation value of the spin, as given by eq. (1.15), marked on the Fermi contours. Top panel illustrates $\langle \hat{\mathbf{S}} \rangle_\pm^{LR}$ for the subband E_+ at different Fermi levels, while the bottom panel presents $\langle \hat{\mathbf{S}} \rangle_\pm^{LR}$ for the both subbands, $E_\pm$, at a single Fermi level. This result, well-known in the literature, demonstrates that in the k-linear Rashba model, spins are locked perpendicular to their momenta, $\mathbf{k}$, with opposite spin orientation for the two spin-splitting states.

Anisotropic k-cubed form of Rashba SOC

The k-linear Rashba spin splitting dominates at low carrier densities, near $k = 0$. However, in a 2DHG in semiconductor heterostructures, for larger k, the spin splitting is dominated by higher-order terms, particularly those proportional to k^3, due to the HH-LH mixing [31]. Thus, it is justified to take into account the cubic form of Rashba SOC, especially at higher carrier densities. Furthermore, recent findings indicate that k-cubed corrections to the Rashba Hamil-

tonian can lead to a reversal of spin-polarization near the Fermi level in non-centrosymmetric semiconductors such as BiTeCl [56].

Moreover, using a low-energy tight-binding (TB) three-band Hamiltonian provided for perovskite oxides interfaces LAO/STO and STO surfaces (see Sec. 1.2.2) it has been shown that the lower bands for d_{xz}/d_{yz} orbitals exhibit a cubic form of Rashba SOI at the Γ point [57–61]. The cubic form of Rashba in LAO/STO structures has also been confirmed in experimental transport studies [54, 62]. The TB Hamiltonian describing the 2DEG at the LAO/STO interface consists of three terms [57–61]:

$$\hat{H} = \hat{H}_{kin} + \hat{H}_{ASO} + \hat{H}_{R}, \tag{1.16}$$

where $\hat{H}_{kin}$ represents the kinetic term describing free electrons in 2DEG, $\hat{H}_{ASO}$ defines the atomic-like SOC, and the third term, $\hat{H}_{R}$, accounts for the interorbital hopping related to the mirror symmetry breaking at the interface. Both $\hat{H}_{ASO}$ and $\hat{H}_{R}$ contribute to the splitting of the middle and bottom band pairs. Figure 1.5(a) depicts the low-energy TB model for the LAO/STO
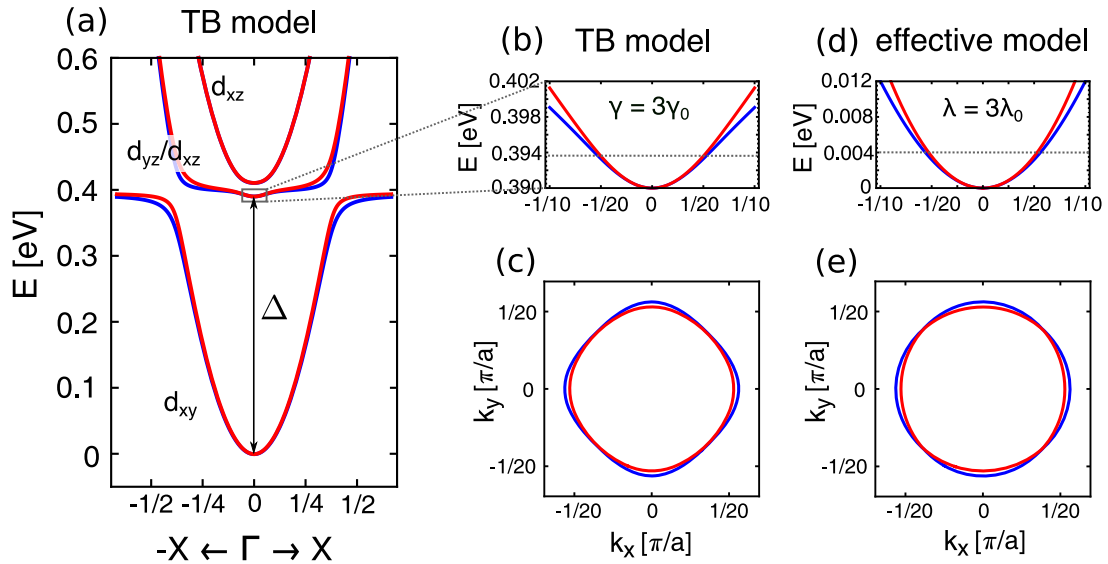
Figure 1.5: (a-c) The band structure of the conduction states at the LAO/STO interface, obtained using the low-energy tight-binding model. (d,e) An effective model, described by Hamiltonian (1.17), for the vicinity of the Γ-point, corresponding to (b,c). (c) and (e) show Fermi contours at 4 meV above the bands minimum for the TB and the effective model, respectively. The parameters for the TB model are taken from [61]. Figure is adapted from [63]

interface. The bands are formed by d-orbitals, specifically d_{xy}, d_{xz} and d_{yz}, originating from the t_{2g} atomic orbitals of the transition-metal atom, Ti. The lowest-energy pair of bands reveals the k-linear form of Rashba SOC, while the highest-energy bands are characterized by k-linear Dresselhaus SOC. In turn, the middle pair of bands corresponds to quasiparticle states determined by the anisotropic k-cubed Rashba SOC, described by the Hamiltonian [61, 64]:

$$\hat{H} = \hat{H}_{kin} + \hat{H}_{aniCR}, \tag{1.17}$$

where the kinetic term $\hat{H}_{kin} = \frac{\hbar^2 k^2}{2m}\sigma_0$ and the anisotropic k-cubed SOI term reads as:

$$\hat{H}_{aniCR} = \alpha \left(k_x^2 - k_y^2 \right) \left(k_x \sigma_y - k_y \sigma_x \right), \tag{1.18}$$

where $k^2 = k_x^2 + k_y^2$, $k_x = k\cos(\phi)$, $k_y = k\sin(\phi)$ and the eigenvalues of the Hamiltonian (1.17) are given by $E_\pm = \frac{\hbar^2 k^2}{2m} \pm \sqrt{\alpha^2 k^6 \cos^2(2\phi)}$.

The Rashba splitting described by Hamiltonian (1.18) is anisotropic in k-space. It is worth noting that, according to group-theoretical analysis for systems characterized by C_{3v} and C_{4v} point-group symmetry, an effective two-band Hamiltonian can only reveal the anisotropy of the Rashba splitting in higher-order terms in k [65], that can be derived using $k \cdot p$ perturbation theory [66][7].

The anisotropic cubic Rashba model, eq. (1.18), is characterized by the anisotropy of Fermi contours in k-space, as depicted in Figure 1.5(e) and Figure 1.4(b) with the expectation value of the spin, $\langle\tilde{\mathbf{S}}\rangle_\pm^{aniCR}$, marked on the sketch, where:

$$\langle\tilde{\mathbf{S}}\rangle_\pm^{aniCR} = \frac{\hbar}{2} \left(\pm \frac{\sin(\phi) - \sin(3\phi)}{2\sqrt{\cos^2(2\phi)}}, \pm \frac{\cos(\phi) + \cos(3\phi)}{2\sqrt{\cos^2(2\phi)}}, 0 \right). \tag{1.19}$$

On the other hand, some experiments suggest the presence of k-linear Rashba SOI at perovskite oxides interfaces [68, 69]. Furthermore, the construction of the tight-binding model, supported by DFT-calculated band structure, analyzed in conjunction with weak antilocalization measurements, indicates that the form of RSOI, whether linear or cubic, can be controlled by the filling of Ti orbitals by carriers [70].

Therefore, it is worthwhile to investigate an effective model that incorporates both forms of Rashba SOC. The energy dispersion and Fermi contour, along with the expectation value of the spin, for such a case are depicted in Figure 1.4(c). One can observe that the linear Rashba SOC dominates at lower energies (referred to as energy level 'A'), whereas the cubic form modifies the band structure and spin expectation value at higher energies (referred to as energy level 'C').

Isotropic k-cubed form of Rashba SOC

As mentioned earlier, the k-linear form of Rashba spin-orbit coupling (SOC) is not valid for describing the spin splitting of heavy-hole states with angular momentum 3/2 in a 2D hole system [31, 71]. Liu et al. [71] derived from Luttinger-Kohn Hamiltonian [72, 73] an effective

---

[7]A different situation occurs for C_{2v} point-group symmetry, describing, e.g., surface states at Au(110). In this case, the k-linear term of the Rashba SOC reveals an anisotropic character due to two independent Rashba parameters, i.e., $H_{aniLR} = \lambda_1 k_x \sigma_y + \lambda_2 k_y \sigma_x$, cf. Hamiltonian (1.14) [67].

model for the lowest heavy-hole valence subband with spin-3/2, where the Rashba SOC arises in a cubic form in the Hamiltonian:

$$\hat{H} = \hat{H}_{kin} + \hat{H}_{isoCR}, \tag{1.20}$$

where the kinetic term is $\hat{H}_{kin} = \frac{\hbar^2 k^2}{2m}\sigma_0$, and the isotropic k-cubed SOI term is given by:

$$\hat{H}_{isoCR} = \mathrm{i}\alpha\left(k_-^3\sigma_+ - k_+^3\sigma_-\right). \tag{1.21}$$

The eigenvalues of Hamiltonian (1.20) are $E_\pm = \frac{\hbar^2 k^2}{2m} \pm \alpha k^3$. The Rashba SOC strength parameter, α, is determined by [71]:

$$\alpha = \frac{512 e F L_z^4 \gamma_2^2}{9\pi^6(3\gamma_1 + 10\gamma_2)(\gamma_1 - 2\gamma_2)}, \tag{1.22}$$

where γ_1 and γ_2 are Luttinger material parameters[8]. Hence, α is proportional to the strength of the asymmetric quantum well potential, F, and depends on the QW width, L_z. The effective mass is expressed as [71]:

$$m = m_0\left(\gamma_1 + \gamma_2 - \frac{256\gamma_2^2}{3\pi^2(3\gamma_1 + 10\gamma_2)}\right)^{-1}. \tag{1.23}$$

Figure 1.6(a) presents the energy dispersion for a 2DEG with isotropic cubic Rashba SOC, described by Hamiltonian (1.20). Unlike the linear Rashba model, the spin splitting in the cubic Rashba model is negligible near $k \approx 0$ and increases with the Fermi energy.

Because the effective Hamiltonian (1.21) for the heavy-hole valence subband with spin-3/2 in 2DHG is derived from the Luttinger-Kohn Hamiltonian by the perturbation and truncation procedure to higher orders, the same approach should be applied to the spin operator. This procedure involves applying two canonical transformations on the 4x4 matrix representing the spinor for spin-3/2. It is crucial to note that in the isotropic cubic Rashba model, the spin matrices are no longer Pauli matrices, and the vector of spin matrices in the lowest heavy-hole basis is given by $\tilde{\mathbf{S}} = (\tilde{S}_x, \tilde{S}_y, \tilde{S}_z)$, where [71]:

$$\tilde{S}_x = \begin{bmatrix} -s_0 k_y & s_1 k_-^2 \\ s_1 k_+^2 & -s_0 k_y \end{bmatrix}, \tag{1.24a}$$

$$\tilde{S}_y = \begin{bmatrix} s_0 k_x & -\mathrm{i}s_1 k_-^2 \\ \mathrm{i}s_1 k_+^2 & s_0 k_x \end{bmatrix}, \tag{1.24b}$$

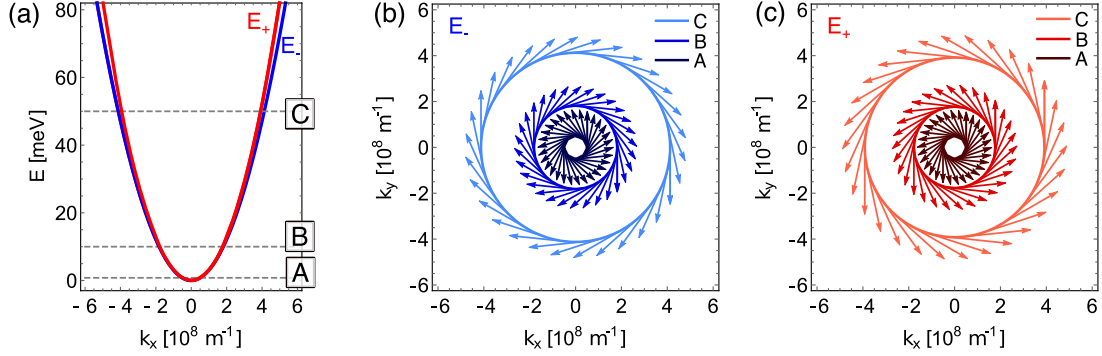$$\tilde{S}_z = \frac{3}{2}\sigma_z. \tag{1.24c}$$

---

[8]The specific values of these parameters for different materials are collected in [74].

with:

$$s_0 = \frac{512 e F L_z^4 \gamma_2 m_0}{9\pi^6 \hbar^2 (3\gamma_1 + 10\gamma_2)(\gamma_1 - 2\gamma_2)}, \tag{1.25}$$

$$s_1 = \left(\frac{3}{4\pi^2} - \frac{256\gamma_2^2}{3\pi^4 (3\gamma_1 + 10\gamma_2)^2} \right) L_z^2. \tag{1.26}$$

Figure 1.6: (a) Energy dispersion for a 2DEG with isotropic k-cubic Rashba SOC described by the Hamiltonian (1.20). Fermi contours for the subbands (b) E_- and (c) E_+ with the expectation value of the spin indicated by the arrows. The parameters are: A = 0.8 meV, B = 10 meV, C = 50 meV, $\alpha = 3.96 \cdot 10^{-29}$ eV m^3, and an effective mass $m = 0.123 m_0$

Figures 1.6(b), and 1.6(c) illustrate the Fermi contours for the subbands E_- and E_+, respectively, (for the Hamiltonian (1.20)) at three different Fermi energies. At low-carrier densities (Fermi level 'A'), the expectation value of the spin operator, $\hat{\mathbf{S}}$, for the n-th band ($n = \pm$)

$$\langle \hat{\mathbf{S}} \rangle_{\pm}^{isoCR} = \hbar \left(-s_0 k \sin\psi \pm s_1 k^2 \sin\psi,\ s_0 k \cos\psi \mp s_1 k^2 \cos\psi,\ 0 \right) \tag{1.27}$$

indicated by the arrows, is the same for both bands. For lower energies, $\langle \hat{\mathbf{S}} \rangle_{\pm}^{isoCR}$ is determined by the term proportional to s_0, which is identical for both subbands. At higher Fermi energies, the spin orientation locks perpendicularly to its momentum, similar to the behavior observed in the linear Rashba model, where the two spin-splitting states have opposite spin values. This issue is analyzed in [71].

Experimental evidence supports using the cubic Rashba model for 2D hole systems, such as strained-Ge/SiGe, rather than the linear model [75]. Additionally, the cubic form of Rashba SOC has been experimentally observed at the surface of perovskite oxide SrTiO$_3$ and at the LaAlO$_3$/SrTiO$_3$ interface [54, 62]. The possibility of describing 2DHG in semiconductor heterostructures and 2DEG at the interfaces of perovskite oxides becomes understandable in light of the investigations provided by L. W. van Heeringen et al. [76]. In their work, the authors highlighted the similarity between p-level valence states in III-V semiconductors and d-level conduction states in SrTiO$_3$.

1.3.5 Dresselhaus-type SOI

III-V semiconductors with a zinc-blende structure exhibit bulk inversion asymmetry (BIA) due to two nonequivalent atoms in the unit cell. This BIA leads to Dresselhaus-type spin-orbit interaction (SOI). The lowest-order contribution to the spin-orbital splitting in the conduction band of a 3D system is described by the Hamiltonian [31, 77–79]:

$$\hat{\mathcal{H}}_D = \gamma[(k_y^2 - k_z^2)k_x\sigma_x + (k_z^2 - k_x^2)k_y\sigma_y + (k_x^2 - k_y^2)k_z\sigma_z], \tag{1.28}$$

where γ stands for the spin-orbit coupling parameter, $p_i = \hbar k_i$ represents the i-th component of the kinetic momentum (wavevector), and σ_i are the Pauli matrices with $i = \{x, y, z\}$. For a quasi-2D system confined in the z-direction, representing a symmetric quantum well grown in the [001] crystallographic direction, the z-component of the wavevector is $k_z = -i\partial_z$, and eq. (1.28) reads[9] [31, 79]:

$$\hat{H} = \hat{H}_{kin} + \hat{H}_D, \tag{1.29}$$

where the kinetic term $\hat{H}_{kin} = \frac{\hbar^2 k^2}{2m}\sigma_0$ and the SOI term reads as:

$$\hat{H}_D = \beta(k_y\sigma_y - k_x\sigma_x) + \gamma(k_x k_y^2 \sigma_x - k_y k_x^2 \sigma_y), \tag{1.30}$$

where $\beta = \gamma \langle k_z^2 \rangle = \gamma (\pi/L)^2$, and L is the quantum well width. The first term in eq. (1.30), proportional to β, is linear in k and provides the dominant contribution to the Dresselhaus SOI. The second one, proportional to γ and cubic in k, becomes significant at higher Fermi levels, particularly in wider, highly doped quantum wells. Eignevalues of the Hamiltonian (1.29) are $E_\pm = \frac{\hbar^2 k^2}{2m} \pm \sqrt{\beta^2 k^2 - k_x^2 k_y^2(4\beta\gamma - \gamma^2 k^2)}$.

The Dresselhaus SOI in a 2D system strongly depends on the direction of the quantum well growth [47]. Interestingly, for growth along the [111] direction, considering only k-linear terms in the Hamiltonian (1.28), the spin orientation at the Fermi contours is the same as for the system with SIA, depicted in Figure 1.4(a). In contrast, when the quantum well is grown in the [111] direction, the spins are oriented perpendicular to the Fermi contour in the (001) plane, with the amplitude varying along the Fermi contour. For a quasi-2D system with the quantum well grown in the [001] direction, (corresponding to the Hamiltonian (1.30)), the spin orientation is perpendicular to the plane, as depicted in Figure 1.7.

Figure 1.7 presents the Fermi contours for a 2DEG with both linear and cubic forms of Dresselhaus SOC, as described by the Hamiltonian (1.29). The arrows indicate the expectation values of the spin, $\langle \hat{\mathbf{S}} \rangle_\pm^D$, that reads:

$$\langle \hat{\mathbf{S}} \rangle_\pm^D = \frac{\hbar\sqrt{2}}{2} \left(\pm\frac{\cos(\phi)\left(2\beta + \gamma k^2 \cos(2\phi) - \gamma k^2\right)}{\xi_{\mathbf{k}}}, \mp\frac{\sin(\phi)\left(2\beta - \gamma k^2 \cos(2\phi) - \gamma k^2\right)}{\xi_{\mathbf{k}}}, 0 \right),$$

---

[9]According to the first-order perturbation theory, the n-th power of $k_z = -i\partial_z$ is replaced by the expectation value $\langle(-i\partial_z)^n\rangle$. Note that if n is odd, then $\langle(-i\partial_z)^n\rangle = 0$, thus $\langle k_z \rangle = 0$. For infinitely-high potential well of width L, $\langle k_z^2 \rangle = (\pi/L)^2$.

where $\xi_{\mathbf{k}} = \sqrt{8\beta^2 + \gamma^2 k^4 + \gamma k^2 \cos(4\phi)(4\beta - \gamma k^2) - 4\beta\gamma k^2}$. The cubic Dresselhaus term influences the spin orientation, $\langle \hat{\mathbf{S}} \rangle_{\pm}^{D}$, at higher energies (contours 'B' and 'C'), where the cubic term becomes more significant, as shown in Fig. 1.7(a),(b).
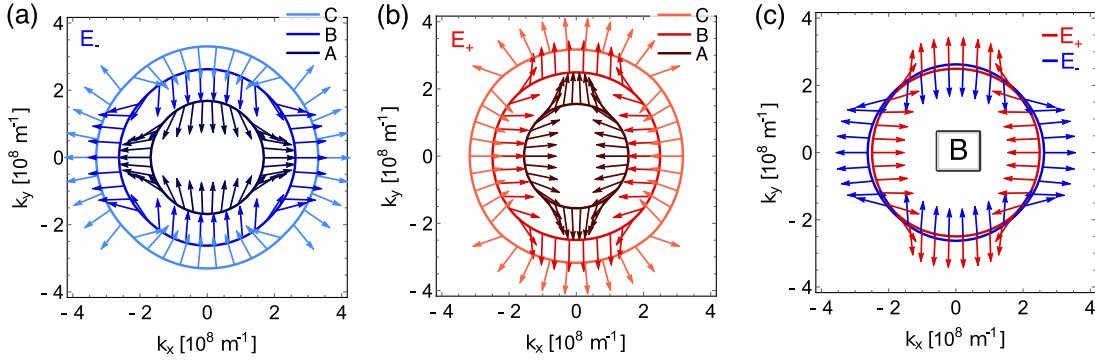
Figure 1.7: Fermi contours at three different Fermi levels, denoted 'A', 'B', and 'C', for a 2D system with k-linear and k-cubed Dresselhaus SOC, described by the Hamiltonian (1.29). Panels show Fermi contours for (a) the subband E_+, (b) the subband E_-, and (c) both subbands at energy 'B'. Arrows on the Fermi contours indicate the expectation value of the spin. The parameters are: $A = 20\,\text{meV}$, $B = 50\,\text{meV}$, $C = 80\,\text{meV}$, $m = 0.05m_0$, $\beta = 1 \cdot 10^{-11}\,\text{eV m}$, $\gamma = 200 \cdot 10^{-30}\,\text{eV m}^3$ (the cubic Dresselhaus term is set higher than in real materials known in the literature to clearly observe the influence of γ in the system)

Theoretical investigations using $\mathbf{k} \cdot \mathbf{p}$ method have determined the cubic Dresselhaus SOC term in GaAlAs/GaAs semiconductor heterostructure to be $\gamma = 21.29 \cdot 10^{-30}\,\text{eV m}^3$ [80]. In turn, experimental determination of the cubic Dresselhaus SOC strength parameter can be conducted through magnetoconductance measurements using weak antilocalization phenomena [52, 53]. In low-dimensional systems, conductivity is affected by quantum interference effect [81]. Specifically, constructive interference between time-reversed closed-loop electron paths after scattering events, known as backscattering, results in a *weak localization* (WL) contribution to the conductance, decreasing it. The phase difference of 2π in spin states for a pair of time-reversed backscattering electron trajectories leads to a spin reverse, causing destructive interference (suppressing backscattering). Consequently, a weak anti-localization (WAL) contribution to the conductance appears, enhancing the conductance. However, an external magnetic field can suppress both WL and WAL quantum corrections to the conductance by introducing a phase shift between pairs of electron closed-loop trajectories. This results in negative magnetoresistance for WL and positive magnetoresistance for WAL [53, 81, 82]. Miller et al. [53] determined the linear Rashba and both linear and cubic Dresselhaus SOC parameters, considering WL/WAL phenomena in GaAs/AlGaAs semiconductor heterostructure grown in the [001] direction, using magnetoconductance measurements and 2D magnetotransport theory account for spin-orbit interaction. In these systems, where both Rashba and Dresselhaus SOC are present, a gate-voltage-induced transition between WL and WAL can differentiate the contributions of each SOC type. Miller et al. found $\beta \approx 4 \pm 1 \cdot 10^{-13}\,\text{eV m}$ and $\gamma \approx 30 \cdot 10^{-30}\,\text{eV m}^3$. Similarly, within magnetoresistance measurements, Dresselhaus et al. found that in GaAs/Al$_{0.3}$Ga$_{0.7}$As (001) heterostructure

$\gamma = 26.1 \pm 0.9 \cdot 10^{-30}$ eV m^3.

Walser at al. [48], employed time-resolved Kerr rotation to determine the linear and cubic Dresselhaus coefficients in (001)-grown GaAs/Al$_{0.3}$Ga$_{0.7}$As quantum wells. They found $\gamma = -11 \pm 2 \cdot 10^{-30}$ eV m^3, while the linear Dresselhaus term increased with decreasing quantum well width, varying from $\beta = 1.2 \cdot 10^{-13}$ eV m to $\beta = 9 \cdot 10^{-13}$ eV m over a range of 6–30 nm. These γ values are consistent with those obtained through Raman spectroscopy, where γ for quantum wells in GaAs/AlGaAs semiconductor heterostructure ranges from $\gamma = 11 \cdot 10^{-30}$ eV m^3 to $\gamma = 34.5 \cdot 10^{-30}$ eV m^3, see in the tabulated values in the Supplementary material of [83].

The cubic form of Dresselhaus SOC is particularly significant in materials with a zinc-blende structure and an asymmetric quantum well, i.e., in the systems where both Rashba and Dresselhaus types of SOC coexist [84–89]. When the k-linear forms of both SOC types are balanced, a unique state known as the *persistent spin helix* (PSH) state emerges [84, 85, 87, 89]. The PSH is characterized by a uniaxial alignment of the spin-orbital field along the [110] or [1$\bar{1}$0] direction, depending on the relative sign between the Rashba and Dresselhaus strength parameters. Such uniaxial alignment of the spins suppresses spin relaxation for components parallel to the spin-orbital field, thus preserving spin precession. Consequently, the PSH state enables simultaneous manipulation and preservation of spin information by the SO field [89]. However, the presence of the cubic Dresselhaus term in such a system can disrupt the PSH state [84, 85, 87].

2

Method

2.1 Introduction

The theoretical analysis of electron transport in solids in response to external fields can be pursued through various methods. One commonly used approach involves identifying and solving the transport equation known as the Boltzmann equation [1, 90]. Another method for analyzing a system response to external perturbations, driving it out of equilibrium, is through the non-equilibrium Green's functions formalism [1, 91]. A third widely used approach employs correlation functions, such as the Kubo formula, which includes current-current correlation functions. In this case, equilibrium Green's functions can be utilized within the Kubo formula alongside diagrammatic perturbation theory [1, 90]. The following chapter provides a detailed description of evaluating the Kubo formula using Green's and Matsubara-Green's functions formalism within the diagrammatic technique.

Green's function

Green's functions powerful tools for solving inhomogeneous differential equations in both classical physics and many-body systems [91].

The fundamental definition of the time-ordered (causal) single-particle Green's function is given by [90–92]:

$$G(\lambda, t, t') = -\frac{\mathrm{i}}{\hbar} \frac{\langle \psi | T\{C_\lambda(t) C_\lambda^\dagger(t')\} | \psi \rangle}{\langle \psi | \psi \rangle}, \tag{2.1}$$

where $|\psi\rangle$ represents the ground state of the system, and $C_\lambda, C_\lambda^\dagger$ denote the time-dependent operators (in the Heisenberg representation) with λ standing for a quantum number, such as wavevector or spin. The time-ordering operator for operators $A(t)$ and $B(t')$ is defined as $T\{A(t)B(t')\} = \Theta(t - t')A(t)B(t') \mp \Theta(t' - t)B(t')A(t)$ with the upper (lower) sign referring to fermions (bosons), and $\Theta(t - t')$ being the step function.

The Green's function provides direct information about measurable quantities in physics. Specifically, using Green's function, one can define the quantum-mechanical expectation (average) value of an operator $\hat{O}_i$ as follows [91, 92]:

$$O_i(t) = -\mathrm{i}\mathrm{Tr}\sum_{\mathbf{k}}\hat{O}_i G_{\mathbf{k}}(t, t + \delta t). \tag{2.2}$$

Another type of Green's function, characterized by poles in only one half-plane, is particularly useful for evaluating physical responses [91, 92]. To analyze the system response at time t to an earlier perturbation at time t', one should use the retarded Green's function, which is non-zero only for times $t \geq t'$:

$$G^R(\lambda, t, t') = -\frac{\mathrm{i}}{\hbar}\Theta(t - t')\frac{\langle\psi|C_\lambda(t)C_\lambda^\dagger(t')|\psi\rangle}{\langle\psi|\psi\rangle}. \tag{2.3}$$

Alternatively, the advanced Green's function, which is finite only for $t \leq t'$, can be used:

$$G^A(\lambda, t, t') = -\frac{\mathrm{i}}{\hbar}\Theta(t' - t)\frac{\langle\psi|C_\lambda(t)C_\lambda^\dagger(t')|\psi\rangle}{\langle\psi|\psi\rangle}. \tag{2.4}$$

For a given non-interacting Hamiltonian, $\hat{H}$, the causal Green's function can be obtained by performing a Fourier transform (thus transitioning from the time domain to the energy domain) as follows [90]:

$$G(\varepsilon) = \left[(\varepsilon + \mu + \mathrm{i}\delta\mathrm{sgn}(\varepsilon))\hat{I} - \hat{H}\right]^{-1}, \tag{2.5}$$

where $\hat{I}$ is the identity matrix, δ is an infinitesimal quantity, and the sign function, $\mathrm{sgn}(\varepsilon)$, depends on the location of the poles in the complex plane.

Kubo formula

In principle, Kubo formula [93, 94] allows the examination of the linear response to any external driving perturbation. The *ac* conductivity in Kubo formalism is given by [90, 91]:

$$\sigma_{\alpha\beta}(\mathbf{q}, \omega) = \frac{\mathrm{i}}{\omega}\left[\Pi_{\alpha\beta}^R(\mathbf{q}, \omega) + \frac{ne^2}{m}\delta_{\alpha\beta}\right], \tag{2.6}$$

where α, β represent cartesian components, $\delta_{\alpha\beta}$ denotes the Kronecker delta and $\Pi_{\alpha\beta}^R(\mathbf{q}, \omega)$ is the retarded two-particle current-current correlation function defined with a Fourier transform [91]:

$$\Pi_{\alpha\beta}^R(\mathbf{q}, \omega) = -\frac{\mathrm{i}}{V}\int_{-\infty}^{\infty}\mathrm{d}t\, \mathrm{e}^{\mathrm{i}\omega(t-t')}\Theta(t - t')\langle\psi|\left[j_\alpha(-\mathbf{q}, t), j_\beta(\mathbf{q}, t')\right]|\psi\rangle, \tag{2.7}$$

where V is the volume of a system, $\Theta(t-t')$ stands for a step function maintaining the time order, and $j_\alpha(-\mathbf{q}, t)$ and $j_\beta(\mathbf{q}, t')$ are current operators. In the zero-temperature limit, $|\psi\rangle$ indicates the ground state of the analyzed Hamiltonian, whereas for finite temperatures – the trace over thermal distribution at nonzero temperatures.

It is important to note that each current operator in eq. (2.7), $j_\alpha(-\mathbf{q}, t)$ and $j_\beta(\mathbf{q}, t')$, involves a product of creation and destruction operator, describing the creation and destruction of two particles. Thus, the conductivity appears from the correlations between these two processes. Therefore, one can evaluate eq. (2.7) with a two-particle Green's function. Nevertheless, for noninteracting electrons, two-particle Green's function can be factorized into a product of two single-particle Green's functions.

2.2 Diagrammatic perturbation theory in the linear response regime

The response of a system to an external driving force, such as the quantum-mechanical expectation value of the charge (or spin) current density operator, as given by eq. (2.2), i.e. [91, 92],

$$O_i(t) = -\mathrm{i}\mathrm{Tr} \sum_{\mathbf{k}} \hat{O}_i G_{\mathbf{k}}(t, t + \delta t),$$

is defined with a causal Green's function, $G_{\mathbf{k}}(t, t + \delta t)$ (eq. (2.1)). The ground state involved in $G_{\mathbf{k}}(t, t + \delta t)$ corresponds to a many-body system, making it challenging to find its explicit form. In most cases the Hamiltonian for an analyzed system can not be solved exactly[1]. A commonly used approach, provided by many-body perturbation theory, involves dividing the Hamiltonian into two parts [90]:

$$\hat{\mathcal{H}} = \hat{H} + V, \tag{2.8}$$

where the Hamiltonian $\hat{H}$ represents the noninteracting system, and V is a perturbation (describing the interaction between the perturbation field and the carriers in the system), small compared to $\hat{H}$. In the investigation of transport effects in the linear response regime, the external driving force, such as an electric field or temperature gradient, is treated as a perturbation, $V \equiv \hat{H}_A$. Consequently, $G_{\mathbf{k}}(t, t + \delta t)$ in eq. (2.2) can be expanded in a series with respect to the perturbation Hamiltonian, $\hat{H}_A(t')$, where $t < t' < t + \delta t$, and t' represents the time when the perturbation occurs. The Green's function is then evaluated based on the unperturbed Hamiltonian, $\hat{H}$. This leads the expectation value of the operator $\hat{O}_i$ taking the form [92]:

$$O_i(t) = -\mathrm{i}\mathrm{Tr} \sum_{\mathbf{k}, t'} \hat{O}_i G_{\mathbf{k}}(t, t') \hat{H}_A(t') G_{\mathbf{k}}(t', t + \delta t). \tag{2.9}$$

---

[1]Strictly speaking, the phrase "solving a Hamiltonian" is industry jargon. It refers to solving the Schrödinger equation for the analyzed Hamiltonian. In other words, one seeks the eigenstates of the system.

Equation (2.9) serves as a starting point for investigating transport effects and can be depicted using the diagrammatic technique, as shown in figure 2.1. All the diagrams presented are utilized
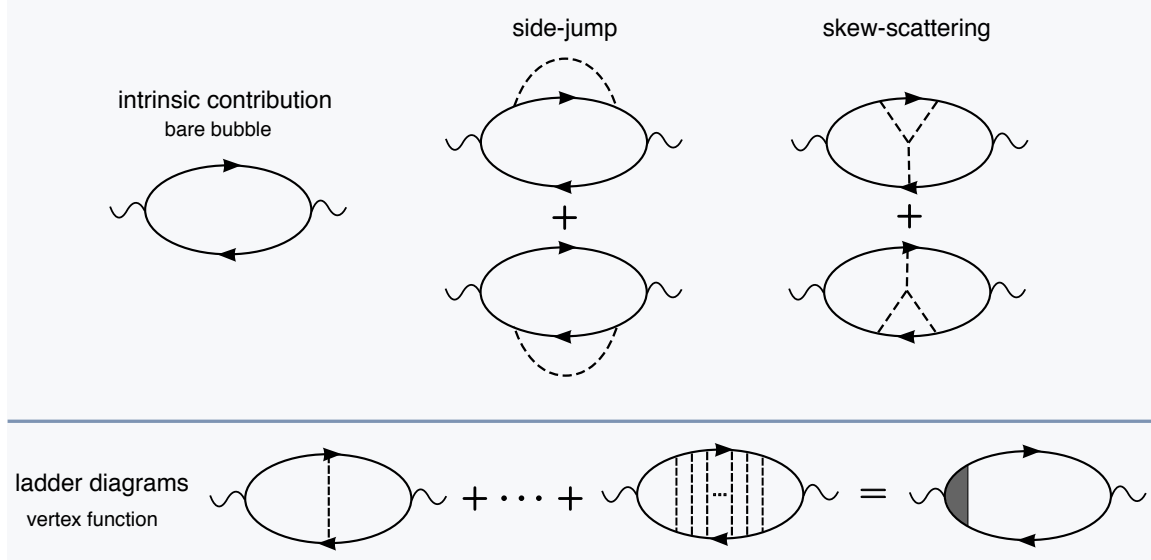
**Figure 2.1:** Feynman diagrams corresponding to the different contributions

within the Kubo formalism. The Green's functions correspond to the solid lines, the vertices of the diagrams represent the response operator, $\hat{O}_i$, and perturbation Hamiltonian, $\hat{H}_A$, and the dashed lines stand for scattering events. The diagram without disorder lines, the *bare bubble*, resembles the intrinsic contribution (see also fig. 2.2). Spin-dependent scattering processes, such as side-jump and skew-scattering, can be included with pairs of mutually conjugated diagrams. In turn, the role of impurities in the system can be analyzed with the vertex correction, introduced through the sum of ladder diagrams.

Green's functions formalism allows obtaining results in the zero-temperature regime, enabling observation of how included interactions influence the system, where temperature smearing does not distort the view. Consequently, zero-temperature results provide a valuable starting point for analyzing the system's behavior. However, for experimental relevance and practical applications, it is essential to also consider the system's thermodynamic properties at finite temperatures.

2.2.1 Matsubara-Green's functions formalism

The role of the temperature was implemented into the Green's functions formalism by Matsubara in 1955 through the imaginary-time formalism [95]. The general formula for the expectation value of the operator $\hat{O}_i$ in the linear response to an external perturbation, $\hat{H}_\mathbf{A}(i\omega_m)$ (fig. 2.2a) is given by [90, 96]:

$$O_i(i\omega_m) = k_B T \sum_{\mathbf{k},n} \text{Tr}\{\hat{O}_i G_\mathbf{k}(i\varepsilon_n + i\omega_m)\hat{H}_\mathbf{A}(i\omega_m)G_\mathbf{k}(i\varepsilon_n)\}, \qquad (2.10)$$
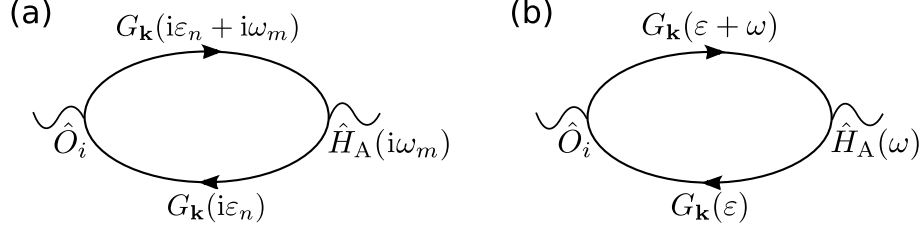
Figure 2.2: Single-loop diagram (*bare bubble*) in Feynman diagrammatic technique describing the expectation value of the operator $\hat{O}_i$ in response to external perturbation $\hat{H}_A$ in (a) finite-temperature and (b) zero-temperature formalism

where i, j stand for cartesian coordinates and $G_{\mathbf{k}}(i\varepsilon_n + i\omega_m)$, $G_{\mathbf{k}}(i\varepsilon_n)$ are Matsubara-Green's functions dependent on Matsubara energies: $\varepsilon_n = (2n+1)\pi k_B T$ with $n = 1, 3, 5, 7, \ldots$ and $\omega_m = 2m\pi k_B T$ with $m = 1$. The perturbation Hamiltonian $\hat{H}_{\mathbf{A}}(i\omega_m)$ represents the external driving force that brings the system out of equilibrium.

For electrically-induced transport effects, the driving force is an electric field applied in the j-direction, represented by a perturbation Hamiltonian describing the interaction of electrons with the electric field: $\hat{H}_{\mathbf{A}}^E(i\omega_m) \equiv \hat{H}_{A_j}^E(i\omega_m) = -\hat{j}_j A_j^E(i\omega_m)$ with electromagnetic vector potential $A_j^E(i\omega_m) = \frac{\hbar}{i\omega_m}(-iE_j(i\omega_m))$, where the charge current density operator $\hat{j}_j = e\hat{v}_j$, and the velocity operator $\hat{v}_j = \frac{1}{\hbar}\frac{\partial \hat{H}}{\partial k_j}$.

For thermally-induced transport phenomena, one can introduce a sort of inhomogeneous gravitational field [97] that induces heat current flow [98, 99]. The perturbation Hamiltonian for this case is defined as a coupling of the heat current density operator to an auxiliary gravitational vector potential amplitude, i.e., for driving force applied in the j-direction: $\hat{H}_{\mathbf{A}}^{\nabla T} \equiv \hat{H}_{A_j}^{\nabla T} = -\hat{j}_j^h A_j^h(i\omega_m)$ where $A_j^h(i\omega_m) = \frac{\hbar}{i\omega_m}\left(-\frac{\nabla_i T}{T}\right)$ and $\hat{j}_j^h = \frac{1}{2}\left[\hat{H} - \mu\hat{I}, \hat{v}_j\right]_+$, with μ standing for the chemical potential, and $\hat{I}$ denoting the identity matrix. The driving force in this case is the temperature gradient ∇T, a statistical force that drives transport as the system approaches equilibrium through irreversible processes.

To study charge conductivity, one replaces the operator $\hat{O}_i$ with the velocity operator $\hat{v}_i$. For spin responses, such as the spin Hall effect or spin polarization, one should consider the spin current density operator, $\hat{j}_i^{s_z}$, or the spin operator, $\hat{s}_i$.

Exempli gratia, to find the non-equilibrium spin polarization induced by the external electric field, the relevant operator is the spin operator, $\hat{O}_i = \hat{s}_i$. Then, the formula for the current-induced spin polarization reads [90, 100]:

$$S_i^{E_j}(i\omega_m) = k_B T \frac{eE_j\hbar}{\omega_m} \sum_{\mathbf{k},n} \mathrm{Tr}\{\hat{s}_i G_{\mathbf{k}}(i\varepsilon_n + i\omega_m)\hat{v}_j G_{\mathbf{k}}(i\varepsilon_n)\}. \tag{2.11}$$

The summation over Matsubara energies, ε_n, can be performed using contour integration methods [90], as illustrated in Fig. 2.3.
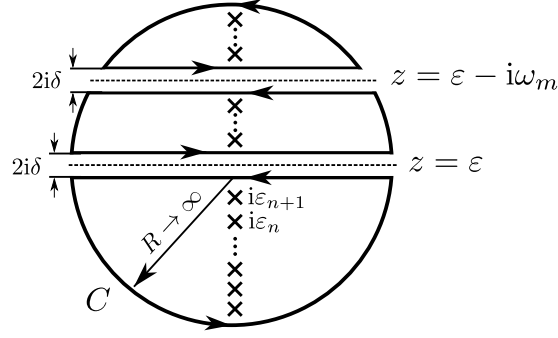
Figure 2.3: Contour C in the complex z-plane used for summing over Matsubara energies, ε. The contour includes two branch cuts: along $z = \varepsilon$ and $z = \varepsilon - \mathrm{i}\omega_m$

Thus, one postulates that [90, 100]:

$$k_B T \sum_n \hat{s}_i G_{\mathbf{k}}(\mathrm{i}\varepsilon_n + \mathrm{i}\omega_m)\hat{v}_j G_{\mathbf{k}}(\mathrm{i}\varepsilon_n) = -\int_C \frac{\mathrm{d}z}{2\pi\mathrm{i}} f(z)\hat{s}_i G_{\mathbf{k}}(z + \mathrm{i}\omega_m)\hat{v}_j G_{\mathbf{k}}(z) = \mathcal{L}, \quad (2.12)$$

where contour integral has two branch cuts: along $z = \varepsilon$ and $z = \varepsilon - \mathrm{i}\omega_m$. The parts of the contour C where $R \to \infty$ are equal to zero, and only the four horizontal lines along the branch cuts remain. The integration over the contour C leads then to [90, 100]:

$$\begin{aligned}
\mathcal{L} = {}& \mathrm{i} \int_{-\infty}^{+\infty} \frac{\mathrm{d}\varepsilon}{2\pi} f(\varepsilon)\hat{s}_i G_{\mathbf{k}}(\varepsilon + \mathrm{i}\omega_m)\hat{v}_j G_{\mathbf{k}}(\varepsilon + \mathrm{i}\delta) \\
& - \mathrm{i} \int_{-\infty}^{+\infty} \frac{\mathrm{d}\varepsilon}{2\pi} f(\varepsilon)\hat{s}_i G_{\mathbf{k}}(\varepsilon + \mathrm{i}\omega_m)\hat{v}_j G_{\mathbf{k}}(\varepsilon - \mathrm{i}\delta) \\
& + \mathrm{i} \int_{-\infty}^{+\infty} \frac{\mathrm{d}\varepsilon}{2\pi} f(\varepsilon - \mathrm{i}\omega_m)\hat{s}_i G_{\mathbf{k}}(\varepsilon + \mathrm{i}\delta)\hat{v}_j G_{\mathbf{k}}(\varepsilon - \mathrm{i}\omega_m) \\
& - \mathrm{i} \int_{-\infty}^{+\infty} \frac{\mathrm{d}\varepsilon}{2\pi} f(\varepsilon - \mathrm{i}\omega_m)\hat{s}_i G_{\mathbf{k}}(\varepsilon - \mathrm{i}\delta)\hat{v}_j G_{\mathbf{k}}(\varepsilon - \mathrm{i}\omega_m),
\end{aligned} \quad (2.13)$$

where $f(\varepsilon)$ is the Fermi-Dirac distribution function, treated as a meromorphic function with poles at odd integers $z = \mathrm{i}\varepsilon_n$. Upon analytical continuation to the complex plane, $\mathrm{i}\omega_m \to \omega + \mathrm{i}\delta$, and considering the complex half-planes for the corresponding advanced and retarded Green's functions, $G_{\mathbf{k}}^{A/R}$, one obtains the formula for the current-induced spin polarization, $S_i^{E_j}(\omega)$ [101]:

$$\begin{aligned}
S_i^{E_j}(\omega) = -\frac{eE_j\hbar}{\omega} \int \frac{\mathrm{d}^2\mathbf{k}}{(2\pi)^2} \int \frac{\mathrm{d}\varepsilon}{2\pi} f(\varepsilon) \operatorname{Tr} \big\{ & \hat{s}_i G_{\mathbf{k}}^R(\varepsilon + \omega)\hat{v}_j \left[G_{\mathbf{k}}^R(\varepsilon) - G_{\mathbf{k}}^A(\varepsilon) \right] \\
& + \hat{s}_i \left[G_{\mathbf{k}}^R(\varepsilon) - G_{\mathbf{k}}^A(\varepsilon) \right] \hat{v}_j G_{\mathbf{k}}^A(\varepsilon - \omega) \big\},
\end{aligned} \quad (2.14)$$

where the summation over $\mathbf{k}$ is converted into an integral, and for a two-dimensional system $\sum_{\mathbf{k}} \to \int \frac{\mathrm{d}^2\mathbf{k}}{(2\pi)^2}$ with $\mathbf{k} = (k_x, k_y)$. The integration over the energy, ε, can be performed using Cauchy's residue integration method (see, e.g., [102, 103]).

2.2.2 Green's functions formalism

Figure 2.2b illustrates the single-loop diagram in the zero-temperature regime. In this diagram, the Green's functions of the non-interacting system, $G_{\mathbf{k}}(\varepsilon + \omega)$ and $G_{\mathbf{k}}(\varepsilon)$, are represented by the solid lines. The vertices symbolize the perturbation Hamiltonian, $\hat{H}_A(\omega)$, which represents the driving force, and the operator, $\hat{O}_i$, which denotes the system response. Applying the Fourier transform with respect to the time variables on eq. (2.9) yields the formula corresponding to the diagram [100]:

$$O_i(\omega) = i\mathrm{Tr} \int \frac{\mathrm{d}^2\mathbf{k}}{(2\pi)^2} \int \frac{\mathrm{d}\varepsilon}{2\pi} \hat{O}_i G_{\mathbf{k}}(\varepsilon + \omega) \hat{H}_A(\omega) G_{\mathbf{k}}(\varepsilon). \tag{2.15}$$

When the perturbation Hamiltonian represents an external electric field, $\hat{H}_A(\omega) = -e\hat{v}_j A_j^E(\omega)$ with the electromagnetic vector potential $A_j^E(\omega) = -i\frac{\hbar}{\omega}E_j(\omega)$, the conductivity tensor, $\sigma_{ij}(\omega) = j_i^E/E_j(\omega)$, is expressed by the Kubo-Středa formula [33, 93, 94] based on the diagram shown in figure 2.2b, and is given by [104]:

$$\sigma_{ij}(\omega) = \frac{e^2\hbar}{\omega} \int \frac{\mathrm{d}^2\mathbf{k}}{(2\pi)^2} \int \frac{\mathrm{d}\varepsilon}{2\pi} \mathrm{Tr}\{\hat{v}_i G_{\mathbf{k}}(\varepsilon + \omega)\hat{v}_j G_{\mathbf{k}}(\omega)\}, \tag{2.16}$$

where $G_{\mathbf{k}}$ is defined by eq. (2.5).

2.3 Self-energy

In a real system, carriers experience scattering processes such as electron-electron interaction, electron-phonon interaction, and scattering on disorders due to impurities or defects in the crystal lattice. These processes are captured by the proper *self-energy*, $\Sigma_{\mathbf{k}}^*$, which describes how interactions with the surrounding many-particle system affect the carriers. While the unperturbed (zero-ordered) Green's function, $G_{\mathbf{k}}^0$, does not account for scattering processes, the exact Green's function, $\bar{G}_{\mathbf{k}}$, incorporates the self-energy. Dyson's equation, which stands for the definition of the proper self-energy, includes an infinite-order approximate series expansion for the Green's function [1, 90–92, 105]:

$$\bar{G}_{\mathbf{k}} = G_{\mathbf{k}}^0 + G_{\mathbf{k}}^0 \Sigma_{\mathbf{k}}^* G_{\mathbf{k}}^0 + G_{\mathbf{k}}^0 \Sigma_{\mathbf{k}}^* G_{\mathbf{k}}^0 \Sigma_{\mathbf{k}}^* G_{\mathbf{k}}^0 + \ldots = G_{\mathbf{k}}^0 + G_{\mathbf{k}}^0 \Sigma_{\mathbf{k}}^* \bar{G}_{\mathbf{k}}. \tag{2.17}$$

After a straightforward algebraic transformation, since $\bar{G}_{\mathbf{k}}$, $G_{\mathbf{k}}^0$, and $\Sigma_{\mathbf{k}}^*$ are all diagonal in matrix indices, the relation simplifies to [1, 90–92, 105]:

$$\left[\bar{G}_{\mathbf{k}}\right]^{-1} = \left[G_{\mathbf{k}}^0\right]^{-1} - \Sigma_{\mathbf{k}}^*, \tag{2.18}$$

which is used to evaluate the proper self-energy.

According to Bloch's theorem, in the *nearly-free electron model*, an electron moving in an ideal periodic crystal lattice does not change its velocity due to the interaction with ions (electron-phonon interaction). In turn, the scattering processes on electrons, i.e., electron-electron (e-e) interaction, are not considered in the non-interacting gas model. It is related to the fact that the relaxation time[2], τ, for e-e interactions is significantly longer than τ associated with deviations in the periodic crystal lattice (mainly due to the Pauli exclusion principle), hence can be neglected in this context [106]. In this thesis, the scattering processes considered are related only to deviations from the periodicity of the crystal potential due to defects in periodic structure or impurities. Consequently, the exact Green's function here is called the *impurity-averaged Green's function*.

Born approximation

Here, impurities are assumed to be randomly distributed, spin-independent, and point-like, giving rise to short-range interaction. Since the impurities are much heavier than the electrons, the impurities can be described with a static potential, $V(\mathbf{r})$, and their collisions are considered elastic (i.e., the electrons scatter from from an initial state with wavevector $\mathbf{k}$ to a final state with wavevector $\mathbf{k}'$ without losing energy, only changing their momentum, see chapter 8.1 in [90]).

If the mean wavelength of the electron is smaller than the characteristic dimension of the impurity field, (i.e, the impurity potential is weak and the momentum transfer $(\mathbf{k} - \mathbf{k}')$ is small), then the scattering event can be approximated using the lowest-order Born approximation. In this approximation, only the first-order contribution to the proper self-energy is considered, $\Sigma_{\mathbf{k}}^* \approx \Sigma_{\mathbf{k}}^{*(1)} \equiv \Sigma_{\mathbf{k}}$ [92], see fig. 2.4.

Figure 2.4: Zero-, first- and second-order contributions to the proper self-energy, $\Sigma_{\mathbf{k}}^{*(n)}$ for $n = \{0, 1, 2\}$. Dashed lines represent the scattering amplitude, $n_i V(\mathbf{k} - \mathbf{k}')$, solid lines correspond to the Green's function, $G_{\mathbf{k}}^0$, and the crosses denote the impurity

For a two-dimensional system, the self-energy in the Born approximation is given by [28]:

$$\Sigma_{\mathbf{k}}^{*(1)} \equiv \Sigma_{\mathbf{k}} = n_i \int \frac{\mathrm{d}^2\mathbf{k}'}{(2\pi)^2} V^2(\mathbf{k} - \mathbf{k}') G_{\mathbf{k}'}^0, \tag{2.19}$$

---

[2]The electron scatters with probability $1/\tau$ in a unit time, where τ is the mean free time between the collisions called the *relaxation time* [106].

34

where n_i is the impurity concentration and $V(\mathbf{k} - \mathbf{k}')$ is the Fourier transform of the single impurity potential. One assumes that electrons scatter off short-range impurities modeled as δ-function scatters. Additionally, for weak impurity interaction (momentum-independent scattering potential), the real part of the self-energy is negligible. Thus, one obtains [28]:

$$\mathrm{Im}[\Sigma_{\mathbf{k}}] = n_i V_0^2 \int \frac{\mathrm{d}^2\mathbf{k}}{(2\pi)^2} G_{\mathbf{k}}^0 = \mathrm{i}\Gamma, \tag{2.20}$$

where Γ denotes the relaxation rate, related to the relaxation time, τ, by $\Gamma = \hbar/(2\tau)$.

It is important to note that the scattering events are treated independently of all other impurities. Consequently, the approach provided above is applicable only at low impurity concentrations.

2.4 Impurity vertex correction

Since the self-energy describes the influence of scattering processes on the carriers themselves, it turns out that including the interaction with surrounding processes only in the self-energy is not enough to analyze the transport properties of a system. Therefore, one must consider a correction that describes the influence of scattering processes on the system response. In the diagrammatic technique, including impurity scattering processes involves renormalizing the operators at the vertices of the diagram, as shown in fig. 2.5, thus the name – *vertex correction*.

As was previously mentioned, the primary relaxation mechanism in this context is scattering on point-like, spin-independent, and randomly distributed impurities located in points $\mathbf{R}_i$. Thus, assuming a white-noise distribution, the impurity potential can be modeled as δ-function scatters: $V_i(\mathbf{r}) = \sum_i V_i \delta(\mathbf{r} - \mathbf{R}_i)$ which means that impurities are static objects with spherically symmetric potentials. While the impurity potential vanishes on average[3], $\langle V_i(\mathbf{r}) \rangle = 0$, the second statistical cumulant is finite and has the form: $\langle |V_i(\mathbf{r})|^2 \rangle = n_i V_0^2$, where n_i is the impurity concentration.

The sketch in figure 2.5a depicts the sum of all ladder diagrams, which are sufficient in the low-impurity regime and result in the vertex correction. The scattering events are represented by dashed electron lines connecting the Green's functions on both sides of the diagram. Each dashed line represents various scattering events due to a single impurity. After summing all scattering events, the vertex diagrams are consolidated into a single diagram where the vertex operator is renormalized with the vertex function. The vertex function appears only at one end of the diagram to avoid overvaluing the vertex terms [90].

To determine the impurity vertex function, $\mathcal{O}_i$, one have to solve the self-consistent equation

---

[3] $\langle \ldots \rangle$ means the ensemble average over disorder configurations.
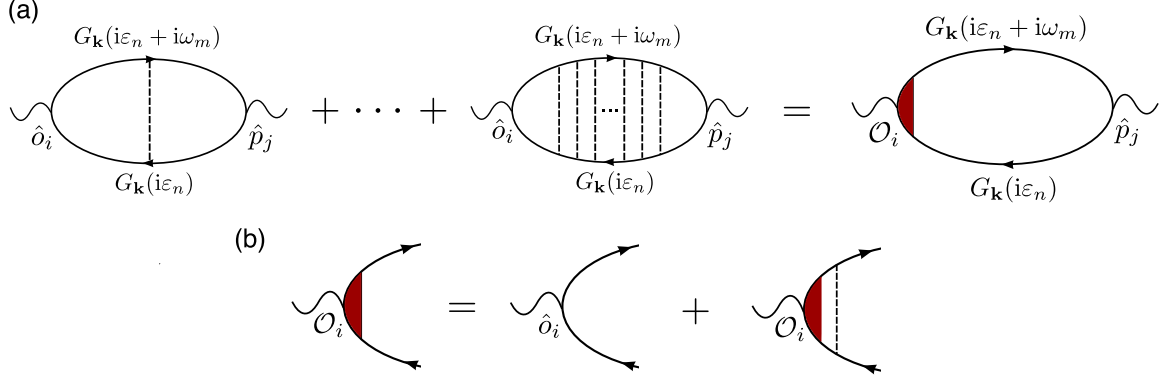
Figure 2.5: (a) Ladder diagrams for vertex corrections to the bare operator $\hat{o}_i$. (b) Diagrammatic representation of the self-consistent impurity-renormalized vertex equation for the vertex function $\mathcal{O}_i$. The figure is taken from [107], © 2022 Elsevier

depicted in figure 2.5b. In general, the vertex function in the Matsubara-Green's functions formalism depends on the Matsubara energies [90]:

$$\mathcal{O}_i(i\varepsilon_n, i\omega_m) = \hat{o}_i + n_i V_0^2 \int \frac{d^2\mathbf{k}}{(2\pi)^2} \, G_\mathbf{k}(i\varepsilon_n)\mathcal{O}_i(i\varepsilon_n, i\omega_m)G_\mathbf{k}(i\varepsilon_n + i\omega_m). \quad (2.21)$$

In the *dc* limit, $\omega \to 0$, and when only the states at the Fermi level, ε_F, are taken into account[4], eq. (2.21) comes down to [108]:

$$\mathcal{O}_i^{XY} = \hat{o}_i + n_i V_0^2 \int \frac{d^2\mathbf{k}}{(2\pi)^2} \, G_\mathbf{k}^X(\varepsilon_F)\mathcal{O}_i G_\mathbf{k}^Y(\varepsilon_F), \quad (2.22)$$

where $G_\mathbf{k}^{X,Y}(\varepsilon_F)$ are advanced or retarded impurity-averaged Green's functions, $X, Y = \{A, R\}$.

---

[4]The vertex correction describes the influence of impurity scattering on the transport properties since only the carriers at the Fermi level are scattered. In turn, the carriers in the Fermi sea, which contribute to the intrinsic part, are robust against impurity scattering and do not need to be included in the vertex correction.

<div style="text-align: right; font-size: 3em;">**3**</div>

Transport phenomena considered in the thesis

3.1 Non-equilibrium spin polarization

The idea of *spin polarization* dates back to the early days of the spin concept and involves a scenario where spin magnetic moments (or just spins) are oriented in a specific direction[1]. In magnetic material, the exchange interaction between the spins of constituent atoms results in magnetic ordering. In ferromagnetic metals, for instance, the majority of spin magnetic moments align parallel to a selected axis (e.g., *spin-up*), while less than half align antiparallel (*spin-down*). This imbalance creates a non-zero net magnetization, and the terms *majority* and *minority spins* are used to describe that case. If the quantities of spin-up and spin-down are equal, the system is spin-unpolarized (nonmagnetic).

Spin polarization, i.e., magnetization, can also be induced in nonmagnetic materials by applying an external magnetic field or through the proximity effect. In the latter case, when a nonmagnetic material is deposited on a magnetic substrate, the exchange interaction between the spins of the atoms in the nonmagnetic material (or the spins of carriers in a 2DEG formed on its surface) and the localized magnetic moments in the substrate induces magnetization in the system.

In the context of current flow, when the spins of the carriers align parallel to a chosen axis, the resulting current is referred to as *spin-polarized current*. One of the most promising phenomena in spintronics is the ability to induce non-equilibrium spin polarization of carriers *via* spin-orbit

---

[1]It is noteworthy that, while it is impossible to measure all components of spin simultaneously, individual components can be measured. For example, stating that a "spin-1/2 is in the z-direction" means that the spin vector lies on a conical shell around the z-axis, with its z-component equal to $\hbar/2$ (see, e.g., chapter 2.1 in [109]).

interaction (SOI) without requiring an external magnetic field. It turns out that, due to the presence of SOI in the system, a direct current can generate a non-equilibrium uniform spin polarization of the carriers in the system, a phenomenon known as *current-induced spin polarization* (CISP) [110]. It is worth noting that CISP is also referred to by various names in the literature, including the inverse spin-galvanic effect, current-induced spin accumulation, magnetoelectric effect, and (Rashba)-Edelstein effect. However, all of these terms describe the same microscopic effect, which is the emergence of non-equilibrium CISP in response to an external electric field (*dc*) in gyrotropic media with intrinsic spin-orbit coupling [111]. On the other hand, when the driving force is a temperature gradient, *thermally-induced spin polarization* (TISP) arises.

3.1.1 Current-induced spin polarization (CISP)

The theoretical prediction of spin polarization by a charge current was made in 1978 by Ivchenko and Pikus [112] for bulk-tellurium crystals, attributing this effect to the unique valence band structure (hybridized spin-up and spin-down bands) in tellurium. In contrast, a distinct microscopic mechanism of CISP in a 2DEG formed in semiconductor quantum wells, associated with *asymmetric spin relaxation*, was predicted by Vas'ko and Prima, Edelstein, and Aranov and Lyanda-Geller [113–115].
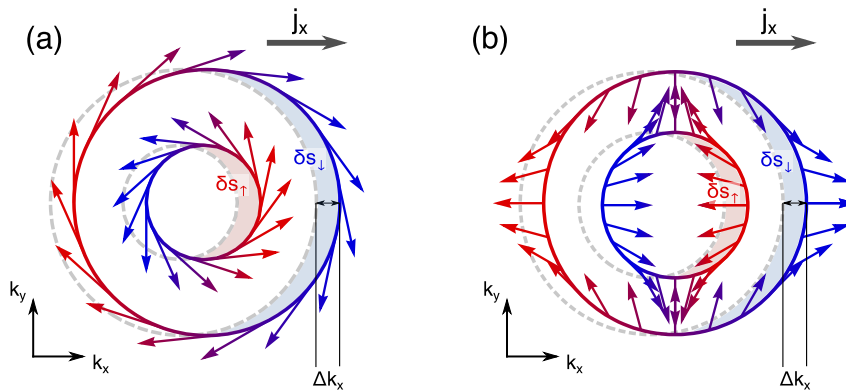
Figure 3.1: Current-induced spin polarization in a 2DEG with intrinsic spin-orbit coupling (a) Rashba type and (b) Dresselhaus type for a quantum well grown along the [001] direction. The 2DEG is formed in the xy-plane. Arrows indicate the expectation value of the carriers' spin related to the SOI. j_x denotes the direction of charge carriers in response to an applied external electric field

The asymmetric scattering mechanism leading to spin polarization of the current is known in the literature as Elliott-Yafet spin relaxation [116]. This effect plays a crucial role in systems where spin-orbit coupling is present. In a 2DEG with intrinsic spin-orbit interaction (Rashba or Dresselhaus type), the spin degeneracy of the bands is lifted. Since the external electric field is applied in the $-x$-direction, charge carriers move along the direction of the applied field, and the Fermi contours are shifted in k-space by Δk_x, see fig. 3.1. This results in a non-equilibrium spin distribution, i.e., $\delta s_\downarrow \neq \delta s_\uparrow$. Consequently, spin-flip scattering processes become unbalanced,

resulting in current-induced spin orientation along the y-direction for a 2D system with Rashba SOC, as indicated in fig. 3.1a, and along the x-direction for a 2DEG with Dresselhaus SOC in a QW grown along the [001] direction, see fig. 3.1b.

D'yakonov and Perel [47, 117] developed another concept for spin polarization of the current, which involves spin precessional processes. Here, the current-induced shift of the Fermi contour decouples the carriers' spin orientation from their momenta, initiating spin precession around the new expected spin orientation and resulting in an additional spin component. Furthermore, this mechanism also contributes to the intrinsic spin Hall effect, a charge-to-spin conversion effect discussed in sec. 3.2.3, which leads to nonuniform spin accumulation at the edges of the system [118]. Thus, having common features in their microscopic origins, CISP often accompanies spin Hall effect [110, 118–120]. Indeed, the first measurements of the CISP were made together with SHE measurement in a strained semiconductor heterostructure n-InGaAs/GaAs using Kerr-Faraday magneto-optical detection [110, 119], as well as in AlGaAs/GaAs heterostructure by angle-resolved polarization detection [120] and spatially resolved scanning Kerr rotation microscopy [121].

Additionally, another source of the CISP is related to asymmetric in momentum space spin-dependent carrier scattering by phonons and defects, due to the presence of an extrinsic spin-orbit interaction in the system. This mechanism does not require spin-splitting the bands and can dominate at higher temperatures [122–124]. It has been theoretically considered in (001)-grown quantum wells in semiconductor heterostructures [122, 123] and experimentally observed in InGaAs deposited on GaAs in the [001] direction with anisotropic spin-orbit field [124]. In these experiment, the strength and orientation of the anisotropic spin-orbit field were tuned through the direction of the electron drift momentum, altered by adjusting the voltage applied to the four contacts at the edges of the sample. The researchers found that strong intrinsic SOC relates to weak CISP and *vice versa*. Thus, the mechanism of spin-dependent scattering events must be considered in such cases.

From an application perspective, an intriguing aspect of non-equilibrium spin polarization is the coupling of the carrier's spin with local magnetization in a magnetized system *via* exchange interaction. This interaction results in a spin torque on the local magnetic moments [125, 126], enabling efficient switching of magnetic domains using an electric current without an applied magnetic field. The control of magnetization *via* spin-orbit field was experimentally demonstrated in 2009 by Chernyshov et al. in p-type ferromagnetic semiconductor, (Ga,Mn)As. In the presence of an external magnetic field and Rashba spin-orbit field (tuned by an external electric field strength), the transverse resistance, and thus the magnetization, changes its sign with the electric field strength. Spin torque induced by current flowing in a system with Rashba SOC was also experimentally investigated in a metallic ferromagnetic system, Pt/Co/AlO$_x$ [127].

3.1.2 Thermally-induced spin polarization (TISP)

Spin polarization in a system can also be induced by a temperature gradient, namely thermally-induced spin polarization (TISP). Unlike electrically-induced spin polarization (CISP), where a mechanical force drives the effect, TISP is driven by statistical forces that induce transport as the system as a result of approaching the equilibrium through irreversible processes.

In the presence of a temperature gradient, the colder and hotter particles move towards a given point from different sides. Due to the different density of states in the two subbands within a 2DEG model with intrinsic spin-orbit interaction, the local distribution of particles with positive and negative wavevector components differs, resulting in nonzero spin polarization [128]. In a system with Rashba-type SOI, the spin polarization occurs in-plane and perpendicular to the driving force, while in the case of Dresselhaus-type SOI, it aligns with the driving force. Moreover, in a 2DEG system with Dresselhaus (Rashba) SOI and an out-of-plane exchange field, a transverse (longitudinal) component of spin polarization also appears.

3.1.3 Key finding in the literature related to the scope of the thesis

Current-induced spin polarization has been studied for a magnetized 2DEG with k-linear form of Rashba SOI [101], as well as for systems with Rashba, Dresselhaus SOI, and extrinsic spin-orbit interaction [129].

In the following thesis, CISP in a 2DEG with Dresselhaus spin-orbit interaction, taking into account also the k-cubic SOI term, is discussed. While CISP for a nonmagnetized 2DEG with the k-linear form of Dresselhaus, or equivalent case with Rashba SOI, is well-known in the literature [101, 129, 130] and recalculated here using Matsubara-Green's functions formalism, the analytical results and detailed analysis for CISP in a magnetized 2DEG with k-linear DSOI, including its correlation with experimental parameters such as quantum-well width, is the novelty in this area. Moreover, a detailed analysis of the influence of the cubic term on the results in both a nonmagnetized (with the analytical formulas) and a magnetized 2DEG is examined as an original contribution to the field [107].

In turn, TISP has been discussed for a 2DEG with the k-linear form of Rashba SOI [98, 131, 132], including scenario with an external magnetic field [128]. However, this work focuses on TISP in a 2DEG with both k-linear and k-cubic forms of Dresselhaus SOI, considering the influence of an out-of-plane exchange field.

3.2 Linear Hall effects

The story began in 1879 when Edwin Hall discovered a "new action of magnetism on electric current," manifesting as the appearance of a potential that is transverse to the electric current when it flows through a conductor in the presence of a steady magnetic field applied in an out-of-plane direction [133]. Nowadays, this phenomenon is known as the *ordinary Hall effect* and has become a valuable tool for material characterization, including resistivity or magnetoresistance measurements, determining conductivity type (*p* or *n*), and measuring carriers concentration in nonmagnetic conductors (metals with valence one, i.e., one electron in the valence shell of a free atom). Additionally, it has found practical applications as Hall sensors in electronics and motorization, among others [134, 135].

The empirical explorations that formed the basis of Edwin Hall's Ph.D. dissertation opened a new chapter in solid-state physics and established Edwin Hall as the father of a range of phenomena, including integer/fractional quantum, anomalous, spin, and even non-linear Hall effects. The common thread among all these phenomena is the transverse current response to an external electric field.

Paying attention to the Hall effect has been highly fruitful, not only from an application point of view but also in triggering the discovery of topological phases of matters. It is worth mentioning the concept of Berry curvature (see p. 43), which not only aids in a better understanding of the anomalous Hall effect (see sec. 3.2.1) but also enables the definition of intrinsic contributions to transport properties that are robust against spin-independent impurities in the system.

3.2.1 Anomalous Hall effect (AHE)

Edwin Hall has already noticed that the transverse charge response was "several times greater" in a plate of iron or nickel (magnetic metals) than in gold, silver, or platinum (non-magnetic conductors) [136]. This observation sparked interest in exploring the role of internal magnetic moments, i.e., spin, in transport properties.

The quest to unravel the origins of the *extraordinary* [137] or *spontaneous* [38] Hall effect aroused a vivid discussion within the scientific community during the latter half of the 20th century. Initially, Robert Karpulus and Joaquin M. Luttinger [137] proposed that the effect stemmed from the "spin-orbit interaction of polarized conduction electrons", a phenomenon now recognized as intrinsic spin-orbit interaction that alters the band structure. However, a young Dutch theorist Jan Smith [38] questioned this idea, arguing that "the only effect which [...] remains as a possible cause of R_s[2] is anisotropic scattering caused by spin-orbit interaction," indicating on the skew-scattering contribution. Luttinger later acknowledged that skew-scattering could

---

[2]additional resistance coming from the anomalous Hall effect

contribute to the effect but maintained that the intrinsic contribution was still significant [138]. Several years later, Swiss physicist Luc Berger [37] added two cents to the discussion by pointing out an additional origin – the side-jump mechanism, an extrinsic type of spin-orbit interaction. This mechanism involves a carrier's displacement during scattering events caused by phonons or impurities.

Nowadays, there is consensus that all three mechanisms mentioned above can induce a charge Hall response in magnetic material, even in the absence of an external magnetic field. However, the dominant contribution varies depending on different systems and operating regimes. In experiments, the primary mechanisms can often be identified using a scaling relation (scaling-law or power-law), which relates the transverse and longitudinal resistivity, expressed as $\rho_{xy} \propto \rho_{xx}^a$. When $a = 2$, the intrinsic and side-jump contributions prevail, while $a = 1$ signifies the dominance of the skew-scattering mechanism (see references in [37, 139] and [140]). *Exempli gratia*, the extrinsic mechanism, skew-scattering, dominates in highly-conductive ferromagnets, such as dilute alloys, whereas the intrinsic mechanism is the leading contribution in metallic ferromagnets with moderate conductivity, like pure iron [36, 37].

Intrinsic AHE

In their microscopic theory [137], Karpulus and Luttinger introduced the concept of carriers acquiring an additional contribution to their group velocity, known as the *anomalous velocity*, $v_{\mathbf{k}}^a$, that is perpendicular to an external electric field applied to the system. Specifically, in a 2DEG with spin-orbit interaction (SOI), the velocity of the carriers reads as $v_{\mathbf{k}} = v_{\mathbf{k}}^0 + v_{\mathbf{k}}^a$, where $v_{\mathbf{k}}^0 = \hbar \mathbf{k}/m$ represents the velocity of Bloch fermions trapped in a potential well, and $v_{\mathbf{k}}^a$ is the anomalous velocity, which carriers acquire due to the presence of SOI in the system [141]. Therefore, the name *anomalous Hall effect* (AHE) was adopted, even though the transverse response is also influenced by the scattering mechanisms mentioned above. However, the anomalous velocity is solely dependent on the band structure (summed over all occupied band states) and is thus considered an intrinsic contribution to AHE.

On the other hand, the introduction of topological concepts into solid-state physics, along with Sir Michael V. Berry's notion of *geometrical phase* [142], has allowed for a reinterpretation of the AHE by linking the anomalous velocity to the *Berry curvature*, highlighting the topological nature of the intrinsic AHE [143].

Using the wavepacket motion of electrons in the Bloch band, the contribution to the Hall effect from the Berry curvature in momentum space was first provided by Ming-Che Chang and Qian Niu [144] for a 2D periodic system with a strong magnetic field, as well as by Ganesh Sundaram and Qian Niu [145] for slowly perturbed crystals. With these works, a connection between the anomalous velocity and the Berry curvature was shown, therefore, utilizing the concept of Berry

curvature to examine the intrinsic anomalous Hall effect became justified.

The connection between anomalous velocity and Berry curvature is particularly evident when considering the Kubo formula for intrinsic anomalous Hall conductivity [36]:

$$
\begin{aligned}
\sigma_{ij}^{intAH} = e^2\hbar \sum_{n\neq m} \int \frac{d\mathbf{k}}{(2\pi)^d} \left[f\left(E_n(\mathbf{k})\right) - f\left(E_m(\mathbf{k})\right) \right] \\
\times \operatorname{Im} \frac{\langle \Psi_n(\mathbf{k}) \left| v_i(\mathbf{k}) \right| \Psi_m(\mathbf{k}) \rangle \langle \Psi_m(\mathbf{k}) \left| v_j(\mathbf{k}) \right| \Psi_n(\mathbf{k}) \rangle}{\left[E_n(\mathbf{k}) - E_m(\mathbf{k}) \right]^2}
\end{aligned}
\tag{3.1}
$$

with $|\Psi_{n,m}(\mathbf{k})\rangle$ and $E_{n,m}(\mathbf{k})$ being eignestates and eigenvalues of the Bloch Hamiltonian, $H(\mathbf{k})$, $f(E_{n,m}(\mathbf{k}))$ representing the distribution functions, and $\{n,m\}$ denoting different bands. The components of the velocity operator $\mathbf{v} = \frac{1}{\hbar}\nabla_{\mathbf{k}} H(\mathbf{k})$ are denoted as $v_{i,j}$. Noting that [36]:

$$
\langle \Psi_n(\mathbf{k}) \left| \nabla_{\mathbf{k}} \right| \Psi_m(\mathbf{k}) \rangle = \frac{1}{\hbar} \frac{\langle \Psi_n(\mathbf{k}) \left| \nabla_k H(\mathbf{k}) \right| \Psi_m(\mathbf{k}) \rangle}{E_m(\mathbf{k}) - E_n(\mathbf{k})},
\tag{3.2}
$$

the intrinsic AHC can be expressed as [36]:

$$
\sigma_{ij}^{intAH} = -\varepsilon_{ij\ell} \frac{e^2}{\hbar} \sum_n \int \frac{d\mathbf{k}}{(2\pi)^d} f\left(E_n(\boldsymbol{k})\right) \mathcal{B}_n^{\ell}(\mathbf{k}),
\tag{3.3}
$$

where $\varepsilon_{ij\ell}$ stands for antisymmetric tensor, and $\mathcal{B}_n^{\ell}(\mathbf{k}) = \mathrm{i}\nabla_{\mathbf{k}} \times \langle \Psi_n | \nabla_{\mathbf{k}} | \Psi_n \rangle$ denotes the ℓ-th component of the Berry curvature for the n-th band.

Equation (3.3) indicates that the intrinsic AHC describes the motion of wavepackets (carriers) in $\mathbf{k}$-space within the Fermi sea, which endows this intrinsic contribution to the AHC with an inherent topological character. Moreover, since the states in the Fermi sea do not interact with impurities (unlike the states at the Fermi surface), this contribution is robust against impurities.

Berry curvature

In the 1980s, Sir Michael V. Berry systematized and popularized the concept of the *geometric phase*, known as the *Berry phase*. The idea extends from the adiabatic theorem, which states that a particle moving in a slowly-varying environment and tracing out *closed loop*[3], acquires an additional phase factor, γ_n, which is given by the path integral over the closed loop C in parameter space [142, 148]:

$$
\gamma_n = \oint_C d\mathbf{R} \cdot \mathcal{A}_n(\mathbf{R}),
$$

where $\mathbf{R}$ denotes a set of parameters describing the system. The vector-valued function $\mathcal{A}_n(\mathbf{R}) = \mathrm{i}\langle \Psi_n | \nabla_{\mathbf{R}} | \Psi_n \rangle$ is known as the *Berry connection* or Berry vector potential, with Ψ_n standing for

---

[3]For an open path, the phase γ is gauge-dependent and accumulates along the path, ultimately canceling out [147].

the eigenvector of considered system. Analogous to electrodynamics, one defines a gauge-field tensor referred to as the *Berry curvature*, which reads as [148]:

$$\mathcal{B}_n(\mathbf{R}) = \nabla_{\mathbf{R}} \times \mathcal{A}_n(\mathbf{R}).$$

While considering a 2D system, e.g., xy-plane, in wavevector space, the Berry curvature has only the z-component ($\nabla_{\mathbf{k}} = \hat{x}\frac{\partial}{\partial k_x} + \hat{y}\frac{\partial}{\partial k_y}$), namely:

$$\mathcal{B}_n^z(\mathbf{k}) = \mathrm{i}\nabla_{\mathbf{k}} \times \langle \Psi_n | \nabla_{\mathbf{k}} | \Psi_n \rangle \tag{3.4}$$

with Ψ_n denoting the eigenvector for the n-th band.

Notably, the gauge-invariance of the Berry phase ensures that it is a physically observable quantity. Moreover, due to its geometric nature, the Berry phase can be expressed in terms of geometrical quantities in the parameter space. For example, when considering the transport properties of systems, the Berry phase is defined for quasi-particles moving in wavevector space. However, what makes Berry's concept a powerful tool in solid-state physics is its close analogy to gauge field theories and differential geometry. Thus, the idea of the geometric phase factor has proven to be a fertile concept, shedding new light on already-known phenomena in physics.

Firstly, Michael V. Berry showed that the geometric phase factor can be considered as a special case of the physical effect of the magnetic vector potential that exists even in the absence of fields, as predicted by Aharonov and Bohm in 1959 [142, 149]. Here, the Berry phase is the equivalent of the Aharonov-Bohm phase that a particle acquires when making a loop in magnetic flux, while the *Berry curvature* acts like a "magnetic field".

Secondly, with the Berry curvature, one can explain the quantization of transverse conductance, i.e., the quantum Hall effect (QHE). This requires an alliance between Berry's concept and topology[4]. Barry Simon initiated this connection [150], interpreting the integers in Hall conductance (i.e., n in $\sigma_H = n(e^2/h)$) introduced by Thouless et al. [151] using Berry's ideas. The key point is that the integral of the Berry curvature over a closed surface quantizes as integers called Chern numbers. The Brillouin zone, considered as a closed surface, allows the integration of the Berry curvature over the entire Brillouin zone, leading to the quantization of the Hall conductance. It's worth emphasizing that the effective models examined in this thesis, by assumption, do not cover the entire Brillouin zone; hence, the evaluated Hall conductance is not quantized.

---

[4]Initially, *topology* was a branch of mathematics, and its concepts have been successfully adapted to solid-state physics, as evidenced by the Nobel Prize in Physics awarded in 2016 to David J. Thouless, F. Duncan M. Haldane, and J. Michael Kosterlitz "for theoretical discoveries of topological phase transitions and topological phases of matter".

3.2.2 Key finding in the literature related to the scope of the thesis

Thomas Jungwirth et al. [143] studied the anomalous Hall effect in ferromagnetic III-V semi-conductors doping with Mn (e.g., InAs and GaAs) using the Luttinger theory and the Berry curvature concept [138, 145], finding good agreement between their approach and experimental results. Dimitrie Culcer et al. [152] later applied the same approach to a paramagnetic 2D system with Rashba SOI. In their work, Culcer and co-authors discussed systems with a zinc-blende structure, where the BIA occurs. However, they modeled such a system with Rashba Hamiltonian, which is appropriate for systems with SIA. Despite this, the results remain valid due to the similar form of the Berry curvature in both cases – differing only in sign. Consequently, in systems where both BIA and SIA are present, the opposite sign of the Berry curvature, and hence the intrinsic AHE, reflect the relative strengths of these SOIs as they vary [153]. In turn, a theoretical analysis of a 2DEG with SIA provided by Vitalii K. Dugaev et al. [154] demonstrated the dominant role of the intrinsic mechanism in the AHE within systems exhibiting strong SOC.

The intrinsic AHC, linked to the non-zero Berry curvature, has already been examined in a magnetized 2DEG with k-linear form of Rashba SOI [71, 154].

However, the anomalous Hall effect in a 2DEG with cubic forms of Rashba and Dresselhaus SOI has not been widely discussed in the literature. Nevertheless, Li and Yi-Ming [155] investigated the AHE in a magnetized 2DEG with the cubic form of Rashba SOC using the Kubo formula and Green's functions formalism, although their analysis focuses solely on the contribution from states at the Fermi surface, omitting the intrinsic contribution.

This dissertation aims to fill that gap by providing both analytical and numerical results for the AHC in a 2DEG with isotropic and anisotropic forms of Rashba SOI, with a specific emphasis on the intrinsic contribution. Additionally, the influence of the cubic form of Dresselhaus SOI on the transverse response in a 2DEG with k-linear and k-cubed forms of SOI is examined. The results of this investigation were published in [63, 107, 156].

3.2.3 Spin Hall effect (SHE)

The spin Hall effect (SHE) highlights the use of electron spin in transport, where a charge current is converted into a transverse spin current with spin polarization perpendicular to the charge and spin current directions [118]. The SHE originates from spin-orbit coupling within the material. Due to SOC, electrons with opposite spins bend in opposite directions, resulting in a spin current flowing perpendicular to the direction of the charge current, as illustrated in figure 3.2(a).

Importantly, SHE can be observed even in nonmagnetic systems, giving rise to what is known as a *pure spin current* – a flow of spin without an accompanying charge current. The concept
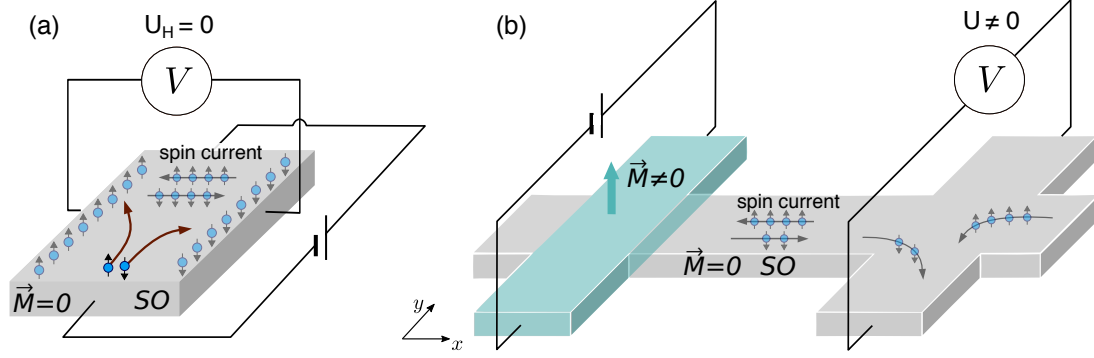
Figure 3.2: (a) Spin Hall effect in a paramagnetic system. (b) Measurement of spin current in the inverse spin Hall effect. Here, $\vec{M} = 0$ represents a non-magnetic system, and SO indicates a material with spin-orbit interaction. Figure (a) comes from [135], published with permission of the journal *Postępy Fizyki*

of electrically-induced spin current flow in a paramagnetic system was first theoretically proposed in 1971 by Mikhail Dyakonov and Vladimir Perel [117, 157], and later named and more precisely described in 1999 by Jorge E. Hirsch [158]. These early studies focused on extrinsic SHE, originating from spin-dependent scattering processes, i.e., side-jump and skew-scattering (extrinsic SOI).

Nevertheless, even without spin-dependent scattering centers, spin accumulation can occur due to intrinsic SOI related to the band structure (i.e., Rashba and Dresselhaus types of SOI, caused by inversion asymmetries in the host crystal), leading to what is known as intrinsic SHE [159, 160]. In this case, the mechanism leading to spin polarization of the current is based on spin precessional processes developed by D'yakonov and Perel [47, 117]. Due to the current-induced shift of the Fermi contour, the spin orientation of the carriers is no longer locked to their momenta, causing spins to precess around the new expected spin orientation, resulting in an additional spin component. For example, in the Rashba model (see fig. 3.1a), spins acquire a component parallel to the z-axis for $k_y > 0$ and antiparallel to the z-axis for $k_y < 0$, resulting in a spin current polarized along the z-axis, flowing in the y-direction [159].

Spin Hall effect measurements detect spin accumulation at the sample edges, which results from SOC-induced spin current flow. When these edges are linked by a conductor characterized by a low spin-flip scattering rate, the spin current generated by the spin accumulation flows in the opposite direction to the SOC-induced spin current, facilitating its measurement. The first experimental observations of the SHE in 2D semiconductor systems[5], made in 2004, used optical techniques to measure electrically induced spin polarization. Kato et al. [119] demonstrated SHE in GaAs thin film using the magnetooptical Kerr effect, attributing spin accumulation to spin-dependent scattering effects. Wunderlich et al. [120] fabricated two light-emitting diodes

---

[5]Although the SHE is not limited to semiconductors and was later observed in single-layered crystals such as graphene [161–163], this discussion focuses on systems where a 2D electron gas forms.

in (Al,Ga)As/GaAs heterostructure and detected spin polarization at the sample edges using circularly polarized light, identifying intrinsic SOC as the primary contribution to SHE.

Direct electrical measurement of the SHE in paramagnetic systems is challenging due to the lack of a transverse voltage associated with pure spin current. However, the first electrical measurements of the *inverse spin Hall effect* (ISHE) in semiconductor systems, which detected a charge current generated by a spin current, were conducted in 2006 [164, 165]. The principle behind measuring ISHE using a double Hall bar device is illustrated in figure 3.2b. First, a spin current, flowing in the x-direction, is generated by spin injection from a ferromagnet (the green part) into a nonmagnetic system (the gray part). Then, due to SOI in the system, electrons with opposite spins bend their trajectories in opposite directions, resulting in voltage generation in the y-direction on the right part of the device.

With the spin Hall effect, a new class of spintronic devices emerges, enabling spin manipulation even in non-magnetic systems without requiring an external magnetic field. *Exempli gratia*, a field-effect spin transistor based on spin current – rather than charge flow, as in traditional transistors – has been proposed [166].

3.2.4   Key finding in the literature related to the scope of the thesis

The intrinsic spin Hall effect in semiconductor systems with Rashba SOI was initially described by Jairo Sinova et al. [159], where Rashba SOI was assumed to be in k-linear form. Later, Schliemann and Loss [167] derived the intrinsic SHE in zero-temperature limit for semiconductors hole systems, where the k-cubed form of Rashba SOI was found.

Here, the finite-temperature results for the intrinsic SOC induced by the cubic form of Rashba SOC are provided, allowing for an analysis of the temperature dependence of SHE in semiconductor hole systems. Moreover, the explicit formula for the spin Hall angle is derived, and the influence of the temperature is studied. Finally, the influence of an out-of-plane magnetization on the SHE is examined. Some of these findings were partially published in [168].

3.3   Thermoelectric effects

3.3.1   Anomalous Nernst effect (ANE)

Among various transport phenomena, the thermoelectric effects are particularly significant, as they play a crucial role in room-temperature transport measurements. On one hand side, a system can be subjected to several forces simultaneously, such as electric or magnetic field and thermal gradient. Secondly, in general, a temperature gradient induces an electrical current, and vice versa [169]. Consequently, a thermal signal can appear as an additional contribution to transport

measurements, influencing the results.

In the linear response regime, one assumes that the temperature difference between the hottest and the coldest edge of the sample is small. This means that the system is exposed to a temperature gradient that is small and uniform across the sample, and the average temperature, T, tends to be constant on the scale of the carrier wavelengths. Under these conditions, the current $\mathbf{j}_i$ induced by a driving force $\mathbf{X}_j$ is given by [90]:

$$\mathbf{j}_i = \sum_j \mathbf{Z}^{ij} \cdot \mathbf{X}_j, \tag{3.5}$$

where $\mathbf{Z}^{ij}$ are measurable coefficients that satisfy the Onsager's relations when the driving forces are properly defined. Specifically, when the driving force is the electric field, then $\mathbf{X}_j^E = -\frac{1}{T}\nabla(\bar{\mu}) = \frac{1}{T}\nabla(\mu + eV)$ where μ stands for the chemical potential, e is the particle charge, and V refers to the electric field potential. In turn, for the temperature gradient acting as the driving force, $\mathbf{X}_j^{\nabla T} = \nabla\left(\frac{1}{T}\right)$.

Thus, the electric (particle) current, $\mathbf{j}_i^E$, and the heat current, $\mathbf{j}_i^h$, in the presence of both an electric field and a temperature gradient can be expressed as (see chapter 17.4.3 in [169], chapter 7.9 in [28] or chapter 3.9.2 in [90]):

$$\begin{aligned}
\mathbf{j}_i^E &= -\sigma_{ij}\frac{\nabla(\bar{\mu})}{T} + \alpha_{ij}\nabla_j\left(\frac{1}{T}\right), \\
\mathbf{j}_i^h &= -\bar{\alpha}_{ij}\frac{\nabla(\bar{\mu})}{T} + \kappa_{ij}\nabla_j\left(\frac{1}{T}\right),
\end{aligned} \tag{3.6}$$

where the first-order kinetic coefficients are: σ_{ij} – conductivity tensor, κ_{ij} – heat conductivity tensor, α_{ij} – thermoelectric tensor and $\bar{\alpha}_{ij}$ – Seebeck coefficient tensor.

The phenomenological reciprocal relations, derived by Lars Onsager[6], reflect the time-reversal invariance of the microscopic equation of motion at the macroscopic level, e.g., $\sigma_{ij} = \sigma_{ji}$, $\kappa_{ij} = \kappa_{ji}$. In turn, in the presence of a magnetic field, $\mathbf{B}$, Onsager's reciprocal relations establish the following relationships between the first-order kinetic coefficients, i.e., the conductivity, σ_{ij}, heat conductivity, κ_{ij}, thermoelectric, α_{ij}, and Seebeck coefficient, $\bar{\alpha}_{ij}$, tensors as follows[7] [28]:

---

[6]The initial extensive works on thermoelectric effects were conducted by William Thomson (Lord Kelvin) [170–173] in the late 19th century. On behalf of his work, in 1931, a recognized chemist Lars Onsager derived "reciprocal relations" [174, 175], linking coefficients describing irreversible processes (for more details see also chapter 4.3 in [173]). Lars Onsager was awarded the Nobel Prize in Chemistry in 1968 "for the discovery of the reciprocal relations bearing his name, which are fundamental for the thermodynamics of irreversible processes".

[7]Note, that if a magnetic field is applied to the system, the particle retraces its path only if both the magnetic field and the particle angular velocity, $\boldsymbol{\omega}$, are reversed. If follows from the expression on the Lorentz force that acts on the carrier moving in a magnetic field, $\mathbf{F} = q\mathbf{v} \times \mathbf{B}$.

$$\sigma_{ij}(\mathbf{B}, \boldsymbol{\omega}) = \sigma_{ji}(-\mathbf{B}, -\boldsymbol{\omega}), \tag{3.7a}$$

$$\kappa_{ij}(\mathbf{B}, \boldsymbol{\omega}) = \kappa_{ji}(-\mathbf{B}, -\boldsymbol{\omega}), \tag{3.7b}$$

$$\bar{\alpha}_{ij}(\mathbf{B}, \boldsymbol{\omega}) = T\alpha_{ij}(-\mathbf{B}, -\boldsymbol{\omega}). \tag{3.7c}$$

In 1853, Wiedemann and Franz observed that thermal conductivity, $\mathbf{K}$, divided by electrical conductivity, $\boldsymbol{\sigma}$, and temperature, T, yields a constant (known as the Lorentz number) for metals [176]. This relation is known as the Wiedemann-Franz law (see also chapter 7.8 in [177] or chapter 7.15 in [178]):

$$\mathbf{K} = \frac{\pi^2}{3} \left(\frac{k_B}{e} \right)^2 T\boldsymbol{\sigma},$$

and is preserved in quite general conditions, i.e., in the linear response regime for non-interacting electrons, assuming elastic scattering on impurities and phonons [179, 180], and even in strong magnetic fields [181].

Another significant relation is the Mott rule [180–182], that enables to express a measurable voltage in response to a temperature gradient, i.e., thermoelectric power, also called the *Seebeck coefficient*, $\mathbf{S}$, *via* the electrical conductivity tensor, $\boldsymbol{\sigma}$ [180–182],

$$\mathbf{S} = \frac{\pi^2}{3} \frac{k_B^2 T}{e} \left(\frac{\partial \ln \boldsymbol{\sigma}(\mu)}{\partial \mu} \right), \tag{3.8}$$

where μ is the chemical potential. The phrase 'Mott-like relations' in the literature, generally refers to such connection between the current responses to an electric field and the temperature gradient [183].

Combining the electric field and temperature gradient with an external magnetic field yields transverse *thermoelectro-magnetic effects* [28, 184], such as the Nernst effect. The Nernst effect can be understood as the thermal counterpart of the Hall effect, where the driving current is generated by a temperature gradient instead of an electric field.

3.3.2 Key finding in the literature related to the scope of the thesis

The application of the Mott relation, eq. (3.8), to the intrinsic contribution to the anomalous Hall and Nernst effects, originating from the Berry curvature, was theoretically predicted by Di Xiao *et al.* [185] and experimentally verified in Mn-doped GaAs ferromagnetic semiconductors [186], ferromagnetic metals [187], and half-metallic ferromagnet LSMO thin films [188].
Furthermore, the temperature-dependent sign change of the ANE, experimentally observed in ferromagnetic semiconductors and half-metallic ferromagnets [186, 188], can be understood in light of the Mott relation.

In this dissertation, the intrinsic (non-dissipative) contribution to both the anomalous Nernst effect and the anomalous Hall effect in a magnetized 2DEG with cubic forms of Rashba spin-orbit interaction is considered [63, 168]. The sign change of the ANE and the connection between ANE and AHE *via* the Mott relation are also analyzed.

3.4 Nonlinear effects

Nonlinear transport effects are characterized by a response current (or voltage) that scales non-linearly with the driving force (represented by current or voltage). It is important to note that the nonlinear phenomena considered in this thesis do not represent higher-order corrections in perturbation theory. They have a different origin than the corresponding linear responses for particular effects. As a result, the nonlinear effects can be observed even in the absence of their linear counterparts. *Exempli gratia*, the nonlinear Hall effect can manifest in systems with time-reversal symmetry, which should be broken to observe the linear Hall effect [189].

In this dissertation, two nonlinear transport phenomena are investigated: the nonlinear Hall effect, introduced in section 3.4.1, and the nonlinear magnetoelectric resistance, known as bilinear magnetoresistance, described in section 3.4.2.

3.4.1 Nonlinear Hall effect (NLHE)

The main idea behind so-called *nonlinear Hall effects* (NLHE) is that the transverse current (or voltage) scales non-linearly with the longitudinal current (or voltage) evoked by an external electric field. Generally, the charge current density, j_a, in response to the electric field, $\mathbf{E}$, can be expressed as a power series [190]:

$$j_a = \sigma_{ab}E_b + \chi_{abc}E_bE_c + \dots, \tag{3.9}$$

where $a, b, c \in \{x, y, z\}$ with $a \neq b$. Here, σ_{ab} denotes the off-diagonal component of the linear conductivity tensor, and χ_{abc} stands for the nonlinear (here quadratic) conductivity tensor. The presence of higher-order terms (3rd, 4rd, etc.) was theoretically suggested and investigated in [191–193]. Subsequently, both theoretical and experimental investigations have explored the 3rd ordered anomalous Hall effect induced by the Berry curvature quadruple in topological magnetic materials such as the kagome antiferromagnet (FeSn) [194, 195]. Nevertheless, this dissertation focuses primarily on nonlinear effects within the context of second-order responses.

The work that can be marked as a milestone in the field of non-linear responses was provided in 2015 by Intii Sodemann and Liang Fu [189]. They suggested that NLHE could be observed in systems with time-reversal symmetry[8], provided that inversion symmetry is broken. Intii Sodemann and Liang Fu proposed a simple model for topological crystalline insulators, namely *tilted*

---

[8]The presence of the Hall effect in time-reversal invariant systems is one of the advantages of phenomena

Dirac cones, where NLHE can be realized. In this model, the tilting of Dirac cones breaks the inversion symmetry, resulting in a non-zero first-order moment of the Berry curvature, i.e., *Berry curvature dipole* (BCD), which induces the nonlinear Hall response in the system (more technical details about BCD are provided at p. 53). Due to the intrinsic character of the Berry curvature dipole, i.e., relation to the band structure modification, the non-linear transverse response induced by the BCD is called the *intrinsic NLHE*. Moreover, in time-reversal broken systems, an intrinsic-type correction to the Berry curvature was identified, arising at the Fermi surface from the field-induced positional shift of Bloch electrons [197, 198].

It was demonstrated in bulk WTe_2 [198] that applying an external electric field lowers the spacial symmetry of the material, thereby inducing a nonlinear response that can be tuned by the electric field. Further theoretical work [199–201] and experimental research [202] have highlighted the extrinsic contributions to the nonlinear Hall effect, such as side-jump and skew-scattering events. For instance, using the example of 2D tilted massive Dirac cones and applying the Boltzmann formalism [199, 201], it has been demonstrated that in systems where both intrinsic and extrinsic contributions are significant, their competition leads to a sign change in the NLHE. Moreover, by examining the gyrotropic Hall effect in two simple models – namely, a 3D non-centrosymmetric Weyl semimetal and a strained 2D transition metal dichalcogenide monolayer – it was found [200] that intrinsic and extrinsic contributions become comparable at frequencies well below the band-splitting, typically within the terahertz (THz) range.

Consequently, due to the various mechanisms contributing to the NLHE, a key challenge in interpreting experimental results is distinguishing between these contributions. For this purpose, one can adopt the scaling law [201, 202], which has been successfully applied in the case of the linear Hall effects. Another approach, proposed by Zongzheng Du et al. [203], involves symmetry analysis. In this method, components of the nonlinear conductivity tensor are classified as either extrinsic or intrinsic based on the specified symmetry point group. Thus, for a defined conductivity tensor, one can classify or predict the NLHE contributions in the analyzed system.

Another significant aspect of the NLHE pertains to the theoretical methods employed to investigate the nonlinear response. According to the literature [189, 199–201, 204], one commonly favored method is the semiclassical Boltzmann approach. In this approach, the distribution function is expanded in terms of the external electric field, E, i.e., $f = f_0 + f_1 + f_2 + \ldots$, where $f_n \propto E^n$.

Alternatively, a quantum description developed by Zongzheng Du et al. [203], employs a diagrammatic technique for the nonlinear response regime. Unlike the Kubo formula and the

---

that extend beyond the linear response regime. Another way to achieve a transverse response in a system with time-reversal symmetry is by utilizing the spin or valley degree of freedom [118, 196].

corresponding bubble diagrams in the linear response regime, in the quadratic response, it is necessary to analyze triangular and two-photon diagrams that represent two inputs and one output. When considering both intrinsic and extrinsic contributions in the weak-disorder limit, this leads to the examination of dozens of charts.

The case study of the 2D Dirac model [203] reveals that the intrinsic contribution, arising from the Berry curvature dipole, is fully consistent in both the semiclassical Boltzmann approach and quantum description using diagrammatic technique. However, the extrinsic contributions, describing the disorder effects, differ in sign between the two approaches, resulting in distinct total NLHE. It is noteworthy that the total NLHE in the quantum diagrammatic approach shares the same sign and a similar behavior with the chemical potential as the intrinsic contribution, but it has a greater magnitude.

When focusing solely on the intrinsic contribution from the Berry curvature dipole, the analysis can be limited to this specific quantity (see p.). This approach is especially justified in systems where the intrinsic contribution to the NLHE is predominant, meaning that scattering events can be safely disregarded. Candidate materials for realizing intrinsic NLHE include low-symmetry crystals where inversion symmetry can be readily broken, such as the surface of 3D topological insulators, 2D transition metal dichalcogenides, or 3D Weyl semimetals [189]. Consequently, a few years after the theoretical proposal of the BCD's role in NLHE, this idea has been experimentally confirmed in non-magnetic systems, specifically, in a few-layer WTe_2 in the absence of an external magnetic field [202, 205].

The experimental setup for NLHE measurements closely resembles that used for linear Hall effect experiments. Typically, a low-frequency alternating current (i.e., ranging in 10–10 000 Hz) is applied, and the transverse voltage is measured at zero- or double-frequency using a lock-in technique. This technique involves multiplying the measured signal, f_s, in the frequency domain (convolution in the time domain) by a reference signal tuned to the same frequency, $f_r = f_s$ yielding harmonics at $f_s = 0$ and $f_s = 2f_r$.

Moreover, the ability to measure the transverse response at zero-frequency in response to alternating current, allows NLHE to find applications in terahertz technology, particularly for high-frequency rectification processes in broadband, long-wavelength photodetection devices [204, 206]. Additionally, NLHE holds the potential application for strain sensors by leveraging the strain-tunable (or strain-induced) Berry curvature dipole [207].

Furthermore, quadratic dependence of the charge current density on the external electric field, $j_a = \chi_{abb}E_b^2$ ($b = c$ in eq. (3.9)), results in a linear relationship between the measured[9] off-diagonal component of the quadratic conductance tensor, σ_{ab}^{NL}, and the electric field amplitude,

---

[9]Conductivity and resistivity are considered as the response functions, while conductance and resistance are the physically measured quantities.

i.e., $j_a/E_b = \sigma_{ab}^{NL} = \chi_{abb}E_b$, and $\sigma_{ab}^{NL}(E_b) = -\sigma_{ab}^{NL}(-E_b)$. In the measurements, the total conductance can have both the linear and the nonlinear parts, i.e., $\sigma_{ab} = \sigma_{ab}^{L}(E_b = 0) + \sigma_{ab}^{NL}(E_b)$. Thus, the presence of NLHE creates the possibility of obtaining a unidirectional response, where measuring resistance in opposite directions yields different results. Such a behavior can be leveraged in the construction of spintronic logic devices, where lower and higher resistances correspond to logic '0' and '1', respectively.

In addition to its device application, the sensitivity of the Berry curvature dipole to breaking of the crystal symmetries offers the potential to use nonlinear response for material characterization. This can be particularly useful for probing topological transitions, such as the transition between trivial and topological insulators by applying pressure in BiTeI [208] or electrically-induced topological transition in twisted doubled bilayer graphene [209].

The concept of nonlinear Hall effects can be extended to other phenomena where the nonlinear response to the driving force takes different forms. *Exempli gratia*, investigating spin current rather than charge current reveals the nonlinear spin Hall effect [210, 211]. On the other hand, applying a temperature gradient instead of an electric field leads to nonlinear thermoelectric (nonlinear Nernst effect – the response is the charge current) or thermal (when a heat current becomes the response) transport effects [212–215].

Berry curvature dipole (BCD)

The a-th component of the charge current density can be expressed as an integral of the carriers' velocity, v_a, multiplied by their distribution function, $f(k)$, over the wavevector space, i.e. [189]:

$$j_a = -e \int \frac{\mathrm{d}^d k}{(2\pi)^d} v_a f(k) \tag{3.10}$$

in d-dimensional system. The electron's velocity, in turn, is a sum of the group velocity of the electron wave and the anomalous velocity arising from the Berry curvature, $\mathcal{B}$ [189]:

$$v_a = \frac{1}{\hbar}\frac{\partial \epsilon(k)}{\partial k_a} + \varepsilon_{abc}\mathcal{B}_b\frac{\mathrm{d}k_c}{\mathrm{d}t}, \tag{3.11}$$

where ε_{abc} is the Levi-Civita symbol, and the canonical momentum of the electron changes in time in response to the external electric field as $\frac{\mathrm{d}k_c}{dt} = -\frac{eE_c(t)}{\hbar}$. One assumes that the electric field oscillates harmonically in time with frequency ω, i.e., $E_c(t) = \mathrm{Re}\{\mathcal{E}_c e^{\imath\omega t}\}$ where $\mathcal{E}_c \in \mathbb{C}$. Since the response up to the second order in the electric field is in one's interest, the distribution function is expanded up to the second order, i.e., $f(k) = \mathrm{Re}\{f_0 + f_1 + f_2\}$. Thus, the rectified and second harmonic components of the a-th component of the charge current density $j_a = $

$\mathrm{Re}\{j_a^0 + j_z^{2\iota\omega t}\}$, eq. (3.10), can be expressed as [189]:

$$j_a^0 = \frac{e^2}{2}\int_k \varepsilon_{abc}\mathcal{B}_b\mathcal{E}_c^* f_1^\omega - \frac{e}{\hbar}\int_k f_2^0 \frac{\partial\epsilon(k)}{\partial k_a},\tag{3.12a}$$

$$j_a^{2\omega} = \frac{e^2}{2}\int_k \varepsilon_{abc}\mathcal{B}_b\mathcal{E}_c f_1^\omega - \frac{e}{\hbar}\int_k f_2^{2\omega} \frac{\partial\epsilon(k)}{\partial k_a},\tag{3.12b}$$

where for the sake of brevity $\int_k \equiv \int \frac{\mathrm{d}^d k}{(2\pi)^d}$, and functions $f_{1,2}^{0,\omega,2\omega}$ are components of the distribution function $f(k)$ expressed in recursive structure, e.g., $f_1^\omega = \frac{e\tau\mathcal{E}_a}{1+i\omega\tau}\frac{\partial f_0}{\partial k_a}$ with τ denoting relaxation time (all expressions detailed in [189]). The second terms in eqs. (3.12) are odd under time reversal and thus vanish, leaving only the first terms in eqs. (3.12), related to the Berry curvature.

In general, the zero- and second-harmonic response in the a-direction can be written as $j_a^0 = \chi_{abc}\mathcal{E}_b\mathcal{E}_c^*$ and $j_a^{2\omega} = \chi_{abc}\mathcal{E}_b\mathcal{E}_c$. According to this analysis, the nonlinear conductivity tensor for the Hall response reads [189, 216]:

$$\chi_{abc} = -\varepsilon_{adc}\frac{e^3\tau}{2(1+\mathrm{i}\omega\tau)}\int_k f_0\frac{\partial\mathcal{B}_d}{\partial k_b},\tag{3.13}$$

where $\int_k f_0\frac{\partial\mathcal{B}_d}{\partial k_b}$ represents the *Berry curvature dipole*[10] (BCD). It is straightforward to verifythat the BCD produces a current orthogonal to the applied electric field, e.g., assuming both applied fields are in the x-direction ($b = c = x$), the response occurs only in the y-direction ($a = y \neq 0$).

In a 2D system (within the xy-plane), the Berry curvature dipole for the n-th band is given by [189]:

$$\mathcal{D}_i^n = \iint \frac{\mathrm{d}k_x\mathrm{d}k_y}{(2\pi)^2} f_0 \frac{\partial}{\partial k_i}\mathcal{B}_z^n(\mathbf{k}),\tag{3.14}$$

where $i = \{x, y\}$, f_0 stands for the equilibrium distribution function in the absence of external fields, and $\mathcal{B}_z^n(\mathbf{k})$ is the Berry curvature for the n-th band.

Key finding in the literature related to the scope of the thesis

Insightful theoretical works, supported by successfully performed experimental measurements of the nonlinear Hall effect in 2D systems, create a valuable opportunity to explore a 2DEG with strong spin-orbit coupling of the Rashba type for the nonlinear effects.

Edouard Lesne et al. [217] modeled a 2DEG at the interface of a (111)-oriented oxide heterostructure (LAO/STO) in the high-temperature trigonal phase with k-linear Rashba SOI and a third-order momentum term allowed by crystalline anisotropy [218, 219]. Using this model,

---

[10]Origin of the name, Berry curvature *dipole*, can be considered as an analogy to the electric dipole defined as the first-order term in the multipole expansion, i.e., the first-order term of a function described the field at some distance from a point-source.

they have reported, providing the experimental realization, a nonlinear Hall response induced by a non-zero Berry curvature dipole.

In turn, Renato M. A. Dantas et al. [220] theoretically analyzed nonlinear transport in both 1D and 2D systems with linear and cubic forms of Rashba SOI under an external magnetic field. They proposed analytical expressions that allow the establishment of Rashba SOC parameters from nonlinear measurements. However, the effective Hamiltonian they investigated includes both isotropic and anisotropic forms of the cubic Rashba SOI. Due to the differences in spin spaces [221], the isotropic cubic Rashba term should not be combined with the linear Rashba term in an unchanged form within a single Hamiltonian.

In this dissertation, the focus is not on exploring nonlinear effects in time-reversal invariant systems but rather on tuning the nonlinear Hall effect using an external in-plane magnetic field within a simple model of a 2DEG with a cubic form of Rashba SOI. Specifically, the Berry curvature-induced nonlinear Hall effect is examined in a 2DEG with the isotropic k-cubed Rashba SOI.

3.4.2 Bilinear magnetoresistance (BMR)

Magnetoresistance (MR), which refers to the change in resistance under different magnetic field directions, has been a well-known phenomenon in condensed matter physics for decades [177, 222, 223]. In metals, MR typically scales quadratically with the magnetic field, B, in the low magnetic field regime. Recent research has revealed that in single crystalline metals, the resistance can scale linearly or quadratically with B, depending on the magnetic field direction [224]. Linear dependence on B has also been observed in density-wave materials (e.g., GdSi, SrAl$_4$) at low temperatures and in low magnetic field limits [225].

Nevertheless, an intriguing phenomenon emerges beyond the linear response regime, where magnetoresistance depends not only on the magnetic but also on the electric field. Experimental findings have demonstrated that in topological insulators (TI) [226–228] as well as in a two-dimensional electron gas [68, 229], an additional magnetoresistance term can be measured, where resistance scales linearly with both the external magnetic and electric fields. This component is named bilinear magnetoresistance (BMR). Due to the unidirectional response characterizing BMR, its potential applications include the spin-logic devices mentioned in section 3.4.1.

The physical mechanism standing behind the BMR can be different. In TIs at higher Fermi energies, BMR is related to the hexagonal warping effect, leading to the nonlinear spin-to-charge current conversion [226, 230]. At the lower Fermi energies in TIs, as well as in a 2DEG with Rashba spin-orbit interaction, a different mechanism is at play [68, 227, 231, 232]. In these

cases, due to spin-momentum locking[11], shifting the Fermi contours under an external electric field causes a non-equilibrium spin polarization in the system. This induced non-equilibrium spin polarization scales linearly with the current along the applied electric field direction. Then, in the presence of an external magnetic field, one can measure the resistance component that is proportional to both the electric and magnetic fields.

3.4.3   Key finding in the literature related to the scope of the thesis

The experimental-theoretical work provided by Diogo C. Vaz et al. [68] considers a 2DEG with k-linear form of Rashba SOI. The mechanism leading to BMR, as introduced in [227], is accomplished due to the non-equilibrium spin polarization in the system.

Further experimental measurements of magnetoresistance in a 2DEG formed at the LAO/STO interface were conducted by Zhang et al. [232]. They have found a BMR signal that scales sinusoidally with the in-plane magnetic field angle, attributing this phenomenon to spin-momentum locking.

In this thesis, the BMR in a 2DEG with an isotropic cubic form of Rashba spin-orbit interaction in the presence of an in-plane magnetic field is examined. The underlying mechanism leading to BMR is assumed to be the same as in [68], where a 2DEG with a linear form of Rashba SOI was under consideration, i.e., BMR is accomplished due to the non-equilibrium spin polarization in the system.

---

[11]In a 2DEG the spin-momentum locking is related to the presence of Rashba SOI in the system. In the case of TI, spin-momentum locking inhomogeneities arise from scattering by spin-orbit structural defects generates [227].

4

Articles constituting the dissertation

In the following chapter, the articles constituting the thesis are attended in chronological order, each accompanied by brief comme. All articles are reprinted with the permission of the respective journals, see App. A.

4.1 Reprint of the article A-1

In the attended manuscript, entitled "Temperature dependence of spin Hall effect in k-cubed Rashba model" the spin Hall effect in a nonmagnetic 2DEG with an isotropic form of k-cubed Rashba SOI is investigated.

The Matsubara-Green's functions formalism and diagrammatic technique in the linear response regime are employed to calculate the spin Hall conductivity at finite temperatures. Additionally, an analytical result for zero-temperature, consistent with the findings in [167], is provided.

Temperature Dependence of Spin Hall Effect in k–Cubed Rashba Model

A. Krzyżewska[a], A. Dyrdał[a,*] and J. Berakdar[b]

[a]Faculty of Physics, Adam Mickiewicz University in Poznań, ul. Umultowska 85, 61-614 Poznań
[b]Institut für Physik, Martin-Luther-Universität Halle–Wittenberg, 06099 Halle (Saale), Germany

Within the Matsubara Green function formalism and linear response theory we considered theoretically the temperature dependences of the spin Hall effect for a two-dimensional gas with an isotropic k–cubed form of the Rashba interaction. We utilize a standard model for treating spin-orbit phenomena in p-doped semiconductor heterostructures and also for an electron gas formed at perovskite oxides interfaces.

1. Introduction

The spin Hall effect [1] is one of the hallmarks in the field of spintronics offering the opportunity to generate and control spin currents in a pure electrical way [2–7]. The detectors based on the inverse spin Hall effect have become a standard tool for sensing spin currents and were instrumental in the discovery of the spin Seebeck phenomenon [8–10]. Recenly, it was also shown that the spin currents generated via spin Hall effect can be large enough to produce sizable spin torque effects (see e.g. [11–14]).

The underlying physics of the spin Hall effect is very rich depending on the nature of the intrinsic spin-orbit coupling of the host material. Impurities and structural defects are further sources of spin-orbit couplings that is of prime imporatnce for spin-dependent scattering phenomena (for review see: [15–17] and references therein). A proper theoretical description of the fundamental physics responsible for the SHE in materials that are potentially important for spintronics is crucial when it comes to the control of spin currents driven by spin Hall effect. Another important issue is the thermal behavior of the spin Hall effect. The role of finite temperatures in the theoretical description of spin-orbital phenomena has been studied in few papers in the context of 2D k–linear Rashba gas (for example [18–23]). However there is still lack of a consistent theory of SHE which takes into account all microscopic mechanisms and describes the spin Hall effects at high temperatures.

The spin Hall effect at zero-temperature is fairly well understood in n-doped semiconductor heterostructures where the simple model describing 2D electron gas with k–linear Rashba and Dresselhaus spin-orbit interaction seems to be valid approximation allowing an analytical description of spin-orbital phenomena. For n-doped semiconductors the Luttinger Hamiltonian is a suitable

framework. Recently, a large Rashba spin-orbit coupling has been experimentally observed at the interface of $LaAlO_3/SrTiO_3$ (LAO/STO) [25]. The interfaces of oxide perovskites such as LAO/STO, where the 2D electron gas has been recently discovered are attracting a great attention both experimentally and theoretically. The transition metal oxides heterostructures show interesting physical properties such as two-dimensional metallic conductivity [26] metal-insulator transition [27, 28], low-temperature superconductivity and ferromagnetism as well as its coexistence [29, 30], or large negative magnetoresistance [31]. The physics for the formation of the electron gas is still not settled for all compounds. One of proposed theoretical models of Rashba 2D gas in STO based heterostructures utilizes the effective k-cubed Rashba Hamiltonian [32, 33] which is well known from the case of heavy-hole model for semiconductor heterostructures [34].

In this paper we discuss the temperature dependences of the spin Hall effect for the k–cubed Rashba Hamiltonian. Our results may be suitable for both p-doped semiconductor heterostructures and oxide perovskites thin films or interfaces.

2. Model and methods

The effective Hamiltonian describing electrons or holes in isotropic k–cubed Rashba gas can be written in the matrix form [35]:

$$\mathcal{H} = \begin{pmatrix} \frac{\hbar^2 k^2}{2m} & i\lambda k_-^3 \\ -i\lambda k_+^3 & \frac{\hbar^2 k^2}{2m} \end{pmatrix}, \tag{1}$$

where $k^2 = k_x^2 + k_y^2$, $k_\pm = k_x \pm i k_y$, and m is the effective mass of the particle defined by Luttinger parameters. λ is the Rashba spin-orbital coupling parameters which depends on Luttinger parameters, width and the potential strength of the quantum well - see Ref. [35].

The casual Green function corresponding to the Hamiltonian (1) can be written in the form:

$$G_{\boldsymbol{k}}(\varepsilon) = G_{\boldsymbol{k}0}\sigma_0 + G_{\boldsymbol{k}x}\sigma_x + G_{\boldsymbol{k}y}\sigma_y \tag{2}$$

with coefficients:

———

*corresponding author; e-mail: adyrdal@amu.edu.pl

(558)

$$G_{\boldsymbol{k}0} = \tfrac{1}{2}(G_{k+} + G_{k-}) \qquad (3)$$

$$G_{\boldsymbol{k}x} = \sin(3\phi)(G_{k+} - G_{k-}) \qquad (4)$$

$$G_{\boldsymbol{k}y} = -\cos(3\phi)(G_{k+} - G_{k-}) \qquad (5)$$

where $G_{k\pm} = [\varepsilon + \mu - E_\pm + \mathrm{i}\delta\,\mathrm{sgn}(\varepsilon)]^{-1}$ and $E_\pm = \frac{\hbar^2 k^2}{2m} \pm \lambda k^3$ denote the energy eigenvalues; σ_0 and σ_α ($\alpha = x, y, z$) are unit and Pauli matrices in spin space.

To obtain the spin Hall conductivity and discuss its temeprature dependence we have used the Matsubara-Green function formalism [36]. In the regime of linear response to the external electromagnetic field the spin Hall current derives from the expression

$$\sigma_{xy}^{s_z}(\mathrm{i}\omega_m) = \qquad (6)$$

$$\frac{1}{\beta}\sum_{\boldsymbol{k},n}\mathrm{Tr}\left\{\hat{j}_x^{s_z}G_{\boldsymbol{k}}(\mathrm{i}\varepsilon_n + \mathrm{i}\omega_m)\hat{H}_{\boldsymbol{A}}^E(\mathrm{i}\omega_m)G_{\boldsymbol{k}}(\mathrm{i}\varepsilon_n)\right\},$$

where $\beta = 1/k_\mathrm{B}T$ and $\hat{H}_{\boldsymbol{A}}^E(\mathrm{i}\omega_m) = -\hat{j}_y A_y(\mathrm{i}\omega_m)$ is the perturbation Hamiltonian defined by the y-component of the current density operator $\hat{j}_y = e\hat{v}_y$ and the y-component of electromagnetic vector potential $A_y(\mathrm{i}\omega_m)$. Operator of the spin current density is defined as an anticommutator of the velocity operator and the z-th component of spin operator ($s_z = 3\hbar\sigma_z/2$), that is $\hat{j}_x^{s_z} = [\hat{v}_x, \hat{s}_z]_+/2$ (note that the velocity operators are defined as $\hat{v}_{x,y} = \partial\hat{H}/\partial k_{x,y}$) and $G_{\boldsymbol{k}}(\mathrm{i}\epsilon_n)$ denotes Matsubara Green function. The equation above leads finally to the frequency-dependent spin Hall conductivity in the form [21]:

$$\sigma_{xy}^{s_z}(\omega) = -\frac{e\hbar}{\omega}\mathrm{Tr}\int\frac{\mathrm{d}^2\boldsymbol{k}}{(2\pi)^2}\int\frac{\mathrm{d}\varepsilon}{2\pi}f(\varepsilon)$$

$$\times\left[\hat{j}_x^{s_z}G_{\boldsymbol{k}}^R(\varepsilon + \omega)\hat{v}_y[G_{\boldsymbol{k}}^R(\varepsilon) - G_{\boldsymbol{k}}^A(\varepsilon)]\right.$$

$$\left. + \hat{j}_x^{s_z}[G_{\boldsymbol{k}}^R(\varepsilon) - G_{\boldsymbol{k}}^A(\varepsilon)]\hat{v}_y G_{\boldsymbol{k}}^A(\varepsilon - \omega)\right]. \qquad (7)$$

Upon tracing and integrating over ε we obtain an expression for the dc-limit

$$\sigma_{xy}^{s_z} = e\frac{9}{16\pi}\frac{\hbar^2}{m}\left[\int\mathrm{d}k\,k\frac{f'(E_+) + f'(E_-)}{1 + (\lambda k^3/\Gamma)^2}\right.$$

$$\left. - \int\frac{\mathrm{d}k}{\lambda k^2}[f(E_+) - f(E_-)]\right] \qquad (8)$$

This is our general result for spin Hall conductivity. Here we should comment that the above expression is obtained in a single-loop approximation which corresponds to the quasi-ballistic limit. Assuming randomly distributed point-like impurities we may find that (i) the relaxation rate Γ is the same for both subbands [35], and (ii) the impurities vertex correction in the ladder approximation vanishes [35, 37].

3. Results and discussion

In the low temperature limit we may find simple analytical expressions in the form

$$\sigma_{xy}^{s_z} = -\frac{9}{16\pi}e\frac{\hbar^2}{m\lambda}\frac{k_{\mathrm{F}+} - k_{\mathrm{F}-}}{k_{\mathrm{F}+}k_{\mathrm{F}-}}$$

$$-\frac{9}{16\pi}e\frac{\hbar^2}{m}\left(\frac{\nu_+}{1 + (\lambda k_{\mathrm{F}+}^3/\Gamma)^2} + \frac{\nu_-}{1 + (\lambda k_{\mathrm{F}-}^3/\Gamma)^2}\right) \qquad (9)$$

where $k_{\mathrm{F}\pm}$ and $\nu_\pm$ are the Fermi vawevectors and density of states related to the $E_\pm$ subband respectively. Assuming $\Gamma \ll \lambda k_{\mathrm{F}\pm}^3$ we obtain

$$\sigma_{xy}^{s_z} = -\frac{9}{16\pi}e\frac{\hbar^2}{m\lambda}\frac{k_{\mathrm{F}+} - k_{\mathrm{F}-}}{k_{\mathrm{F}+}k_{\mathrm{F}-}}. \qquad (10)$$

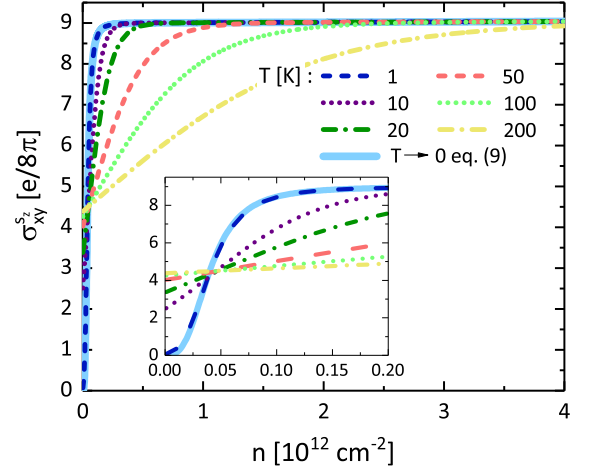This result is consistent with result in Ref. [38].

Fig. 1. Spin Hall conductivity as a function of carrier density. Different curves correspond to indicated values of temperature. The solid blue line corresponds to the analytical expression (Eq. (10)) obtained in the zero-temperature limit. In numerical calculations it was assumed that $\lambda = 3.96 \cdot 10^{-29}$ eV m^3, $\Gamma = 5 \cdot 10^{-6}$ eV.
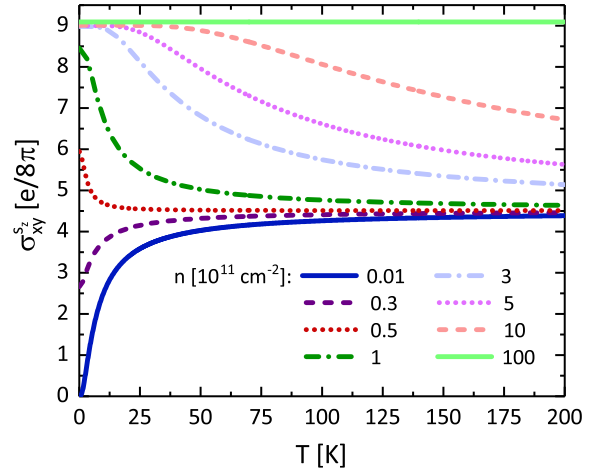

Fig. 2. Spin Hall conductivity as a function of temperature for fixed values of carrier density. Other parameters are as in Fig. 1.

Figures 1 and 2 present some numerical results for spin Hall conductivity obtained based on Eq.(8) and expressed in terms of carrier density n. In case of the model under consideration the relations between $k_{\mathrm{F}\pm}$, n and chemical potential are simple and can be found e.g. in [38].

In Fig. 1 we show the spin Hall conductivity plotted as a function of carrier density for fixed values of temperature. The analytical result (for $T \to 0$) is also indicated. Fig. 2 presents the spin Hall conductivity as a function of the temperature for different charge concentrations.

To conclude, we considered theoretically the temperature dependence of Spin Hall effect in 2D electron gas with isotropic $\boldsymbol{k}$–cubed Rashba interaction that formed at the perovskite oxides interfaces. The model under consideration is a basic model suitable not only for some group of perovskite oxides but also for p-doped semiconductor heterostructures.

Acknowledgments

References

[1] J.E. Hirsch, *Phys. Rev. Lett.* **83**, 1834 (1999).

[2] Y.K. Kato, R.C. Myers, A.C. Gossard, D.D. Awschalom, *Science* **306**, 1910 (2004).

[3] S.O. Valenzuela, M. Tinkham, *Nature* **442**, 176 (2006).

[4] L. Vila, T. Kimura, Y. Otani, *Phys. Rev. Lett.* **99**, 226604 (2007).

[5] K. Ando, J. Ieda, K. Sasage, S. Takahashi, S. Maekawa, E. Saitoh, *Appl. Phys. Lett.* **94**, 262505 (2009).

[6] C.Brune, A. Roth, E.G. Novik, M. KÃśnig, H. Buhmann, E.M. Hankiewicz, W. Hanke, J. Sinova, L.W. Molenkamp, *Nature Physics* **6**, 448 (2010).

[7] J. Wunderlich, B.-G. Park, A. C. Irvine, L. P. Zarbo, E. Rozkotova, P. Nemec, V. Novak, J. Sinova, T. Jungwirth, *Science* **330**, 1801 (2010).

[8] K. Uchida, S. Takahashi, K. Harii, J. Ieda, W. Koshibae, K. Ando, S. Maekawa, E. Saitoh *Nature* **455**, 778(2008).

[9] K. Uchida, J. Xiao, H. Adachi, J. Ohe, S. Takahashi, J. Ieda, T. Ota, Y. Kajiwara, H. Umezawa, H. Kawai, G.E.W. Bauer, S. Maekawa, E. Saitoh, *Nature Materials* **9**, 894 (2010).

[10] C.M. Jaworski, J. Yang, S. Mack, D.D. Awschalom, J.P. Heremans, S. Mahrlein, *Nature Materials* **9**, 898 (2010).

[11] L. Liu, T. Moriyama, D.C. Ralph, R.A. Buhrman, *Phys. Rev. Lett.* **106**, 036601 (2011).

[12] I.M. Miron, K. Garello, G. Gaudin, P.-J. Zermatten, M.V. Costache, S. Auffret, S. Bandiera, B. Rodmacq, A. Schuhland P. Gambardella, *Nature* **476**, 189 (2011).

[13] L. Liu, Ch.-F. Pai, Y. Li, H. W. Tseng, D. C. Ralph, R. A. Buhrman, *Science* **336**, 555 (2012).

[14] M. Cecot, L. Karwacki, W. Skowronski, J. Kanak, J. Wrona, A. Zywczak, L. Yao, S. Dijken, J. Barnas, T. Stobiecki, *Scientific Reports* **7**, 968 (2017).

[15] J. Sinova, S.O. Valenzuela, J. Wunderlich, C.-H. Back, T. Jungwirth, *Rev. Mod. Phys.* **87**, 1213 (2015).

[16] G. Vignale, *J. Supercond. Nov. Magn.* **23**, 3 (2010).

[17] H.-A. Engel, E.I. Rashba, B.I. Halperin, in: *Handbook of Magnetism, Advanced Magnetic Materials*, Eds. H. Kronmüller, S. Parkin, John Wiley, Sons Ltd, Chichester, UK 2007, p. 2858.

[18] K. Bencheikh, G. Vignale, *Phys. Rev. B* **77**, 155315 (2008).

[19] J. Borge, C. Gorini, R. Raimondi, *Phys. Rev. B* **87**, 085309 (2013).

[20] C. Gorini, U. Eckern, R. Raimondi, *Phys. Rev. Lett.* **115**, 076602 (2015).

[21] A. Dyrdal, J. Barnas, V.K. Dugaev, *Phys. Rev. B* **94**, 035306 (2016).

[22] A. Dyrdal, V. K. Dugaev, J. Barnas, *Phys. Rev. B* **94**, 205302 (2016).

[23] A. Dyrdal, J. Barnas, V. K. Dugaev, *Phys. Rev B* **95**, 245302 (2017).

[24] A. Soumyanarayanan, N. Reyren, A. Fert, Ch. Panagopoulos, *Nature* **539**, 509 (2016).

[25] E. Lesne, Yu Fu, S. Oyarzun, J.C. Rojas-Sanchez, D.C. Vaz, H. Naganuma, G. Sicoli, J.-P. Attane, M. Jamet, E. Jacquet, J.-M. George, A. Barthelemy, H. Jaffres, A. Fert, M. Bibes, L. Vila, *Nature Materials* **15**, 1261 (2016).

[26] A. Ohtomo, H.Y. Hwang, *Nature (London)* **427**, 423 (2004).

[27] S. Thiel, G. Hammerl, A. Schmehl, C. W. Schneider, J. Mannhart, *Science* **313**, 1196 (2006).

[28] C. Cen, S. Thiel, G. Hammerl, C.W. Schneider, K.E. Andersen, C.S. Hellberg, J. Mannhart, J. Levy, *Nature Materials* **7**, 298, (2008).

[29] L. Li, C. Richter, J. Mannhart, R.C. Ashoori, *Nature Physics* **7**, 762, (2011).

[30] A.J. Bert, B. Kalisky, Ch. Bell, M. Kim, Y. Hikita, H.Y. Hwang, K.A. Moler, *Nature Physics* **7**, 767 (2011).

[31] A. Brinkma, M. Huijben, M. van Zalk, J. Huijben, U. Zeitler, J.C. Maan, W.G. van der Wiel, G. Rijnders, D.H.A. Blank, H. Hilgenkamp, *Nature Matterials* **6**, 493 (2007).

[32] H. Nakamura, T. Koga, T. Kimura, *Phys. Rev. Lett.* **108**, 206601 (2012).

[33] L.W. Feeringen, A. MacCollam, G.A. de Wijs, A. Fasolino, *Phys. Rev. B* **95**, 155134 (2017).

[34] R. Winkler, *Spin-Orbit Coupling Effects in Two-Dimensional Electron, Hole Systems*, Springer-Verlag, Berlin Heidelberg 2003.

[35] C.-X. Liu, B. Zhou, S.-Q. Shen, B.-F. Zhu, *Phys. Rev. B* **77**, 125345 (2008).

[36] G.D. Mahan, *Many Particle Physics.* Kluwer Academic/Plenum Publishers, New York 2000.

[37] S. Murakami, *Phys. Rev. B* **69**, 241202(R) (2004).

[38] J. Schliemann, D. Loss, *Phys. Rev. B* **71**, 085308 (2005).

Discussion

Article A-1 is supplemented with calculations involving the spin Hall angle and spin Hall effect in a magnetized 2DEG, presented below.

Spin Hall angle

Kubo formula for the longitudinal charge conductivity induced by an electric field applied in the y-direction in Matsubara-Green's functions formalism is as follows:

$$\sigma_{yy}^{E_y}(\omega) = -\frac{e^2\hbar}{\omega} \int \frac{\mathrm{d}k\,k}{(2\pi)^2} \int \frac{d\varepsilon}{2\pi} f(\varepsilon) \int \mathrm{d}\phi \left[\mathrm{Tr}\left\{ \hat{v}_y\, G_{\mathbf{k}}^R(\varepsilon+\omega)\, \hat{v}_y \left[G_{\mathbf{k}}^R(\varepsilon) - G_{\mathbf{k}}^A(\varepsilon) \right] \right\} \right.$$
$$\left. + \mathrm{Tr}\left\{ \hat{v}_y \left[G_{\mathbf{k}}^R(\varepsilon) - G_{\mathbf{k}}^A(\varepsilon) \right] \hat{v}_y\, G_{\mathbf{k}}^A(\varepsilon-\omega) \right\} \right]. \tag{4.1}$$

In *dc* limit ($\omega \to 0$) one gets:

$$\sigma_{yy} = -\frac{e^2\hbar}{8\pi\Gamma} \left[\frac{6\alpha}{m} \int \mathrm{d}k\,k^4 \left(f'(E_+) - f'(E_-) \right) \right.$$
$$+ \frac{9\alpha^2}{\hbar^2} \int \mathrm{d}k\,k^5 \left(1 + \frac{1}{1+(\alpha k^3/\Gamma)^2} \right) \left(f'(E_+) + f'(E_-) \right) \tag{4.2}$$
$$\left. + \frac{\hbar^2}{m^2} \int \mathrm{d}k\,k^3 \left(f'(E_+) + f'(E_-) \right) \right],$$

which in the low-temperature limit, $T \to 0$, leads to:

$$\sigma_{yy} = \frac{e^2\hbar}{8\pi\Gamma} \left[\frac{6\alpha}{m} \left(k_+^3 \nu_+ - k_-^3 \nu_- \right) \right.$$
$$+ \frac{9\alpha^2}{\hbar^2} \left[k_+^4 \nu_+ \left(1 + \frac{1}{1+(\alpha k_+^3/\Gamma)^2} \right) + k_-^4 \nu_- \left(1 + \frac{1}{1+(\alpha k_-^3/\Gamma)^2} \right) \right] \tag{4.3}$$
$$\left. + \frac{\hbar^2}{m^2} \left(k_+^2 \nu_+ + k_-^2 \nu_- \right) \right].$$

In the low carriers concentration limit, $n \to 0$, where the Rashba SOI plays a less significant role, the third term in equation (4.3) is the dominant contribution. Therefore, the longitudinal charge conductivity is given by:

$$\sigma_{yy}^{n\to 0} = \frac{\hbar^2}{m^2} \left(k_+^2 \nu_+ + k_-^2 \nu_- \right). \tag{4.4}$$

In general, the spin Hall angle is expressed as the ratio between the spin Hall conductivity and the longitudinal charge conductivity: $\theta_{SH} = \sigma_{xy}^{s_z}/\sigma_{yy}$.

Figure 4.1 shows the spin Hall angle, θ_{SH}, as a function of carriers density, n, in (a) for different Rashba parameter, α, and in (b) for different temperature, T. Figure 4.1(a) was created using
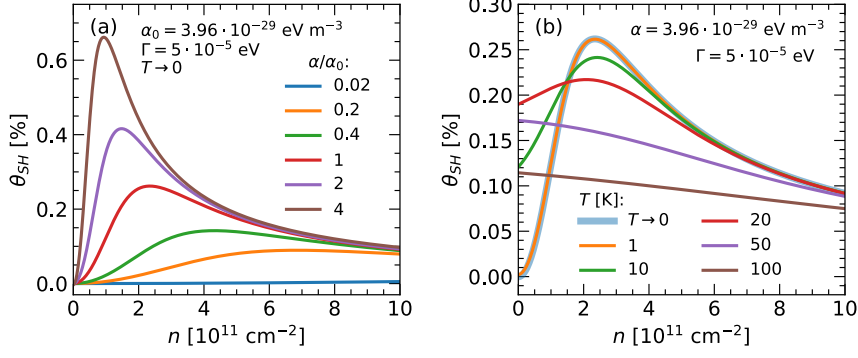
Figure 4.1: Spin Hall angle, θ_{SH}, as a function of carriers density, n. (a) $\theta_{SH}(n)$ for fixed Rashba SOI parameter, α, plotted using zero-temperature formulae, eqs. (9) and (4.3). (b) $\theta_{SH}(n)$ for fixed temperature, T, plotted with finite-temperature formulae, eqs. (8) and (4.2)

analytical zero-temperature formulas. One can observe a peak in the $\theta_{SH}(n)$ dependence that flattens and shifts up to higher n with a decrease in the strength of the Rashba SOI in the system. The influence of temperature on θ_{SH} is presented in figure 4.1(b), where temperature smearing leads to a non-zero spin Hall angle for lower carriers concentration, $n \to 0$, and flattens the peak in n-dependence, decreasing the θ_{SH} value.

Spin Hall effect in a magnetized 2DEG with k-cubed Rashba SOC

The inclusion of an out-of-plane magnetization field in the system modifies the analyzed Hamiltonian in the following way:

$$H = \frac{\hbar^2 k^2}{2m}\sigma_0 + i\alpha \left(k_-^3 \sigma_+ - k_+^3 \sigma_- \right) + M\sigma_z, \tag{4.5}$$

where $M\sigma_z$ represents the exchange interaction between the spin of quasiparticles and the magnetic substrate or external magnetic field, expressed in energy units (eV). Subsequently, the spin Hall conductivity (SHC) takes the form:

$$\sigma_{xy}^{s_z} = -\frac{9}{16\pi}e\frac{\hbar^2}{m}\left[\int dk \frac{k^7 \alpha^2 \left[f(E_+) - f(E_-)\right]}{\left(M^2 + \alpha^2 k^6\right)^{3/2}} - \int dk \frac{k^7 \alpha^2 \Gamma^2 \left[f'(E_+) + f'(E_-)\right]}{\left(M^2 + \alpha^2 k^6\right)\left(M^2 + \alpha^2 k^6 + \Gamma^2\right)} \right], \tag{4.6}$$

which for $M = 0$ reduces to equation (9) in the paper.

Figure 4.2 presents the spin Hall conductivity as a function of saturation magnetization, M_0, temperature, T, and chemical potential, μ. It is observed that due to the presence of the exchange field in the system, SHC decreases, especially in the weak cubic Rashba SOI regime, i.e., when M_0 dominates, see Fig. 4.2a, and for lower chemical potential values, see Fig. 4.2c. In Figure 4.2b, Bloch's law is assumed for the temperature dependence of magnetization preceding the Curie temperature, T_c, i.e., $M = M_0 \left[1 - (T/T_C)^{3/2}\right]$. Thus, the magnetization field decreases with the temperature up to T_c, where the system becomes non-magnetic. This behavior of M is reflected in the $\sigma_{xy}^{s_z}(T)$ dependence, where SHC is suppressed with increasing M.
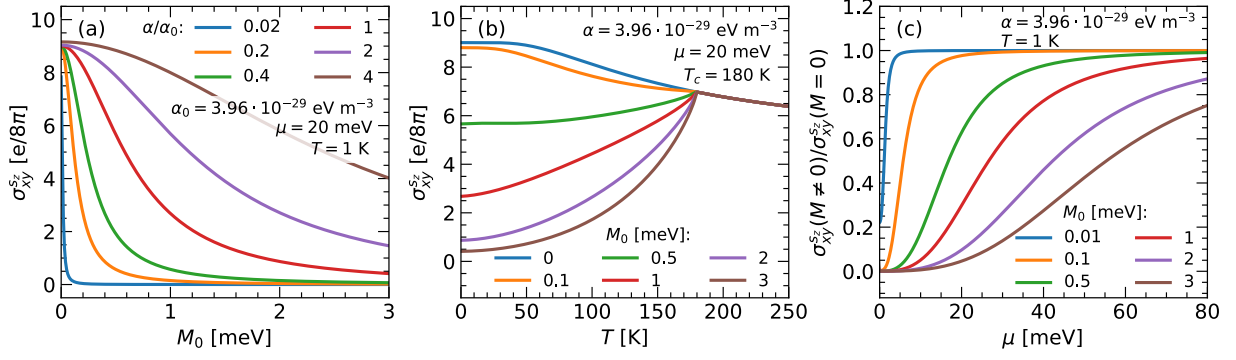
Figure 4.2: Spin Hall conductivity, $\sigma_{xy}^{s_z}$, eq. (4.6). (a) $\sigma_{xy}^{s_z}$ as a function of saturation magnetization, M_0, for fixed Rashba SOI parameter, α/α_0. (b) $\sigma_{xy}^{s_z}$ as a function of temperature, T, for different M_0 value. For temperature dependence of magnetization field, M, preceding the Curie temperature, T_c, the Bloch's law is assumed, $M = M_0 \left[1 - (T/T_c)^{3/2} \right]$. (c) Normalized SHC, $\sigma_{xy}^{s_z}/\sigma_{xy}^{s_z}(M=0)$, as a function of chemical potential for fixed saturation magnetization, M_0. For non-magnetized system, $M = 0$, chemical potential $\mu = 80$ meV corresponds to the carriers density $n = 41.4 \cdot 10^{11}$ cm^{-2}. Parameters: $T_c = 180$ K, $\Gamma = 5 \cdot 10^{-6}$ eV

Summary

The zero-temperature, as well as finite-temperature results for the intrinsic spin Hall conductivity (SHC) and the spin Hall angle (SHA) in a 2DEG with an isotropic cubic form of SOI, are provided.

It is worth noting that the analytical calculations provided by [221, 233] show that the vertex correction due to impurity scattering on isotropic short-range potential vanishes in the analyzed system. Thus, the spin Hall conductivity in a system with spin-independent impurities reproduces its intrinsic value, obtained from a clean system without impurities. This behavior is in contrast to the model of a 2DEG with a linear form of Rashba SOC [159], where the vertex correction cancels SHE [234, 235] and thus the intrinsic[1] spin Hall effect vanishes in the weak disorder limit.

The influence of temperature on the SHA is similar to that observed for the SHC with respect to carrier density. As the strength of Rashba SOC increases in the system, the SHA peak is both enhanced and shifted towards lower carrier densities.

The influence of out-of-plane magnetization on SHE was also investigated. One can conclude that magnetization suppresses the spin Hall response in the system, especially if magnetization dominates the cubic Rashba SOI, i.e., for lower Rashba parameter strength and at higher energies (higher chemical potential).

---

[1] Besides, one can refer to the *extrinsic spin Hall effect* when the leading source of SOI has an external character, i.e., is related to scattering events on spin-dependent impurities like side-jump and skew-scattering processes. Here, in a clean limit, the extrinsic processes are not under investigation.

4.2 Reprint of the article A-2

The article entitled "Anomalous Hall and Nernst effects in 2D systems: role of cubic Rashba spin-orbit coupling" provides the analysis of the anomalous Hall conductivity (AHC) and its thermal counterpart, anomalous Nernst conductivity (ANC) in a 2DEG where the isotropic k-cubed form of Rashba spin-orbit interaction is present. The out-of-plane magnetization field in the system can arise due to the proximity effect, i.e., the coupling of quasiparticles' spin with the magnetic substrate.

It is shown, using Matsubara-Green's functions (MGF) formalism, that the non-dissipative component of AHC, coming from the states in the Fermi sea, is linked to the Berry curvature. Thus, both approaches to investigate the intrinsic AHC, i.e., MGF formalism and using the Berry curvature concept, are equivalent.

Anomalous Hall conductivity takes the highest value where the cubic Rashba energy, E_R, and magnetization (in energy units), E_M, are comparable, i.e., $M \approx k^3 \alpha$ (see Fig. 1a, where for $\mu = 60$ meV, $E_R \approx E_M \approx 3$ meV). When one of these interactions, Rashba or exchange field, dominates, the anomalous Hall response takes the lower values.

An intriguing feature of ANC is the change of the sign preceding the magnetic phase transition indicated by the Curie temperature, T_C, observed for higher chemical potential, μ, and saturation magnetization, M_0, Fig. 2b,d. This behavior has already been observed experimentally, e.g., in thin film of LSMO ($La_{2/3}Sr_{1/3}MnO_3$) [188] and ferromagnetic semiconductors like $Ga_{1-x}Mn_xAs$ [186].

The sign change of α_{xy} with μ occurs when the Rashba SOC and exchange interaction are comparable. For example, in Fig. 2a, the green dashed line shows a sign change at $\mu \approx 30$ meV, where $E_R = k_F^3 \alpha = M$ (k_F is the Fermi wavevector)[2]. Regarding the AHC, it reaches its maximum when $M \approx E_R$, which corresponds to the point where the ANC vanishes. This behavior supports the Mott relation between AHC and ANC, as the Mott relation [186–188] indicates that ANC (thermal counterpart of AHC) is proportional to the derivative of AHC with respect to μ, eq. (3.8). Additionally, ANC takes negative (positive) values when the exchange interaction (Rashba SOI) dominates.

---

[2]Here, one should take in mind the influence of the temperature on magnetization $M = M_0 \left[1 - (T/T_C)^{3/2} \right]$, as well as the temperature smearing that blurs the ANC dependency.

Anomalous Hall and Nernst Effects in 2D Systems: Role of Cubic Rashba Spin–Orbit Coupling

Anna Krzyżewska, Anna Dyrdał,* Józef Barnaś, and Jamal Berakdar

The anomalous Hall and Nernst effects are considered theoretically for the model Hamiltonian describing properties of electronic states formed at the interfaces of semiconductor heterostructures or perovskite oxide junctions and surfaces. Using the Matsubara Green's function formalism and linear response theory we find, among others, substantial intrinsic contributions to both effects. Additionally, a change of sign in the anomalous Nernst conductivity occurs for temperatures preceding the magnetic phase transition.

The anomalous Hall effect[1] (AHE) is a phenomenon which is widely used for experimental characterization of electronic transport and topological properties of various systems, especially two-dimensional ones.[2,3] The long debate on the physical origins of AHE started already at the end of 1950's by the theory proposed by Karplus and Luttinger.[4,5] Now it is clear that this phenomenon is due to not only scattering mechanisms (*side jump*[6] and *skew scattering*[7]) but also due to intrinsic properties of materials, that are reflected in the topology of electronic bands (for reviews and further literature we refer to Refs. [8–11]). The latter contribution to AHE, also called intrinsic or topological one, is due to states below the Fermi level. The underlying physics of this contribution became clear when applying methods relying on the Berry phase.[12,13] The topological contribution is significant for systems with a non-trivial topology of electronic energy bands and is robust to relaxation processes. Its magnitude may reach much larger values than the contribution due to spin-dependent scattering processes.[14–18] Experimentally AHE is instrumental in delivering information not only on the magnetization and transport properties but also on the system topology. For a proper interpretation of experimental data a detailed understanding of the anomalous Hall conductivity beyond the zero temperature limit is crucial. The thermal counterpart of AHE, known as the anomalous Nernst effect (ANE),[19] is also an important transport phenomenon. ANE appears, for example, as an additional signal in many experimental realizations of transport measurements, thermal spin–orbit torques, and other thermally induced effects measured in systems with strong spin–orbit coupling.[20,21] The anomalous Nernst conductivity yields information on the topological properties of the system, too. However, contrary to the AHE, it depends only on the Berry phase at the Fermi level.[22,23] Moreover, the anomalous Nernst conductivity is also a natural characteristics for determining magnetic fluxes and transverse entropy flow in Fermi liquids and superconductors.

The physics behind AHE and ANE is especially intriguing in more complicated structures such as spin glasses, antiferromagnets, and other systems with a helical orientation of magnetic moments. In such a case AHE takes significant values, even though the net magnetization is zero or close to zero. These results do not reflect the simple proportionality of AHE signal to magnetization, and follow from an enhancement of spin–orbit coupling and a non-trivial topological properties of the electronic structure.

For spintronics applications low dimensional systems and heterostructures are of special interest. For instance, metallic multilayers, semiconductor heterostructures, and van der Waals heterostructures as well as thin layers of perovskite oxides and their interfaces were in the focus of research. This letter is devoted to the anomalous Hall and Nernst effect in magnetized two-dimensional systems described by the effective Hamiltonian with isotropic *k*-cubed Rashba spin–orbit interaction. This model is not only widely used for the description of p-doped semiconductor heterostructures, but also (according to some experimental data[24]) can be useful for modeling of spin–orbit phenomena at surfaces or interfaces of n-doped perovskite oxides.[25,26] We will show, among others, that the anomalous Hall conductivity contains a significant topological contribution, not included in recent description of AHE within this model.[27]

Model and Method: We consider an effective Hamiltonian that describes a 2D magnetized electron gas with isotropic *k*-cubed Rashba spin–orbit interaction[25,27,28]:

$$\widehat{H} = \frac{\hbar^2 k^2}{2m}\sigma_0 + i\lambda\left(k_-^3\sigma_+ - k_+^3\sigma_-\right) + M\sigma_z \tag{1}$$

A. Krzyżewska, Dr. A. Dyrdał, Prof. J. Barnaś
Faculty of Physics
Adam Mickiewicz University
ul. Umultowska 85, 61-614 Poznań, Poland
E-mail: anna.dyrdal@physik.uni-halle.de

Dr. A. Dyrdał, Prof. J. Berakdar
Institut für Physik
Martin-Luther Universität Halle-Wittenberg
D-06099 Halle, Germany

Prof. J. Barnaś
Institute of Molecular Physics
Polish Academy of Sciences
ul. M. Smoluchowskiego 17, 60-179 Poznań, Poland

The ORCID identification number(s) for the author(s) of this article can be found under https://doi.org/10.1002/pssr.201800232.

with $k = \sqrt{k_x^2 + k_y^2}$, $k_\pm = (k_x \pm i k_y)$, and $\sigma_\pm = \frac{1}{2}(\sigma_x \pm i\sigma_y)$. The effective mass, m, and Rashba coupling constant, λ, are defined by material parameters such as the width and the potential of the quantum well, and Luttinger parameters.[25,28] The effective exchange field **M** is normal to the plane of 2D electron system (along the z direction) and is defined in energy units. We are interested in the temperature dependences of the anomalous Hall and Nernst effects.

To determine the anomalous Hall and Nernst conductivities, we use the Matsubara Green's function formalism and calculate the linear response of the system to external perturbations, that is to the electric field and to the temperature gradient. The general expression for the charge current in the Matsubara formalism has the following form[29]:

$$j_a = \frac{1}{\beta} \sum_{k,n} \mathrm{Tr}\left\{ \hat{j}_a G_k(i\varepsilon_n + i\omega_m) \hat{H}_A(i\omega_m) G_k(i\varepsilon_n) \right\} \quad (2)$$

where $\beta = 1/k_B T$ (k_B is the Boltzmann constant), $G_k(i\varepsilon_n)$ is the Matsubara Green's function corresponding to the Hamiltonian (1) $\varepsilon_n = (2n+1)\pi/\beta$, $\omega_m = 2m\pi/\beta$, and stand for Matsubara energies. The charge current density operator is expressed by the velocity operator: $\hat{j}_a = e\hat{v}_a$ and $\hat{v}_a = \frac{1}{\hbar}\frac{\delta \hat{H}}{\delta k_a}$ (with $a = x,y$). Hereafter, we assume that the driving force (electric field or temperature gradient) is oriented in the y-direction. Thus the charge current that appears due to AHE/ANE flows in the x direction. For electric field as the driving force, the Hamiltonian describing perturbation reads $H_A(i\omega_m) = -\hat{j}_y A_y^E(i\omega_m)$, where the amplitude of electromagnetic vector potential is related to the electric field through the relation: $A_y^E(i\omega_m) = -i\hbar \frac{E_y(i\omega_m)}{i\omega_m}$. In turn, when the temperature gradient $\nabla_y T$ appears in the system, the perturbation Hamiltonian may be defined by the coupling of heat current density to auxiliary vector potential,[30–32] $H_A(i\omega_m) = -\hat{j}_y^h A_y^T(i\omega_m)$. The heat current density operator is defined as the following anticommutator $\hat{j}_y^h = \frac{1}{2}\left[\hat{H} - \mu\sigma_0, \hat{v}_y \right]_+$ (μ denotes the chemical potential) and the amplitude of the auxiliary vector potential is connected to the temperature gradient via the following relation: $A_y(i\omega_m) = -\frac{\hbar}{i(i\omega_m)}\frac{\nabla_y T}{T}$.

Based on Equation (2), after some standard calculations like summation over the Matsubara energies and analytical continuation,[29] we obtain the following expressions for the anomalous Hall and Nernst conductivities:

$$\sigma_{xy} = j_x/E_y = -\frac{e^2\hbar}{\omega}\mathrm{Tr}\int\frac{d^2\mathbf{k}}{(2\pi)^2}\int\frac{d\varepsilon}{2\pi}f(\varepsilon)\left[\hat{v}_x G_\mathbf{k}^R(\varepsilon+\omega)\hat{v}_y\left[G_\mathbf{k}^R(\varepsilon) - G_\mathbf{k}^A(\varepsilon)\right]\right.$$
$$\left. + \hat{v}_x\left[G_\mathbf{k}^R(\varepsilon) - G_\mathbf{k}^A(\varepsilon)\right]\hat{v}_y G_\mathbf{k}^A(\varepsilon-\omega)\right] \quad (3)$$

$$a_{xy} = j_x/(-\nabla_y T) = -\frac{e\hbar}{\omega}\mathrm{Tr}\int\frac{d^2\mathbf{k}}{(2\pi)^2}\int\frac{d\varepsilon}{2\pi}f(\varepsilon)\left[\hat{v}_x G_\mathbf{k}^R(\varepsilon+\omega)\hat{j}_y^h\left[G_\mathbf{k}^R(\varepsilon) - G_\mathbf{k}^A(\varepsilon)\right]\right.$$
$$\left. + \hat{v}_x\left[G_\mathbf{k}^R(\varepsilon) - G_\mathbf{k}^A(\varepsilon)\right]\hat{j}_y^h G_\mathbf{k}^A(\varepsilon-\omega)\right] \quad (4)$$

where $G_\mathbf{k}^{R/A}(\varepsilon) = \left[(\varepsilon + \mu \pm i\Gamma)\sigma_0 - \hat{H}\right]^{-1}$ is the retarded/advanced Green's function, respectively, with Γ denoting the relaxation rate. It should be noted that Equations (3) and (4) are obtained in the single loop approximation.[29] These equations are adequate since we consider randomly distributed point-like non-magnetic impurities. In such a case it was shown that, the impurity vertex correction does not provide additional contributions to the transport properties in the k-cubed Rashba model.[25,33] Furthermore, the relaxation rate Γ (obtained as the imaginary part of the self-energy in the Born approximation) is the same for both energy subbands. Furthermore, we operate within the limit of low impurities concentration treating Γ as a small parameter.

Anomalous Hall Conductivity: Integrating over the angle ϕ (describing orientation of the vector **k**) and ε in Equation (3) leads to a general formula that should be integrated over k. According to the standard convention we can split the anomalous Hall conductivity into two components: $\sigma_{xy} = \sigma_{xy}^I + \sigma_{xy}^{II}$, where $\sigma_{xy}^I = \sigma_{xy}^I\left[f'(E_i)\right]$ corresponds to the states at the Fermi level and $\sigma_{xy}^{II} = \sigma_{xy}^{II}[f(E_i)]$ describes the contribution from all states in the Fermi sea (note that E_i [with $i = \pm$] denotes the i-th subband). For the model under consideration, these two contributions have the following explicit form:

$$\sigma_{xy}^I = -\frac{9e^2 M\lambda^2}{4\pi\hbar}\int dk\, k^2\left[f'(E_+) + f'(E_-)\right]$$
$$\times\left(\frac{1}{M^2 + \lambda^2 k^6} - \frac{1}{(M^2 + \lambda^2 k^6) + \Gamma^2}\right) \quad (5)$$

$$\sigma_{xy}^{II} = -\frac{9e^2 M\lambda^2}{4\pi\hbar}\int dk\, k^5\frac{f(E_-) - f(E_+)}{(M^2 + \lambda^2 k^6)^{3/2}} \quad (6)$$

In our considerations and discussions on the temperature variation of the anomalous Hall and Nernst conductivity, we assume that the carriers time scale is much faster that the magnetization dynamics which is generally fulfilled away from the magnetic phase transition and carrier densities such as those considered here. This allows a parametric treatment of the temperature dependence of the effective exchange field M (magnetization in the energy units) while considering transport. This dependence is assumed to follow the Bloch relation: $M = M_0[1 - (T/T_c)^{3/2}]$ (here M_0 is the saturation magnetization, $M_0 = M$ ($T = 0$), T is the temperature while T_c stands for the Curie temperature).

In the low-temperature regime, after integration over k, we find

$$\sigma_{xy} = -\frac{9e^2 M\lambda^2}{4\pi\hbar}\left[\frac{k_+^4 \nu_+}{(M^2 + \lambda^2 k_+^6) + \Gamma^2} + \frac{k_-^4 \nu_-}{(M^2 + \lambda^2 k_-^6) + \Gamma^2} - \frac{k_+^4 \nu_+}{M^2 + \lambda^2 k_+^6}\right.$$
$$\left. - \frac{k_-^4 \nu_-}{M^2 + \lambda^2 k_-^6} - \frac{1}{3\lambda^2}\left(\frac{1}{\sqrt{M^2 + \lambda^2 k_-^6}} - \frac{1}{\sqrt{M^2 + \lambda^2 k_+^6}}\right)\right] \quad (7)$$

where $k_\pm$ and $\nu_\pm$ are the Fermi wave vectors and the density of states at the Fermi level for the $i = \pm$ subband, respectively. The first line of the above expression originates from the integrals

related to the product of the retarded and advanced Green's functions. This term was already obtained in the earlier study of AHE in the model under consideration. The last two lines, in turn, are related to the integrals containing the product of two retarded or two advanced Green's functions. This contribution was neglected in previous calculations. However, in systems with broken time-reversal symmetry (here due to the presence of magnetization), this contribution is non-zero and follows from intrinsic (topological) properties of the system, that is, from the Fermi-sea states. When the concentration of impurities is small, $\Gamma \to 0$, the first and second line of (7) cancel each other and only the term that comes from the σ^{II}-component survives. Thus, the topological terms cannot be neglected. Moreover, in the case of almost pure systems (quasi-ballistic limit), the topological contribution to the anomalous Hall conductivity dominates. This behavior is clearly seen in **Figure 1**(a and c), where the anomalous Hall conductivity is plotted as a function of the saturated magnetization, M_0 and temperature T, respectively. To show the role of individual components, we plotted separately σ^I and σ^{II} as well as the total anomalous Hall conductivity. For the relaxation rates Γ smaller than 0.1 meV, the contribution σ^I is reduced and the total anomalous Hall conductivity is determined by the topological contribution. In turn, Figure 1(b and d) show variation of the anomalous Hall conductivity with the Fermi level and temperature. These figures show that the magnitude of the Hall conductivity grows with increasing μ.

To conclude this part, we stress that for small concentration of impurities, the component σ^I vanishes and the anomalous Hall effect is described by the topological term. Hence the

anomalous Hall conductivity can be written in the following general form:

$$\sigma_{xy} = -\frac{e^2}{\hbar}\sum_i \int \frac{d^2\mathbf{k}}{(2\pi)^2} B_i^z(\mathbf{k}) f(E_i) \qquad (8)$$

where $B_i^z(\mathbf{k}) = i\nabla_\mathbf{k} \times \langle \Psi_i|\nabla_\mathbf{k}|\Psi_i\rangle$ denotes the Berry curvature for the i-th band and Ψ_i is the eigenvector of the i-th band that corresponds to the eigenvalue E_i. For the model under consideration, the Berry curvature has the following explicit form[26]:

$$B_\pm^z(\mathbf{k}) = \pm\frac{9}{2}\frac{M\lambda^2 k^4}{\left(M^2 + \lambda^2 k^6\right)^{3/2}} \qquad (9)$$

Anomalous Nernst Conductivity. The anomalous Nernst conductivity within the Matsubara Green's function formalism and linear response theory is described by Equation (4). However, it is well known and already discussed in the literature, that thermal transport coefficients obtained in the linear response theory (Kubo and Kubo-like formalism) behave unphysically when $T \to 0$. Thus, the magnetization currents should be taken into account to obtain the correct thermoelectric coefficients, which satisfy the Onsager relations and do not contradict the third thermodynamic law. This issue has been explained by Obraztsov[37] and then widely discussed in the context of quantum Hall effect, Nernst, and spin Nernst effect as well as in the context of graphene-like 2D materials.[22,38–45] To obtain physically correct results for the anomalous Nernst conductivity one should add to Equation (4) the component related to the orbital magnetization current density. Since calculations of the orbital magnetization are a little bit tedious, we use the symmetry properties of the thermal kinetic coefficients, as well the fact that the anomalous Hall conductivity in the considered model is determined by the topological component. Namely, the Nernst conductivity, a_{xy}, is related to the transverse heat conductivity, β_{xy}, by the Onsager relation[29]: $\beta_{xy} = a_{xy}T$. In turn, the heat conductivity may be expressed by the Berry curvature and the entropy density of the electron gas[22,23,46–48]:

$$\beta_{xy} = a_{xy}T = \frac{ek_B T}{\hbar}\sum_n \int \frac{d^2\mathbf{k}}{(2\pi)^2} B_n^z(\mathbf{k}) S_n(\mathbf{k}) \qquad (10)$$

Taking into account the explicit form of Berry curvature given by Equation (9) and the fact that the entropy density of the electron gas is defined as $S_n(\mathbf{k}) = -f_\mathbf{k}\ln(f_\mathbf{k}(E_n)) - (1 - f_\mathbf{k}(E_n))\ln(1 - f_\mathbf{k}(E_n))$, one can easily obtain the anomalous Nernst conductivity. This conductivity behaves strongly non-monotonous as a function of chemical potential, which follows from the interplay between the Rashba and exchange coupling, see **Figure 2**(a). For a relatively large value of μ, the anomalous Nernst conductivity decreases. Thus, the most interesting behavior of ANE is observable for smaller values of the chemical potential, where the spin–orbit coupling dominates. For higher energies, the influence of the spin–orbit coupling on the band structure is negligible, and therefore ANE vanishes. For a small but fixed
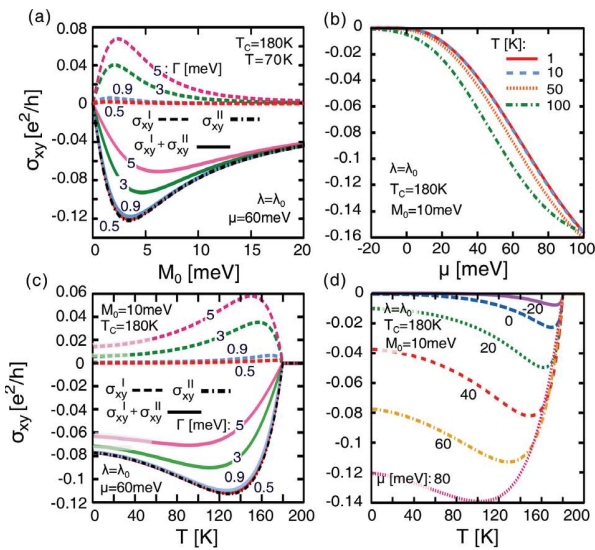
Figure 1. Anomalous Hall conductivity as a function of: saturation magnetization M_0 for fixed values of relaxation rate Γ (a); chemical potential μ for fixed temperatures T (b); and temperature for indicated relaxation rates (c) and chemical potentials (d). Other parameters are: $\lambda_0 = 3.96 \cdot 10^{-29}$ eVm^3, $\Gamma = 0.005$ meV, and $m = 0.123\, m_0$ (with m_0 being the electron rest mass). The Rashba coupling constant and effective mass are chosen based on Refs. [24,25,28,34–36]. The shaded parts of some curves in (c) correspond to the temperature range where the condition $\Gamma < k_B T$ is not obeyed.
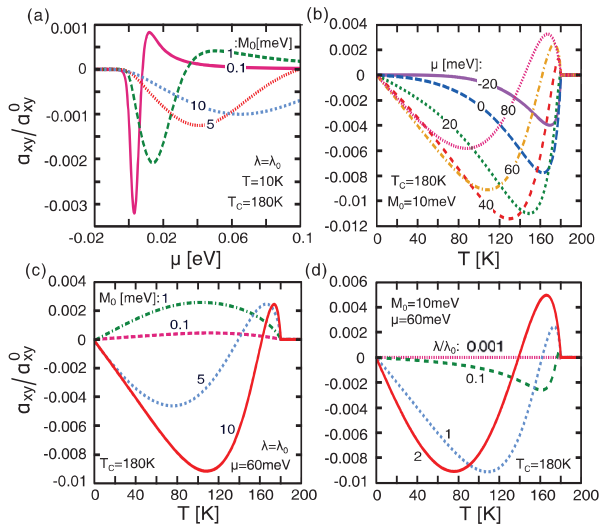
Figure 2. Anomalous Nernst conductivity normalized to $\alpha_{xy}^0 = ek_B/\hbar$, shown as a function of the chemical potential μ for fixed values of the saturation magnetization M_0 (a) and as a function of the temperature T for fixed values of chemical potential μ (b); saturation magnetization (c); and Rashba coupling constant λ (d). Other parameters are as in Figure 1.

chemical potential, the Nernst conductivity reaches a maximal value (positive) at a certain temperature, and then decreases with increasing T, eventually changing sign. The maximal value of the anomalous Nernst conductivity is reduced with increasing μ and then changes sign. Furthermore, the temperature at maximum shifts from larger to lower values when the chemical potential decreases, see Figure 2(b). Additionally, for relatively large saturation magnetization of the system, sign of a_{xy} is reversed at a temperature below the phase transition from the ferromagnetic state to paramagnetic one, where $M = 0$ and ANE disappears (Figure 2c,d).

Summary and Conclusions: We considered the anomalous Hall and Nernst effects in the 2D magnetized electron gas with k-cubed form of the Rashba spin–orbit interaction. We showed that both the anomalous Hall and Nernst conductivities include terms that are determined by the topological properties of the system. The corresponding topological contributions are robust against impurity scattering processes. Interestingly, the sign of the anomalous Nernst conductivity can be changed by tuning the temperature. This change of sign appears below the critical temperature of magnetic phase transition.

Acknowledgement

Conflict of Interest

The authors declare no conflict of interest.

[1] E. Hall, *Philos. Mag.* **1881**, *12*, 157.
[2] C. L. Chien, C. R. Westgate, *The Hall Effect and Its Applications*, Plenum, New York **1979**.
[3] H. Ohno, F. Matsukura, Y. Ohno, *Solid State Commun.* **2001**, *119*, 281.
[4] R. Karplus, J. M. Luttinger, *Phys. Rev.* **1954**, *95*, 1154.
[5] J. M. Luttinger, *Phys. Rev.* **1958**, *112*, 739.
[6] L. Berger, *Phys. Rev. B* **1970**, *2*, 4559.
[7] J. Smit, *Physica (Amsterdam)* **1985**, *24*, 39.
[8] A. Crepieux, P. Bruno, *Phys. Rev. B* **2001**, *64*, 014416.
[9] N. Nagaosa, *J. Phys. Soc. Jpn.* **2006**, *75*, 042001.
[10] N. A. Sinitsyn, *J. Phys.: Condens. Matter* **2008**, *20*, 023201.
[11] N. Nagaosa, J. Sinova, S. Onoda, A. H. MacDonald, N. P. Ong, *Rev. Mod. Phys.* **2010**, *82*, 1539.
[12] M. V. Berry, *Proc. R. Soc. Lond. Ser. A* **1984**, *392*, 45.
[13] G. Sundaram, Q. Niu, *Phys. Rev. B* **1999**, *59*, 14915.
[14] T. Jungwirth, Q. Niu, A. H. MacDonald, *Phys. Rev. Lett.* **2002**, *88*, 207208.
[15] M. Onoda, N. Nagaosa, *J. Phys. Soc. Jpn.* **2002**, *71*, 19; *Phys. Rev. Lett.* **2003**, *90*, 206601.
[16] Z. Fang, N. Nagaosa, K. S. Takahashi, A. Asamitsu, R. Mathieu, T. Ogasawara, H. Yamada, H. Kawasaki, Y. Tokura, K. Terakura, *Science* **2003**, *302*, 92.
[17] D. Culcer, A. H. NiuMacDonald, Q. Niu, *Phys. Rev. B* **2003**, *68*, 045327.
[18] D. Culcer, J. Sinova, N. A. Sinitsyn, T. Jungwirth, A. H. MacDonald, Q. Niu, *Phys. Rev. Lett.* **2004**, *93*, 046602.
[19] A. W. Smith, *Phys. Rev.* **1911**, *33*, 295.
[20] T. Miyasato, N. Abe, T. Fujii, A. Asamitsu, S. Onoda, Y. Onose, N. Nagaosa, Y. Tokura *Phys. Rev. Lett.* **2007**, *99*, 86602.
[21] Y. Pu, D. Chiba, F. Matsukura, H. Ohno, J. Shi, *Phys. Rev. Lett.* **2008**, *101*, 117208.
[22] D. Xiao, Y. Yao, Z. Fang, Q. Niu, *Phys. Rev. Lett.* **2006**, *97*, 026603.
[23] D. Xiao, M.-C. Chang, Q. Niu, *Rev. Mod. Phys.* **2010**, *82*, 1959.
[24] H. Nakamura, T. Koga, T. Kimura, *Phys. Rev. Lett.* **2012**, *108*, 206601.
[25] C.-X. Liu, B. Zhou, S.-Q. Shen, B.-F. Zhu, *Phys. Rev. B* **2008**, *77*, 125345.
[26] L. Karwacki, A. Dyrdal, J. Berakdar, J. Barnas, *Phys. Rev. B* **2018**, *97*, 235302.
[27] R. Li, M. Yi-Ming, *Commun. Theor. Phys.* **2010**, *54*, 559.
[28] R. Winkler, *Spin–Orbit Coupling Effects in Two-Dimensional Electron and Hole Systems*, Springer-Verlag, Berlin, Heidelberg **2003**.
[29] D. Mahan, *Many Particle Physics*, Kluwer Academic/Plenum Publishers, New York **2000**.
[30] G. Strinati, C. Castellani, *Phys. Rev. B* **1987**, *36*, 2270.
[31] A. Dyrdal, M. Inglot, V. K. Dugaev, J. Barnas, *Phys. Rev. B* **2013**, *87*, 245309.
[32] G. Tatara, *Phys. Rev. Lett.* **2015**, *114*, 196601; *Phys. Rev. B* **2015**, *92*, 064405.
[33] S. Murakami, *Phys. Rev. B* **2004**, *69*, 241202(R).
[34] L. W. van Heeringen, G. A. de Wijs, A. McCollam, J. C. Maan, A. Fasolino, *Phys. Rev. B* **2013**, *88*, 205140; L. W. van Heeringen, A. McCollam, G. A. de Wijs, A. Fasolino, *Phys. Rev. B* **2017**, *95*, 155134.
[35] Z. Zhong, A. Toth, K. Held, *Phys. Rev. B* **2013**, *87*, 161102(R).

[36] H. Liang, L. Cheng, L. Wei, Z. Luo, G. Yu, Ch. Zeng, Z. Zhang, *Phys. Rev. B* **2015**, *92*, 075309.

[37] N. Yu Obraztsov, *Fiz. Tverd. Tela* **1964**, *6*, 414; *Sov. Phys. Solid State* **1964**, *6*, 331.

[38] L. Smrcka, P. Streda, *J. Phys. C* **1977**, *10*, 2153.

[39] P. Streda, *J. Phys. C* **1982**, *15*, L717.

[40] M. Jonson, S. M. Girvin, *Phys. Rev. B* **1984**, *29*, 1939.

[41] H. Oji, P. Streda, *Phys. Rev. B* **1985**, *31*, 7291.

[42] T. Qin, Q. Niu, J. Shi, *Phys. Rev. Lett.* **2011**, *107*, 236601.

[43] N. R. Cooper, B. I. Halperin, I. M. Ruzin, *Phys. Rev. B* **1997**, *55*, 2344.

[44] V. P. Gusynin, S. G. Sharapov, A. A. Varlamov, *Phys. Rev. B* **2014**, *90*, 155107; V. P. Gusynin, S G. Sharapov, A. A. Varlamov, *Low Temp. Phys.* **2015**, *41*, 342.

[45] A. Dyrdal, V. K. Dugaev, J. Barnas, *Phys. Rev. B* **2016**, *94*, 205302; *Phys. Rev. B* **2016**, *94*, 035306.

[46] Ch. Zhang, S. Tewari, V. M. Yakovenko, Das Sarma, *Phys. Rev. B* **2008**, *78*, 174508.

[47] Ch. Zhang, S. Tewari, Das Sarma, *Phys. Rev. B* **2009**, *79*, 245424.

[48] Z.-G. Zhu, J. Berakdar, *New J. Phys.* **2013**, *15*, 073028.

4.3 Reprint of the article A-3

The work entitled "Anomalous Hall and Nernst effects in a two-dimensional electron gas with an anisotropic cubic Rashba spin-orbit interaction" addresses two transverse charge transport effects, driven by an electric field or temperature gradient. The analyzed model, a 2D system with an anisotropic form of k-cubed Rashba spin-orbit interaction, applies to both the interfaces or surfaces of perovskite oxides and semiconductor heterostructures.

In low-impurity concentrations, the anomalous Hall effect exhibits an intrinsic character, where only the states in the Fermi sea contribute to transport, and AHC can be described with the Berry curvature. The change in the sign of ANC with temperature, chemical potential, and the strength of both the Rashba SOC and exchange interaction has been demonstrated. This behavior of ANC is associated with the interplay between Rashba spin-orbit interaction and exchange interaction in the system. Furthermore, it has been observed that both investigated effects (AHC and ANC) behave qualitatively similarly in both isotropic and anisotropic cubic Rashba models, cf. [156].

Research articles

Anomalous Hall and Nernst effects in a two-dimensional electron gas with an anisotropic cubic Rashba spin-orbit interaction

A. Krzyżewska[a], A. Dyrdał[a,b,*]

[a] Faculty of Physics, Adam Mickiewicz University, 61-614 Poznań, Poland
[b] Institut für Physik, Martin-Luther-Universität Halle-Wittenberg, 06099 Halle (Saale), Germany

ARTICLE INFO

ABSTRACT

The anomalous Hall and Nernst effects are considered theoretically within Matsubara Green's function formalism. The effective Hamiltonian of a magnetized two-dimensional electron gas with cubic Rashba spin-orbit interaction may describe transport properties of electronic states at the interfaces or surfaces of perovskite oxides or another type of heterostructures that, due to symmetry, may be described by the same effective model. In the quasi-ballistic limit, both effects are determined by the topological (Fermi sea) contribution whereas the states at the Fermi level gives a negligibly small response. For a wide range of parameters describing the considered system, the anomalous Nernst conductivity reveals a change of the sign before the magnetic phase transition.

1. Introduction

Spin-orbit interaction is the origin of various phases and phenomena observed in the physics of solid-state providing pure electric control of the spin degree of freedom [1]. Nowadays, the spin-orbit driven transport phenomena, such as anomalous and spin Hall effects, has become a fundamental tool for generation spin accumulation and detection of spin currents and topological character of quasiparticles states. Moreover, pure electrical control of the spin degree of freedom is one of the crucial ideas of spintronics, according to which spin-based electronics should provide smaller, cheaper and faster electronic devices with high functionality (e.g., data storage and logic operations in one material) and low energy consumption at room temperatures [2–6].

It is known that spin-orbit interaction strongly depends on the type of impurities and the crystallographic potential of the host material and is especially enhanced in low dimensional systems. In such a case the space inversion symmetry is broken at the surfaces or interfaces what results in an additional component of the spin-orbit interaction, called the Bychkov-Rashba interaction [7–10]. This type of spin-orbit interaction, resulting from structural inversion asymmetry, has been described initially in the context of a two-dimensional electron gas forming at the interfaces of semiconductor heterostructures [8]. For symmetry reasons, Rashba Hamiltonian is odd in quasiparticle momentum what leads in the simplest approximation to the well known **k**-linear dependence. However, in various 2D systems, terms with a cubic momentum dependence play also an important role. The so-called cubic Rashba interaction is responsible, e.g., for spin and transport

properties of a two-dimensional hole gas formed at the interfaces of III-V semiconductor heterostructures [11–16]. Recently, the cubic character of Rashba interaction has also been found in a two-dimensional electron gas at the perovskite oxides surfaces and interfaces such as $LaAlO_3/SrTiO_3$ (LAO/STO) [17–20].

The thin films or heterointerfaces of perovskite oxides are a diverse group of materials with intriguing aspects of fundamental physics. For instance, the interfaces of insulating nonmagnetic oxide perovskites reveal interesting physical properties such as two-dimensional metallic conductivity, large negative magnetoresistance, metal-insulator transition, low-temperature superconductivity, and ferromagnetism as well as their coexistence [21–24]. Moreover, experimental data indicate strong spin-to-charge interconversion effects governed by spin-orbit coupling [25–28].

Here, we investigate anomalous Hall and Nernst effects in a two-dimensional electron gas with anisotropic **k**-cubed Rashba spin-orbit coupling. Anomalous Hall effect has become nowadays one of the most important and commonly used experimental tools, delivering information about magnetization, transport properties, and the system topology [29]. Although the behavior of anomalous Hall conductivity in the presence of linear Rashba coupling has been investigated intensively, the influence of the cubed Rashba coupling on it has got much less attention. Therefore, the purpose of this paper is to provide the theoretical description of the anomalous Hall and Nernst effects in magnetized 2D electron gas with cubic Rashba coupling. Since perovskite oxides have become recently very promising materials for spintronics applications, the effective Hamiltonian derived for 2DEG at LAO/STO interface is considered. However, the

presented model and qualitative results may also be applied to other structures that, due to symmetry arguments, can be described by the same Hamiltonian.

In Section 2 the effective low-energy Hamiltonian describing electronic states of 2DEG with cubic Rashba spin-orbit coupling is described. In this section, the Matsubara Green's function formalism is applied to the anomalous Hall and Nernst effects. The Berry phase approach is also introduced. The discussion of numerical results is given in Section 3. Finally, Section 4 contains the final remarks and summary of this work.

2. Model and method

2.1. Effective Hamiltonian

The electronic energy spectrum describing STO surfaces and STO/LAO interfaces has been calculated recently within the tight-binding approach and DFT modeling [17,18,30–33]. Based on these calculations the effective Hamiltonian describing the neighborhood of the Γ point in the Brillouin zone has been derived [17–20]. This energy spectrum is formed by three pairs of bands as presented in Fig. 1(a). These bands are created by d-orbitals (d_{xy}, d_{xz} and d_{yz}) originating from t_{2g} atomic orbitals of Ti. The effective Hamiltonian describing the lowest pair of bands is formed by d_{xy} orbital and has a form of $\mathbf{k}$-linear Rashba Hamiltonian with a negative coupling constant. The middle pair of bands around Γ point is described by spin-orbit coupling term which is not only anisotropic in a $\mathbf{k}$-space but also has a cubic dependence on $\mathbf{k}$ (Fig. 1(b)–(e)). The highest, in energy, pair of bands is characterized by effective Hamiltonian with $\mathbf{k}$-linear Dresselhaus-like form of spin-orbit [20]. Since electronic transport characteristics in a system with conventional Rashba term is rather well described, within this article, we focus only on the transport properties of quasiparticles from the middle pair of bands. Another word, the aim is to describe transport properties related to quasiparticle states determined by anisotropic $\mathbf{k}$-cubed Rashba spin-orbit interaction. The effective Hamiltonian describing the system under consideration has the following form:

$$\widehat{H} = \frac{\hbar^2 k^2}{2m}\sigma_0 + \lambda\left(k_x^2 - k_y^2\right)\left(k_x\,\sigma_y - k_y\,\sigma_x\right) + M\,\sigma_z, \tag{1}$$

where $k^2 = k_x^2 + k_y^2$ and $k_x = k\cos(\phi)$, $k_y = k\sin(\phi)$ are the wavevector components, m is an effective mass of quasiparticle. The Rashba coupling constant is defined as $\lambda = a^3\gamma\,(t_1 + t_3 - t_2)/\Delta$, where a is the lattice constant for perovskite oxides, γ and Δ stands for the effective hopping amplitude and energy difference between the d_{xy} orbital and the d_{xz} and

d_{yz} orbitals, respectively while $t_{1,2,3}$ are the tight-binding parameters describing the virtual hopping between d-orbital states via p-orbitals of the oxygen [20,30,31]. The last term in the Hamiltonian describes effective exchange interaction with parameter M describing effective magnetization in energy units. The magnetization is oriented in z-direction (out-of 2DEG plain) and depends on temperature according to the Bloch relation [34]: $M = M_0\left[1 - (T/T_C)^{3/2}\right]$, where M_0 is the saturation magnetization, $M_0 = M(T = 0)$, T is the temperature and T_C denotes Curie temperature. Here it should be stressed that the above effective Hamiltonian is unbounded from below for large wavevectors what is unphysical. Thus the considerations within this model are restricted only to small quasiparticle densities. Thus, one needs to define the cut-off energy, E_c (and corresponding to it cut-off wavevector) below which the states might be occupied and require that chemical potential is far below the cut-off energy, that is $\mu \ll E_c$. Accordingly, for numerical calculations, the module of cut-off wavevector, k_c, is defined as $k_c = \hbar^2/(3m\lambda)$ and corresponds to the local maximum of the energy dispersion for the lower (i.e., E_-) branch (see inset in the upper right corner of Fig. 1(f)). Since the cut-off wavevector depends on the effective mass and Rashba coupling constant, thus the energy window related to the reasonable changes of the chemical potential also strongly depend on them. This is shown in Fig. 1(f), where k_c is plotted as a function of the quasiparticle effective mass. Additionally, the Fermi contours fixed for the same Fermi energy, for different values of effective mass are shown. Evidently, the anisotropy of energy bands is more pronounced at higher effective masses.

The casual Green function corresponding to the Hamiltonian (1) has the following explicit form:

$$G_{\mathbf{k}}(\varepsilon) = G_{\mathbf{k}0}\,\sigma_0 + G_{\mathbf{k}x}\,\sigma_x + G_{\mathbf{k}y}\,\sigma_y \tag{2}$$

with coefficients:

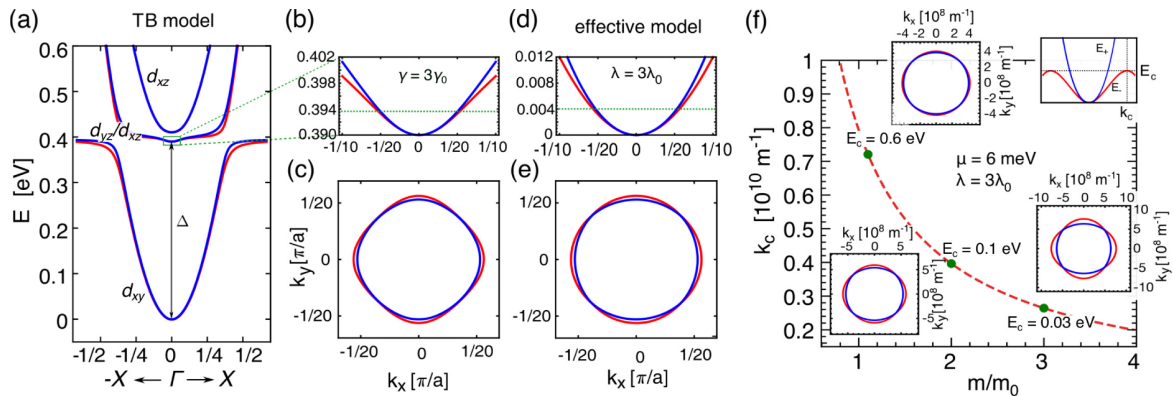$$G_{\mathbf{k}0} = \frac{1}{2}(G_{\mathbf{k}+} + G_{\mathbf{k}-}), \tag{3}$$

$$G_{\mathbf{k}x} = \frac{\lambda k^3}{4\xi_{\mathbf{k}}}\left(\sin(\phi) - \sin\left(3\phi\right)\right)(G_{\mathbf{k}+} - G_{\mathbf{k}-}), \tag{4}$$

$$G_{\mathbf{k}y} = \frac{\lambda k^3}{4\xi_{\mathbf{k}}}\left(\sin(\phi) + \sin\left(3\phi\right)\right)(G_{\mathbf{k}+} - G_{\mathbf{k}-}), \tag{5}$$

$$G_{\mathbf{k}z} = \frac{M}{2\xi_{\mathbf{k}}}(G_{\mathbf{k}+} - G_{\mathbf{k}-}), \tag{6}$$

where $G_{\mathbf{k}\pm} = [\varepsilon + \mu - E_\pm + i\delta\,\mathrm{sgn}(\varepsilon)]^{-1}$ with the eigenvalues $E_\pm = \epsilon_k \pm \xi_{\mathbf{k}}$ ($\epsilon_k = \hbar^2 k^2/2m$ and $\xi_{\mathbf{k}} = \sqrt{M^2 + \lambda^2 k^6\cos^2(2\phi)}$).

Fig. 1. Band structure of the electronic states at the interface of LAO/STO obtained based on TB model (a)–(c) and effective model for close vicinity of the Γ point (d), (e). The lowest in energy pair of bands originates mainly from the d_{xy} orbital, the middle pair of bands originates from the mixing of d_{xz} and d_{yz} orbitals, whereas the highest in energy pair of bands is formed mainly by the orbital d_{xz}. Figures (c) and (e) show constant energy contours at 4 meV above the bands minima in TB and effective model respectively. The anisotropy of energy spectrum in the $\mathbf{k}$-space is seen in both models. Figure (f) presents the cut-off wavevector as a function of the effective mass, and Fermi contours obtained for selected values of effective mass. The TB model and parameters such as lattice constant $a = 4.05$ Å, hopping integrals: $t_1 = 0.227$ eV, $t_2 = 0.031$ eV, $t_3 = 0.076$ eV, parameters $\Delta = 0.4$ eV, $\gamma = 0.02$ eV, and atomic spin-orbit coupling parameter $\Delta_{ASO} = 0.01$ eV are taken from Ref. [20].

2.2. Anomalous Hall conductivity

To calculate the anomalous Hall conductivity (AHC), the Matsubara Green's function formalism has been used (see e.g. [35–39]). In the linear response regime, the transverse charge current density induced by external electric field can be derived based on the following expression:

$$j_x\left(i\omega_m\right) = k_B T \sum_{\mathbf{k},n} \text{Tr}\{\hat{j}_x\, G_\mathbf{k}(i\varepsilon_n + i\omega_m)\widehat{H}_\mathbf{A}(i\omega_m)G_\mathbf{k}(i\varepsilon_n)\},\tag{7}$$

where $G_\mathbf{k}(i\varepsilon_n)$ denotes Matsubara Green's function corresponding to the unperturbed Hamiltonian (1) with $\varepsilon_n = (2n+1)\pi k_B T$, $\omega_m = 2m\pi k_B T$ being Matsubara energies, and k_B is the Boltzmann constant. The charge current density operator is defined as $\hat{j}_i = e\hat{v}_i$ where e is the electron charge and the velocity operator is defined as $\hat{v}_i = \hbar^{-1}\partial_{k_i}\widehat{H}$. The perturbation Hamiltonian $\widehat{H}_\mathbf{A}$ describing the coupling of quasiparticles with an external electric field is given in the form:

$$\widehat{H}_\mathbf{A}(i\omega_m) = -\hat{j}_y A_y(i\omega_m),\tag{8}$$

where the amplitude of electromagnetic field is linked with the amplitude of electric field through the well known relation: $A_y(i\omega_m) = -i\hbar E_y(i\omega_m)/i\omega_m$. The sum over Matsubara energies has been done using the method of contour integration and analytical continuation for Green's function [35]. Finally, the expression for AHC receives the following form:

$$\sigma_{xy}(\omega) = -\frac{e^2\hbar}{\omega}\text{Tr}\int\frac{d^2\mathbf{k}}{(2\pi)^2}\int\frac{d\varepsilon}{2\pi}f(\varepsilon)[\hat{v}_x G_\mathbf{k}^R(\varepsilon+\omega)\hat{v}_y[G_\mathbf{k}^R(\varepsilon) - G_\mathbf{k}^A(\varepsilon)] + \hat{v}_x[G_\mathbf{k}^R(\varepsilon) - G_\mathbf{k}^A(\varepsilon)]\hat{v}_y G_\mathbf{k}^A(\varepsilon-\omega)],\tag{9}$$

where $G_\mathbf{k}^{R/A} = [(\varepsilon + \mu \pm i\Gamma)\sigma_0 - \widehat{H}]^{-1}$ stands for retarded/advanced Green's function, Γ is a quasiparticle relaxation rate ($\Gamma = \hbar/2\tau$, τ – relaxation time), μ is a chemical potential, and $f(\varepsilon)$ denotes the Fermi-Dirac distribution function. The Eq. (9) is a starting formula for further numerical and analytical calculations.

2.3. Anomalous Nernst conductivity

The anomalous Nernst conductivity (ANC) can be also found based on Matsubara Green's function formalism. One can start from equation similar to Eq. (7), but with the perturbation Hamiltonian defining as follows:

$$\widehat{H}_\mathcal{A}(i\omega_m) = -\hat{j}_y^h\, \mathcal{A}_y(i\omega_m),\tag{10}$$

where $\hat{j}_y^h$ is a heat current density operator and $\mathcal{A}$ is an artificial gravitational vector potential amplitude related to the temperature gradient by the following expression: $\mathcal{A}(i\omega_m) = i\hbar\nabla_y T(i\omega_m)/(i\omega_m T)$ (for details see e.g. [38,40–42]).

In turn, it is also known that some thermal transport coefficients obtained within the Kubo-like formalism behave unphysically when the temperature tends to zero. Thus, to satisfy the Onsager relations, the magnetization currents should be taken into account. Other words, for the anomalous Nernst effect, to obtain results satisfying the third thermodynamic law, one should add to the expression derived from the Kubo formula an additional term related to the orbital magnetization current density. In this manuscript, quite tedious calculations of the orbital magnetization are omitted due to the fact that in the model under consideration the AHE is determined by the topological component. In such a case it is easier to calculate the transverse heat current conductivity, β_{xy}, which intrinsic contribution is expressed by the entropy density of the electron gas, $S_n(\mathbf{k})$, and the Berry curvature, $\mathscr{B}_n^z$. Since the transverse heat current conductivity is related to the transverse heat conductivity by the Onsager relation, $\beta_{xy} = \alpha_{xy}T$, ANC is

given by the following expression [43,44]:

$$\alpha_{xy} = \frac{ek_B}{\hbar}\sum_{n=\pm}\int\frac{d^2\mathbf{k}}{(2\pi)^2}\mathscr{B}_n^z(\mathbf{k})S_n(\mathbf{k}).\tag{11}$$

The entropy density for the n-th subband is given by the equation:

$$S_n(\mathbf{k}) = -f_\mathbf{k}(E_n)\ln[f_\mathbf{k}(E_n)] - (1 - f_\mathbf{k}(E_n))\ln[1 - f_\mathbf{k}(E_n)]\tag{12}$$

and the Berry curvature is calculated from the expression:

$$\mathscr{B}_n^z(\mathbf{k}) = i\,\nabla_\mathbf{k}\times\langle\Psi_n|\nabla_\mathbf{k}|\Psi_n\rangle,\tag{13}$$

with Ψ_n standing for the eigenvector related to the n-th eigenvalue of the Hamiltonian (1).

3. Results and discussion

Evaluation of the Eq. (9) for AHC and Eq. (11) for ANC allows to obtain analytical and numerical results. Eq. (9) has to be integrated analytically over ε and next the dc-limit ($\omega\to 0$) has to be taken. Moreover, after a long discussion about different origins of AHE and proper nomenclature related to its different origins (see, e.g., [29]), the AHC is commonly expressed as a sum of two components:

$$\sigma_{xy} = \sigma_{xy}^I + \sigma_{xy}^{II}.\tag{14}$$

The first component, $\sigma_{xy}^I[f'(E_\pm)]$, is the contribution from the states at the Fermi level and the second one, $\sigma_{xy}^{II}[f(E_\pm)]$, describes contribution from all states below the Fermi level (so-called Fermi sea or topological component).

Here we consider the quasi-ballistic limit, that means low impurities concentration and weak scattering on impurities, which results in $\Gamma\to 0$. In this case, we found that the component σ_{xy}^I is a few orders of magnitude smaller than the contribution from σ_{xy}^{II} and can be neglected. Thus, the electronic properties of the system described by anisotropic $\mathbf{k}$-cubed Rashba model is determined by the quasi-particle states from the Fermi sea, and:

$$\sigma_{xy}^{II} = -\frac{3e^2M\lambda^2}{8\pi^2\hbar}\int d\phi dk\,\frac{k^5}{\xi_\mathbf{k}^3}\cos^2\left(2\phi\right)[f(E_-) - f(E_+)].\tag{15}$$

This result might be verified easily taking into account the fact that the topological contribution to the AHC may be derived based on the knowledge of the local value of the Berry phase in the system [45–47]:

$$\sigma_{xy}^{II} = -\frac{e^2}{\hbar}\sum_{n=\pm}\int\frac{d^2\mathbf{k}}{(2\pi)^2}\mathscr{B}_n^z(\mathbf{k})f(E_n).\tag{16}$$

The Berry curvature for the considered model has the following explicit form:

$$\mathscr{B}_\pm^z(\mathbf{k}) = \mp\frac{3}{2\xi_\mathbf{k}^3}k^4M\lambda^2\cos^2\left(2\phi\right).\tag{17}$$

Thus, inserting (17) into (16) gives immediately Eq. (15). In turn, taking into account Eq. (11) the expression for ANC reads:

$$\alpha_{xy} = \frac{3eM\lambda^2 k_B}{8\pi^2\hbar}\int d\phi dk\,\frac{k^5\cos^2(2\phi)}{\xi_\mathbf{k}^3}[S_-(\mathbf{k}) - S_+(\mathbf{k})].\tag{18}$$

Fig. 2 presents numerical results for anomalous Hall conductivity as a function of temperature, T, saturation magnetization, M_0, and Rashba coupling constant, λ. The AHC increases slightly with the temperature reaching a maximum at certain value of T, and next decreasing to vanish at T equal the Curie temperature ($T = T_C$), where the phase

A. Krzyżewska and A. Dyrdał
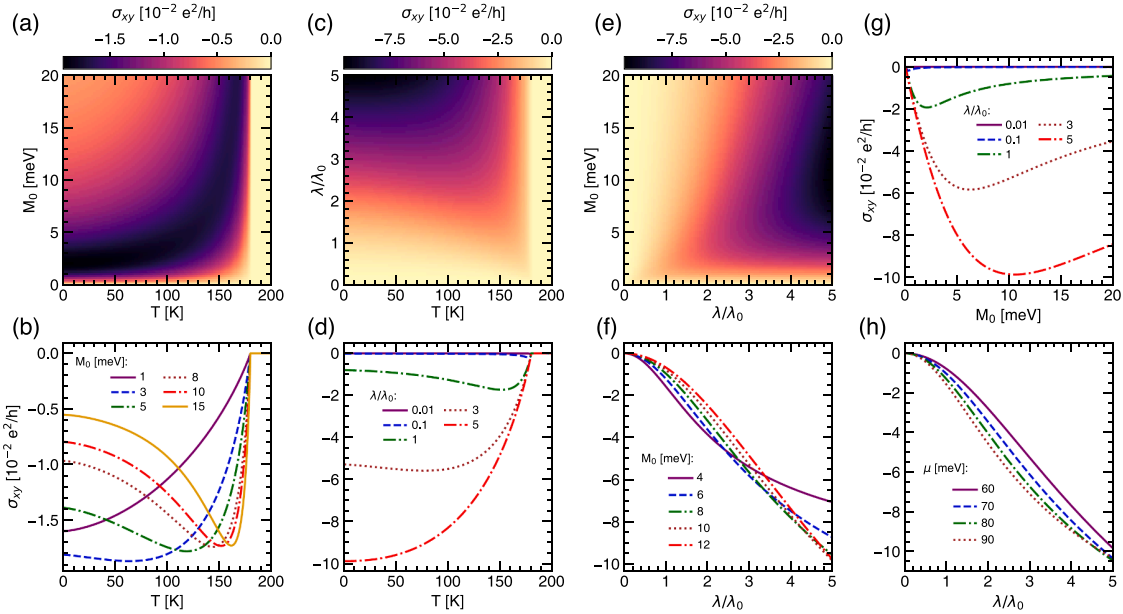
Fig. 2. Anomalous Hall conductivity as a function of temperature, T, and saturation magnetization, M_0, (a), (b), (g); temperature and Rashba coupling constant, λ, (c), (d); Rashba constant and saturation magnetization (e), (f), (h); Other parameters (unless otherwise specified): $\mu = 60$ meV, $M_0 = 10$ meV, $\lambda_0 = 1.07 \cdot 10^{-30}$ eV m^3, $T = 10$ K, $T_C = 180$ K, $\Gamma = 0.005$ meV, $m = 1.14 m_0$.
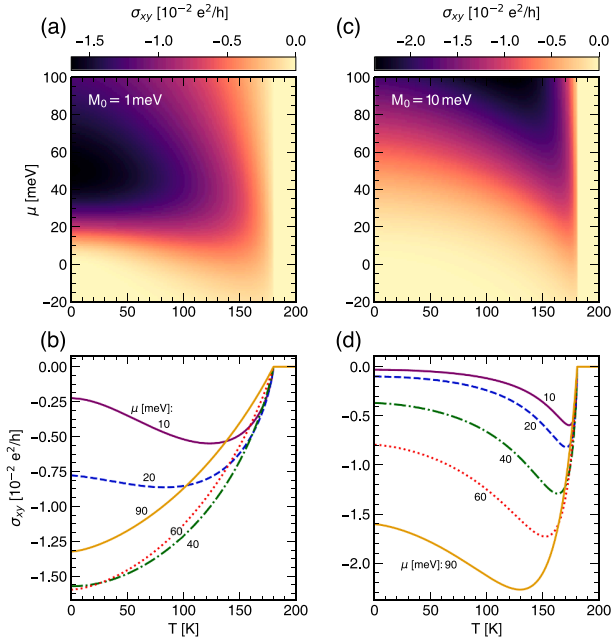
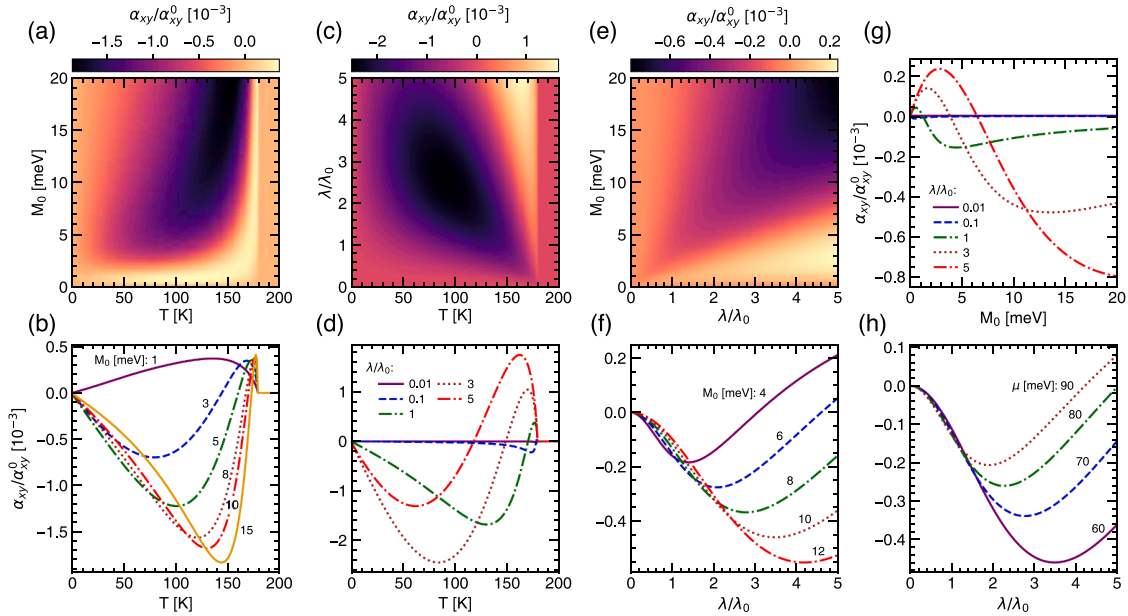
Fig. 3. Anomalous Hall conductivity as a function of chemical potential, μ, and temperature T (a), (c). The cross sections of the plots (a) and (c) at fixed values of μ (b), (d). Other parameters are the same as in Fig.2.

transition occurs, and a system becomes nonmagnetic (Fig. 2(a)–(d)). Moreover, one can easily see that the maximum value of AHC is shifted to higher temperatures with increasing the saturation magnetization (Fig. 2(a) and (b)). For higher temperatures and larger M_0 the maximum of AHC is well pronounced and precedes the magnetic phase transition. Furthermore, the competition between the strength of spin-orbit coupling and saturation magnetization is clearly seen in Fig. 2(e)–(h). AHC increases with the saturation magnetization, reaches a maximum, and then saturates. In general, for the fixed M_0 and μ, the absolute value of the anomalous Hall conductivity increases with

increasing λ. Note that the chemical potential is fixed with changing the temperature, that is, the number of quasiparticles may be changed. With increasing the temperature the magnetization decreases and the subbands splitting degeneracy also decreases. Moreover, the blurring of quasiparticles distribution also increases. In consequence, the AHC decreases with temperature. The AHC behave quite non-monotonous with the variation of the chemical potential. For the fixed value of saturation magnetization, we observe that AHC increases with increasing the chemical potential but after reaching maximum it decreases and becomes zero at $T = T_C$ (Fig. 3(a) and (b)). Moreover, the maximum of the absolute value of AHC moves to higher values of μ and T if the saturation magnetization, M_0, in the system is higher (compare Fig. 3(a) and (b) with (c) and (d)). Note also that the AHC is almost zero when only one subband is occupied (that is, for Fermi level in the Zeeman gap). Only when the temperature is sufficiently large, in comparison to M_0, the thermal smearing of charge carriers distribution in both bands leads to nonzero AHC, also for negative values of μ, what is seen in Fig. 3.

Fig. 4 shows the anomalous Nernst conductivity as a function of the same parameters as for AHC, that is the temperature, T, saturation magnetization, M_0, and Rashba constant, λ. For fixed value of chemical potential (here $\mu = 60$ meV), and sufficiently large saturation magnetization one can observe that the anomalous Nernst conductivity increases almost linearly with temperature and then, for a certain value of T, decreases abruptly and change the sign to reach well define pick for temperatures preceding the Curie temperature (Fig. 4(a)–(d)). Both maxima (maximal negative and positive values) occur for higher temperatures when saturation magnetization, M_0 is higher (Fig. 4(b)) or the spin-orbit coupling parameter is smaller, λ (Fig. 4(d)). Moreover, one can see very non-monotonous behavior of ANC as a function of both M_0 and λ (Fig. 4(e)–(h)). When the spin-orbit coupling is sufficiently large (i.e., it dominates the exchange interaction), ANC takes positive values and increases with M_0. After reaching a maximum, the ANC decreases, and for a certain value of M_0 it changes sign and approaches minimum. Finally, the absolute value of ANC slightly decreases and saturates for sufficiently large values of M_0. When exchange interaction dominates the Rashba one, the ANC is always negative. This is also very good seen in Fig. 5 where ANC is presented as a function of temperature and

Fig. 4. Anomalous Nernst conductivity as a function of temperature, T, and saturation magnetization, M_0, (a), (b), (g); temperature and Rashba coupling constant, α, (c), (d); Rashba constant and saturation magnetization (e), (f), (h). Other parameters are as in the Fig. 2.
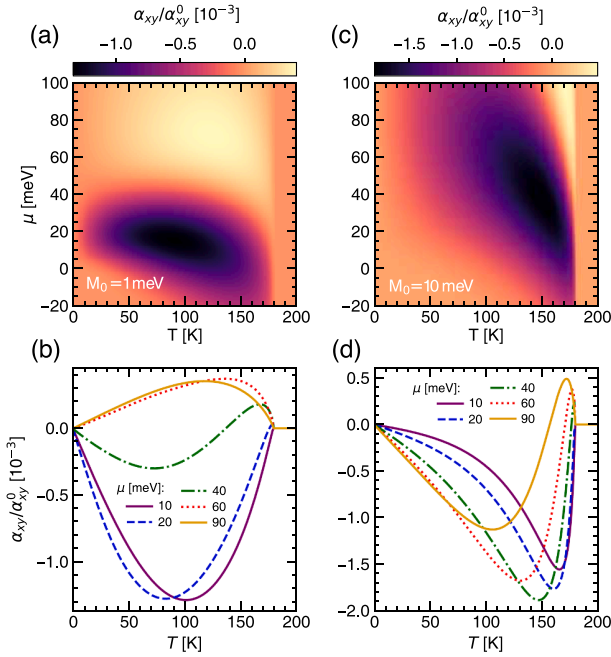
Fig. 5. ANC as a function of chemical potential, μ, and temperature, T (a), (c). The cross sections of the plots (a) and (c) at fixed values of μ (b), (d). Other parameters are the same as in Fig. 2.

chemical potential for the two different values of M_0.

One of the most important features in the behavior of ANC is the change of its sign, that occurs for temperatures preceding the magnetic phase transition. The similar sign reversal of ANC as a function of temperature has been observed experimentally in different oxides materials (such as LSMO thin layers and SRO crystals) [48,49] as well as in ferromagnetic semiconductors [50]. In the case of all these experimental data, the intrinsic mechanism has been confirmed as a dominant one. This behavior seems to be in agreement with our theoretical studies that show unambiguously that the topological contribution governs the behavior of both anomalous Hall and anomalous Nernst effect.

Moreover, this is also consistent with our previous study for the two-dimensional gas with isotropic cubic Rashba coupling [51].

4. Conclusions

The anomalous Hall and Nernst effect have been studied in the magnetized two-dimensional electron gas with anisotropic **k**-cubed Rashba spin-orbit interaction. It has been shown that the topological term determines anomalous Hall and anomalous Nernst conductivity. The contribution from the states at the Fermi level to both conductivities are few orders of magnitude smaller and does not affect the total system responses. Such behavior of AHE (ANE) in the systems revealing **k**-cubic Rashba interaction is distinct in comparison to the systems with **k**-linear Rashba coupling where AHE is nonzero only when the carriers relaxation times are finite and spin-dependent (see, e.g., [52]). Moreover, the change of sign in ANC has been observed in temperature dependences. The sign reversal precedes the magnetic phase transition and has been observed recently in experiments for magnetic perovskite oxides. The system responses for the model studied in this paper might be changed when one takes into account scattering processes (taking corrections related to the vertex correction, skew-scattering, and side-jump, randomness of spin-orbit coupling, etc.) related to the impurities with a magnetic moment and spin-orbit coupling. All these processes (that will be studied separately elsewhere) may modify the contribution from the states at the Fermi level remaining the topological contribution unchanged.

References

[1] A. Soumyanarayanan, N. Reyren, A. Fert, C. Panagopoulos, Emergent phenomena induced by spin–orbit coupling at surfaces and interfaces, Nature 539 (2016) 509.
[2] D.D. Awschalom, R. Epstein, R. Hanson, The diamond age diamond age of spintronics, Sci. Am. 297 (2007) 84.
[3] S.D. Bader, S.S.P. Parkin, Spintronics, Annu. Rev. Condens. Matter Phys. 1 (2010) 71.

[4] J. Sinova, I. Žutić, New moves of the spintronics tango, Nat. Mater. 11 (2012) 368.

[5] D.D. Awschalom, M.E. Flatté, Challenges for semiconductor spintronics, Nat. Phys. 3 (2007) 153.

[6] J. Fabian, A. Matos-Abiaguea, C. Ertler, P. Stano, I. Žutić, Semiconductor spin-tronics, Acta Phys. Slovaca 57 (2007) 565.

[7] Yu.A. Bychkov, E.I. Rashba, Properties of a 2D electron gas with lifted spectral degeneracy, Soviet J. Exp. Theor. Phys. Lett. 39 (1984) 78.

[8] R. Winkler, Spin-Orbit Coupling Effects in Two-Dimensional Electron and Hole Systems, Springer, Berlin, Heidelberg, 2003.

[9] H.-A. Engel, E.I. Rashba, B.I. Halperin, Theory of Spin Hall effects in semi-conductors, in: H. Kronmüller, S. Parkin (Eds.), Handbook of Magnetism and Advanced Magnetic Materials, John Wiley & Sons Ltd, Chichester, UK, 2007, pp. 2858–2877.

[10] D. Bercioux, P. Lucignano, Quantum transport in Rashba spin–orbit materials: a review, Rep. Prog. Phys. 78 (2015) 106001.

[11] J.M. Luttinger, W. Kohn, Motion of electrons and holes in perturbed periodic fields, Phys. Rev. 97 (1955) 869.

[12] J.M. Luttinger, Quantum theory of cyclotron resonance in semiconductors: general theory, Phys. Rev. 102 (1956) 1030.

[13] R. Winkler, Rashba spin splitting in two-dimensional electron and hole systems, Phys. Rev. B 62 (2000) 4245.

[14] R. Winkler, D. Culcer, S.J. Papadakis, B. Habib, M. Shayegan, Spin orientation of holes in quantum wells, Semicond. Sci. Technol. 23 (2008) 114017.

[15] C.-X. Liu, B. Zhou, S.-Q. Shen, B.-F. Zhu, Current-induced spin polarization in a two-dimensional hole gas, Phys. Rev. B 77 (2008) 125345.

[16] R. Moriya, K. Sawano, Y. Hoshi, S. Masubuchi, Y. Shiraki, A. Wild, C. Neumann, G. Abstreiter, D. Bougeard, T. Koga, T. Machida, Cubic Rashba spin-orbit interaction of a two-dimensional hole gas in a strained-Ge/SiGe quantum well, Phys. Rev. Lett. 113 (2014) 086601.

[17] Y. Kim, R.M. Lutchyn, C. Nayak, Origin and transport signatures of spin-orbit interactions in one- and two-dimensional SrTiO3-based heterostructures, Phys. Rev. B 87 (2013) 245121.

[18] K.V. Shanavas, Theoretical study of the cubic Rashba effect at the SrTiO$_3$(001) surfaces, Phys. Rev. B 93 (2016) 045108.

[19] J. Zhou, W.-Y. Shan, D. Xiao, Spin responses and effective Hamiltonian for the two-dimensional electron gas at the oxide interface LaAlO$_3$/SrTiO$_3$, Phys. Rev. B 91 (2015) 241302.

[20] G. Seibold, S. Caprara, M. Grilli, R. Raimondi, Theory of the Spin galvanic effect at oxide interfaces, Phys. Rev. Lett. 119 (2017) 256801.

[21] A. Brinkman, M. Huijben, M. van Zalk, J. Huijben, U. Zeitler, J.C. Maan, W.G. van der Wiel, G. Rijnders, D.H.A. Blank, H. Hilgenkamp, Magnetic effects at the inter-face between non-magnetic oxides, Nat. Mater. 6 (2007) 493.

[22] N. Reyren, S. Thiel, A.D. Caviglia, L.F. Kourkoutis, G. Hammerl, C. Richter, C.W. Schneider, T. Kopp, A.-S. Rüetschi, D. Jaccard, M. Gabay, D.A. Muller, J.-M. Triscone, J. Mannhart, Superconducting interfaces between insulating oxides, Science 317 (2007) 1196.

[23] K. Michaeli, A.C. Potter, P.A. Lee, Superconducting and ferromagnetic phases in SrTiO$_3$/LaAlO$_3$ oxide interface structures: possibility of finite momentum pairing, Phys. Rev. Lett. 108 (2012) 117003.

[24] A. Mawrie, T.K. Ghosh, Optical conductivity of a 2DEG with anisotropic Rashba interaction at the interface of SrTiO$_3$/LaAlO$_3$, J. Phys.: Condens. Matter 28 (2016) 42530.

[25] E. Lesne, Y. Fu, S. Oyarzun, J.C. Rojas-Sánchez, D.C. Vaz, H. Naganuma, G. Sicoli, J.-P. Attané, M. Jamet, E. Jacquet, J.-M. George, A. Barthélémy, H. Jaffrés, A. Fert, M. Bibes, L. Vila, Highly efficient and tunable spin-to-charge conversion through Rashba coupling at oxide interfaces, Nat. Mater. 15 (2016) 1261.

[26] J.-Y. Chauleau, M. Boselli, S. Gariglio, R. Weil, G. de Loubens, J.-M. Triscone, M. Viret, Efficient spin-to-charge conversion in the 2D electron liquid at the LAO/STO interface, EPL 116 (2016) 17006.

[27] Q. Song, H. Zhang, T. Su, W. Yuan, Y. Chen, W. Xing, J. Shi, J. Sun, W. Han, Observation of inverse Edelstein effect in Rashba-split 2DEG between SrTiO$_3$ and LaAlO$_3$ at room temperature, Sci. Adv. 3 (2017) e1602312.

[28] Y. Wang, R. Ramaswamy, M. Motapothula, K. Narayanapillai, D. Zhu, J. Yu, T. Venkatesan, H. Yang, Room-temperature giant charge-to-spin conversion at the SrTiO$_3$/LaAlO$_3$ oxide interface, Nano Lett. 17 (2017) 7659.

[29] N. Nagaosa, J. Sinova, S. Onoda, A.H. MacDonald, N.P. Ong, Anomalous Hall effect, Rev. Mod. Phys. 82 (2010) 1539.

[30] G. Khalsa, B. Lee, A.H. MacDonald, Theory of t_2g) electron-gas Rashba interac-tions, Phys. Rev. B 88 (2013) 041302.

[31] Z. Zhong, A. Tóth, K. Held, Theory of spin-orbit coupling at LaAlO3/SrTiO3 inter-faces and SrTiO3 surfaces, Phys. Rev. B 87 (2013) 161102.

[32] Z.S. Popović, S. Satpathy, R.M. Martin, Origin of the two-dimensional electron gas carrier density at the LaAlO$_3$ on SrTiO$_3$ interface, Phys. Rev. Lett. 101 (2008) 256801.

[33] K.V. Shanavas, Z.S. Popović, S. Satpathy, Theoretical model for Rashba spin-orbit interaction in d electrons, Phys. Rev. B 90 (2014) 165108.

[34] N. Ashcroft, N. Mermin, Magnetic Ordering, Saunders College, Philadelphia, 1976.

[35] G.D. Mahan, Many-Particle Physics, Springer, US, 2000.

[36] A.L. Fetter, J.D. Walecka, Quantum Theory of Many-particle Systems, Courier Corporation, 2003.

[37] P. Streda, Theory of quantised Hall conductivity in two dimensions, J. Phys. C: Solid State Phys. 15 (1982) L717.

[38] A. Dyrdał, J. Barnaś, V.K. Dugaev, Spin Hall and spin Nernst effects in a two-di-mensional electron gas with Rashba spin-orbit interaction: temperature depen-dence, Phys. Rev. B 94 (3) (2016) 035306.

[39] T.S. Nunner, N.A. Sinitsyn, M.F. Borunda, V.K. Dugaev, A.A. Kovalev, Ar. Abanov, C. Timm, T. Jungwirth, J.-I. Inoue, A.H. MacDonald, J. Sinova, Anomalous Hall effect in a two-dimensional electron gas, Phys. Rev. B 76 (2007) 235312.

[40] J.M. Luttinger, Theory of thermal transport coefficients, Phys. Rev. 135 (1964) A1505.

[41] A. Dyrdał, M. Inglot, V.K. Dugaev, J. Barnaś, Thermally induced spin polarization of a two-dimensional electron gas, Phys. Rev. B 87 (2013) 245309.

[42] G. Tatara, Thermal vector potential theory of transport induced by a temperature gradient, Phys. Rev. Lett. 114 (2015) 196601.

[43] D. Xiao, Y. Yao, Z. Fang, Q. Niu, Berry-phase effect in anomalous thermoelectric transport, Phys. Rev. Lett. 97 (2) (2006) 026603.

[44] C. Zhang, S. Tewari, V.M. Yakovenko, S. Das Sarma, Anomalous Nernst effect from a chiral d-density-wave state in underdoped cuprate superconductors, Phys. Rev. B 78 (2008) 174508.

[45] D.J. Thouless, M. Kohmoto, M.P. Nightingale, M. Den Nijs, Quantized Hall con-ductance in a two-dimensional periodic potential, Phys. Rev. Lett. 49 (1982) 405.

[46] F.D.M. Haldane, Berry curvature on the fermi surface: anomalous Hall effect as a topological fermi-liquid property, Phys. Rev. Lett. 93 (2004) 206602.

[47] D. Xiao, M.-C. Chang, Q. Niu, Berry phase effects on electronic properties, Rev. Mod. Phys. 82 (2010) 1959.

[48] C.T. Bui, F. Rivadulla, Anomalous and planar Nernst effects in thin films of the half-metallic ferromagnet La$_{2/3}$MnO$_3$, Phys. Rev. B 90 (2014) 100403.

[49] T. Miyasato, N. Abe, T. Fujii, A. Asamitsu, S. Onoda, Y. Onose, N. Nagaosa, Y. Tokura, Crossover behavior of the anomalous Hall effect and anomalous Nernst effect in itinerant ferromagnets, Phys. Rev. Lett. 99 (2007) 086602.

[50] Y. Pu, D. Chiba, F. Matsukura, H. Ohno, J. Shi, Mott relation for anomalous Hall and Nernst effects in Ga$_{1-x}$Mn$_x$As ferromagnetic semiconductors, Phys. Rev. Lett. 101 (2008) 117208.

[51] A. Krzyżewska, A. Dyrdał, J. Barnaś, J. Berakdar, Anomalous Hall and Nernst effects in 2D systems: role of cubic rashba spin-orbit coupling, Phys. Status Solidi RRL 12 (2018) 1800232.

[52] J.-I. Inoue, T. Kato, Y. Ishikawa, H. Itoh, G.E.W. Bauer, L.W. Molenkamp, Vertex corrections to the anomalous Hall effect in spin-polarized two-dimensional electron gases with a rashba spin-orbit interaction, Phys. Rev. Lett. 97 (2006) 046604.

4.4 Reprint of the article A-4

The presented article entitled "Non-equilibrium spin polarization in magnetic two-dimensional electron gas with k-linear and k-cubed Dresselhaus spin-orbit interaction" provides the analysis of spin polarization induced by the external electric field in a 2D system of zinc-blende structure with symmetric quantum well grown in the [001]-direction.
In general, the exchange field in the out-of-plane direction is assumed. The exchange field emerges when the electron gas forms at the interfaces, e.g., n-type diluted magnetic semiconductor heterostructures (n-type DMS). Another possibility is that the magnetization in the 2DEG results from a proximity effect, i.e., due to coupling with a magnetic substrate.

The Kubo formula within Matsubara-Green's functions formalism is used to analyze current-induced spin polarization (CISP) in both non-magnetic and magnetic systems. Specifically, the influence of the cubic Dresselhaus term on the results is investigated. Additionally, the intrinsic contribution to the system's response, namely, the transverse component of non-equilibrium spin polarization and anomalous Hall effect, is identified.

Non-equilibrium spin polarization in magnetic two-dimensional electron gas with k-linear and k-cubed Dresselhaus spin–orbit interaction

A. Krzyżewska, A. Dyrdał*

Department of Mesoscopic Physics, ISQI, Faculty of Physics, Adam Mickiewicz University, ul. Uniwersytetu Poznańskiego 2, 61-614 Poznań, Poland

A R T I C L E   I N F O

A B S T R A C T

The current-induced spin polarization (CISP) of charge carriers is one of the main mechanisms of spin-to-charge interconversion effects that can be used in new spintronics devices. Here, CISP is studied theoretically in symmetric quantum wells growing in [001] crystallographic direction, where both k-linear and k-cubed Dresselhaus spin–orbit interactions are present. The exchange interaction responsible for perpendicular to plane net magnetization is also taken into account. The main focus is on the influence of cubic Dresselhaus term on CISP and the interplay between spin–orbit interaction (SOI) and the exchange field. The analytical and numerical results are derived within the linear response theory and Matsubara Green's function formalism. Apart from detailed numerical results, we also provide some analytical expressions that may be useful for interpretation of experimental results and for characterization of quantum wells with Dresselhaus SOI. Analytical expressions for the relevant Berry curvature are also derived, and it is shown that the Berry curvature in magnetic 2DEG with cubic Dresselhaus interaction oscillates in the k-space, while its averaged value is reduced. We also analyze the temperature behavior of CISP and calculate the low-temperature spin polarizability due to heat current.

1. Introduction

The efficient control of the spin degree of freedom is nowadays one of the most important aspect of solid state physics and cornerstone for further development of spin electronics. The spin–orbit interaction couples intrinsically orbital and spin degrees of freedom and provides a variety of phenomena enabling all-electric control of the spin. The spin Hall effect (SHE) is probably the most prominent example where the charge current (i.e., external electric field) in a non-magnetic sample generates pure transverse spin current (or spin accumulation at the sample edges) [1–3]. Additionally the electric current flowing through the sample induces a non-equilibrium spin polarization of charge carriers. This phenomenon is known as the Edelstein effect or inverse spin galvanic effect [4–7]. Both effects after only fifteen years of their experimental observation [8–11], have become widely used tools for generation and control of spin currents and spin accumulation. They are also strong enough to induce magnetoresistance effects and spin dynamics [12–14].

The semiconductor heterostructures, with a two-dimensional electron gas (2DEG) forming at the interface, serve as a platform for the spin-to-charge interconversion effects. This is mainly due to well established methods of fabrication and externally tunable electronic properties (via doping, gating or strain). Moreover, structural and bulk inversion asymmetries lead to spin–orbit interactions of different nature (depending on gate voltage and growth direction with respect to the crystallographic axes), and in consequence, to various spin textures and spin dependent system responses [15–19]. The Rashba spin–orbit interaction is a consequence of the so-called structural inversion asymmetry. Here, the confinement potential of quantum well is asymmetric. Importantly, the strength of Rashba coupling can be tuned by the gate voltage or doping. In turn, the spin–orbit interaction related to the bulk inversion asymmetry of the underlying crystal is known as Dresselhaus spin–orbit coupling [20] and its form depends on the growth direction with respect to the crystallographic axis. Both Rashba and Dresselhaus spin–orbit couplings are proportional to odd powers of wavevector **k** with the dominant contribution of k-linear and k-cubed terms.

Recently, in the context of spin-to-charge interconversion phenomena, the Rashba spin–orbit coupling focuses enormous attention [21, 22]. It is studied not only in semiconductor heterostructures but also in other structures without inversion symmetry, i.e., at the interfaces of perovskite oxides, perovskite halides thin films, surface or subsurface states of germanium Ge[111], gold Au[111], bismuth Bi[111], and Bi/Ag alloys [111] [23–29]. The anomalous and spin Hall effect, as well as the current-induced spin polarization have been extensively discussed within the Rashba 2DEG in the presence and absence of

---

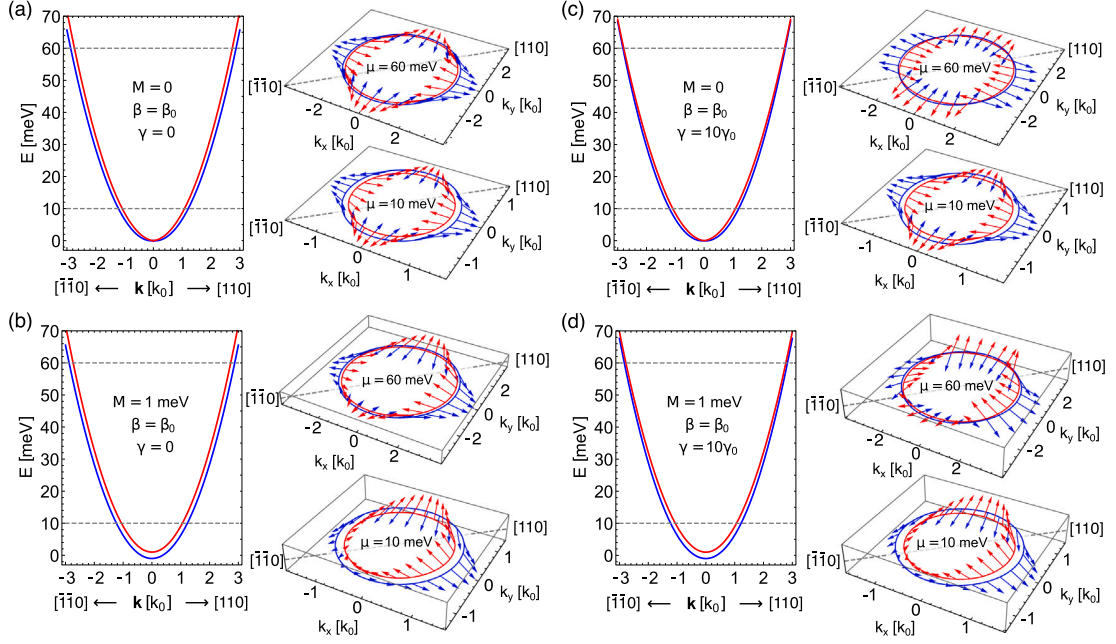**Fig. 1.** Dispersion curves in nonmagnetic ((a), (c)) and magnetic ((b), (d)) 2DEG with linear Dresselhaus spin–orbit interaction in the presence ((c), (d)) and absence ((a), (b)) of cubic Dresselhaus spin–orbit coupling term γ. The right side of each part shows the corresponding expectation values of spin for two different values of chemical potential ($\mu = \{10, 60\}$ eV m). The linear and cubic Dresselhaus coupling constants are equal respectively $\beta_0 = 1 \cdot 10^{-11}$ eV m, and $\gamma_0 = 20 \cdot 10^{-30}$ eV m³, effective mass $m = 0.05 m_0$ and $k_0 = 10^8$ m⁻¹.

external magnetic field, or different types of scattering potentials (see reviews e.g., [3,30] and references therein).

Here we focus on 2D electron gas with Dresselhaus spin–orbit interaction, as a basic model describing symmetric semiconducting quantum wells, and present detail characteristics of the current-induced spin polarization. In case of quantum wells growing in the [001] crystallographic direction, build by semiconductors with zinc-blende structure, the lowest order contribution to conduction band spin–orbital splitting is given by the following Hamiltonian [19,20]:

$$\hat{\mathcal{H}}^D = \gamma[(k_y^2 - k_z^2)k_x\sigma_x + (k_z^2 - k_x^2)k_y\sigma_y + (k_x^2 - k_y^2)k_z\sigma_z],$$

where γ is spin–orbit coupling parameter. Since the quantum well is confined in the z-direction it is assumed for the lowest energy subband that $\langle k_z \rangle = 0$ and $\langle k_z^2 \rangle = \pi^2/L^2$, where L is a thickness of the quantum well. Accordingly, the dominant contribution to the Dresselhaus spin–orbit interaction comes from the linear in k term proportional to the coupling constant $\beta = \gamma\langle k_z^2 \rangle$. The k-cubed term manifests in wider, highly doped quantum wells, where its presence, in addition to k-linear Rashba and/or Dresselhaus term, can have important consequences. It leads, e.g., to the nonvanishing spin Hall effect in nonmagnetic 2DEG with scalar impurities, and nonzero anomalous Hall effect under uniform exchange field when two subbands are occupied [31–33]. It plays also an important role in the case of persistent spin-helix state detuning. Current-induced spin–orbit interaction in 2DEG with the linear in **k** Dresselhaus coupling has been studied, especially in the context of its interplay with linear Rashba interaction [34–36]. However, detailed characteristics of CISP for the model with both k-linear and k-cubic terms have got less attention [32,33,37]. Thus, we present results of detailed study of 2DEG with Dresselhaus spin orbit interaction defined by the above Hamiltonian. We focus, among others, on the role of the k-cubed Dresselhaus term and the role of temperature and net magnetization on the system response.

The paper is organized as follows. In Section 2 we introduce the model and formalism used for description of the non-equilibrium spin polarization. In Section 3 we consider nonmagnetic 2DEG with linear and cubic spin–orbit interaction, whereas in Section 4 we analyze in details the magnetic 2DEG in the presence of linear Dresselhaus SOC as

well as the most general case, i.e., magnetic 2DEG with both k-linear and k-cubic Dresselhaus terms. We discuss also the relation between the Berry curvature and anomalous Hall effect, as well as the component of spin polarization that appears only in the presence of exchange field. In Section 5 we discuss the thermally-induced spin polarization, that is related to the electrically-induced spin polarization at the low temperature by the Mott relation. The final discussion and summary is provided in Section 6.

2. Model and method

Here we focus on a magnetic two-dimensional electron gas forming at the interfaces in a symmetric quantum well. In such a case the Rashba spin–orbit coupling is reduced and the leading source of spin–orbit interaction originates from the bulk inversion asymmetry. The model Hamiltonian can be written as follows [18,19]:

$$\hat{\mathcal{H}} = \hat{\mathcal{H}}^{KIN} + \hat{\mathcal{H}}^D + \hat{\mathcal{H}}^M, \tag{1}$$

where the kinetic term, $\mathcal{H}^{KIN}$ has the well known form:

$$\hat{\mathcal{H}}^{KIN} = \varepsilon_k\sigma_0, \tag{2}$$

where $\varepsilon_k = \frac{\hbar^2 k^2}{2m}$ with $k^2 = k_x^2 + k_y^2$ and m being an effective mass of quasiparticles. The second term describes spin–orbit interaction of the Dresselhaus type, which in the case of 2DEG at the surface [001] has two components, i.e., k-linear and k-cubed respectively:

$$\hat{\mathcal{H}}^D = \hat{\mathcal{H}}^{LD} + \hat{\mathcal{H}}^{CD} \tag{3a}$$

$$\hat{\mathcal{H}}^{LD} = \beta(k_y\sigma_y - k_x\sigma_x), \tag{3b}$$

$$\hat{\mathcal{H}}^{CD} = \gamma(k_x k_y^2\sigma_x - k_y k_x^2\sigma_y). \tag{3c}$$

The spin–orbit coupling parameters β and γ are related to each other, i.e., $\beta = \gamma\langle k_z^2 \rangle$, where $\langle k_z^2 \rangle$ is the expectation value of k_z^2 with respect to the subband wave functions of quasiparticles in the quantum well, and γ depends on the underlying semiconductor bulk material. The last term in (1), $\hat{\mathcal{H}}^M$, describes the exchange interaction between spins of conduction electrons and localized magnetic moments, i.e., a net

A. Krzyżewska and A. Dyrdał

magnetization **M** oriented in the z-direction (normal to the plane of 2DEG), and takes the following explicit form:

$$\hat{H}^M = M\sigma_z. \qquad (4)$$

Here, the exchange energy is given by the parameter M in energy units. The matrices σ_0 and σ_α (where $\alpha = \{x, y, z\}$) are the identity and Pauli matrices acting in the spin space.

The eigenvalues corresponding to the Hamiltonian (1) have the following form: $E_\pm = \varepsilon_k \pm \xi_\mathbf{k}$, where $\xi_\mathbf{k} = \left[M^2 + \beta^2 k^2 - k_x^2 k_y^2 (4\beta\gamma - \gamma^2 k^2) \right]^{1/2}$. Fig. 1 presents the energy spectra corresponding to the all cases considered in this paper, that is: nonmagnetic (Fig. 1(a),(c)) and magnetic (Fig. 1(b),(d)) Dresselhaus 2DEG in the presence (Fig. 1(c),(d)) and absence (Fig. 1(a),(b)) of k-cubic correction to the Dresselhaus spin–orbit interaction. The expectation values of quasiparticles spin are also presented to emphasize how the out-of plane magnetization and the cubic Dresselhaus interaction modify equilibrium orientations of spins at the Fermi contours, and therefore the spin-dependent properties of 2DEG.

The non-equilibrium current-induced spin polarization may be found in the linear response to the external electric field within the Matsubara Green's function formalism [38]:

$$S_i(i\omega_m) = \Xi \sum_{\mathbf{k},n} \text{Tr}\left\{\hat{s}_i G_\mathbf{k}(i\varepsilon_n + i\omega_m)\hat{H}_\mathbf{A}(i\omega_m)G_\mathbf{k}(i\varepsilon_n)\right\}, \qquad (5)$$

where $\Xi = k_B T$ (k_B — Boltzmann constant, T — temperature), $\hat{s}_i = \frac{\hbar}{2}\sigma_i$ is i-th component of the spin operator, and $\hat{H}_\mathbf{A}$ is a perturbation Hamiltonian describing the interaction of electrons with an external electric field:

$$\hat{H}_\mathbf{A}(i\omega_m) = -\hat{v}_j A_j(i\omega_m). \qquad (6)$$

Here $\hat{v}_j$ is a j-th component of the velocity operator, and the amplitude of the electromagnetic vector potential has the following explicit form: $A_j(i\omega_m) = \hbar\frac{E_j(i\omega_m)}{i(i\omega_m)}$. $G_\mathbf{k}(i\varepsilon_n)$ stands for the Matsubara Green's functions, were $\varepsilon_n = (2n+1)\pi \Xi$ and $\omega_m = 2m\pi \Xi$ define Matsubara energies.

Eq. (5), after summation over Matsubara energies, takes the form:

$$S_i = \chi_{ij} e E_j, \qquad (7)$$

where the response function, χ_{ij}, also called the spin polarizability, can be written as follows:

$$\chi_{ij}(\omega) = -\frac{\hbar}{\omega}\text{Tr}\int \frac{d^2\mathbf{k}}{(2\pi)^2}\int \frac{d\varepsilon}{2\pi} f(\varepsilon)\mathcal{T}_{ij}(\mathbf{k}, \varepsilon). \qquad (8)$$

Here $f(\varepsilon)$ is the Fermi–Dirac distribution function, and:

$$\mathcal{T}_{ij}(\mathbf{k}, \varepsilon) = \text{Tr}\left\{\hat{s}_i\left[G_\mathbf{k}^R(\varepsilon+\omega)\hat{v}_j[G_\mathbf{k}^R(\varepsilon) - G_\mathbf{k}^A(\varepsilon)]\right.\right.$$
$$\left.\left. + [G_\mathbf{k}^R(\varepsilon) - G_\mathbf{k}^A(\varepsilon)]\hat{v}_j G_\mathbf{k}^A(\varepsilon-\omega)]\right\}\right. \qquad (9)$$

with $G_\mathbf{k}^{X=R,A}$ defining retarded or advanced Green's function. The expression (8) is the starting point for detailed analysis of spin polarization in our model. Without loosing the generality one can assume that electric field is oriented in the $\hat{x}$ direction, and therefore we discuss the response functions χ_{ix}.

In our considerations the main source of relaxation is the scattering on randomly distributed, spin-independent, point-like impurities. Accordingly, assuming white-noise distribution, the impurity potential is given in the form: $V_0(\mathbf{r}) = \sum_i V_0\delta(\mathbf{r} - \mathbf{R}_i)$ and vanishes on average, i.e., $\langle V_0(\mathbf{r})\rangle = 0$, whereas the second statistical cumulant is finite $\langle |V_{0\mathbf{kk'}}|^2\rangle = n_i V_0^2$ (n_i — impurity concentration). The scattering on impurity potential is taken into account by averaging the quantum–mechanical expectation value for spin polarization over impurities configuration. This has been done, by averaging the combination of operators in Eq. (9) over impurities configuration, i.e., $\langle \hat{s}_i G^X \hat{v}_j G^Y\rangle$. The localization corrections, as vanishingly small in the low impurity concentration, are not taken into account. Thus, the disorder average is evaluated here in the ladder approximation, that is $\langle \hat{s}_i G^X \hat{v}_j G^Y\rangle = S_i\langle G^X\rangle \hat{v}_j\langle G^Y\rangle$, where S_i is the renormalized spin vertex function, and
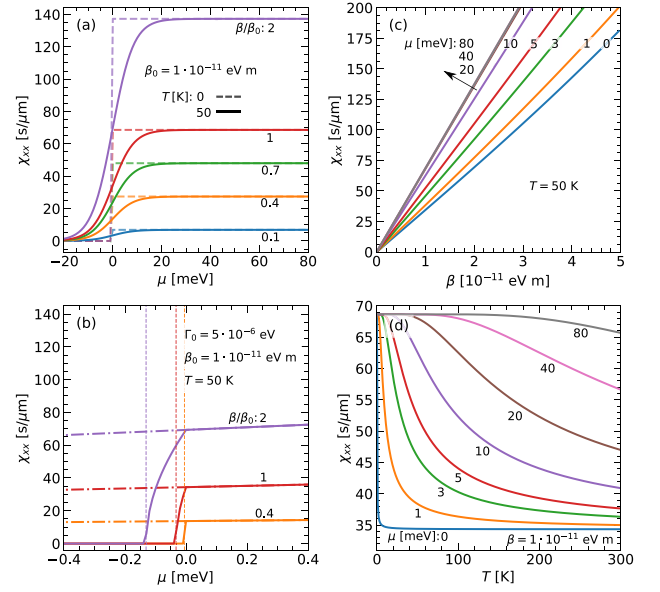

Fig. 2. Spin susceptibility χ_{xx} as a function of (a), (b) chemical potential μ, (c) linear Dresselhaus spin–orbit parameter β, and (d) temperature T. The effective mass $m = 0.05m_0$ and other parameters as indicated.

$\langle G^X\rangle = [\varepsilon - \hat{H} - \Sigma^X]^{-1}$ is the configurational averaged Green's function, that contains the impurity self-energy Σ^X. Information about derivation of self-energy and spin vertex function, S_i, is provided in Appendix A.

In next sections we study in details the behavior of current-induced spin polarization in 2DEG with Dresselhaus spin–orbit interaction. In Section 3 we will focus on nonmagnetic 2DEG, whereas in Section 4 we present results for magnetic systems.

3. CISP in nonmagnetic 2DEG

The non-equilibrium spin-polarization has been studied in details for Rashba systems, and partially for Dresselhaus spin–orbit interaction [39,40]. However, according to our knowledge, there is still a lack of detailed studies of CISP for systems with both linear and cubic Dresselhaus spin–orbit interaction. Thus, for the consistency of this paper we study the Dresselhaus 2DEG described by the Hamiltonian (1) for some special limits. In this section we consider the nonmagnetic case, i.e., we assume that the exchange field M vanishes.

3.1. 2DEG with linear Dresselhaus SOC ($\beta \neq 0$ and $\gamma = 0$)

We start our considerations assuming that the linear Dresselhaus spin–orbit interaction dominates whereas the cubic term may be neglected. In such a case the Hamiltonian (1) takes the following form: $\hat{H} = \hat{H}^{KIN} + \hat{H}^{LD}$, with eigenvalues: $E_\pm = \varepsilon_k \pm \beta k$. The corresponding energy dispersion is presented in Fig. 1(a). In this case, only the x-component of non-equilibrium spin polarization appears, that is the component in plane of 2DEG and collinear to the external electric field. This is also easy to understand when we plot the equilibrium expectation values of spin for fixed energy and wavevector $\mathbf{k}$ (right panel of Fig. 1(a)). The average spin in each subband vanishes at equilibrium. When external electric field is applied in the x-direction, the Fermi contour is shifted. In consequence of spin-momentum locking, triggered by linear Dresselhaus spin–orbit coupling, one observes a nonzero x-component of spin density. The Eqs. (7) and (8) (i.e., single loop or 'bare bubble' approximation [38]) leads to the following formula:

$$S_x^0 = eE_x\hbar\frac{\beta}{8\Gamma}\int\frac{dk\,k}{2\pi}\left[\frac{k^2\beta^2 + 2\Gamma^2}{k^2\beta^2 + \Gamma^2}[f'(E_-) + f'(E_+)]\right.$$

3
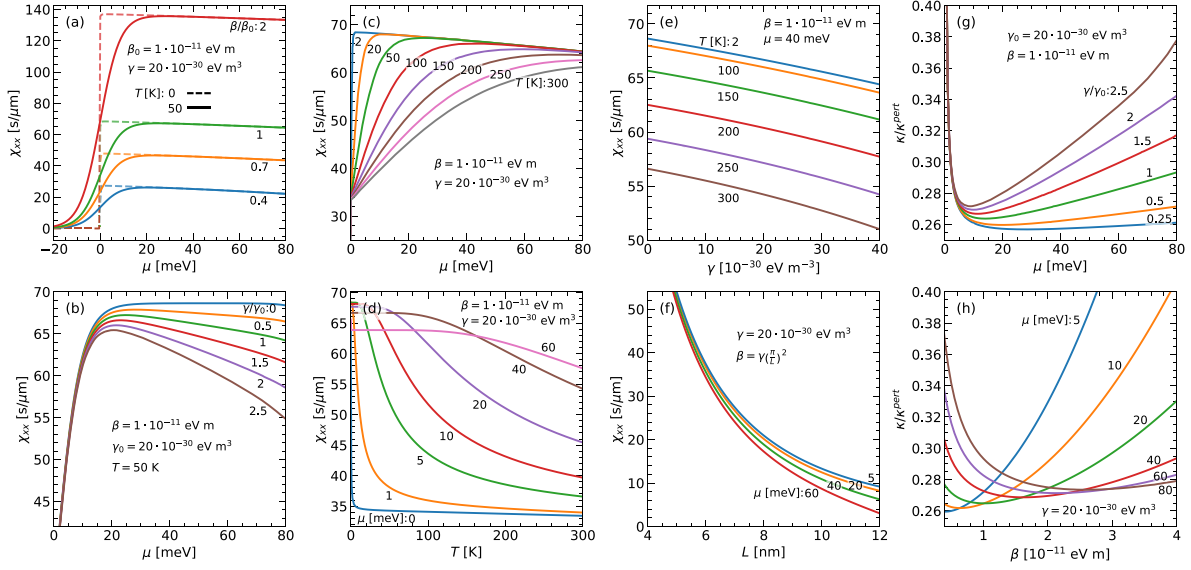
Fig. 3. Spin susceptibility χ_{xx} as a function of set of parameters. (a)–(c) χ_{xx} as a function of chemical potential μ, for selected values of parameters β, γ, and T respectively; (d) χ_{xx} as a function of temperature T for selected values of chemical potential, and (e) as a function of parameter γ for selected temperatures; (f) χ_{xx} presented as a function of the quantum well width for different positions of Fermi level μ. (g), (h) The κ parameter normalized to κ^{pert}, as a function of μ and β respectively. Effective mass as in Fig. 2 and other parameters as indicated.

$$+ \frac{k\hbar^2}{m\beta}[f'(E_+) - f'(E_-)]\Bigg]. \tag{10}$$

The above equation, in the limit of low impurity concentration and at low temperatures (i.e., $T \to 0$), takes the following form for $\mu > 0$:

$$S_x^{0\,(T=0)} = eE_x \frac{m\beta}{8\pi\hbar\Gamma} \equiv s_x, \tag{11}$$

where the relaxation rate, Γ, is:

$$\Gamma = n_i V_0^2 \frac{m}{2\hbar^2} \equiv \Gamma_0. \tag{12}$$

Taking into account the averaging over impurities configuration by the renormalization of the spin vertex operator (see Appendix A.2) one gets:

$$S_x = \eta S_x^0, \tag{13}$$

where η is a numerical factor renormalizing the spin vertex function. In this case η is equal to two (details of calculations are given in the end of Appendix A). The Eq. (13), in the limit $T \to 0$ and $\Gamma \to 0$, gives us the final analytical result for non-equilibrium spin polarization in 2DEG with linear Dresselhaus spin–orbit interaction:

$$S_x = eE_x \frac{m\beta}{4\pi\Gamma\hbar} \equiv 2s_x. \tag{14}$$

The non-equilibrium spin polarization, in this case, is indeed μ independent and constant for specific system (for constant β, m, n_i, and V_0).

When Fermi level lies below the subbands crossing point, that is for the range $-\frac{\beta^2 m}{2\hbar^2} < \mu < 0$, the relaxation rate takes the following explicit form:

$$\Gamma = \Gamma_0 \frac{m\beta}{\sqrt{2m\mu\hbar^2 + m^2\beta^2}} = \Gamma_0 \frac{n^*}{n}, \tag{15}$$

where n is quasiparticle density at the Fermi level, i.e., $n(\mu < 0) = \frac{m\beta}{\pi\hbar^4}\sqrt{m^2\beta^2 + 2\hbar^2 m\mu}$ and $n^* = n(\mu = 0) = m^2\beta^2/\pi\hbar^4$. In this case the non-equilibrium spin polarization can be expressed as follows:

$$S_x = 2s_x \frac{n}{n^*}. \tag{16}$$

These results are in agreement with those in the previous literature [40], and show the linear dependence of the non-equilibrium spin polarization on the relaxation time, and the spin–orbit coupling

parameter. Moreover, CISP in such system is oriented in the plane of 2DEG and collinear with the external electric field.

Fig. 2(a) and (b) present the spin polarizability χ_{xx} of the nonmagnetic 2DEG when the cubic Dresselhaus spin–orbit coupling is neglected, i.e., $\gamma = 0$. Here χ_{xx} is plotted as a function of chemical potential, μ, for several values of the coupling parameter β. The solid lines in Fig. 2(a) correspond to the numerical results, obtained based on Eqs. (10) and (13), whereas the dashed lines correspond to the analytical expressions (Eq. (14) and (16)). The range of negative chemical potential is very narrow and presented separately in Fig. 2(b). Here, the numerical results are plotted for two cases, i.e., when (i) Γ is a μ-dependent function (as in Eq. (15)), and when (ii) Γ is treated as a constant, μ-independent, parameter. Note, that in the second case, the constant value of Γ when μ changes means that the concentration of impurities or the impurity potential are variable.

At this point it should be stressed that in general, when chemical potential approaches the edge of the lower subband (i.e., $\mu \to \mu_{min}$ and $n \to 0$), the relaxation rate diverges (according to Eq. (15)) and the role of disorder increases. In such a case the Ioffe–Regel localization criterion imposes a constrain on μ. Therefore, from the equation $\mu^* - \mu_{min} \simeq \Gamma(\mu^*)$ one can find the chemical potential, μ^*, below which the states become localized and the conductivity is suppressed. Since we do not consider in this paper the localization processes, in the following sections we restrict our considerations mainly to the range of positive values of chemical potential or far above the bottom of the lower subband. Accordingly, everywhere we present the μ dependence, the relaxation rate Γ is treated as a constant parameter independent on μ (i.e., the impurity concentration changes) and we do not determine μ^*, below which the conductivity and also the spin polarization is suppressed. Note, this happens above the bottom of the lower band, i.e., for chemical potentials larger than the temperature smearing of Fermi–Dirac distribution function.

Fig. 2(c) shows the spin polarizability as a function of the spin–orbit coupling parameter β. Thus, χ_{xx} is almost a linear function of β. For sufficiently large values of chemical potential the rate of increase of χ_{xx} as a function of β does not change, what coincides with Fig. 2(a). Finally, Fig. 2(d) presents the spin susceptibility as a function of temperature. One can see that χ_{xx} is reduced by approximately half when the temperature increases. The decrease of χ_{xx} is abrupt for smaller chemical potentials, whereas for large chemical potentials it is only slightly modified.

3.2. 2DEG with linear and cubic Dresselhaus SOC ($\beta \neq 0$ and $\gamma \neq 0$)

In a more general case, when both k-linear and k-cubed terms of Dresselhaus spin–orbit interaction are nonzero, the Hamiltonian (1) has the following components $\hat{H} = \hat{H}^{KIN} + \hat{H}^{LD} + \hat{H}^{CD}$. The eigenvalues corresponding to this Hamiltonian can be written in the form: $E_\pm = \frac{\hbar^2 k^2}{2m} \pm \xi_{\mathbf{k}}(M = 0)$. The corresponding energy spectrum is presented in Fig. 1(c). The influence of the k-linear Dresselhaus term on the electronic states is mostly visible around the subbands crossing point, i.e. for small values of chemical potential (low carrier concentration). In turn, the k-cubed Dresselhaus term might be important at larger values of μ, that is for quantum wells with higher electron concentration. Since the expressions that follow from Eq. (8), as well as the impurity vertex function are rather cumbersome, (for the details see Appendix A.2), they are evaluated numerically and presented in Fig. 3.

Fig. 3(a)–(d) present spin polarizability χ_{xx}, plotted as a function of chemical potential μ (note that Γ is fixed here). Comparing Fig. 3(a),(b) and Fig. 2(a) one can clearly see how the nonzero cubic Dresselhaus term modifies the spin polarizability. Namely, for the positive chemical potentials (two subbands occupied) one observes almost linear drop in the value of spin susceptibility with an increase in the value of chemical potential. The modification is also evident in temperature dependences and for higher values of chemical potentials (compare Fig. 3(c)–(e) and Fig. 2(d)).

When $\gamma k_F^2 \ll \beta$, the cubic Dresselhaus term in the Hamiltonian can be treated perturbatively. Performing the expansion of the Green's functions with respect to $\hat{H}^{CD}$ one can continue our calculations analytically (see Appendix B). As a result, in the low temperature regime, one finds (up to the linear term in γ) the final expression in a simple analytical form. Thus, for $\mu > 0$:

$$S_x \cong 2 s_x \left(1 - \frac{\gamma}{\beta} k_{F0}^2\right), \tag{17}$$

where $k_{F0} = \sqrt{2m\mu}/\hbar$ is a Fermi wavevector of a degenerate 2DEG. Based on this expression, it is clear that the cubic Dresselhaus spin–orbit coupling modifies the current-induced spin polarization through the term proportional to the chemical potential, μ. Taking into account the relation between parameters β and γ, the Eq. (17) can be written as:

$$S_x \cong 2 s_x \left(1 - \frac{L^2}{\pi^2} k_{F0}^2\right). \tag{18}$$

These approximate formulas may be useful as they combine CISP with the quantum well width, L, and Fermi wavevector k_{F0} (or electron mobility), that is with the quantities provided by typical transport experiments. The dependence of spin susceptibility on the quantum well width is presented in Fig. 3(f). The fact that χ_{xx} in symmetric quantum wells can be tuned by μ or L seems to be important for possible applications, making it controllable by external means.

One can also introduce a parameter κ defined as:

$$\kappa = \frac{\chi_{xx}(\gamma = 0) - \chi_{xx}(\gamma \neq 0)}{\chi_{xx}(\gamma = 0)}. \tag{19}$$

Thus, κ is a characteristic parameter that describes directly the influence of cubic Dresselhaus SOC on non-equilibrium spin polarization. Regarding to the analytical result obtained perturbatively, i.e., Eqs. (17) and (18), one finds immediately the κ parameter in the following form:

$$\kappa \cong k_{F0}^2 \frac{\gamma}{\beta} = k_{F0}^2 \frac{L^2}{\pi^2} \equiv \kappa^{\text{pert}}. \tag{20}$$

Fig. 3(g),(h) present κ normalized to κ^{pert}. One can see that the perturbative treatment of cubic Dresselhaus spin–orbit interaction leads to the revalued influence of this term on the total non-equilibrium spin polarization. The ratio $\kappa/\kappa^{\text{pert}}$ is a slowly varying function of μ, for $\mu \gg 0$ and for small values of spin–orbit coupling parameter γ. In turn, when $\mu \to 0$ it increases rapidly. Similarly, when γ is larger

than $\gamma_0 = 20 \cdot 10^{-30}$ eV m^3, the linear increase of κ with increasing μ becomes visible (see Fig. 3(g)). The cubic Dresselhaus term changes the spin polarization about $10\% - 30\%$ for higher values of μ with respect to the μ-independent spin polarization.

4. CISP in magnetic 2DEG

Now, let us discuss the influence of exchange field on CISP. Similarly as in the previous section we start our discussion assuming that the cubic Dresselhaus term is vanishingly small, and can be neglected. Then we discuss the case of magnetic 2DEG in the presence of both linear and cubic Dresselhaus spin–orbit coupling. We will focus, among other, on temperature behavior of spin polarization. We assume here that M varies with temperature according to the Bloch's law, i.e., $M(T) = M_0 \left[1 - (T/T_C)^{3/2}\right]$, where $M_0 = M(T = 0)$, and T_C denotes the Curie temperature.

4.1. Magnetic 2DEG with linear Dresselhaus SOC ($\beta \neq 0$, $\gamma = 0$)

The Hamiltonian (1) is now reduced to the following form $\hat{H} = \hat{H}^{KIN} + \hat{H}^{LD} + \hat{H}^M$ and the eigenvalues take simple form: $E_\pm = \varepsilon_k \pm \sqrt{\beta^2 k^2 + M^2} \equiv \varepsilon_k \pm \lambda_k$. In this case, we get, in the single loop approximation, the following expressions:

$$S_x^0 = \frac{e E_x \hbar \beta}{8\pi \Gamma} \int dk \, k \left[\frac{(k^2 \beta^2 + 2\Gamma^2)}{\lambda_k^2 + \Gamma^2}[f'(E_+) + f'(E_-)] \right.$$
$$\left. + \frac{k^2 \hbar^2}{m \lambda_k}[f'(E_+) - f'(E_-)] \right], \tag{21}$$

$$S_y^0 = e E_x \hbar \int \frac{dk \, k}{\pi} \frac{M\beta}{(2\lambda_k)^3} \left[f(E_+) - f(E_-) \right.$$
$$\left. - \frac{\Gamma^2}{\lambda_k} \frac{[f'(E_+) + f'(E_-)]}{[1 + (\Gamma/\lambda_k)^2]} \right], \tag{22}$$

and $S_z^0 = 0$. Note, that in the limit of low impurity concentration, the second term in expression describing S_y^0 vanishes. Thus, the non-equilibrium spin polarization has two components: The x-component which survives even if M vanishes, and the y-component that appears only in the presence of M. Moreover, the y-component, as originating from the Fermi sea contribution, is independent of relaxation processes and can be easily linked to Berry curvature.

The detailed calculations show that the impurity vertex function modifies only the x-component of spin polarization, whereas the y-component remains unchanged. Thus, one can write:

$$S_x = \eta S_x^0, \quad S_y = S_y^0. \tag{23}$$

As in the previous section, η is a factor that comes from the impurity vertex correction. In this case, η ranges between 1 and 2 and its value reflects the interplay between exchange interaction and spin–orbit coupling. When Fermi level crosses only one subband, i.e., it lies in the energy gap which appears as a consequence of the exchange interaction, $\eta \to 1$. Thus, η reflects the fact that the exchange interaction dominates the spin–orbital one (there is no renormalization of the spin vertex function when SOC disappears). In turn, $\eta \to 2$ when two subbands are occupied, and is equal 2 in the range of μ, where the spin–orbit interaction completely dominates the exchange one. This behavior is shown in Fig. 4, where the vertex correction, η, is plotted as a function of chemical potential μ and spin–orbit coupling parameter β (Fig. 4(a)), chemical potential and magnetization M (Fig. 4(b)), and as a function of β and M (Fig. 4(c)). Moreover, Fig. 4(d) presents the cross sections of Fig. 4(c). The numerical results for η are obtained assuming Γ as a constant parameter. This simplification may be not adequate when μ approaches the bottom of the lower subband, where Γ and η are energy dependent functions (as discussed in Section 3.1).

In low temperature limit, the Eq. (21) and (22) can be evaluated analytically. Thus, in the low concentration of impurities, the analytical expressions are presented below, where s_x is defined in Eq. (11).

5
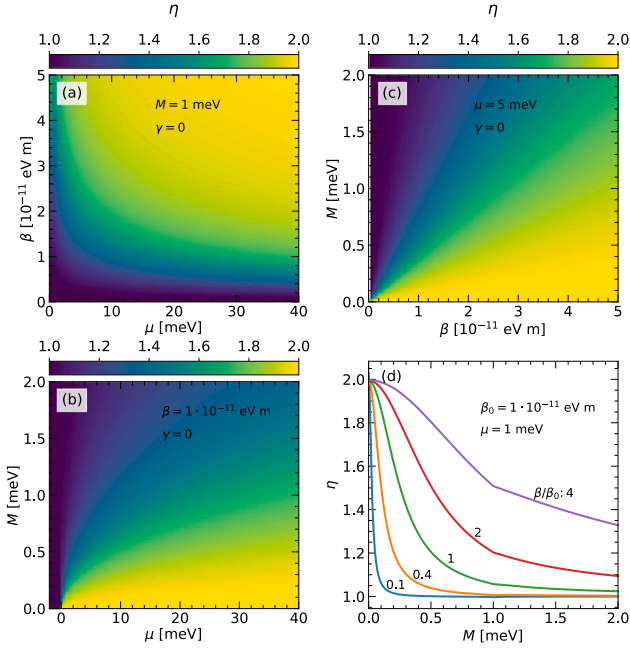
Fig. 4. Renormalized spin vertex function η plotted as a function of (a) spin–orbit coupling parameter β and chemical potential μ, (b) magnetization M and chemical potential, and (c) magnetization and spin–orbit coupling parameter; (d) η as a function of M for different ratio of β to β_0. The other parameters as indicated, whereas the effective mass, m, is the same as in Fig. 2.

Fig. 5. Current-induced spin polarizability χ_{xx} and χ_{yx} as a function of (a),(c) chemical potential μ, for selected values of linear Dresselhaus coupling parameter β and (b),(d) as a function of temperature T for selected values of μ. Solid lines correspond to the temperature $T = 50$ K and dashed lines correspond to zero-temperature formulas given by Eqs. (24)–(29). The Curie temperature is set to $T_C = 180$ K. The results include the vertex correction. The other parameters are indicated and the effective mass is the same as in Fig. 2.

For the S_x component of spin polarization one finds:

$$S_x = \eta\, s_x \left(\frac{\varepsilon_{k_-}}{\lambda_{k_-}} - \frac{\varepsilon_{k_+}}{\lambda_{k_+}} \right) \tag{24}$$

for $\mu \geq M$,

$$S_x = \eta\, s_x \frac{\varepsilon_{k_-}}{\lambda_{k_-}} \tag{25}$$

for $-M \leq \mu < M$, and

$$S_x = \eta\, s_x \left(\frac{\varepsilon_{k^\pm}}{\lambda_{k^\pm}} - \frac{\varepsilon_{k_-}}{\lambda_{k_-}} \right) \tag{26}$$

for $-\frac{\varepsilon_\beta}{2}\left(1 + \frac{M^2}{\varepsilon_\beta^2}\right) \leq \mu < -M$, where $\varepsilon_\beta = \frac{m\beta^2}{\hbar^2}$.

The S_y component is given by the following equations, where $s_y = \frac{eE_x\hbar}{8\pi\beta}$:

$$S_y = -s_y M \left(\frac{1}{\lambda_{k+}} - \frac{1}{\lambda_{k-}} \right) \tag{27}$$

for $\mu \geq M$,

$$S_y = -s_y \left(1 - \frac{M}{\lambda_{k-}} \right) \tag{28}$$
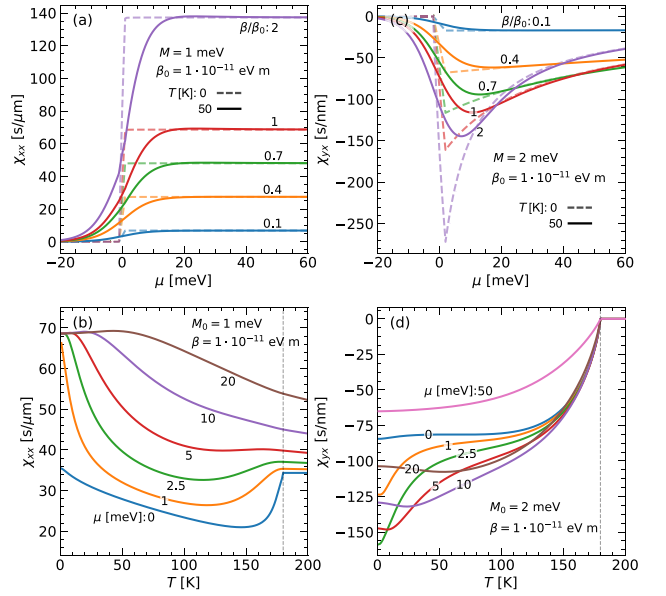
for $-M \leq \mu < M$, and

$$S_y = -s_y M \left(\frac{1}{\lambda_{k^\pm}} - \frac{1}{\lambda_{k_-}} \right) \tag{29}$$

for $-\frac{\varepsilon_\beta}{2}\left(1 + \frac{M^2}{\varepsilon_\beta^2}\right) \leq \mu < -M$. In the above equations, the Fermi wavevectors take the form
$k_\pm = \left[2m\left(\varepsilon_\beta + \mu \mp [\varepsilon_\beta^2 + 2\mu\varepsilon_\beta + M^2]^{1/2} \right) \right]^{1/2}$ for $\mu \geq -M$, and $k_-^\pm = k_\mp$ for $\mu \in \left[-\frac{\varepsilon_\beta}{2}\left(1 + \frac{M^2}{\varepsilon_\beta^2}\right); -M \right]$ (see Fig. 12 in Appendix C).

The analytical results given by Eqs. (24)–(29) are presented in Fig. 5. The spin susceptibilities, χ_{xx} and χ_{yx}, are plotted as a function

of chemical potential μ for fixed value of M and the temperature $T = 50$ K (solid lines), as well as in the limit of $T \to 0$ (dashed lines) (Fig. 5(a)–(c)). In the low impurity concentration regime the spin susceptibility χ_{yx} is robust to impurity scattering processes. Precisely, we found that χ_{yx} does not depend on the relaxation time and impurity vertex correction. Additionally, one can see that χ_{yx} increases rapidly when only single band is occupied, reaches maximum and next slowly decreases with increasing μ. In turn, χ_{xx} is only slightly modified by magnetization in comparison to the nonmagnetic case when both subbands are occupied. The main difference between dependences presented in Fig. 3(a) and Fig. 5(a) is pronounced in the low temperature regime when chemical potential lies in the range $-M < \mu < M$. In this case the only single subband is occupied and the x-component of the spin polarization increases linearly with μ. This behavior is however blurred at higher temperatures due to the smearing of Fermi contours by Fermi–Dirac distribution function. It should be stressed that χ_{yx} is about three orders of magnitude smaller than χ_{xx}. Indeed, comparing s_x and s_y one finds:

$$s_y = \frac{\Gamma}{2\varepsilon_\beta} s_x. \tag{30}$$

Thus, as long as we keep the limit $\Gamma \ll \varepsilon_\beta$, the S_y component of spin polarization is always negligibly small in comparison to S_x component.

The non-equilibrium spin polarization depends also on temperature. In general, within the model considered in this paper, the temperature affects the system response in two ways: (i) by thermal broadening of Fermi surface, and (ii) by thermal decrease of magnetization. Fig. 4(b),(d) presents temperature dependences of χ_{xx} and χ_{yx}. In numerics, M decreases with temperature according to the Bloch's law and the Curie temperature is assumed to be $T_C = 180$ K. This is easy to observe, since χ_{yx} approaches 0 above T_C (where $M = 0$), and χ_{xx} reaches values observed for the nonmagnetic case.

4.2. Magnetic 2DEG with linear and cubic Dresselhaus SOC ($\beta \neq 0$, $\gamma \neq 0$)

In this section we present the most general case in our considerations, i.e., magnetic 2DEG with k-linear and k-cubic Dresselhaus
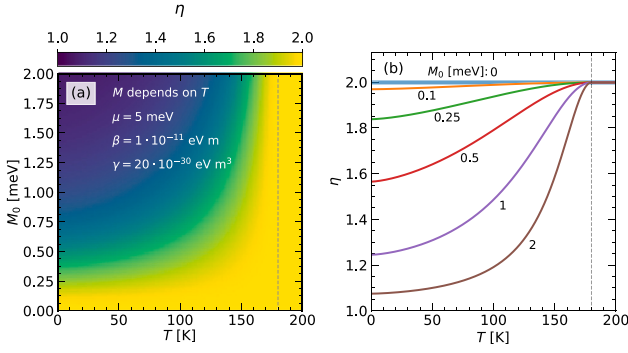
6

Fig. 6. Temperature dependences for the renormalized spin vertex function η. (a) η as a function of zero-temperature magnetization $M_0 \equiv M(T = 0)$ and temperature T. (b) The temperature dependences for selected values of M_0. The Curie temperature $T_C = 180$ K. The magnetization M is dependent on the temperature according to the Bloch's law. The effective mass is the same as in Fig. 2 and other parameters are as indicated. .

spin–orbit coupling. We trace the numerical results and discuss the behavior of Berry curvature in 2DEG with k-cubed contribution to SOC.

Numerical results: As discussed in the preceding section, the net magnetization in the system is in general a temperature dependent. In such a case the impurity vertex function is also temperature dependent via the $M(T)$ dependence. This is shown in Fig. 6, where the vertex function, η, is presented as a function of temperature, T, and zero-temperature magnetization, M_0. The parameter η increases with increasing T, and reaches $\eta = 2$ when $T = T_C$. However, since the presence of k-cubic Dresselhaus term does not change qualitatively the general dependences of impurity vertex function presented in the previous subsection (Fig. 5), numerical results for the impurity spin vertex function when $\gamma \neq 0$ are presented only in Appendix D.

Fig. 7 contains the full information about spin polarizability, i.e., the impurity vertex function is included. The dependence of χ_{xx} on the chemical potential μ (Fig. 7(a),(b),(d),(e)) is modified by the cubic Dresselhaus spin–orbit coupling when $\mu \gg M$. However, the general dependences do not change qualitatively with regard to the previous case, when $\gamma = 0$. Thus, we describe in more details only the dependences for χ_{yx}, i.e. the spin polarizability related to the y-component of spin polarization that are presented in Fig. 7(g),(h),(j),(k). Accordingly, when only a single subband is occupied, that is when $-M < \mu < M$, χ_{yx} is almost a linear function of μ. The absolute value of χ_{yx} takes maximum when $\mu = M$, and decreases with further increase of μ. As a consequence, S_y component reveals a sharp asymmetric peak at lower temperatures and for chemical potential ranging in the vicinity of $\mu = M$, whereas it vanishes for largest values of μ. This peak is the most visible when Dresselhaus SOC dominates the exchange interaction.

Fig. 7 presents also the temperature dependences of χ_{xx} and χ_{yx} for the fixed range of zero-temperature magnetization M_0 (Fig. 7(c), (f) and (i), (l) respectively). The spin polarizability χ_{xx} decreases with increasing temperature similarly as in the case of nonmagnetic 2DEG. The qualitative difference in temperature dependence of χ_{xx} with respect to the nonmagnetic case appears for temperatures preceding the transition between magnetic to nonmagnetic phase, where spin polarizability reveals local minimum. In turn, the absolute value of χ_{yx} decreases with temperature for small values of M_0. This local maximum moves to higher temperature range (close vicinity of $T = T_C$). The absolute value of χ_{yx} reveals the local maximum, that moves from lower to higher temperatures when M_0 increases.

Berry curvature, S_y and anomalous Hall effect: The y-component of spin polarization, in low impurity concentration limit, is robust to scattering processes. That is, the dissipative part of χ_{yx} vanishes, and only nondissipative component remains. This is clearly seen in Eq. (22)

describing the magnetic Dresselhaus 2DEG with $\gamma = 0$. In the weak scattering limit, $\Gamma \to 0$, this equation reduces to:

$$S_y = eE_x\hbar \int \frac{dk\,k}{8\pi} \frac{\beta M}{\lambda_k^3} \left[f(E_+) - f(E_-) \right] \tag{31}$$

Interestingly, the y-component of the non-equilibrium spin polarization can be expressed directly by the Berry curvature of the n-th subband $\mathbf{B}_n(\mathbf{k}) = \nabla_\mathbf{k} \times \mathbf{A}_n(\mathbf{k})$, where $\mathbf{A}_n(\mathbf{k}) = i\langle \Psi_n | \nabla_\mathbf{k} | \Psi_n \rangle$ is Berry connection, and $|\Psi_{n=\pm}\rangle$ are normalized eigenvectors of the investigated Hamiltonian. For 2D systems Berry curvature has only z-component. Indeed, in the case of magnetic 2DEG with linear Dresselhaus spin–orbit interaction one gets:

$$B_{n=\pm}^z = \pm \frac{M\beta^2}{2\lambda_k^3}. \tag{32}$$

Combining this result with Eq. (31) one finds immediately:

$$S_y = \frac{eE_x\hbar}{4\pi\beta} \sum_{n=\pm} \int dk\,k B_n^z f(E_n). \tag{33}$$

In the general case, i.e., for the system described by the Hamiltonian (1), the Berry curvature can be written in the following form:

$$B_n^z = \pm \frac{M}{2\xi_\mathbf{k}^3} \left[\beta(\beta - \gamma k^2) - 3\gamma^2 k_x^2 k_y^2 \right]. \tag{34}$$

Berry curvature corresponding to the E_+ subband is presented in Fig. 8(a), and (b). The cubic Dresselhaus spin–orbit interaction introduces anisotropy of the energy subbands and therefore anisotropy in Berry curvature. Moreover, $B_\pm^z$ integrated over angle decreases with increasing γ.

In Matsubara Green's function formalism we get the formula for S_y component of non-equilibrium spin polarization that can be expressed by Berry curvature in the following way:

$$S_y = S_y[f(E_\pm)] + S_y[f'(E_\pm)], \tag{35}$$

where

$$S_y[f(E_\pm)] = eE_x\hbar \sum_{n=\pm} \int \frac{d^2\mathbf{k}}{(2\pi)^2} \mathcal{W}(\mathbf{k}) B_n^z f(E_n) \tag{36}$$

with:

$$\mathcal{W}(\mathbf{k}) = \frac{\beta - \gamma k_y^2}{2[\beta(\beta - \gamma k^2) - 3\gamma^2 k_x^2 k_y^2]}, \tag{37}$$

and $S_y[f'(E_\pm)]$ is the dissipative part of S_y, i.e., it depends on derivatives of Fermi–Dirac distribution:

$$S_y[f'(E_\pm)] = -eE_x\hbar \sum_{n=\pm} \int \frac{d^2\mathbf{k}}{(2\pi)^2} \frac{\Gamma^2}{4\xi_\mathbf{k}^2} \frac{M\left(\beta - \gamma k_y^2\right)}{\left(\Gamma^2 + \xi_\mathbf{k}^2\right)} f'(E_n) \tag{38}$$

In the limit of low impurity concentration, $\Gamma \to 0$, one finds $S_y[f'(E_n)] \to 0$ and S_y is determined wholly by Eq. (36).

As we mentioned before, S_y component is few orders of magnitude smaller than the S_x component, and therefore it has a negligible role in the total non-equilibrium spin polarization. However, the fact that S_y is nonzero and robust to impurities may be important in systems with higher impurity concentrations. In such a case S_x component decreases and, in consequence, the amplitudes of both components are comparable. Additionally, S_y can be important in spin dynamics.

Our study also shows that Berry curvature is decreased by the cubic Dresselhaus component. Interestingly this has a negligible impact on S_y component of spin polarization (see Fig. 8(c)), but leads to a visible decrease in the anomalous Hall conductivity (Fig. 8(d)), especially at higher values of chemical potential, μ. Note, that anomalous Hall conductivity has been derived in the same approach as CISP. The numerical results presented in Fig. 8(d) are achieved based on the formulas given in Appendix E.
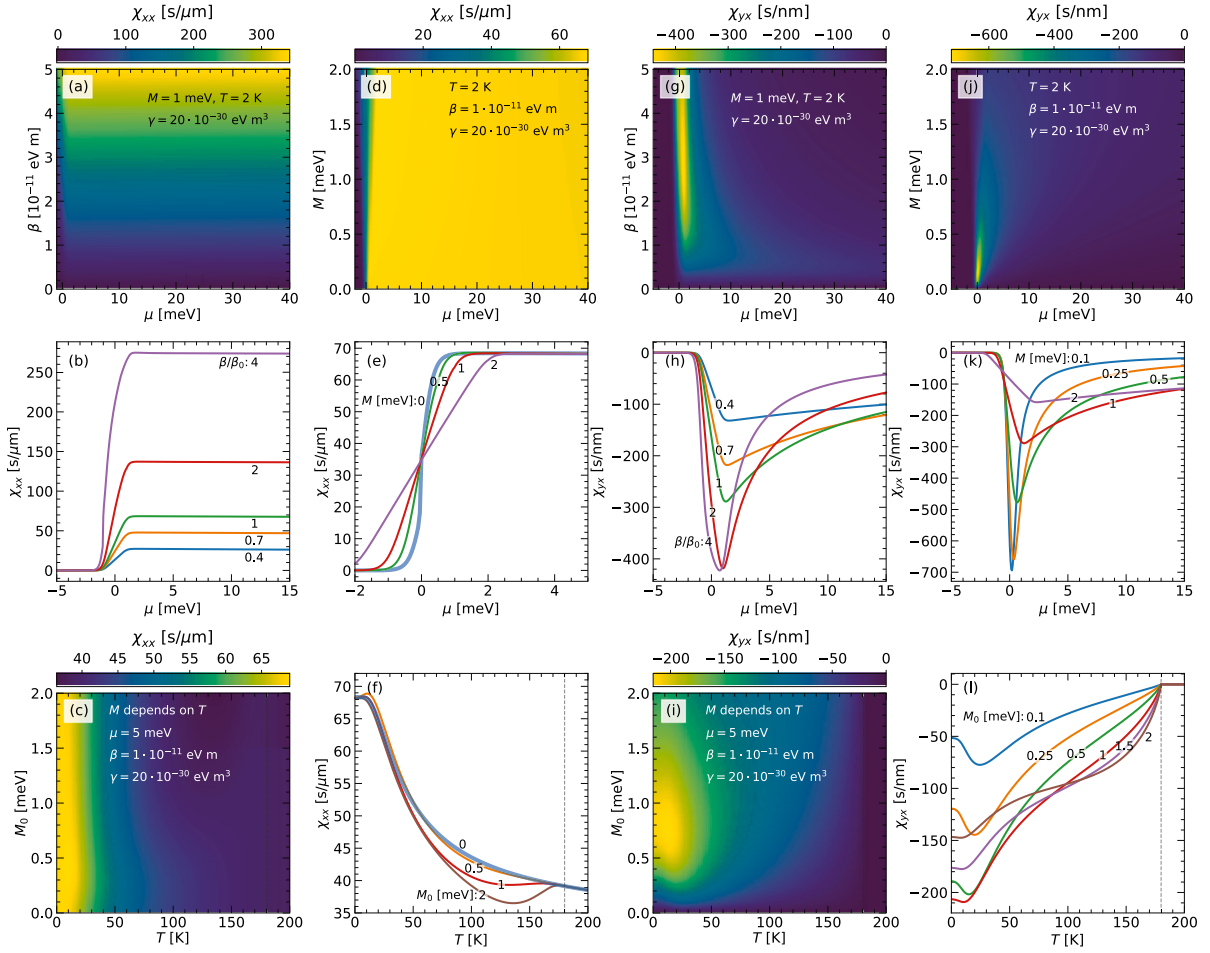
Fig. 7. Spin polarizability (a)–(f) χ_{xx}^v and (g)–(l) χ_{yx} as a function of different parameters. The first row presets χ_{xx} and χ_{yx} as a function of chemical potential μ and linear Dresselhaus coupling parameter β, and as a function of chemical potential and magnetization M. The second row presents the corresponding horizontal cross sections (for a few parameters β or M respectively). Spin polarizability χ_{xx} and χ_{yx} is also plotted as a function of temperature T and zero-temperature magnetization M_0 — Fig. (c) and (i) respectively. Fig. (f) and (l) show the corresponding cross sections for a few values of M_0. The Curie temperature $T_C = 180$ K, and effective mass is the same as in Fig. 2.

5. Thermally-induced spin polarization

In systems with spin–orbit interaction one can define not only the spin polarization induced by the electric field, but also the thermally-induced spin polarization. In such a case the non-equilibrium spin polarization appears as a system response to heat current (temperature gradient). At finite temperatures, the spin polarization is calculated as a linear response to $\nabla T / T$. However, to work within the linear response formalism, one needs to assume that the temperature gradient is small and uniform across the whole sample, and the average temperature T is basically constant on the scale of the carrier wavelengths. Accordingly, one can define the spin polarizability χ_{ij}^T as:

$$S_i = \chi_{ij}^T \frac{\nabla_j T}{T}. \tag{39}$$

The thermal spin polarizability can be determined within the linear response theory and Green function formalism in a similar way to the electric spin polarizability, as presented recently [41,42]. On the other hand, neglecting the non dissipative S_y component, one can apply the relation between thermal spin polarizability and its electrical counterpart. That is, one can define the so-called Mott relation between zero-temperature spin polarizability, χ_{ij}, and thermal spin polarizability, χ_{ij}^T, as follows [41]:

$$\chi_{ij}^T = -\frac{\pi^2}{3}(k_B T)^2 \partial_\mu \chi_{ij}. \tag{40}$$

Fig. 9(a),(b) presents the heat current polarizability as a function of chemical potential for a few different values of linear Dresselhaus spin–orbit coupling parameter, and for a few different values of M, respectively. The heat spin polarizability is nonzero only for a well defined range of chemical potential, that is for $-M < \mu < M$. Moreover the peak of χ_{xx}^T increases with increasing β. It also decreases when M increases. Thus, similarly to the Rashba 2DEG [41,42], the thermal spin susceptibility reveals the well defined energetic window $2M$, for which it takes nonzero value, with the peak width and height controllable by material parameters β and M.

6. Summary and outlook

In this work we have considered the non-equilibrium spin polarization in the two-dimensional electron gas forming at the interface of symmetric semiconductor quantum wells. Precisely, we presented analytical and numerical results for the nonmagnetic and magnetic 2DEG in the presence of magnetization oriented perpendicularly to the plane of the electron gas. We have focused on the role of k-cubed Dresselhaus interaction on the system responses. As we have shown, the cubic Dresselhaus term seems to be important for higher values of chemical potential, leading to the almost linear decrease of spin polarization with increasing chemical potential. In magnetic 2DEG the cubic Dresselhaus interaction introduces Berry curvature oscillations in the **k**-space and reduction of its averaged value. This,
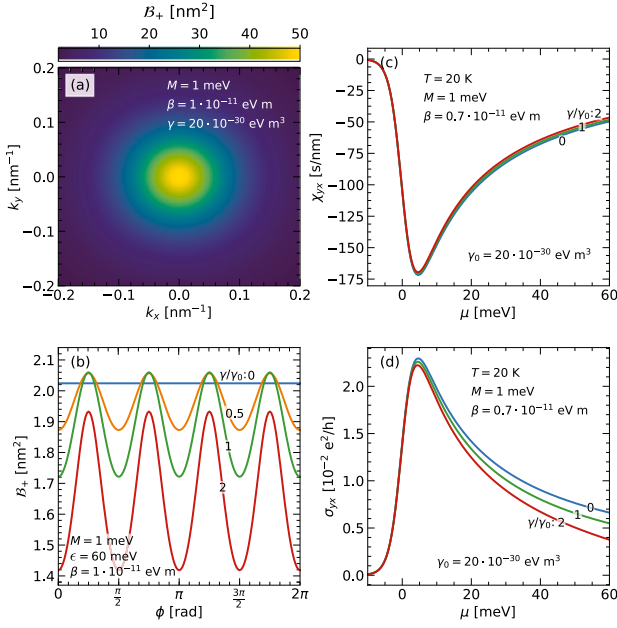
Fig. 8. Berry curvature plotted (a) in the wavevector space and (b) as a function of the azimuthal coordinate of the wavevector ϕ, for isoenergetic surface being the solution of $E_+(k,\phi) = \epsilon$, where $\epsilon = 60$ meV. (c) The spin polarizability χ_{yx} and (d) the intrinsic anomalous Hall conductivity as a function of chemical potential μ for a few values of spin–orbit coupling parameter γ. Effective mass is the same as in Fig. 2 and the other parameters are indicated.
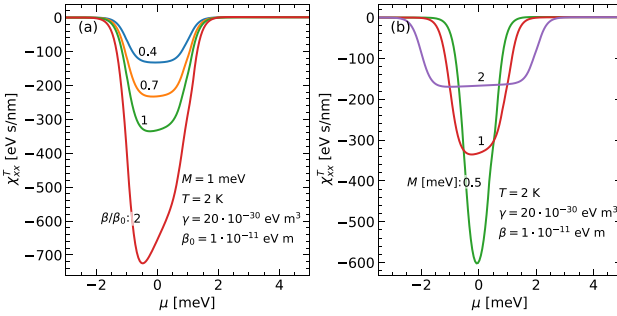
Fig. 9. Thermally-induced spin polarizability χ_{xx}^T as a function of (a) chemical potential μ for selected values of linear Dresselhaus coupling parameter β and fixed magnetization M; (b) χ_{xx}^T for a few selected values of M when β is fixed. The effective mass is the same as in Fig. 2 and the other parameters are indicated.

in turn, reduces anomalous Hall conductivity. We have also studied the temperature behavior of CISP. Finally, using Mott-like relation, we calculated the low-temperature spin polarizability due to heat current. Notably, the thermal spin polarizability reveals the well-defined range of chemical potential where it is nonzero. Presented numerical results and analytical expressions may be useful for interpreting experimental results and further theoretical study of spin-to-charge interconversion phenomena in semiconductor structures.

Declaration of competing interest

The authors declare that they have no known competing financial interests or personal relationships that could have appeared to influence the work reported in this paper.

Acknowledgments

This work was supported by the National Science Center in Poland (NCN) under the project no. DEC-2018/31/D/ST3/02351.

Appendix A. Self-energy and impurity vertex correction

A.1. Self-energy and relaxation time

The impurity-averaged Green's function, $G_{\mathbf{k}}^{R/A}$, can be found from the Dyson equation:

$$\left[G_{\mathbf{k}}^{R/A}\right]^{-1} = \left[G_{\mathbf{k}}^{0\,R/A}\right]^{-1} - \Sigma^{R/A}, \tag{41}$$

where $\Sigma^{R/A}$ denotes the impurity self-energy. In case of point-like spin-independent impurity potential the self-energy can be calculated in Born approximation based on the following expression:

$$\Sigma^R = n_i V_0^2 \int \frac{d^2\mathbf{k}}{(2\pi)^2} G_{\mathbf{k}}^{0R}, \tag{42}$$

where n_i is the impurity concentration and V_0 represents the scattering potential of the impurities. For the momentum-independent potential (s-wave scatterers) one can neglect the real part of self-energy, i.e., $\Sigma^R \approx -i|\operatorname{Im}\Sigma^R|$.

Thus, for the nonmagnetic 2DEG with linear Dresselhaus spin–orbit interaction described by the zero-order Green's functions:

$$G_{\mathbf{k}}^{0R/A} = G_{\mathbf{k}0}^{0R/A}\sigma_0 + G_{\mathbf{k}x}^{0R/A}\sigma_x + G_{\mathbf{k}y}^{0R/A}\sigma_y, \tag{43a}$$

$$G_{\mathbf{k}0}^{0R/A} = \frac{1}{2}\left[G_+^{0R/A} + G_-^{0R/A}\right], \tag{43b}$$

$$G_{\mathbf{k}x}^{0R/A} = \frac{-k_x}{2k}\left[G_+^{0R/A} - G_-^{0R/A}\right], \tag{43c}$$

$$G_{\mathbf{k}y}^{0R/A} = \frac{k_y}{2k}\left[G_+^{0R/A} - G_-^{0R/A}\right], \tag{43d}$$

with $G_{n=\pm}^{0R/A} = \left[\epsilon + \mu - E_n \pm i0^+\right]^{-1}$ ($E_{n=\pm}$ stands for the n-th eigenvalue), one finds $\Sigma^R \approx -i\Gamma\sigma_0$, where Γ has the meaning of the relaxation rate, i.e., $\Gamma = \frac{\hbar}{2\tau}$ and τ is the relaxation time. The relaxation rate evaluated, based on Eq. (42), for nonmagnetic 2DEG for $\mu > 0$ and $\mu < 0$ is given by Eqs. (12) and (15) respectively. The impurity-averaged Green's functions take the following form: $G_{\mathbf{k}}^{R/A} = \left[\epsilon - \mu - E_\pm \pm i\Gamma\right]^{-1}$.

A.2. Impurity vertex correction

The self-consistent equation presented in Fig. 10 has to be solved to find the impurity spin vertex function S_i:

$$S_i = \hat{s}_i + n_i V_0^2 \int \frac{d^2\mathbf{k}}{(2\pi)^2}\, G_{\mathbf{k}}^R(\varepsilon_F) S_i G_{\mathbf{k}}^A(\varepsilon_F), \tag{44}$$

where impurity-averaged Green's functions can be expressed as $G_{\mathbf{k}}^X = G_{\mathbf{k}0}^X\sigma_0 + G_{\mathbf{k}x}^X\sigma_x + G_{\mathbf{k}y}^X\sigma_y + G_{\mathbf{k}z}^X\sigma_z$. Assuming the following form of the impurity vertex function:

$$S_i = a\sigma_0 + b\sigma_x + c\sigma_y + d\sigma_z \tag{45}$$

and inserting it into Eq. (44) one can find the set of algebraic equations for the coefficients a, b, c, d. This set of equations can be written as follows:

$$\begin{bmatrix} 0 \\ -\frac{\hbar}{2} \\ 0 \\ 0 \end{bmatrix} = \begin{bmatrix} A_0 - 1 & B_0 & C_0 & D_0 \\ A_x & B_x - 1 & C_x & D_x \\ A_y & B_y & C_y - 1 & D_y \\ A_z & B_z & C_z & D_z - 1 \end{bmatrix}\begin{bmatrix} a \\ b \\ c \\ d \end{bmatrix}, \tag{46}$$

where the coefficients denoted by the capital letters are determined by certain integrals of the products of Green's functions, as presented in the following. In our case for S_x, after some algebraic transformations end evaluation of the integrals one finds the following solution for the coefficients $a - d$:

$$a = 0, \tag{47a}$$
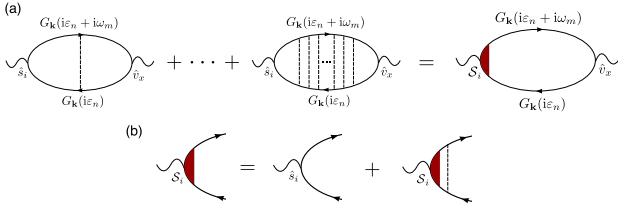
9

A. Krzyżewska and A. Dyrdał

Fig. 10. Ladder diagrams for vertex corrections to the bare spin operator $\hat{s}_i$ (upper line) and the diagrammatic representation of the self-consistent impurity-renormalized vertex equation for the renormalized spin vertex S_i.

$$b = \frac{\hbar}{2} \frac{C_y - 1}{(-B_x C_y + B_x + B_y C_x + C_y - 1)}, \tag{47b}$$

$$c = \frac{\hbar}{2} \frac{-B_y}{(-B_x C_y + B_x + B_y C_x + C_y - 1)}, \tag{47c}$$

$$d = 0, \tag{47d}$$

where:

$$B_x = C_y = n_i V_0^2 \int \frac{d^2\mathbf{k}}{(2\pi)^2} \left[G_{\mathbf{k}0}^A G_{\mathbf{k}0}^R - G_{\mathbf{k}z}^A G_{\mathbf{k}z}^R \right], \tag{48a}$$

$$C_x = -B_y = n_i V_0^2 \int \frac{d^2\mathbf{k}}{(2\pi)^2} \, \mathrm{i} \left[G_{\mathbf{k}0}^A G_{\mathbf{k}z}^R - G_{\mathbf{k}z}^A G_{\mathbf{k}0}^R \right]. \tag{48b}$$

In the limit of low impurity concentration, the integral C_x is also negligible, so the vertex function takes the following form:

$$S_x = \frac{\hbar}{2} \frac{1}{(1 - B_x)} \sigma_x = \frac{\hbar}{2} \eta \sigma_x. \tag{49}$$

The factor η is the renormalization of the spin vertex function and has the meaning of τ_{so}/τ where τ is the momentum relaxation time and τ_{so} is the spin relaxation due to spin–orbit coupling (see also Ref. [6]).

Considering, as an example, the nonmagnetic 2DEG with linear Dresselhaus SOC one can find η analytically. Thus, combining Eq. (48a) with Eqs. ((43)a–d), one finds the integral B_x in the following form:

$$
\begin{aligned}
B_x &= \frac{n_i V_0^2}{4} \int \frac{d^2\mathbf{k}}{(2\pi)^2} \left[G_+^A G_+^R + G_+^A G_-^R + G_-^A G_+^R + G_-^A G_-^R \right] \\
&= \frac{n_i V_0^2}{8\Gamma} \frac{m(k_+ + k_-)}{\sqrt{\beta^2 m^2 + 2\mu m \hbar^2}} = \frac{1}{2}
\end{aligned} \tag{50}
$$

where relaxation rate, Γ, and Fermi wavevectors, $k_\pm$, are defined in Section 3.1. Accordingly, we get immediately that the renormalization of the spin vertex function is:

$$\eta = \frac{1}{1 - B_x} = 2. \tag{51}$$

Appendix B. CISP in the presence of linear and cubic Dresselhaus SOC. Perturbative approach

Here we present some details of the calculations leading to analytical expressions discussed in Section 3.2. Assuming that cubic Dresselhaus interaction is only a small perturbation with respect to the linear one the Hamiltonian describing our system is: $\hat{\mathcal{H}} = \hat{\mathcal{H}}^{KIN} + \hat{\mathcal{H}}^{LD} \equiv \hat{\mathcal{H}}_0$. In such a case, one can perform series expansion of the Green's functions with respect to $\hat{\mathcal{H}}^{CD}$ given by Eq. (3c). Fig. 11 presents Feynman diagrams, including impurity vertex functions, that have to be calculated in this case. The current-induced spin polarization corresponding to these diagrams can be written as:

$$S_i^v = -\frac{eE_x \hbar}{\omega} \int \frac{d^2\mathbf{k}}{(2\pi)^2} \int \frac{d\varepsilon}{2\pi} \left(\widetilde{T}_1^v + \widetilde{T}_2^v + \widetilde{T}_3^v \right), \tag{52}$$

where $\widetilde{T}_{1-3}^v$ correspond to diagrams (1)–(3) presented in Fig. 11. After evaluation of the diagrams we get:

$$\widetilde{T}_1^v = \widetilde{T}_{11}^v + \widetilde{T}_{12}^v + \widetilde{T}_{13}^v, \tag{53a}$$
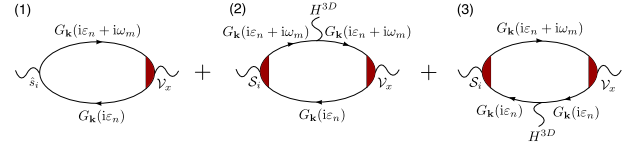

Fig. 11. Diagrammatic representation of the conductivity up to first order in cubic Dresselhaus spin–orbit term.
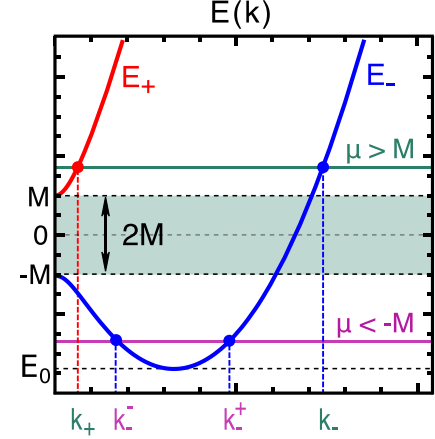

Fig. 12. Schematic energy spectrum for magnetized 2DEG with linear Dresselhaus spin–orbit interaction.

$$\widetilde{T}_{11}^v = f(\varepsilon) \, \mathrm{Tr} \left\{ \hat{s}_i G_{\mathbf{k}}^R(\varepsilon + \omega) \mathcal{V}_{\mathbf{k},x}^{RR}(\varepsilon, \omega) G_{\mathbf{k}}^R(\varepsilon) \right\}, \tag{53b}$$

$$
\begin{aligned}
\widetilde{T}_{12}^v &= [f(\varepsilon + \omega) - f(\varepsilon)] \\
&\quad \times \mathrm{Tr} \left\{ \hat{s}_i G_{\mathbf{k}}^R(\varepsilon + \omega) \mathcal{V}_{\mathbf{k},x}^{RA}(\varepsilon, \omega) G_{\mathbf{k}}^A(\varepsilon) \right\},
\end{aligned} \tag{53c}
$$

$$\widetilde{T}_{13}^v = -f(\varepsilon + \omega) \, \mathrm{Tr} \left\{ \hat{s}_i G_{\mathbf{k}}^A(\varepsilon + \omega) \mathcal{V}_{\mathbf{k},x}^{AA}(\varepsilon, \omega) G_{\mathbf{k}}^A(\varepsilon) \right\}, \tag{53d}$$

$$\widetilde{T}_2^v = \widetilde{T}_{21}^v + \widetilde{T}_{22}^v + \widetilde{T}_{23}^v, \tag{54a}$$

$$
\begin{aligned}
\widetilde{T}_{21}^v &= f(\varepsilon) \, \mathrm{Tr} \left\{ S_{\mathbf{k},i}^{RR}(\varepsilon, \omega) G_{\mathbf{k}}^R(\varepsilon + \omega) \hat{\mathcal{H}}^{CD} \right. \\
&\quad \left. \times G_{\mathbf{k}}^R(\varepsilon + \omega) \mathcal{V}_{\mathbf{k},x}^{RR}(\varepsilon, \omega) G_{\mathbf{k}}^R(\varepsilon) \right\},
\end{aligned} \tag{54b}
$$

$$
\begin{aligned}
\widetilde{T}_{22}^v &= [f(\varepsilon + \omega) - f(\varepsilon)] \, \mathrm{Tr} \left\{ S_{\mathbf{k},i}^{AR}(\varepsilon, \omega) G_{\mathbf{k}}^R(\varepsilon + \omega) \hat{\mathcal{H}}^{CD} \right. \\
&\quad \left. \times G_{\mathbf{k}}^R(\varepsilon + \omega) \mathcal{V}_{\mathbf{k},x}^{RA}(\varepsilon, \omega) G_{\mathbf{k}}^A(\varepsilon) \right\},
\end{aligned} \tag{54c}
$$

$$
\begin{aligned}
\widetilde{T}_{23}^v &= -f(\varepsilon + \omega) \, \mathrm{Tr} \left\{ S_{\mathbf{k},i}^{AA}(\varepsilon, \omega) G_{\mathbf{k}}^A(\varepsilon + \omega) \hat{\mathcal{H}}^{CD} \right. \\
&\quad \left. \times G_{\mathbf{k}}^A(\varepsilon + \omega) \mathcal{V}_{\mathbf{k},x}^{AA}(\varepsilon, \omega) G_{\mathbf{k}}^A(\varepsilon) \right\},
\end{aligned} \tag{54d}
$$

and

$$\widetilde{T}_3^v = \widetilde{T}_{31}^v + \widetilde{T}_{32}^v + \widetilde{T}_{33}^v, \tag{55a}$$

$$
\begin{aligned}
\widetilde{T}_{31}^v &= f(\varepsilon) \, \mathrm{Tr} \left\{ S_{\mathbf{k},i}^{RR}(\varepsilon, \omega) G_{\mathbf{k}}^R(\varepsilon + \omega) \right. \\
&\quad \left. \times \mathcal{V}_{\mathbf{k},x}^{RR}(\varepsilon, \omega) G_{\mathbf{k}}^R(\varepsilon) \hat{\mathcal{H}}^{CD} G_{\mathbf{k}}^R(\varepsilon) \right\},
\end{aligned} \tag{55b}
$$

$$
\begin{aligned}
\widetilde{T}_{32}^v &= [f(\varepsilon + \omega) - f(\varepsilon)] \, \mathrm{Tr} \left\{ S_{\mathbf{k},i}^{AR}(\varepsilon, \omega) G_{\mathbf{k}}^R(\varepsilon + \omega) \right. \\
&\quad \left. \times \mathcal{V}_{\mathbf{k},x}^{RA}(\varepsilon, \omega) G_{\mathbf{k}}^A(\varepsilon) \hat{\mathcal{H}}^{CD} G_{\mathbf{k}}^A(\varepsilon) \right\},
\end{aligned} \tag{55c}
$$

$$
\begin{aligned}
\widetilde{T}_{33}^v &= -f(\varepsilon + \omega) \, \mathrm{Tr} \left\{ S_{\mathbf{k},i}^{AA}(\varepsilon, \omega) G_{\mathbf{k}}^A(\varepsilon + \omega) \right. \\
&\quad \left. \times \mathcal{V}_{\mathbf{k},x}^{AA}(\varepsilon, \omega) G_{\mathbf{k}}^A(\varepsilon) \hat{\mathcal{H}}^{CD} G_{\mathbf{k}}^A(\varepsilon) \right\}.
\end{aligned} \tag{55d}
$$

One finds that in the limit of low impurity concentration $S_{\mathbf{k},i}^{RR} = S_{\mathbf{k},i}^{AA} = \hat{s}_i$ and $\mathcal{V}_{\mathbf{k},x}^{RR} = \mathcal{V}_{\mathbf{k},x}^{AA} = \hat{v}_x$. Thus, there is no vertex correction
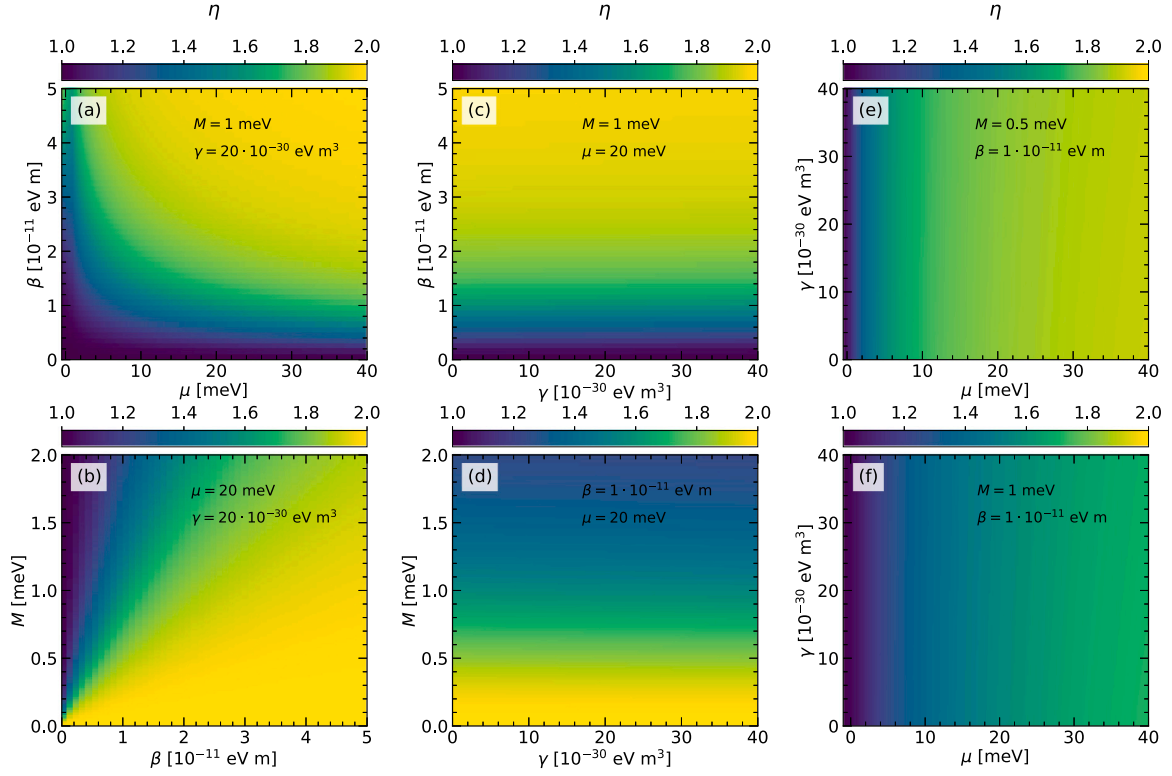
10

Fig. 13. The density plots presenting the impurity vertex function, η, in magnetic system with linear and cubic Dresselhaus SOC as discussed in Section 4.2. The effective mass is the same as in Fig. 2 and the other parameters are indicated.

to non equilibrium spin polarization for the equations containing the product of two retarded or two advanced Green's functions. In the low temperature limit, $T \to 0$, the spin polarization takes the following form:

$$S_x^{v,(T=0)} = \frac{e\hbar}{2\pi} E_x \int \frac{d^2\mathbf{k}}{(2\pi)^2} \left\{ \mathrm{Tr} \left[\hat{s}_x G_{\mathbf{k}}^{0R}(\varepsilon_F) \mathcal{V}_x G_{\mathbf{k}}^{0A}(\varepsilon_F) \right] \right.$$
$$+ \mathrm{Tr} \left[S_x G_{\mathbf{k}}^{0R}(\varepsilon_F) \hat{\mathcal{H}}^{CD} G_{\mathbf{k}}^{0R}(\varepsilon_F) \mathcal{V}_x G_{\mathbf{k}}^{0A}(\varepsilon_F) \right]$$
$$\left. + \mathrm{Tr} \left[S_x G_{\mathbf{k}}^{0R}(\varepsilon_F) \mathcal{V}_x G_{\mathbf{k}}^{A0}(\varepsilon_F) \hat{\mathcal{H}}^{CD} G_{\mathbf{k}}^{0A}(\varepsilon_F) \right] \right\}, \tag{56}$$

where $S_x = \hbar\sigma_x$ and $\mathcal{V}_x = \frac{\hbar k_x}{m}\sigma_0$ are spin and velocity vertex functions renormalized by scalar point-like impurity potential, and the impurity-averaged retarded/advanced Green's function are $G_{\mathbf{k}}^{0R/0A}(\mu) = \left[\mu - \hat{\mathcal{H}}_0 \pm i\Gamma \right]^{-1}$ where Γ is the relaxation rate. The Eq. (56) leads to the following formula:

$$S_x^{v,(T=0)} = \frac{e\hbar}{2\pi} E_x \int \frac{dk\, k}{(2\pi)^2} \left[\frac{k\pi\hbar^2}{2m} (G_-^A G_-^R - G_+^A G_+^R) \right.$$
$$\left. + \frac{k^4\pi\hbar^2\gamma}{8i\Gamma m} \left(G_-^A G_-^A - G_-^R G_-^R + G_+^A G_+^A - G_+^R G_+^R \right) \right], \tag{57}$$

where $G_\pm^R = \left[\mu - E_\pm + i\Gamma_0 \right]^{-1}$ and $G_\pm^A = \left[\mu - E_\pm - i\Gamma_0 \right]^{-1}$. Finally one finds the current-induced spin polarization in the perturbative approach, which for $\mu > 0$ takes the form:

$$S_x^{v,(T=0)} = e\hbar E_x \frac{m\beta}{4\pi\Gamma\hbar^2} - \frac{eE_x m^2 \gamma\mu}{2\pi\Gamma\hbar^3}. \tag{58}$$

Appendix C. Magnetic 2DEG with linear Dresselhaus spin–orbit interaction

The schematic picture of the energy dispersion curves in magnetic 2DEG with linear Dresselhaus spin–orbit interaction (Fig. 12), as discussed in Section 4.1. The picture presents Fermi wavevectors $k_\pm^+$, $k_\mp^-$ that appear in Eqs. (24)–(29).

Appendix D. Magnetic 2DEG with linear and cubic Dresselhaus spin–orbit coupling: Numerical results for the impurity vertex function

Fig. 13 presents the numerical results for impurity vertex function in the most general case considered in this paper, i.e., for magnetic 2DEG with both linear and cubic Dresselhaus spin–orbit coupling. The results clearly show that the coupling parameter of cubic Dresselhaus spin–orbit coupling does not affect qualitatively the impurity vertex function.

Appendix E. Anomalous Hall conductivity

The formalism introduced in Section 2 can be applied to the anomalous Hall conductivity. Thus, the general expression describing the off-diagonal element of the conductivity tensor within Matsubara Green's function formalism has the following form:

$$\sigma_{yx}(i\omega_m) = \Xi \sum_{\mathbf{k},n} \mathrm{Tr} \left\{ \hat{v}_y G_{\mathbf{k}}(i\varepsilon_n + i\omega_m) \hat{\mathcal{H}}_{\mathbf{A}}(i\omega_m) G_{\mathbf{k}}(i\varepsilon_n) \right\}. \tag{59}$$

Note that we keep the same notation as in Section 2. Similar procedure as described in this paper for CISP leads to the anomalous Hall conductivity in the dc limit:

$$\sigma_{yx} = \sigma_{yx}[f(E_\pm)] + \sigma_{yx}[f'(E_\pm)], \tag{60}$$

where

$$\sigma_{yx}[f(E_\pm)] = -\frac{e^2}{\hbar} \sum_{n=\pm} \int \frac{d^2\mathbf{k}}{(2\pi)^2} B_n^z f(E_n) \tag{61}$$

and

$$\sigma_{yx}[f'(E_\pm)] = \frac{e^2}{\hbar} \sum_{n=\pm} \int \frac{d^2\mathbf{k}}{(2\pi)^2} \frac{\Gamma^2}{2\xi_{\mathbf{k}}^2} \frac{M(\beta^2 - \beta\gamma k^2 - 3\gamma^2 k_x^2 k_y^2)}{\xi_{\mathbf{k}}^2 + \Gamma^2} f'(E_n). \tag{62}$$

The above expressions are analogous to Eqs. (35)–(38) for the y-component of spin polarization. The dissipative part of anomalous Hall conductivity vanishes in the limit of $\Gamma \to 0$ and $\sigma_{yx} \approx \sigma_{yx}[f(E_\pm)]$.

References

[1] M.I. D'Yakonov, V.I. Perel, Possibility of orienting electron spins with current, Sov. J. Exp. Theor. Phys. Lett. 13 (1971) 467, http://www.jetpletters.ac.ru/ps/1587/article_24366.shtml; JTPP Lett. 13 (1971) 467.

[2] J.E. Hirsch, Spin hall effect, Phys. Rev. Lett. 83 (9) (1999) 1834–1837, http://dx.doi.org/10.1103/PhysRevLett.83.1834.

[3] J. Sinova, S.O. Valenzuela, J. Wunderlich, C.H. Back, T. Jungwirth, Spin hall effects, Rev. Modern Phys. 87 (4) (2015) 1213–1260, http://dx.doi.org/10.1103/RevModPhys.87.1213.

[4] E.L. Ivchenko, G.E. Pikus, New photogalvanic effect in gyrotropic crystals, Pis'Ma Zh. Eksp. Teor. Fiz. 27 (11) (1978) 640–643, http://www.jetpletters.ac.ru/ps/1554/article_23792.shtml; JETP Lett. 27 (1978) 604.

[5] F.T. Vas'ko, N.A. Prima, Fiz. Tverd. Tela 21 (1979) 1734; Sov. Phys. Solid State 21 (1979) 994.

[6] A.G. Aronov, Y.B. Lyanda-Geller, Nuclear electric resonance and oreintation of carrier spins by an electric field, Pis'Ma Zh. Eksp. Teor. Fiz. 50 (9) (1989) 398–400, http://www.jetpletters.ac.ru/ps/1132/article_17140.shtml; JETP Lett. 50 (1989) 431.

[7] V.M. Edelstein, Spin polarization of conduction electrons induced by electric current in two-dimensional asymmetric electron systems, Solid State Commun. 73 (3) (1990) 233–235, http://dx.doi.org/10.1016/0038-1098(90)90963-C.

[8] Y.K. Kato, R.C. Myers, A.C. Gossard, D.D. Awschalom, Observation of the spin hall effect in semiconductors, Science 306 (5703) (2004) 1910–1913, http://dx.doi.org/10.1126/science.1105514, http://arxiv.org/abs/15539563.

[9] Y.K. Kato, R.C. Myers, A.C. Gossard, D.D. Awschalom, Current-induced spin polarization in strained semiconductors, Phys. Rev. Lett. 93 (17) (2004) 176601, http://dx.doi.org/10.1103/PhysRevLett.93.176601.

[10] J. Wunderlich, B. Kaestner, J. Sinova, T. Jungwirth, Experimental observation of the spin-hall effect in a two-dimensional spin–orbit coupled semiconductor system, Phys. Rev. Lett. 94 (4) (2005) 047204, http://dx.doi.org/10.1103/PhysRevLett.94.047204.

[11] S.D. Ganichev, S.N. Danilov, P. Schneider, V.V. Bel'kov, L.E. Golub, W. Wegscheider, D. Weiss, W. Prettl, Electric current-induced spin orientation in quantum well structures, J. Magn. Magn. Mater. 300 (1) (2006) 127–131, http://dx.doi.org/10.1016/j.jmmm.2005.10.048.

[12] H. Nakayama, M. Althammer, Y.-T. Chen, K. Uchida, Y. Kajiwara, D. Kikuchi, T. Ohtani, S. Geprägs, M. Opel, S. Takahashi, R. Gross, G.E.W. Bauer, S.T.B. Goennenwein, E. Saitoh, Spin hall magnetoresistance induced by a nonequilibrium proximity effect, Phys. Rev. Lett. 110 (20) (2013) 206601, http://dx.doi.org/10.1103/PhysRevLett.110.206601.

[13] H. Nakayama, Y. Kanno, H. An, T. Tashiro, S. Haku, A. Nomura, K. Ando, Rashba-Edelstein magnetoresistance in metallic heterostructures, Phys. Rev. Lett. 117 (11) (2016) 116602, http://dx.doi.org/10.1103/PhysRevLett.117.116602.

[14] T.S. Ghiasi, A.A. Kaverzin, P.J. Blah, B.J. van Wees, Charge-to-spin conversion by the Rashba–Edelstein effect in two-dimensional van der Waals heterostructures up to room temperature, Nano Lett. 19 (9) (2019) 5959–5966, http://dx.doi.org/10.1021/acs.nanolett.9b01611.

[15] S.D. Ganichev, L.E. Golub, Interplay of Rashba/Dresselhaus spin splittings probed by photogalvanic spectroscopy –A review, Phys. Status Solidi b 251 (9) (2014) 1801–1823, http://dx.doi.org/10.1002/pssb.201350261.

[16] J. Schliemann, Colloquium: Persistent spin textures in semiconductor nanostructures, Rev. Modern Phys. 89 (1) (2017) 011001, http://dx.doi.org/10.1103/RevModPhys.89.011001.

[17] S.D. Ganichev, M. Trushin, J. Schliemann, M. Trushin, J. Schliemann, Spin polarization by current, in: Spintronics Handbook, Second Edition: Spin Transport and Magnetism, CRC Press, Boca Raton, FL, USA, 2019, pp. 317–338, http://dx.doi.org/10.1201/9780429434235-8.

[18] R. Winkler, Spin-dependent transport of carriers in semiconductors, in: Handbook of Magnetism and Advanced Magnetic Materials, John Wiley & Sons, Ltd, Chichester, England, UK, 2007, http://dx.doi.org/10.1002/9780470022184.hmm532.

[19] R. Winkler, Spin–Orbit Coupling Effects in Two-Dimensional Electron and Hole Systems, Springer-Verlag, Berlin, Germany, 2003, http://dx.doi.org/10.1007/978-3-540-01187-3.

[20] G. Dresselhaus, Spin–orbit coupling effects in zinc blende structures, Phys. Rev. 100 (2) (1955) 580–586, http://dx.doi.org/10.1103/PhysRev.100.580.

[21] A. Soumyanarayanan, N. Reyren, A. Fert, C. Panagopoulos, Emergent phenomena induced by spin-orbit coupling at surfaces and interfaces, Nature 539 (7630) (2016) 509–517, http://dx.doi.org/10.1038/nature19820.

[22] A. Manchon, H.C. Koo, J. Nitta, S.M. Frolov, R.A. Duine, New perspectives for Rashba spin–orbit coupling, Nature Mater. 14 (9) (2015) 871–882, http://dx.doi.org/10.1038/nmat4360.

[23] M. Kim, J. Im, A.J. Freeman, J. Ihm, H. Jin, Switchable S = 1/2 and j = 1/2 Rashba bands in ferroelectric halide perovskites, Proc. Natl. Acad. Sci. USA 111 (19) (2014) 6900, http://dx.doi.org/10.1073/pnas.1405780111.

[24] L. Bawden, J.M. Riley, C.H. Kim, R. Sankar, E.J. Monkman, D.E. Shai, H.I. Wei, E.B. Lochocki, J.W. Wells, W. Meevasana, T.K. Kim, M. Hoesch, Y. Ohtsubo, P. Le Fèvre, C.J. Fennie, K.M. Shen, F. Chou, P.D.C. King, Hierarchical spin–orbital polarization of a giant Rashba system, Sci. Adv. 1 (8) (2015) e1500495, http://dx.doi.org/10.1126/sciadv.1500495.

[25] M. Kepenekian, J. Even, Rashba and dresselhaus couplings in halide perovskites: Accomplishments and opportunities for spintronics and spin–orbitronics, J. Phys. Chem. Lett. 8 (14) (2017) 3362–3370, http://dx.doi.org/10.1021/acs.jpclett.7b01015.

[26] H. Maaß, H. Bentmann, C. Seibel, C. Tusche, S.V. Eremeev, T.R.F. Peixoto, O.E. Tereshchenko, K.A. Kokh, E.V. Chulkov, J. Kirschner, F. Reinert, Spin-texture inversion in the giant Rashba semiconductor BiTeI, Nature Commun. 7 (11621) (2016) 1–7, http://dx.doi.org/10.1038/ncomms11621.

[27] L. Zhu, T. Zhang, G. Chen, H. Chen, Huge Rashba-type spin–orbit coupling in binary hexagonal PX nanosheets (X = As, Sb, and Bi), Phys. Chem. Chem. Phys. 20 (48) (2018) 30133–30139, http://dx.doi.org/10.1039/C8CP05426F.

[28] A.D. Caviglia, M. Gabay, S. Gariglio, N. Reyren, C. Cancellieri, J.-M. Triscone, Tunable Rashba spin–orbit interaction at oxide interfaces, Phys. Rev. Lett. 104 (12) (2010) 126803, http://dx.doi.org/10.1103/PhysRevLett.104.126803.

[29] K. Gopinadhan, A. Annadi, Y. Kim, A. Srivastava, B. Kumar, J. Chen, J.M.D. Coey, Ariando, T. Venkatesan, Gate tunable in- and out-of-plane spin–orbit coupling and spin-splitting anisotropy at LaAlO3/SrTiO3 (110) interface, Adv. Electron. Mater. 1 (8) (2015) 1500114, http://dx.doi.org/10.1002/aelm.201500114.

[30] N. Nagaosa, J. Sinova, S. Onoda, A.H. MacDonald, N.P. Ong, Anomalous hall effect, Rev. Modern Phys. 82 (2) (2010) 1539–1592, http://dx.doi.org/10.1103/RevModPhys.82.1539.

[31] A.G. Mal'shukov, K.A. Chao, Spin Hall conductivity of a disordered two-dimensional electron gas with Dresselhaus spin–orbit interaction, Phys. Rev. B 71 (12) (2005) 121308, http://dx.doi.org/10.1103/PhysRevB.71.121308.

[32] H. Zhu, Anomalous Hall effect in paramagnetic 2DEG with linear and cubic Dresselhaus spin–orbit coupling, Internat. J. Modern Phys. B 24 (14) (2010) 2107–2112, http://dx.doi.org/10.1142/S0217979210049800.

[33] B. Zhou, Intrinsic anomalous Hall effect in spin-polarized two-dimensional electron gases with Dresselhaus spin–orbit interaction, Phys. Rev. B 81 (7) (2010) 075318, http://dx.doi.org/10.1103/PhysRevB.81.075318.

[34] C.P. Weber, J. Orenstein, B.A. Bernevig, S.-C. Zhang, J. Stephens, D.D. Awschalom, Nondiffusive spin dynamics in a two-dimensional electron gas, Phys. Rev. Lett. 98 (7) (2007) 076604, http://dx.doi.org/10.1103/PhysRevLett.98.076604.

[35] J.D. Koralek, C.P. Weber, J. Orenstein, B.A. Bernevig, S.-C. Zhang, S. Mack, D.D. Awschalom, Emergence of the persistent spin helix in semiconductor quantum wells, Nature 458 (7238) (2009) 610–613, http://dx.doi.org/10.1038/nature07871.

[36] B.A. Bernevig, J. Orenstein, S.-C. Zhang, Exact SU(2) symmetry and persistent spin helix in a spin–orbit coupled system, Phys. Rev. Lett. 97 (23) (2006) 236601, http://dx.doi.org/10.1103/PhysRevLett.97.236601.

[37] A. Maleki Sheikhabadi, I. Miatka, E.Y. Sherman, R. Raimondi, Theory of the inverse spin galvanic effect in quantum wells, Phys. Rev. B 97 (23) (2018) 235412, http://dx.doi.org/10.1103/PhysRevB.97.235412.

[38] G.D. Mahan, Many-Particle Physics, Springer US, New York, NY, USA, 2000, http://dx.doi.org/10.1007/978-1-4757-5714-9.

[39] A. Dyrdał, J. Barnaś, V.K. Dugaev, Current-induced spin polarization of a magnetized two-dimensional electron gas with Rashba spin–orbit interaction, Phys. Rev. B 95 (24) (2017) 245302, http://dx.doi.org/10.1103/PhysRevB.95.245302.

[40] S.D. Ganichev, M. Trushin, J. Schliemann, M. Trushin, J. Schliemann, Spin polarization by current, in: Spintronics Handbook, Second Edition: Spin Transport and Magnetism, CRC Press, 2019, pp. 317–338, http://dx.doi.org/10.1201/9780429434235-8.

[41] A. Dyrdał, J. Barnaś, V.K. Dugaev, J. Berakdar, Thermally induced spin polarization in a magnetized two-dimensional electron gas with Rashba spin–orbit interaction, Phys. Rev. B 98 (7) (2018) 075307, http://dx.doi.org/10.1103/PhysRevB.98.075307.

[42] N. Zhang, Y. Wang, J. Berakdar, C. Jia, Giant spin–orbit torque and spin current generation in carriers at oxide interfaces, New J. Phys. 18 (9) (2016) 093034, http://dx.doi.org/10.1088/1367-2630/18/9/093034.

Discussion

Anomalous Hall effect

Eq. (61) in A-4, the intrinsic anomalous Hall conductivity (AHC) in a magnetized 2DEG with k-linear Dresselhaus SOI, can be written as:

$$\sigma_{xy}^{II} = -\frac{e^2 M \beta^2}{2\pi\hbar} \int \mathrm{d}k\, k \frac{f(E_+) - f(E_-)}{2(M^2 + \beta^2 k^2)^{3/2}}. \tag{4.7}$$

The above result can be compared with the intrinsic AHC for a magnetized 2DEG with a k-linear Rashba-type spin-orbit interaction, as analyzed in the work by Dugaev et al. [154]. It turns out that the result aligns in both models (c.f. eq. (4.7) and eq. (25) in [154]). Therefore, one can conclude that for both types of spin-orbit interaction – Rashba and Dresselhaus – the intrinsic transverse charge response in a magnetized 2DEG is the same, regardless of the sign, which is consistent with [153].

In the low-temperature limit, eq. (4.7) is formulated through the analytical expression:

$$\sigma_{xy}^{(T=0)} = \frac{e^2 M}{4\pi\hbar} \times \begin{cases} \left(\frac{1}{\lambda_{k_+}} - \frac{1}{\lambda_{k_-}} \right) & \text{for} \quad \mu \geq M, \\[2mm] \left(\frac{1}{M} - \frac{1}{\lambda_{k_-}} \right) & \text{for} \quad -M \leq \mu < M, \\[2mm] \left(\frac{1}{\lambda_{k_+^-}} - \frac{1}{\lambda_{k_-^-}} \right) & \text{for} \quad -\frac{\varepsilon_\beta}{2}\left(1 + \frac{M^2}{\varepsilon_\beta^2}\right) \leq \mu < -M. \end{cases} \tag{4.8}$$

If both forms of Dresselhaus SOI are included, i.e., $\beta \neq 0$ and $\gamma \neq 0$, the intrinsic AHC is expressed in the form [107]:

$$\sigma_{xy} = -\frac{e^2 M}{2\pi\hbar} \int \mathrm{d}k\, k \frac{\beta(\beta - \gamma k^2) - 3\gamma^2 k_x^2 k_y^2}{2(M^2 + \beta^2 k^2)^{3/2}} \left[f(E_+) - f(E_-)\right]. \tag{4.9}$$

Summary

Applying an external electric field in (001)-plane to a 2D system with symmetric quantum well grown in the [001]-direction, modeled by a 2DEG with Dresselhaus SOI, results in an in-plane carrier's spin orientation. In a nonmagnetic system, the spins are polarized parallel to the electric field, and the non-equilibrium current-induced spin polarization (CISP) appears. Figure 4.3 illustrates the longitudinal spin polarizability[3], χ_{xx}, plotted as a function of chemical potential, μ, in the weak cubic Dresselhaus SOI limit, $\beta k \gg \gamma k^3$, (solid orange and dashed blue lines), and beyond this limit (solid red and dashed green lines). Solid (dashed) lines represent cases with (without) the inclusion of the impurity vertex correction. Zero-temperature results are shown in Figures 4.3a,c, while finite-temperature outcomes are depicted in Figures 4.3b,d.

---

[3]Spin polarizability (the response function) is expressed *via* spin polarization, S_x, as: $\chi_{xx} = S_x/(eE_x)$, where e – charge of an electron, E_x – amplitude of an external electric field in x-direction.
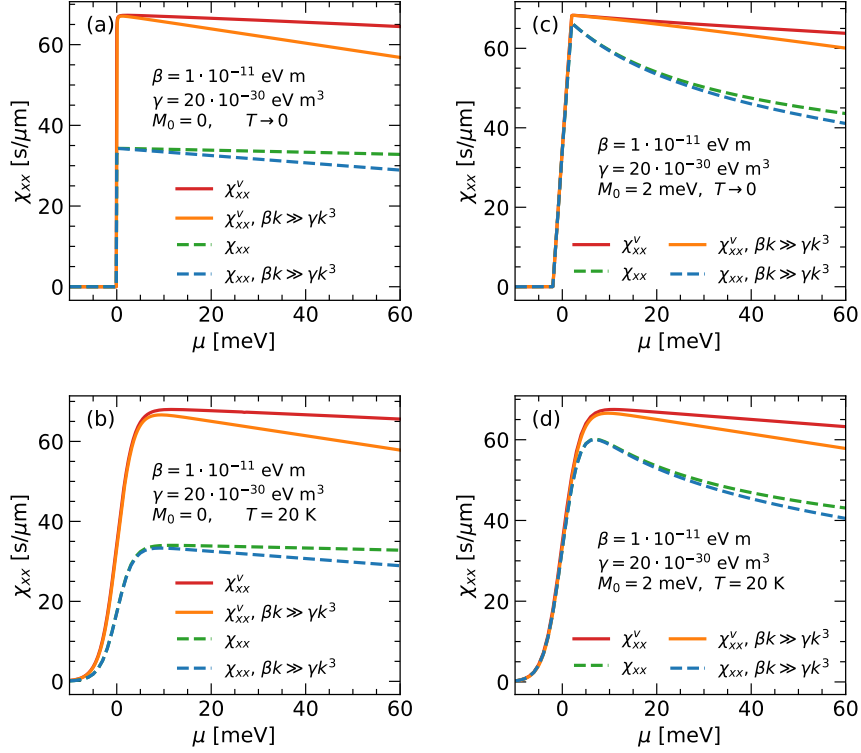
Figure 4.3: Spin polarizability, χ_{xx}, as a function of chemical potential, μ, with (a),(b) corresponding to a nonmagnetic 2DEG and (c),(d) including an out-of-plane exchange field in the system. Solid (dashed) lines represent outcomes with (without) impurity vertex correction. In (a) and (c), χ_{xx} is obtained using a formula derived for the zero-temperature limit, while (b) and (d) display χ_{xx} for $T = 20$ K, calculated using the finite-temperature Matsubara-Green's functions formalism. The solid orange and dashed blue lines present the results in the weak cubic Dresselhaus SOC limit, $\beta k \gg \gamma k^3$.

Figures 4.3a,b display χ_{xx} for a nonmagnetized 2DEG, and Figures 4.3c,d present results for a magnetized 2DEG. One can observe, that the cubic term of Dresselhaus SOI reduces the CISP as the chemical potential, μ, increases. Moreover, in the limit of weak cubic Dresselhaus SOI, $\beta k \gg \gamma k^3$, there is an underestimation of the CISP, which corresponds to an overestimation of the influence of the cubic Dresselhaus SOC term (this is illustrated by the differences between the dashed lines and the solid lines in each plot of Figure 4.3). The influence of the impurity vertex correction on χ_{xx} indicates, that the scattering processes at short-range spin-independent impurities increase the dissipative CISP component (parallel to the applied electric field) up to twice when spin-orbit coupling dominates the exchange field (Fig. 4.3a,b).

Additionally, in a system with an out-of-plane exchange interaction, a response perpendicular to the driving force emerges. Specifically, the transverse components of non-equilibrium spin polarization and anomalous Hall conductivity are identified. The main contribution to both of these transverse effects originates from the states in the Fermi sea, which makes them non-dissipative, and having an intrinsic character linked to the Berry curvature.

If a temperature gradient is applied to the system instead of an electric field, thermally-induced

spin polarization (TISP) appears. The dissipative component of TISP, determined by the states at the Fermi level, is connected through a Mott-like relation with electrically-induced spin polarization.The TISP takes non-zero values in the energy gap and can be easily tuned with the out-of-plane exchange field. In turn, TISP vanishes for higher μ, where the cubic Dresselhaus SOI influences the results; thus, the cubic term does not distinctly modify TISP. Furthermore, the behavior of TISP is similar to the case of a 2DEG trapped in an asymmetric quantum well, where Rashba-type SOC occurs. The key difference is that the dissipative component of the spin polarization in the Rashba model is not perpendicular but parallel to the driving force [128].

4.5   Reprint of the article A-5

The manuscript titled "Bilinear magnetoresistance in a 2DEG with isotropic cubic Rashba spin-orbit interaction" provides analytical results on the magnetoresistance term that scales linearly with both external electric and magnetic fields in a 2DEG with isotropic cubic form of Rashba spin-orbit interaction.

The bilinear magnetoresistance (BMR) term is evoked by an effective spin-orbital field that couples to the electron spin. The spin-orbital field, in turn, originates from the non-equilibrium spin polarization induced by the external electric field. Here, Green's functions formalism is utilized, where the external in-plane magnetic field is treated as a perturbation. This assumption is justified by the fact that the considered effect, BMR, depends on the presence of Rashba SOI in the system and is expected to manifest even in a weak magnetic field.

It was found that the BMR signal varies sinusoidally with the angle of the in-plane magnetic field, reaching its maximum amplitude when the magnetic field is applied perpendicular to the electric field. Furthermore, the BMR contribution is most pronounced at lower carrier concentrations and increases with a stronger Rashba spin-orbital field. Finally, while a stronger magnetic field enhances the BMR values, observing the BMR effect does not require a large magnetic field.

Research article

Bilinear magnetoresistance in 2DEG with isotropic cubic Rashba spin–orbit interaction

A. Krzyżewska, A. Dyrdał [*]

Faculty of Physics, ISQI, Adam Mickiewicz University in Poznań, ul. Uniwersytetu Poznańskiego 2, 61-614 Poznań, Poland

ARTICLE INFO

ABSTRACT

Bilinear magnetoresistance has been studied theoretically in 2D systems with isotropic cubic form of Rashba spin–orbit interaction. We have derived the effective spin–orbital field due to current-induced spin polarization and discussed its contribution to the unidirectional system response. The analyzed model can be applied to the semiconductor quantum wells as well as 2DEG at the surfaces and interfaces of perovskite oxides.

1. Introduction

The magnetotransport is a phenomenon that is known in condensed matter physics for more than hundred years [1–3]. The associated magnetoresistance is currently also a hallmark of spin electronics, that was developed after the discovery of giant magnetoresistance in metallic multilayers at the end of 80's [4–6]. Nowadays spintronics takes advantage of spin-to-charge interconversion effects [7–10] that lead to new magnetoresistance phenomena such as spin magnetoresistance and various unidirectional magnetotransport effects [11–16].

The magnetoresistance (MR) is typically a quadratic function of the magnetic field (or magnetization) amplitude. The linear scaling with magnetic field/magnetization is rather unique and dictated by specific symmetry requirements. Recently, the linear dependence on the magnetic field has been reported in single crystals of antiferromagnetic metals (i.e., TmB_4), where MR can be tuned from quadratic to linear one depending on the orientation of magnetic field [17,18]. It has been shown in recent years, that the spin–orbit interaction can lead to spin-currents and non-equilibrium spin polarization, that can coupled to the external magnetic field or equilibrium magnetization of the system leading to unidirectional magnetotransport [19–23]. The unidirectional spin magnetoresistance in general is a consequence of non-equilibrium spin polarization at the interface of the hybrid structures consisting of a ferromagnetic thin film and a layer of heavy metal or topological insulator. Interestingly, it has been shown that the unidirectional magnetoresistance also appears in nonmagnetic materials. This effect is called bilinear magnetoresistance, BMR, as it scales linearly with the charge current density and external magnetic field. The BMR effect can be a consequence of the strong spin–orbit interaction in systems

with highly anisotropic Fermi contours. This is for example a case of topological insulators with strong hexagonal warping [19,20]. In this case the nonlinear spin currents appear in the system, which in the presence of external magnetic field are partially converted to the non-linear charge current. Another mechanism was proposed to explain the bilinear magnetoresistance in systems with isotropic Fermi contours. This mechanism is related to the non-equilibrium spin-polarization (also known as inverse spin-galvanic effect or Edelstein effect) that appears in the system under external electric field and leads to the effective spin–orbital field that couples to the electron spin. [22]. The Berry curvature dipole can also give contribution to the unidirectional magnetotransport.

In this work we analyze the BMR in the 2D system with isotropic cubic form of Rashba spin–orbit coupling (SOC). Such a form of Rashba SOC can be found in 2DEG emerging in the semiconductor quantum wells as well as 2DEG at the surfaces and interfaces of perovskite oxides [22,24–32]. The detailed description of the model of 2DEG electron gas in the presence of isotropic cubic Rashba SOC can be found, e.g., in [33,34].

The paper is organized as follows. In Section 2 we will present the effective Hamiltonian describing 2DEG with isotropic cubic Rashba coupling and formalism that will be used to describe transport characteristics. Next, in Section 3, we will derive analytical expressions for charge current density and non-equilibrium spin polarization in the absence of external magnetic field. The main results will be presented in Section 4, where we will present derived analytical expressions for bilinear magnetoresistance. Next, we will present numerical results. The general conclusions and summary will be provided in Section 5.

* Corresponding author.
  E-mail address: adyrdal@amu.edu.pl (A. Dyrdał).

2. Model and method

2.1. Effective Hamiltonian

We consider the effective Hamiltonian, obtained upon two canonical transformations from 8×8 Luttinger Hamiltonian for p-doped semiconductor quantum wells with structural inversion asymmetry [35,36], and takes form [33]:

$$\hat{H} = \frac{\hbar^2 k^2}{2m^*}\sigma_0 + i\alpha(k_-^3\sigma_+ - k_+^3\sigma_-) + \mathbf{B}\cdot\hat{\mathbf{s}} + \mathbf{B}_{\mathrm{so}}\cdot\hat{\mathbf{s}}, \tag{1}$$

where $k = \sqrt{k_x^2 + k_y^2}$ is the wavevector amplitude, m^* is the effective mass. The second therm describes the effect of cubic Rashba SOI [33] and is expressed by Rashba coupling parameter, α, and $k_{\pm} = (k_x \pm ik_y)$. In addition, $\sigma_{\pm} = \frac{1}{2}(\sigma_x \pm i\sigma_y)$, where σ_n ($n = x, y, z$) denotes nth Pauli matrix. Note that, m^* and α are material parameters and are defined in Appendix A. The effect of the external in-plane magnetic field, $\mathbf{B}$, is taken into account by the Zeeman term, where $\mathbf{B} = \{B_x, B_y, 0\}$ is in the energy units, that is $\mathbf{B} = g\mu_B\mathbf{b}$ (g - g-factor, μ_B - Bohr magneton, $\mathbf{b}$ - magnetic field in Tesla), and spin operators are 2×2 matrices that can be written by the identity matrix and Pauli matrices as:

$$\hat{s}_\alpha = \sum_{\beta=0,x,y,z} s_\beta^\alpha \sigma_\beta, \tag{2}$$

where the coefficients s_β^α are provided in Appendix A.

Finally, the last term in the Hamiltonian describes the coupling of electron spins to the effective spin–orbital field, $\mathbf{B}_{\mathrm{so}}$, that can be expressed by the non-equilibrium spin polarization emerging due to the inverse spin-galvanic effect and proportional to the charge current density (and thus to the external electric field), i.e, $\mathbf{B}_{\mathrm{so}} \sim \mathbf{S} \sim \mathbf{j}$. As the effective cubic Rashba model considered here is defined by much more complex spin operators, the coupling between spin polarization and electron spin is defined by the two coupling constants: J_0 that couples non-equilibrium spin polarization to the part of the spin operator proportional to the identity matrix σ_0, and coupling constant J_1 that couples spin polarization to the part of spin operator proportional to Pauli matrices $\sigma_{x,y}$,

$$\mathbf{B}_{\mathrm{so}}\cdot\hat{\mathbf{s}} = J_0 S_\alpha s_0^\alpha \sigma_0 + J_1 S_\alpha (s_x^\alpha \sigma_x + s_y^\alpha \sigma_y) \tag{3}$$

where S_α is α-th component of the non-equilibrium spin polarization. The coupling constants $J_{0,1}$ have been derived and presented in Appendix B. Here we stress that non-equilibrium spin polarization induced by the charge current in 2DEG with isotropic cubic Rashba SOC has been studied recently in detail by Karwacki et al. [34]. Here, we will use the general results for current-induced spin polarization presented in [34], and adapt them to derive the theoretical description of BMR.

2.2. Model assumptions

Without losing the generality in our further analysis the external electric field is applied in the x-direction. This means that current-induced spin polarization, under zero magnetic field, has only y-component. We focus on the (unidirectional) bilinear correction to the magnetoresistance, i.e., we characterize the term in magnetoresistance that is proportional to the in-plane magnetic field and simultaneously to the charge current density (electric field). The higher order terms with respect to B and j, that can eventually appear and lead to additional corrections in magnetoresistance (e.g., in strong magnetic fields) are not considered here. Accordingly, we treat perturbatively the terms proportional to the in-plane magnetic field and spin–orbital field in Hamiltonian (1), i.e., $H = H_0 + H_{pert}$, where:

$$H_0 = \frac{\hbar^2 k^2}{2m^*}\sigma_0 + i\alpha(k_-^3\sigma_+ - k_+^3\sigma_-), \tag{4}$$

and the perturbation is defined as:

$$H_{\mathrm{pert}} = \sum_{\beta=0,x,y} b_{\mathrm{eff}\beta}\,\sigma_\beta \tag{5}$$

where

$$b_{\mathrm{eff}\,0} = B_x s_0^x + (B_y + J_0 S_y)s_0^y \tag{6}$$

$$b_{\mathrm{eff}\,x} = B_x s_x^x + (B_y + J_1 S_y)s_x^y \tag{7}$$

$$b_{\mathrm{eff}\,y} = B_x s_y^x + (B_y + J_1 S_y)s_y^y \tag{8}$$

Thus, the H_{pert} has a form of Zeeman-like term acting in the pseudospin space.

Note, that the effective spin–orbital field is approximated in our calculations by the non-equilibrium spin polarization under zero magnetic field. This simplification is justified as the additional components of spin polarization that appear in the presence of an external magnetic field are a few orders of magnitude smaller than the component which survives under zero magnetic field. The magnetic field contribution to the leading term of spin polarization results in higher order terms in magnetoresistance that are neglected here.

2.3. Method

To obtain magnetotransport characteristics, we have used Matsubara-Green's function formalism within linear response theory [37] and used the following formula for the quantum-mechanical average value of the observable, O_n corresponding to the operator $\hat{O}_n$:

$$O_\alpha = -\lim_{\omega\to0}\frac{eE_\beta\hbar}{(2\pi)^3\omega}\int d^2\mathbf{k}\int d\varepsilon f(\varepsilon)\,\mathrm{Tr}\left\{\hat{O}_\alpha G_\mathbf{k}^R(\varepsilon+\omega)\hat{v}_\beta\Delta_\mathbf{k}^{RA}(\varepsilon) \right.$$
$$\left. + \hat{O}_\alpha\Delta_\mathbf{k}^{RA}(\varepsilon)\hat{v}_\beta G_\mathbf{k}^A(\varepsilon-\omega)\right\} \tag{9}$$

where $\Delta_\mathbf{k}^{RA}(\varepsilon) = \left[G_\mathbf{k}^R(\varepsilon) - G_\mathbf{k}^A(\varepsilon)\right]$ and $G_\mathbf{k}^{R/A}(\varepsilon)$ is the retarded/advanced Green function related to the Hamiltonian $\hat{H}_0$. Derivation of this formula can be found, e.g., in [34,37,38]. The operator corresponding to nth component of the charge current density is

$$\hat{j}_\alpha = e\hat{v}_\alpha = \frac{e}{\hbar}\frac{\partial\hat{H}_0}{\partial k_\alpha}, \tag{10}$$

and spin-polarization should be derived using the spin operators given by Eq. (2).

3. Spin-to-charge interconversion: limit of zero magnetic field

In the first step we consider 2DEG with cubic Rashba SOC under zero magnetic field. Based on Eq. (9) the general relation between dc charge current density and spin polarization can be derived. This relation is starting point for our further consideration of nonlinear magnetotransport.

3.1. Charge current density

In the dc limit, the charge current density, calculated based on Eq. (9), takes the following form:

$$j_x = -\frac{e^2\hbar E_x}{4\pi\Gamma_0}\int dk\left\{\frac{3\alpha k^4}{m}[f'(E_+) - f'(E_-)]\right.$$
$$+ \frac{k^3\hbar^2}{2m^2}[f'(E_+) + f'(E_-)]$$
$$\left. + \frac{9\alpha^2 k^5}{2\hbar^2}\left(1 + \frac{1}{(\alpha k^3/\Gamma)^2 + 1}\right)[f'(E_+) + f'(E_-)]\right\} \tag{11}$$

In the low-temperature limit, the above expression leads to:

$$j_x = \frac{e^2\hbar E_x}{4\pi\Gamma}\left\{\frac{9\alpha^2}{2\hbar^2}\left(k_{F-}^4 v_- + k_{F+}^4 v_+\right)\right.$$
$$+ \frac{3\alpha}{m}\left(k_{F+}^3 v_+ - k_{F-}^3 v_-\right) + \frac{\hbar^2}{2m^2}\left(k_{F-}^2 v_- + k_{F+}^2 v_+\right)$$
$$\left. + \frac{9\alpha^2}{2\hbar^2}\left(\frac{k_{F-}^4 v_-}{(\alpha k_{F-}^3/\Gamma)^2 + 1} + \frac{k_{F+}^4 v_+}{(\alpha k_{F+}^3/\Gamma)^2 + 1}\right)\right\} \tag{12}$$
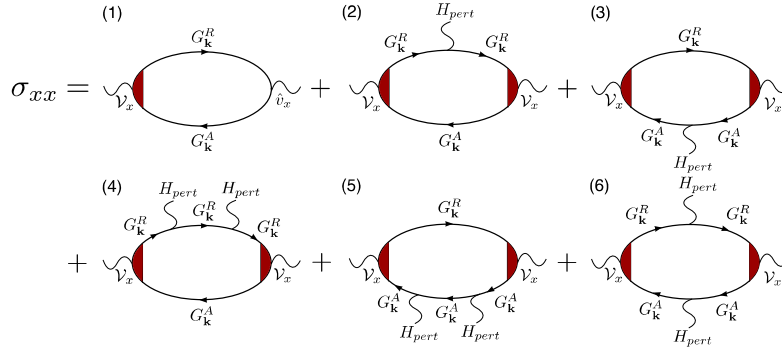
Fig. 1. Feynman diagrams for diagonal conductivity up to the second order perturbation due to $\mathbf{b}_{\mathrm{eff}}$.

where $k_{F\pm}$ are the Fermi wavevectors [39]:

$$
k_{F\pm} = \mp \frac{1}{2} \frac{\hbar^2}{2m\alpha} \left(1 - \sqrt{1 - 4\pi n \left(\frac{2m\alpha}{\hbar^2} \right)} \right)
$$
$$
+ \left[-\frac{1}{2} \left(\frac{\hbar^2}{2m\alpha} \right)^2 \left(1 - \sqrt{1 - 4\pi n \left(\frac{2m\alpha}{\hbar^2} \right)} \right) + 3\pi n \right]^{1/2}
\tag{13}
$$

with n denoting the charge carrier density and $\nu_\pm$ having sense of density of states:

$$
\nu_\pm = \frac{m}{\hbar^2 \left(1 \pm \frac{3\alpha m}{\hbar^2} k_{F\pm} \right)}
\tag{14}
$$

In the presence of randomly distributed point-like impurities, the relaxation rate, $\Gamma = \frac{\hbar}{2\tau}$ (τ is the relaxation time), takes the form $\Gamma = n_i V_0^2 \left(\nu_+ + \nu_- \right) / 4$ where n_i is the concentration of impurities and V_0 is the impurity potential.

3.2. Current-induced spin polarization

The non-equilibrium spin polarization, S_y, in dc limit takes the form:

$$
S_y = -\frac{e\hbar E_x}{4\pi} s_0 \int dk \left\{ \frac{3\alpha k^4}{2\Gamma} [f'(E_+) - f'(E_-)] \right.
$$
$$
\left. + \frac{k^3 \hbar^2}{2m\Gamma} [f'(E_+) + f'(E_-)] \right\}
$$
$$
- \frac{e\hbar E_x}{4\pi} s_1 \int dk \left\{ \frac{k^4 \hbar^2}{2m\Gamma} [f'(E_+) - f'(E_-)] \right.
$$
$$
\left. + \frac{3\alpha}{2} k^5 \left(\frac{1}{\Gamma} + \frac{1}{(k^6 \alpha^2 + \Gamma^2)} \right) [f'(E_+) + f'(E_-)] \right\},
\tag{15}
$$

that in the low-temperature limit can be written as:

$$
S_y = \frac{e\hbar E_x}{8\pi\Gamma} s_0 \left\{ \frac{\hbar^2}{m} \left(k_{F+}^2 \nu_+ + k_{F-}^2 \nu_- \right) + 3\alpha \left(k_{F+}^3 \nu_+ - k_{F-}^3 \nu_- \right) \right\}
$$
$$
+ \frac{e\hbar E_x}{8\pi\Gamma} s_1 \left\{ 3\alpha \left(k_{F+}^4 \nu_+ - k_{F-}^4 \nu_- \right) + \frac{\hbar^2}{m} \left(k_{F+}^3 \nu_+ + k_{F-}^3 \nu_- \right) \right.
$$
$$
\left. + 3\alpha \left[\frac{k_{F+}^4 \nu_+}{\left(\alpha k_{F+}^3 / \Gamma \right)^2 + 1} + \frac{k_{F-}^4 \nu_-}{\left(\alpha k_{F-}^3 / \Gamma \right)^2 + 1} \right] \right\}.
\tag{16}
$$

Note that in the above expressions $s_{0,1}$ are material parameters, that characterize the material and define the spin operators. Their explicit forms are provided in Appendix A. Combining (12) and (16) it is possible to express the spin polarization by the charge current density:

$$
S_y = \frac{s_0 S_{s0} - s_1 S_{s1}}{e\xi} j_x
\tag{17}
$$

where $\xi = \frac{3\alpha}{\hbar^2} \left(k_{F+}^3 - k_{F-}^3 \right) + \frac{1}{m} \left(k_{F+}^2 + k_{F-}^2 \right)$.

In the limit of $\gamma_1 \gg \gamma_2$ one finds:

$$
S_y = s_0 \frac{m}{e} j_x,
\tag{18}
$$

where

$$
j_x = \frac{e^2}{4\pi} \xi \tau E_x.
\tag{19}
$$

with τ denoting relaxation time linked to the relaxation rate, Γ, through the simple relation $\Gamma = \hbar/(2\tau)$.

4. Magnetoresistance

4.1. Longitudinal charge conductivity in the presence of magnetic field

The current-induced spin polarization determines the spin–orbital field. Treating the effective field $\mathbf{b}_{\mathrm{eff}}$ as a perturbation the diagonal conductivity can be expressed as:

$$
\sigma_{xx} = \frac{j_x}{E_x} = \frac{e^2 \hbar}{2\pi} \int \frac{d^2\mathbf{k}}{(2\pi)^2} \mathrm{Tr}\{ \hat{v}_x \bar{G}_{\mathbf{k}}^R \hat{v}_x \bar{G}_{\mathbf{k}}^A \}
\tag{20}
$$

where $\bar{G}_{\mathbf{k}}^{A/R}$ are impurity-averaged advanced and retarded Greens' functions in the weak magnetic field limit: $\bar{G}_{\mathbf{k}}^{R/A} = G_{\mathbf{k}}^{R/A} + G_{\mathbf{k}}^{R/A} H_{\mathrm{pert}} G_{\mathbf{k}}^{R/A} + G_{\mathbf{k}}^{R/A} H_{\mathrm{pert}} G_{\mathbf{k}}^{R/A} H_{\mathrm{pert}} G_{\mathbf{k}}^{R/A}$. Note that contributions related to two retarded and two advanced Green's functions (see Eq. (9)) have been neglected, as they do not affect the final results.

Based on Eq. (20) and diagrammatic theory one finds six diagrams, depicted in Fig. 1, that can be grouped into three terms, according to the order of perturbation:

$$
\sigma_{xx} = \frac{e^2 \hbar}{8\pi^3} \left(\mathcal{D}_1 + \mathcal{D}_{2,3} + \mathcal{D}_{4-6} \right)
\tag{21}
$$

The first diagram, related to the expression $\mathcal{D}_1$ describes the conductivity in the absence of $\mathbf{b}_{\mathrm{eff}}$, and is given by:

$$
\mathcal{D}_1 = \pi^2 \left[\frac{\xi}{\Gamma} + \frac{9\alpha^2 \Gamma}{\hbar^2} \left(\frac{k_{F-}^4 \nu_-}{\Gamma^2 + \alpha^2 k_{F-}^6} + \frac{k_{F+}^4 \nu_+}{\Gamma^2 + \alpha^2 k_{F+}^6} \right) \right],
\tag{22}
$$

which in the low-impurity concentration limit, $\Gamma \to 0$, leads to:

$$
\mathcal{D}_1 = \pi^2 \frac{\xi}{\Gamma}.
\tag{23}
$$

The second and the third diagrams do not contribute, as $\mathcal{D}_{2,3} = 0$. The diagrams $(4) - (6)$ lead to $\mathcal{D}_{4-6}$ that contains B-linear and B-quadratic terms:

$$
\mathcal{D}_{4-6} = \left[B^2 \left(\mathcal{F}_1^{B^2} + \mathcal{F}_2^{B^2} \cos(2\psi) \right) + B \sin(\psi) S_y \mathcal{F}^{jB} \right],
\tag{24}
$$

with $\mathcal{F}$s being rather cumbersome functions of $k_\pm$, $\nu_\pm$ and α, thus not shown here.
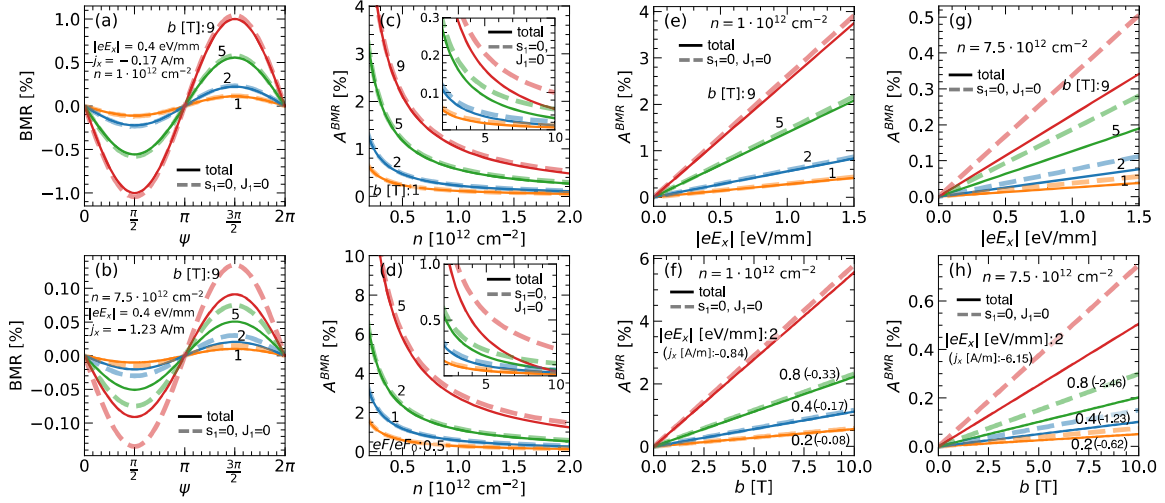
Fig. 2. Bilinear magnetoresistance, BMR, as a function of the angle ψ (the angle between the in-plane magnetic field and $\hat{x}$-axis) for different values of magnetic field, b, (a,b). The amplitude of BMR, $A^{\mathrm{BMR}} = \mathrm{BMR}(\psi = 3\pi/2)$, as a function of carrier density, n, for the indicated values of magnetic field, b (c) and for the indicated values of the quantum well potential, eF/eF_0, (d). A^{BMR} as a function of the external electric field, eE_x, for the indicated values of magnetic field, b, and for the carrier density $n = 1 \cdot 10^{12}$ cm^{-2} (e) and $n = \{1, 7.5\} \cdot 10^{12}$ cm^{-2} (g). A^{BMR} as a function of the in-plane magnetic field, b, for the indicated values of electric field, eE_x, and for the carrier density $n = 1 \cdot 10^{12}$ cm^{-2} (f) and $n = \{1, 7.5\} \cdot 10^{12}$ cm^{-2} (h). The solid lines represent the total formula on BMR, Eq. (26), while the light dashed lines correspond to the formula in the limit $\gamma_1 \gg \gamma_2$, Eq. (28), i.e., for $s_1 = 0$ and $J_1 = 0$. Other parameters are taken from Refs. [26,34] for an STO-surface, i.e.,: $eF_0 = 450 \cdot 10^6$ eV/m, $\gamma_1 = 0.66$, $\gamma_2 = 0.003$, $L_z = 100 \cdot 10^{-10}$ m, $m = 1.5 m_0$ and $J_1/J_0 \cong -0.23$.

4.2. Bilinear magnetoresistance

The magnetoresistance can be expressed in a standard form MR $= (\rho_{xx} - \rho_{xx}^0)/\rho_{xx}^0$, where $\rho_{xx}^0 = 1/\sigma_{xx}^{(1)}$ is the diagonal resistance in the absence of magnetic field and $\rho_{xx} = 1/(\sigma_{xx}^{(1)} + \sigma_{xx}^{(4-6)})$. Note that the transverse conductivity, σ_{xy}, (planar Hall effect) is much smaller than σ_{xx} and has been neglected here.

The unidirectional (bilinear) contribution to magnetoresistance is defined as:

$$\mathrm{BMR} = \frac{1}{2}\left[\mathrm{MR}(j_x = j) - \mathrm{MR}(j_x = -j)\right]. \tag{25}$$

Since the effect of in-plane magnetic field is assumed to be small, i.e., $\mathcal{D}_1 \gg \mathcal{D}_{4-6}$, the diagonal resistance can be written as $\rho_{xx} = \rho_{xx}^0(1 - \mathcal{D}_{4-6}/\mathcal{D}_1)$, and BMR can be described as $\mathrm{BMR} = -\left[\mathcal{D}_{4-6}(j_x = +j) - \mathcal{D}_{4-6}(j_x = -j)\right]/(2\mathcal{D}_1)$. Finally, the BMR can be written in the form:

$$\begin{aligned}\mathrm{BMR} = &-\frac{j_x B \sin(\psi)}{e\xi^2}(s_0 S_{s0} - s_1 S_{s1}) \\ &\times \left[J_0 s_0^2 C_{s0} + (J_0 + J_1)s_0 s_1 C_{s0s1} + J_1 s_1^2 C_{s1}\right],\end{aligned} \tag{26}$$

where

$$C_{s0} = \left[\frac{15}{2\hbar^2}(v_+ + v_-) - \frac{3\hbar^2}{2m^2}\left(v_+^3 + v_-^3\right) - \frac{9\alpha}{4m}\left(k_{F+}v_+^3 - k_{F-}v_-^3\right)\right] \tag{27a}$$

$$\begin{aligned}C_{s0s1} = &\left[-\frac{6}{\alpha\hbar^2} - \frac{9\alpha}{4m}\left(k_{F-}^2 v_-^3 + k_{F+}^2 v_+^3\right)\right. \\ &\left. + \frac{9}{4m}\left(k_{F+}v_+^2 - k_{F-}v_-^2\right) + \frac{3}{\alpha m}(v_- + v_+)\right]\end{aligned} \tag{27b}$$

$$\begin{aligned}C_{s1} = &\left[\frac{9\alpha}{4m}\left(k_{F+}^3 v_+^3 - k_{F-}^3 v_-^3\right) - \frac{3}{m}\left(k_{F-}^2 v_-^2 + k_{F+}^2 v_+^2\right)\right. \\ &\left. + \frac{2}{\alpha\hbar^2}(k_{F+} - k_{F-}) + \frac{29}{4\alpha m}(k_{F-}v_- - k_{F+}v_+)\right]\end{aligned} \tag{27c}$$

Eq. (26) is the main result of this article.

4.3. The limit: $\gamma_1 \gg \gamma_2$

When $\gamma_1 \gg \gamma_2$, the coefficients $s_0 \gg s_1$ and $J_0 \gg J_1$. In such a case the spin polarization and charge current density are given

by Eqs. (18), (19), whereas the spin–orbital field $\mathbf{B}_{so} \approx J_0 S_y$. The expression describing bilinear magnetoresistance simplifies to

$$\mathrm{BMR} = -\frac{j_x B \sin(\psi)}{e\xi^2}J_0 s_0^3 S_{s0}C_{s0}. \tag{28}$$

Taking explicit forms of J_0, S_{s0}, C_{s0} we finally get the following formula:

$$\mathrm{BMR} = \frac{3}{2}\pi s_0 \frac{\hbar}{e}\frac{\eta}{\xi^2}j_x B \sin(\psi) \tag{29}$$

where $\eta = \frac{\hbar^2}{m}\left(10(v_- + v_+) - \frac{\hbar^2}{m}(v_-^2 + v_+^2) - \frac{\hbar^4}{m^2}(v_-^3 + v_+^3)\right)$.

4.4. Numerical results

Fig. 2 collects numerical results, obtained based on formula (26). Figs. 2 (a),(b) present the BMR as a function of the angle ψ defining the relative orientation of charge current density and external in-plane magnetic field (i.e., ψ defines the orientation of in-plane magnetic field with respect to the $\hat{x}$-axis). Linear dependencies of the BMR signal amplitude, A^{BMR}, as a function of the amplitude of magnetic field, b, and electric field, eE_x, are presented in Figs. 2(e)–(h). Finally Fig. 2(c) shows A^{BMR} as a function of the carrier concentration, n, for the fixed amplitude of the in-plane magnetic field b, whereas Fig. 2(d) presents A^{BMR} as a function of n for the fixed strength of quantum well potential, eF. The presented results reflect the linear dependence of BMR with respect to both electric and magnetic fields. Moreover, for the low carrier density, the simplified expressions (18), (19) and (28) are sufficient to describe the charge current, spin polarization, and BMR. In Fig. 2, the results obtained from the simplified expressions are indicated by the dashed lines, whereas the solid lines present the BMR described by the full expression (26). For higher charge carrier concentrations, one can note a deviation of the results obtained form the simplified expression from those based on the full formula. In turn, the BMR signal decreases with increasing n. Accordingly, the simplified expression is sufficient in the carrier concentration range for which one can expect the strongest BMR signal.

5. Summary

We have studied theoretically the unidirectional magnetoresistance in a 2D electron gas with the isotropic cubic form of Rashba spin–orbit coupling under external in-plane magnetic field. The mechanism leading to the unidirectional magnetoresistance response is here based on the effective spin–orbital field originated from non-equilibrium spin polarization. The obtained analytical results indicate that BMR can be of an order of a few percent in a range of low carrier densities. The results presented in the manuscript have been derived for the model Hamiltonian that may be used for the description of electronic properties of p-doped semiconductor quantum wells as well as for the description of electron gas emerging at surfaces or interfaces of perovskite oxides (for a certain energy window). Thus, these results may be useful for interpretation of experimental data of a relatively large group of materials. For example, the bilinear magnetoresistance has been measured recently in LAO/STO [23], where a new scheme for determining the linear Rashba parameter has been proposed. The theoretical model provided in our article allows determining the cubic form of Rashba coupling parameter in such structures, with chemical potential gated above the Lifshitz point, where energy subbands reveal strong anisotropy due to cubic Rashba term.

CRediT authorship contribution statement

A. Krzyżewska: Data curation, Formal analysis, Investigation, Software, Validation, Visualization, Writing – original draft. **A. Dyrdał:** Conceptualization, Data curation, Formal analysis, Funding acquisition, Methodology, Project administration, Supervision, Validation, Writing – original draft, Writing – review & editing.

Declaration of competing interest

The authors declare that they have no known competing financial interests or personal relationships that could have appeared to influence the work reported in this paper.

Data availability

Data will be made available on request.

Acknowledgments

Appendix A. Linking the effective Hamiltonian (1) to the materials parameters

This appendix collects explicit forms of the parameters and spin operators corresponding to Hamiltonian (1). Accordingly, the effective mass takes the form:

$$m^* = m_0 \left(\gamma_1 + \gamma_2 - \frac{256\gamma_2^2}{3\pi^2(3\gamma_1 + 10\gamma_2)} \right)^{-1}, \tag{A.1}$$

with the electron rest mass m_0, and $\gamma_{1,2}$ denoting phenomenological parameters of the Luttinger Hamiltonian [35,36]. The Rashba coupling parameter, α is defined by the following expression:

$$\alpha = \frac{512 e F L_z^4 \gamma_2^2}{9\pi^6 (3\gamma_1 + 10\gamma_2)(\gamma_1 - 2\gamma_2)} \tag{A.2}$$

where L_z and eF are the width and potential of the quantum well, respectively. Hamiltonian (1) has been obtained perturbatively based on 8×8 Luttinger Hamiltonian and mapping into the lowest heavy-hole subbands [33], thus, spin operators are no longer simply expressed by Pauli matrices σ_n. To obtain proper spin operators one needs to perform

the same unitary transformations as that made to obtain Hamiltonian (1) [33]. The explicit forms of spin operators are listed below:

$$\hat{s}_\alpha = \sum_{\beta=0,x,y,z} s_\beta^\alpha \sigma_\beta, \tag{A.3}$$

$s_0^x = -s_0 k_y$, $s_0^y = s_0 k_x$, $s_x^x = s_y^y = s_1(k_x^2 - k_y^2)$, $s_y^x = 2s_1 k_x k_y$, $s_x^y = -s_y^x$, $s_0^z = s_x^z = s_y^z = 0$, $s_z^z = 3\hbar/2$. The parameters $s_{0,1}$ are material parameters defined as follows:

$$s_0 = \frac{512 e F L_z^4 \gamma_2 m_0}{9\pi^6 \hbar^2 (3\gamma_1 + 10\gamma_2)(\gamma_1 - 2\gamma_2)} \tag{A.4}$$

$$s_1 = \left(\frac{3}{4\pi^2} - \frac{256\gamma_2^2}{3\pi^4(3\gamma_1 + 10\gamma_2)^2} \right) L_z^2. \tag{A.5}$$

It should be stressed that in the energy window for which the considered model Hamiltonian is applicable (i.e., small carriers concentration) one finds $\gamma_1 \gg \gamma_2$ and contribution to the spin-dependent transport properties proportional to s_1 is rather small, and can be negligible (see for example data collected in Tab. I in [34]). In such a case:

$$\hat{s}_x \approx -s_0 k_y \sigma_0, \quad \hat{s}_y \approx s_0 k_x \sigma_0, \quad \hat{s}_z = \frac{3}{2}\sigma_z \tag{A.6}$$

$$H_{\text{pert}} = b_{\text{eff}\,0}\,\sigma_0 \tag{A.7}$$

In this paper, we consider magnetoresistance for the general effective Hamiltonian, as well as for the simplified model that leads to simpler analytical expressions applicable in the limit $\gamma_1 \gg \gamma_2$.

Appendix B. Estimation of $J_{0,1}$ parameter

Under an external electric field, the Fermi contour is shifted in the momentum space by $\Delta k_x = -\frac{e\tau}{\hbar} E_x$. In turn, the diagonal charge current density is given by Eq. (19) (the leading term), thus one finds the relation between Δk_x and j_x in the form $\Delta k_x = -\frac{4\pi}{e\hbar\xi} j_x$.

Due to the correction originating from the non-equilibrium shift in the momentum space, the Hamiltonian H_0, Eq. (4), takes the form $H_0(k_x + \Delta k_x) = H_0 + H_{\Delta k_x}$, where:

$$H_{\Delta k_x} = \frac{\hbar^2}{2m} k_x \Delta k_x \sigma_0 + 6\alpha k_x k_y \Delta k_x \sigma_x - 3\alpha(k_x^2 - k_y^2)\Delta k_x \sigma_y + O((\Delta k_x)^2). \tag{B.1}$$

In turn, the effective spin–orbital field introduced to our theory in (1) is defined as:

$$B_{so\,y}\hat{s}_y = JS_y\hat{s}_y = JS_y s_0 k_x \sigma_0 - JS_y 2s_1 k_x k_y \sigma_x + JS_y s_1 (k_x^2 - k_y^2)\sigma_y \tag{B.2}$$

By the comparison of terms standing in front of the same Pauli matrices in Eqs. (B.1) and (B.2) one finds:

$$JS_y s_0 = \frac{\hbar^2}{2m} \Delta k_x \tag{B.3}$$

$$-s_1 JS_y = 3\alpha \Delta k_x \tag{B.4}$$

$$s_1 JS_y = -3\alpha \Delta k_x \tag{B.5}$$

Accordingly, the above relations indicate that two coupling constants should be introduced. From the first equality, one finds $J = J_0$, whereas the second and third equalities are identical and result in $J = J_1$. Thus the parameters $J_{0,1}$ reads

$$J_0 = -\frac{2\pi\hbar}{ms_0}(s_0 S_{s0} - s_1 S_{s1})^{-1} \tag{B.6}$$

$$J_1 = \frac{4\pi}{\hbar}\frac{3\alpha}{s_1}(s_0 S_{s0} - s_1 S_{s1})^{-1} \tag{B.7}$$

where

$$S_{s0} = 3\alpha\left(k_{F-}^3 v_- + k_{F+}^3 v_+\right) + \frac{\hbar^2}{m}\left(k_{F-}^2 v_- + k_{F+}^2 v_+\right)$$

$$= k_{F+}^2 + k_{F-}^2 \tag{B.8a}$$

$$S_{s1} = 3\alpha\left(k_{F-}^4 v_- + k_{F+}^4 v_+\right) + \frac{\hbar^2}{m}\left(k_{F-}^3 v_- + k_{F+}^3 v_+\right)$$

$$= k_{F+}^3 - k_{F-}^3 \tag{B.8b}$$

5

References

[1] L.L. Campbell, Galvanomagnetic and Thermomagnetic Effects: The Hall and Allied Phenomena, Longmans, Green & Co., London, 1923, 1923.

[2] J.M. Ziman, Transport properties, in: Principles of the Theory of Solids, second ed., Cambridge University Press, 1972, pp. 211–254, http://dx.doi.org/10.1017/CBO9781139644075.009.

[3] A.B. Pippard, Magnetoresistance in Metals, Cambridge University Press, Cambridge, England, UK, 1989.

[4] J. Barnaś, A. Fuss, R.E. Camley, P. Grünberg, W. Zinn, Novel magnetoresistance effect in layered magnetic structures: Theory and experiment, Phys. Rev. B 42 (1990) 8110–8120, http://dx.doi.org/10.1103/PhysRevB.42.8110.

[5] M.N. Baibich, J.M. Broto, A. Fert, F.N. Van Dau, F. Petroff, P. Etienne, G. Creuzet, A. Friederich, J. Chazelas, Giant magnetoresistance of (001)Fe/(001)Cr magnetic superlattices, Phys. Rev. Lett. 61 (1988) 2472–2475, http://dx.doi.org/10.1103/PhysRevLett.61.2472.

[6] R.E. Camley, J. Barnaś, Theory of giant magnetoresistance effects in magnetic layered structures with antiferromagnetic coupling, Phys. Rev. Lett. 63 (1989) 664–667, http://dx.doi.org/10.1103/PhysRevLett.63.664.

[7] J. Sinova, S.O. Valenzuela, J. Wunderlich, C.H. Back, T. Jungwirth, Spin Hall effects, Rev. Modern Phys. 87 (2015) 1213–1260, http://dx.doi.org/10.1103/RevModPhys.87.1213.

[8] Y. Ando, M. Shiraishi, Spin to charge interconversion phenomena in the interface and surface states, J. Phys. Soc. Japan 86 (1) (2017) 011001, http://dx.doi.org/10.7566/JPSJ.86.011001.

[9] A. Soumyanarayanan, A. Reyren, et al., Emergent phenomena induced by spin–orbit coupling at surfaces and interfaces, Nature 539 (2016) 509–517, http://dx.doi.org/10.1038/nature19820.

[10] Y. Wu, Y. Xu, Z. Luo, Y. Yang, H. Xie, Q. Zhang, X. Zhang, Charge–spin interconversion and its applications in magnetic sensing, J. Appl. Phys. 129 (6) (2021) 060902, http://dx.doi.org/10.1063/5.0039926.

[11] Y.-T. Chen, S. Takahashi, H. Nakayama, M. Althammer, S.T.B. Goennenwein, E. Saitoh, G.E.W. Bauer, Theory of spin Hall magnetoresistance, Phys. Rev. B 87 (2013) 144411, http://dx.doi.org/10.1103/PhysRevB.87.144411.

[12] H. Nakayama, M. Althammer, Y.-T. Chen, K. Uchida, Y. Kajiwara, D. Kikuchi, T. Ohtani, S. Geprägs, M. Opel, S. Takahashi, R. Gross, G.E.W. Bauer, S.T.B. Goennenwein, E. Saitoh, Spin Hall magnetoresistance induced by a nonequilibrium proximity effect, Phys. Rev. Lett. 110 (2013) 206601, http://dx.doi.org/10.1103/PhysRevLett.110.206601.

[13] J. Kim, P. Sheng, S. Takahashi, S. Mitani, M. Hayashi, Spin Hall magnetoresistance in metallic bilayers, Phys. Rev. Lett. 116 (2016) 097201, http://dx.doi.org/10.1103/PhysRevLett.116.097201.

[14] C. Avci, A. Garello, et al., Unidirectional spin Hall magnetoresistance in ferromagnet/normal metal bilayers, Nat. Phys. 11 (2015) 570–575, http://dx.doi.org/10.1038/nphys3356.

[15] Y. Lv, J. Kally, D. Zhang, J.S. Lee, M. Jamali, N. Samarth, J.-P. Wang, Unidirectional spin-Hall and Rashba-Edelstein magnetoresistance in topological insulator-ferromagnet layer heterostructures, Nature Commun. 9 (111) (2018) 1–7, http://dx.doi.org/10.1038/s41467-017-02491-3.

[16] Y. Tokura, N. Nagaosa, Nonreciprocal responses from non-centrosymmetric quantum materials, Nature Commun. 9 (2018) 3740, http://dx.doi.org/10.1038/s41467-018-05759-4.

[17] S. Mitra, J.G.S. Kang, J. Shin, J.Q. Ng, S.S. Sunku, T. Kong, P.C. Canfield, B.S. Shastry, P. Sengupta, C. Panagopoulos, Quadratic to linear magnetoresistance tuning in TmB₄, Phys. Rev. B 99 (4) (2019) 045119, http://dx.doi.org/10.1103/PhysRevB.99.045119.

[18] Y. Feng, Y. Wang, D.M. Silevitch, J.-Q. Yan, R. Kobayashi, M. Hedo, T. Nakama, Y. Ōnuki, A.V. Suslov, B. Mihaila, P.B. Littlewood, T.F. Rosenbaum, Linear magnetoresistance in the low-field limit in density-wave materials, Proc. Natl. Acad. Sci. USA 116 (23) (2019) 11201–11206, http://dx.doi.org/10.1073/pnas.1820092116.

[19] P. He, S.S.-L. Zhang, D. Zhu, Y. Liu, Y. Wang, J. Yu, G. Vignale, H. Yang, Bilinear magnetoelectric resistance as a probe of three-dimensional spin texture in topological surface states - Nature Physics, Nat. Phys. 14 (5) (2018) 495–499, http://dx.doi.org/10.1038/s41567-017-0039-y.

[20] S.S.-L. Zhang, G. Vignale, Theory of bilinear magneto-electric resistance from topological-insulator surface states, 2018, http://dx.doi.org/10.1117/12.2323126, arXiv, arXiv:1808.06339.

[21] S.S.-L. Zhang, G. Vignale, Theory of bilinear magneto-electric resistance from topological-insulator surface states, in: Spintronics XI, vol. 10732, SPIE, 2018, pp. 97–107, http://dx.doi.org/10.1117/12.2323126.

[22] A. Dyrdał, J. Barnaś, A. Fert, Spin-momentum-locking inhomogeneities as a source of bilinear magnetoresistance in topological insulators, Phys. Rev. Lett. 124 (4) (2020) 046802, http://dx.doi.org/10.1103/PhysRevLett.124.046802.

[23] D.C. Vaz, F. Trier, A. Dyrdał, A. Johansson, K. Garcia, A. Barthélémy, I. Mertig, J. Barnaś, A. Fert, M. Bibes, Determining the Rashba parameter from the bilinear magnetoresistance response in a two-dimensional electron gas, Phys. Rev. Mater. 4 (7) (2020) 071001, http://dx.doi.org/10.1103/PhysRevMaterials.4.071001.

[24] R. Moriya, K. Sawano, Y. Hoshi, S. Masubuchi, Y. Shiraki, A. Wild, C. Neumann, G. Abstreiter, D. Bougeard, T. Koga, T. Machida, Cubic Rashba spin-orbit interaction of a two-dimensional hole gas in a strained-Ge/SiGe quantum well, Phys. Rev. Lett. 113 (8) (2014) 086601, http://dx.doi.org/10.1103/PhysRevLett.113.086601.

[25] H. Liang, L. Cheng, L. Wei, Z. Luo, G. Yu, C. Zeng, Z. Zhang, Nonmonotonically tunable Rashba spin-orbit coupling by multiple-band filling control in SrTiO₃-based interfacial *d*-electron gases, Phys. Rev. B 92 (7) (2015) 075309, http://dx.doi.org/10.1103/PhysRevB.92.075309.

[26] H. Nakamura, T. Koga, T. Kimura, Experimental evidence of cubic Rashba effect in an inversion-symmetric oxide, Phys. Rev. Lett. 108 (20) (2012) 206601, http://dx.doi.org/10.1103/PhysRevLett.108.206601.

[27] Z. Zhong, A. Tóth, K. Held, Theory of spin-orbit coupling at LaAlO₃/SrTiO₃ interfaces and SrTiO₃ surfaces, Phys. Rev. B 87 (16) (2013) 161102, http://dx.doi.org/10.1103/PhysRevB.87.161102.

[28] G. Khalsa, B. Lee, A.H. MacDonald, Theory of t_{2g} electron-gas Rashba interactions, Phys. Rev. B 88 (4) (2013) 041302, http://dx.doi.org/10.1103/PhysRevB.88.041302.

[29] Y. Kim, R.M. Lutchyn, C. Nayak, Origin and transport signatures of spin-orbit interactions in one- and two-dimensional SrTiO₃-based heterostructures, Phys. Rev. B 87 (24) (2013) 245121, http://dx.doi.org/10.1103/PhysRevB.87.245121.

[30] K.V. Shanavas, Theoretical study of the cubic Rashba effect at the SrTiO₃(001) surfaces, Phys. Rev. B 93 (4) (2016) 045108, http://dx.doi.org/10.1103/PhysRevB.93.045108.

[31] G. Seibold, S. Caprara, M. Grilli, R. Raimondi, Theory of the spin galvanic effect at oxide interfaces, Phys. Rev. Lett. 119 (25) (2017) 256801, http://dx.doi.org/10.1103/PhysRevLett.119.256801.

[32] D.C. Vaz, P. Noël, A. Johansson, B. Göbel, F.Y. Bruno, G. Singh, S. McKeown-Walker, F. Trier, L.M. Vicente-Arche, A. Sander, S. Valencia, P. Bruneel, M. Vivek, M. Gabay, N. Bergeal, F. Baumberger, H. Okuno, A. Barthélémy, A. Fert, L. Vila, I. Mertig, J.-P. Attané, M. Bibes, Mapping spin–charge conversion to the band structure in a topological oxide two-dimensional electron gas - Nature Materials, Nature Mater. 18 (11) (2019) 1187–1193, http://dx.doi.org/10.1038/s41563-019-0467-4.

[33] C.-X. Liu, B. Zhou, S.-Q. Shen, B.-f. Zhu, Current-induced spin polarization in a two-dimensional hole gas, Phys. Rev. B 77 (12) (2008) 125345, http://dx.doi.org/10.1103/PhysRevB.77.125345.

[34] Ł. Karwacki, A. Dyrdał, J. Berakdar, J. Barnaś, Current-induced spin polarization in the isotropic *k*-cubed Rashba model: Theoretical study of *p*-doped semiconductor heterostructures and perovskite-oxide interfaces, Phys. Rev. B 97 (23) (2018) 235302, http://dx.doi.org/10.1103/PhysRevB.97.235302.

[35] J.M. Luttinger, W. Kohn, Motion of electrons and holes in perturbed periodic fields, Phys. Rev. 97 (1955) 869–883, http://dx.doi.org/10.1103/PhysRev.97.869, URL https://link.aps.org/doi/10.1103/PhysRev.97.869.

[36] J.M. Luttinger, Quantum theory of cyclotron resonance in semiconductors: General theory, Phys. Rev. 102 (1956) 1030–1041, http://dx.doi.org/10.1103/PhysRev.102.1030, URL https://link.aps.org/doi/10.1103/PhysRev.102.1030.

[37] G.D. Mahan, Many-Particle Physics, Springer US, New York, NY, USA, 2000, http://dx.doi.org/10.1007/978-1-4757-5714-9.

[38] A. Dyrdał, J. Barnaś, V.K. Dugaev, Spin Hall and spin Nernst effects in a two-dimensional electron gas with Rashba spin-orbit interaction: Temperature dependence, Phys. Rev. B 94 (3) (2016) 035306, http://dx.doi.org/10.1103/PhysRevB.94.035306.

[39] J. Schliemann, D. Loss, Spin-Hall transport of heavy holes in III-V semiconductor quantum wells, Phys. Rev. B 71 (8) (2005) 085308, http://dx.doi.org/10.1103/PhysRevB.71.085308.

4.6 Reprint of the article A-6

The manuscript entitled "Nonlinear Hall effect in isotropic k-cubed Rashba model: Berry-curvature-dipole engineering by in-plane magnetic field" is devoted to the nonlinear anomalous Hall effect, which is controlled *via* an in-plane magnetic field in a model describing a magnetized 2DEG with isotropic cubic form of Rashba spin-orbit interaction.

Here the role of both the intrinsic and dissipative components of the linear and nonlinear contributions to the anomalous Hall conductivity (AHC) are investigated. The intrinsic component, related to the states in the Fermi sea, originates in Berry curvature and Berry curvature dipole for linear and nonlinear AHC components, respectively.

It was found that in low in-plane magnetic field regime (the value of the in-plane magnetic field is lower than the out-of-plane magnetization component), the linear AHC is dominated by the intrinsic part, while for higher values of the in-plane magnetic field, the dissipative component originating from the states at the Fermi level begins to influence the results. Interestingly, in the case of the nonlinear component of the AHC, the dissipative component governs the transport in both regimes.

Furthermore, the intrinsic part of the linear AHC reveals π-periodicity with respect to the angle of the in-plane magnetic field, while the nonlinear AHC exhibits a 2π-periodicity with the in-plane magnetic field angle. It is worth noting that the AHC is governed by the intrinsic part when the in-plane magnetic field is applied perpendicular to the external electric field.

physica
status
solidi
pss rrl

www.pss-rapid.com

Check for updates

Nonlinear Hall Effect in Isotropic k-Cubed Rashba Model: Berry-Curvature-Dipole Engineering by In-Plane Magnetic Field

Anna Krzyżewska and Anna Dyrdał*

The linear and nonlinear Hall effects in 2D electron gas are considered theoretically within the isotropic k-cubed Rashba model. It is shown that the presence of an out-of-plane external magnetic field or net magnetization is a necessary condition to induce a nonzero Berry curvature in the system, whereas an in-plane magnetic field tunes the Berry curvature leading to the Berry curvature dipole. Interestingly, in the linear response regime, the conductivity is dominated by the intrinsic component (Berry curvature component), whereas the second-order correction to the Hall current (i.e., the conductivity proportional to the external electric field) is dominated by the component independent of the Berry curvature dipole.

1. Introduction

Spin-orbit coupling (SOC) of Rashba type[1–3] is a consequence of structural inversion asymmetry in a system and originally has been studied in the context of semiconductor surfaces and heterostructures with asymmetric confining potentials. In the current relevant literature, the Rashba spin-orbit coupling usually means the spin-orbital interaction arising in systems without the inversion center, that can be described as an effective internal and odd-momentum-dependent Zeeman-like field acting on the electron spin.[4,5] Consequently, the spin-orbit interaction leads to the so-called spin-momentum locking phenomenon, that is, to a fixed orientation of quasiparticle spin with respect to its momentum. This, in turn, is responsible for fascinating electrical and optical effects, that are currently a hallmark of spin orbitronics.[6–11] In the context of electric transport, especially important consequences of spin-momentum locking are the spin-to-charge interconversion effects, such as current-induced spin polarization (also known as Edelstein effect)[12–14] and the spin-Hall effect.[13,15–20] Recently, in the context of spin orbitronics, nonlinear transport effects, that is, bilinear magnetotransport[21–25] and nonlinear Hall effect (NLHE), are of special attention.

A. Krzyżewska, A. Dyrdał
Faculty of Physics
ISQI
Adam Mickiewicz University in Poznań
ul. Uniwersytetu Poznańskiego 2, 61–614 Poznań, Poland
E-mail: anna.dyrdal@amu.edu.pl

The ORCID identification number(s) for the author(s) of this article can be found under https://doi.org/10.1002/pssr.202400123.

The NLHE[26–30] is an intriguing member of the family of Hall effects, as it can arise in time-reversal symmetric systems. The only condition that is required is the absence of inversion symmetry.[26,27] Similar to the anomalous Hall effect[31] (AHE), one can define intrinsic and extrinsic microscopic mechanisms responsible for NLHE.[30,32] The intrinsic contribution has a geometric nature, namely, the positive and negative Berry curvature hotspots are located in slightly different regions of the Brillouin zone, leading to the dipole moment that is called Berry curvature dipole (BCD).[26] This intrinsic contribution, even originating in case of nonzero Berry curvature, is different from the intrinsic AHE, where the conductivity is robust to scattering and is dissipationless. This is because the intrinsic component of NLHE is nonzero only when the Fermi level crosses the energy bands (i.e., the BCD disappears in the energy gap), and consequently, the effects of disorder are unavoidable. The BCD has been reported in topological crystalline insulators (e.g., the (001) surface of SnTe, $Pb_{1-x}Sn_xTe$, $Pb_{1-x}Sn_xSe$),[26,32] Weyl semimetals,[33] and transition metal dichalcogenides.[28,32,34–36] In turn, the extrinsic contribution to NLHE is related to spin-dependent scattering processes, also well known from the theory of AHE, that is, to the skew scattering and side jump.[28,29,32,36]

In this work, we develop the concept of externally controlled NLHE. We show that the Berry curvature and BCD can emerge as a consequence of external magnetic field, which additionally allows to control the properties of BCD and nonlinear system response. Such external control of nonlinear (unidirectional) electronic transport provides an additional degree of freedom in the design of new spintronics devices. Accordingly, we demonstrate the BCD engineering by external magnetic field and present a detailed study of the linear and nonlinear Hall response in 2D electron gas with isotropic cubic form of Rashba spin-orbit interaction. The Berry curvature in such a system appears as a consequence of nonzero out-of-plane external magnetic field or magnetization. In turn, the BCD emerges (and simultaneously can be controlled) due to an in-plane magnetic field. In consequence, the Hall conductivity contains linear and nonlinear components. The linear system response contains the contributions due to anomalous and planar Hall effects, whereas the nonlinear Hall response is determined by BCD.

Our proposition of magnetic control of Berry curvature and BCD is quite general and can be applied to any kind of system that, under zero external fields, reveals only the lack of spatial

inversion symmetry. Thus we decided to consider the effective model describing 2D quasiparticles in the presence of isotropic cubic form of Rashba SOC. This kind of Rashba spin-orbit coupling determines the spectra of p-states in p-doped zinc-blende III–V semiconductor heterostructures (heavy holes in 2DHG).[2,37–40] Interestingly, the same kind of spin-orbital splitting, that is, the same symmetry of low-energy electronic states, associated with t_{2g} orbitals, is observed for 2D electron gas emerging at the surface states of cubic perovskites, such as $SrTiO_3$ (STO) and STO-based interfaces, that is, $LaAlO_3/SrTiO_3$.[40–43] The 2D electron gas at surfaces and interfaces of cubic perovskite oxides attracts large interest, mainly because of its high electron mobility and enhanced spin-orbit interaction that leads to strong spin-to-charge interconversion.[44–46] This makes oxide perovskites attractive materials for spintronics.

This work is organized as follows. In Section 2, we introduced an effective Hamiltonian describing 2D electron gas with isotropic cubic Rashba SOC. In Section 3, we present semiclassical formulas describing linear and nonlinear Hall conductivity. Next, in Section 4.A, we present Berry curvature and BCD as a function of the in-plane magnetic field and parameters of the effective Hamiltonian. Section 4.2 contains a detailed discussion of the behavior of Hall conductivity in the in-plane magnetic field. Finally, Section 5. contains the summary and final remarks.

2. 2D Electron Gas with k-Cubed Rashba SOC

We consider that effective low-energy Hamiltonian of 2D light electrons (2D heavy holes) with the isotropic cubic form of Rashba SOC[38,39,41] takes the following form [39]

$$H = \frac{\hbar^2 k^2}{2m}\hat{\sigma}_0 + i\alpha(k_-^3\hat{\sigma}_+ - k_+^3\hat{\sigma}_-) + \mathbf{\Delta} \times \mathbf{s} \quad (1)$$

where $k^2 = k_x^2 + k_y^2$, and m is the effective mass that in the systems under consideration is described by the following formula [39]

$$m = m_0\left(\gamma_1 + \gamma_2 - \frac{256\gamma_2^2}{3\pi^2(3\gamma_1 + 10\gamma_2)}\right)^{-1} \quad (2)$$

with m_0 denoting the electron rest mass, and $\gamma_{1,2}$ stands for the Luttinger parameters. The second term of Equation (1) describes isotropic cubic Rashba SOC, where $k_\pm \equiv (k_x \pm ik_y)$, $\hat{\sigma}_\pm \equiv \frac{1}{2}(\hat{\sigma}_x \pm i\hat{\sigma}_y)$, and $\hat{\sigma}_{0,x,y,z}$ are the identity and Pauli matrices. The Rashba parameter α reads[39]

$$\alpha = \frac{512eFL_z^4\gamma_2^2}{9\pi^6(3\gamma_1 + 10\gamma_2)(\gamma_1 - 2\gamma_2)} \quad (3)$$

where L_z is the quantum well width and F is the electric field describing the asymmetric quantum well potential. The last term in Hamiltonian (1) is a Zeeman-like term that describes the coupling of electron spin, $\mathbf{s}$, with magnetization and/or external magnetic field, that for keeping the generality is denoted here as $\mathbf{\Delta}$ (note that $\mathbf{\Delta}$ is defined in the energy units). The spin operators, $\mathbf{s} = (\hat{s}_x, \hat{s}_y, \hat{s}_z)$, in this model are defined as follows.[39]

$$\hat{s}_x = -s_0 k_y\hat{\sigma}_0 + s_1(k_-^2\hat{\sigma}_+ + k_+^2\hat{\sigma}_-) \quad (4a)$$

$$\hat{s}_y = s_0 k_x\hat{\sigma}_0 + is_1(k_-^2\hat{\sigma}_+ - k_+^2\hat{\sigma}_-) \quad (4b)$$

$$\hat{s}_z = \frac{3}{2}\hat{\sigma}_z \quad (4c)$$

and their forms are a consequence of two canonical transformations that need to be performed on the Luttinger Hamiltonian to obtain the effective Hamiltonian (1) (for details, see ref. [39]). The coefficients $s_{0,1}$ are defined as[39]

$$s_0 = \frac{512eFL_z^4\gamma_2 m_0}{9\pi^6\hbar^2(3\gamma_1 + 10\gamma_2)(\gamma_1 - 2\gamma_2)} \quad (5)$$

and

$$s_1 = \left[\frac{3}{4\pi^2} - \frac{256\gamma_2^2}{3\pi^4(3\gamma_1 + 10\gamma_2)^2}\right]L_z^2 \quad (6)$$

The material parameters that characterize different systems (e.g., surfaces of $SrTiO_3$, interfaces of $LaAlO_3/SrTiO_3$, $LaVO_3/SrTiO_3$, and $Ge/Si_{0.2}Ge_{0.8}$)[40–43] have been collected for example in ref. [47]. Here, following another study,[39] we chose the parameters $\gamma_1 = 7$, $\gamma_2 = 1.9$ $eF = 5 \times 10^6$ eV m^{-1}, and $L_z = 8.3$ nm. As the necessary condition to obtain a nonzero Berry curvature is to have a nonzero z-component of $\Delta_z = B_z$ (i.e., a nonzero macroscopic magnetization oriented out of plane of 2DEG or out-of-plane component of magnetic field), whereas to induce and tune the BCD we need in addition an in-plane component of magnetic field, we introduce the following generalized notation: $\mathbf{\Delta} = (B_x, B_y, \Delta_z)$. Here B_{xy} denotes the external in-plane components of magnetic field in the energy units, $\Delta_z = B_z$ or $\Delta_z = M_z$, where B_z and M_z denote the z-component of external magnetic field and the out-of-plane macroscopic magnetization, respectively.

3. Hall Conductivity

Within the semiclassical picture (as provided, e.g., in refs. [26,30,32]), the charge current density driven by AC longitudinal electric field can be described—in the constant relaxation time approximation and up to the second order in the electric field—by the following formula

$$j_\alpha = \text{Re}\{j_\alpha^0 + j_\alpha^1 \exp(i\omega t) + j_\alpha^2 \exp(i2\omega t)\} \quad (7)$$

where the first term describes the rectification effect

$$j_\alpha^0 = -\frac{e^3 E_\beta E_\gamma^*}{2\hbar^2}\frac{\tau}{1 + i\omega\tau}\sum_l \int \frac{d^2\mathbf{k}}{(2\pi)^2}\left(\varepsilon_{\alpha\gamma\delta}\Omega_\delta^l\partial_\mathbf{k}^\beta + \tau v_\alpha^l\partial_\mathbf{k}^\gamma\partial_\mathbf{k}^\beta\right)f_0^l \quad (8)$$

the second term describes the linear response

$$j_\alpha^1 = -\frac{e^2}{\hbar}E_\beta\sum_l \int \frac{d^2\mathbf{k}}{(2\pi)^2}\left(\varepsilon_{\alpha\beta\gamma}\Omega_\gamma^l + \frac{\tau v_\alpha^l}{1 + i\omega\tau}\partial_\mathbf{k}^\beta\right)f_0^l \quad (9)$$

and the last term is the second harmonic response

$$j_\alpha^2 = -\frac{e^3 E_\beta E_\gamma}{2\hbar^2} \frac{\tau}{1+i\omega\tau} \sum_l \int \frac{d^2\mathbf{k}}{(2\pi)^2} \left(\varepsilon_{\alpha\gamma\delta}\Omega_\delta^l \partial_\mathbf{k}^\beta + \frac{\tau v_\alpha^l}{1+i2\omega\tau} \partial_\mathbf{k}^\gamma \partial_\mathbf{k}^\beta \right) f_0^l \tag{10}$$

In the above expressions, l numerates the sub-bands, f_0^l is the Fermi–Dirac distribution function for the l-th sub-band, $\{\alpha, \beta, \gamma, \delta\} = \{x, y, z\}$, and Ω_α^l is the α-th component of the Berry curvature calculated for the l-th sub-band.[48]

$$\Omega_\gamma^l = \nabla_\mathbf{k} \times \Lambda_l(\mathbf{k}) \tag{11}$$

where $\Lambda_l = i\langle \psi_l | \nabla_\mathbf{k} | \psi_l \rangle$ is the Berry connection.

Accordingly, in the DC limit, one can write

$$j_\alpha = -\frac{e^2}{\hbar} E_\beta \sum_l \int \frac{d^2\mathbf{k}}{(2\pi)^2} \left(\varepsilon_{\alpha\beta\gamma}\Omega_\gamma^l + \tau v_\alpha^l \partial_\mathbf{k}^\beta \right.$$
$$\left. + \frac{eE_\gamma\tau}{\hbar} \left(\varepsilon_{\alpha\gamma\delta}\Omega_\delta^l \partial_\mathbf{k}^\beta + \tau v_\alpha^l \partial_\mathbf{k}^\gamma \partial_\mathbf{k}^\beta \right) \right) f_0^l \tag{12}$$

Thus, the Hall conductivity can be written as follows

$$\sigma_{\alpha\beta} = \sigma_{\alpha\beta}^\mathrm{I} + \sigma_{\alpha\beta}^\mathrm{II} + \chi_{\alpha\beta\gamma}^\mathrm{I} E_\gamma + \chi_{\alpha\beta\gamma}^\mathrm{II} E_\gamma \tag{13}$$

Here, $\sigma_{\alpha\beta}^\mathrm{I,II}$ are the components, which are well known from the theory of AHE. Thus, the first term describes the contributions from the electronic states at the Fermi level (dissipative term), that in the simplest form[49] reads

$$\sigma_{\alpha\beta}^\mathrm{I} = -\frac{e^2}{\hbar}\tau \sum_l \int \frac{d^2\mathbf{k}}{(2\pi)^2} v_\alpha^l \partial_\mathbf{k}^\beta f_0^l \tag{14}$$

whereas the second term describes the contribution from the electronic states below the Fermi level, that is, the Fermi sea (nondissipative) component. This term is fully intrinsic and determined by the Berry curvature

$$\sigma_{\alpha\beta}^\mathrm{II} = -\frac{e^2}{\hbar} \sum_l \int \frac{d^2\mathbf{k}}{(2\pi)^2} \varepsilon_{\alpha\beta\gamma}\Omega_\gamma^l f_0^l \tag{15}$$

The third and fourth terms of Equation (13) describe nonlinear Hall response. The third term is fully semiclassical, with electric susceptibility heaving the form

$$\chi_{\alpha\beta\gamma}^\mathrm{I} = -\frac{e^2}{\hbar}\frac{e\tau^2}{\hbar} \sum_l \int \frac{d^2\mathbf{k}}{(2\pi)^2} v_\alpha^l \partial_\mathbf{k}^\gamma \partial_\mathbf{k}^\beta f_0^l \tag{16}$$

whereas the fourth term has quantum origin and the corresponding electric susceptibility takes the form

$$\chi_{\alpha\beta\gamma}^\mathrm{II} = -\frac{e^2}{\hbar}\frac{e\tau}{\hbar} \sum_l \int \frac{d^2\mathbf{k}}{(2\pi)^2} \varepsilon_{\alpha\gamma\delta}\Omega_\delta^l \partial_\mathbf{k}^\beta f_0^l = -\frac{e^2}{\hbar}\frac{e\tau}{\hbar} \sum_l \varepsilon_{\alpha\gamma\delta} D_{\gamma\delta}^l \tag{17}$$

where $D_{\gamma\delta}$ is the BCD which in 2D systems (for which Berry curvature has only $\hat{z}$-component) reads

$$D_{\alpha\beta}^l \overset{2D}{=} D_\alpha^l = \int \frac{d^2\mathbf{k}}{(2\pi)^2} f_0^l \partial_\mathbf{k}^\alpha \Omega_z^l \tag{18}$$

4. Results

4.1. Berry Curvature and Berry Curvature Dipole

The eigenvalues, $E_{l=\pm}$, of Hamiltonian (1) take the form

$$E_\pm = \frac{k^2\hbar^2}{2m} + s_0(B_y k_x - B_x k_y) \pm \frac{1}{2}\xi(\mathbf{k}) \tag{19}$$

and the corresponding eigenfunctions are

$$\Psi_{l=\pm} = \begin{pmatrix} \pm i\Phi(\mathbf{k}) \\ 1 \end{pmatrix} \tag{20}$$

In the above expressions, we introduced the parameters: $\xi(\mathbf{k}) = [9\Delta_z^2 + 4k^4(B^2 s_1^2 + k^2\alpha^2 - 2\alpha(B_y k_x - B_x k_y)s_1)]^{1/2}$ and $\Phi(\mathbf{k}) = \frac{\pm 3\Delta_z + \xi(\mathbf{k})}{2k_+^2(\alpha k_- + i(B_x - B_y)s_1)}$. Accordingly, the Berry curvature corresponding to the sub-bands $E_\pm$ has the following form:

$$\Omega_z^\pm = \mp \frac{6\Delta_z k^2}{(\xi(\mathbf{k}))^3} \left[4B^2 s_1^2 + 12\alpha(B_x k_y - B_y k_x)s_1 + 9\alpha^2 k^2 \right] \tag{21}$$

where $B^2 = B_x^2 + B_y^2$ denotes the amplitude of the in-plane component of external magnetic field. In addition, one usually defines $(B_x/B, B_y/B) = (\cos\psi, \sin\psi)$, where ψ determines the orientation of vector $\mathbf{B}$ with respect to the $\mathbf{x}$-axis.

Both eigenvalues and Berry curvature are presented in **Figure 1a–d**. Figure 1a shows the cross sections of energy bands $E_\pm$ (solid lines) and Berry curvatures corresponding to these eigenvalues. The Berry curvatures have also been plotted in the case, when the coefficient s_1 is taken into account in the definition of spin operators (dotted lines). Figure 1b–d shows selected constant-energy contours and density plots for Berry curvature, Ω_z^+, for a fixed value of Δ_z and for different amplitudes of the in-plane magnetic field, B. One can see that the nonzero in-plane magnetic field, B, leads to a Fermi contours anisotropy in the k-space by shifting the energy sub-bands (e.g., in the k_x direction when the in-plane magnetic field is oriented along the y direction). For higher energies, where the spin-orbit coupling also plays an important role, the B-field leads to a degeneracy of the sub-bands. Obviously, the Berry curvature reveals the highest signal in the crossing points. Moreover, the positions of positive and negative Berry curvature hot spots are also more pronounced at higher energies, and their position in the k-space is controlled by the in-plane orientation of the magnetic field (as indicated in Figure 1f–h). Figure 1e presents the BCD calculated for E_+ and E_- energy branches, respectively, as well as their superposition. Importantly, depending on which component, D_y^+ or D_y^-, dominates, the sum, D_y, can change the sign by changing the chemical potential.

4.2. Hall Conductivity

Now, without loss of generality, we assume that the external electric field is oriented in the y-direction. Accordingly, the Hall response is described by the off-diagonal conductivity $\sigma_{xy} = \sigma_{xy}^\mathrm{I} + \sigma_{xy}^\mathrm{II} + \chi_{xyy}^\mathrm{I} E_y + \chi_{xyy}^\mathrm{II} E_y$. The first two terms describe
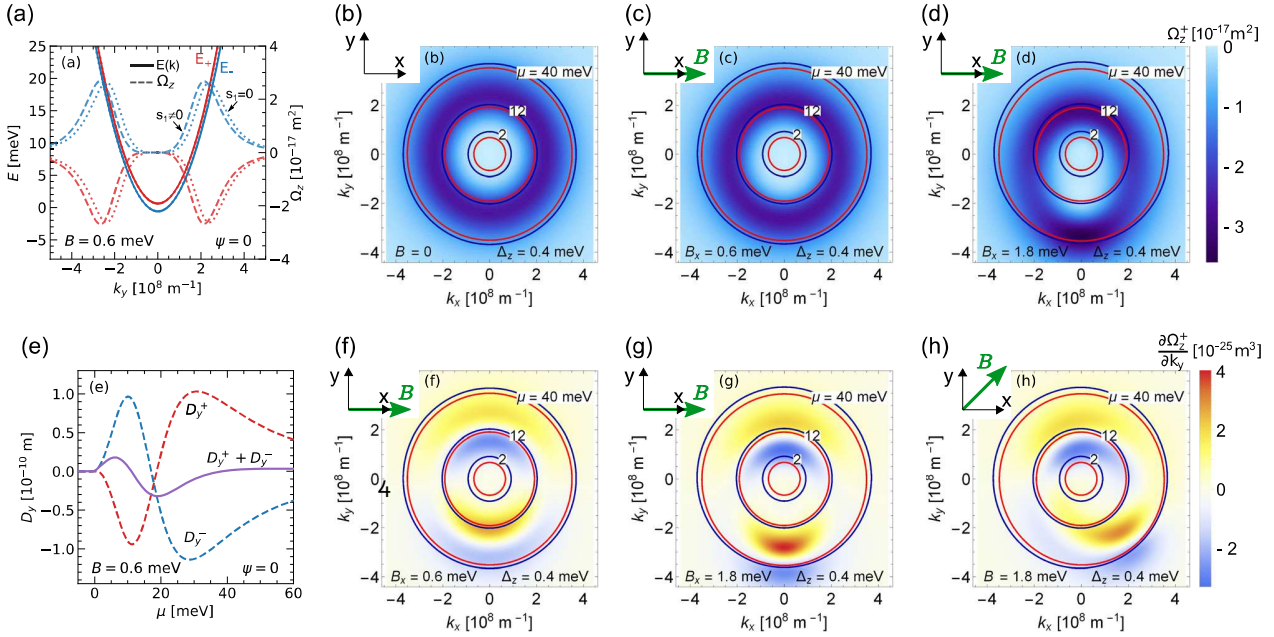
Figure 1. a–d) Berry curvature and e) BCD, as well as f-h) derivative of the Berry curvature with respect to k_x plotted in k-space for indicated values of Δ_z and $\boldsymbol{B}$. The other parameters are: $\gamma_1 = 7$, $\gamma_2\gamma_2 = 1.9$, $eF = 5 \times 10^6$ eV m^{-1}, $L_z = 8.3$ nm.

the linear, with respect to E_y, system response, that is, $\sigma_{xy}^I = \sigma_{xy}^I + \sigma_{xy}^{II}$, whereas the last two terms describe the nonlinear (second-order) response, that is, $\sigma_{xy}^{nl} = (\chi_{xyy}^I + \chi_{xyy}^{II})E_y$. All these components are presented in **Figure 2** (where the contributions from each of the subbands are also plotted) and in **Figure 3**, where all conductivity components are presented as a function of the angle, ψ, and chemical potential, μ, for two amplitudes of the in-plane magnetic field, that is, for $B = 0.2$ and 1.8 meV. These two values of B represent two regimes: $B < \Delta_z$ and $B > \Delta_z$, respectively. Additionally, it should be stressed that the formalism used here is applicable to the constant relaxation time approximation. This is a quite reasonable approach, as Murakami[50] showed that the vertex correction to the velocity operator due to randomly distributed point-like impurities vanishes. We also did not take into account spin-orbital scatterers that may lead to skew-scattering and side-jump processes. Thus, the presented approach allows calculating (in the simplest possible way) the consistent results for linear and nonlinear Hall conductivity, emphasizing the effect of external magnetic field.

When $B < \Delta_z$, the intrinsic component, induced by the Berry curvature, dominates the linear system response. The component σ_{xy}^{II} does not depend on the orientation of in-plane magnetic field (described by the angle ψ, defined as the angle between x-direction and $\boldsymbol{B}$-vector), whereas the component σ_{xy}^I is a periodic function of ψ, with the oscillation period equal to π. In turn, the nonlinear conductivity, σ_{xy}^{nl}, reveals ψ-dependent oscillations, with the oscillation period of 2π. The oscillation period 2π is a signature of nonlinear with respect to the external electric field system response. Opposite to σ_{xy}^I, the topological term originating from the BCD is smaller than the nonlinear contribution originating from the states at the Fermi level. Both χ_{xyy}^I and

χ_{xyy}^{II} are nonmonotonous functions of chemical potential. In Figure 3d, the nonlinear conductivity, σ_{xy}^{nl}, and its two components are plotted as a function of μ for $\psi = 3\pi/4$. From this plot, one can see that χ_{xyy}^I at first decreases with increasing value of μ, reaches minimum around 9 meV and then increases, crosses 0, takes maximum around $\mu = 20$ meV, and next it decreases. In turn, χ_{xyy}^{II} is originally positive and takes maximum around $\mu = 9$ meV, then it decreases, crosses zero, and takes minimum at $\mu = 20$ meV and vanishes with further increase in μ. As a result, σ_{xy}^{nl} is a negative function having a local minimum around $\mu = 9$ meV and a local maximum around $\mu = 20$ meV.

When $B > \Delta_z$, the two components contributing to σ_{xy}^I, that is, σ_{xy}^I and σ_{xy}^{II}, are of the same order. Accordingly, σ_{xy}^I reveals well-defined oscillations with a π-periodicity. The component σ_{xy}^{nl} has periodicity of 2π. In addition, χ_{xyy}^I has a local maximum at $\psi = \pi/2$ and a local minimum at $\psi = 3\pi/2$, which indicates the presence of not only B linear but also B cubed terms. This means that when $\boldsymbol{B}$ is strong enough, not only the bilinear term, $B_x E_y$, but also $B_x^3 E_y$ term should be taken into account to describe properly σ_{xy}^{nl}. For $\psi = 3\pi/4$ the nonlinear contribution σ_{xy}^{nl} is again a negative function, having a local minimum around $\mu = 9$ meV and a local maximum around $\mu = 20$ meV. We note that we have presented here numerical data only for the chemical potentials up to 40 meV, as the effective Hamiltonian given by Equation (1) is valid only for small particle density (small wave numbers).[38,39]

The symmetric part of the off-diagonal conductivity, $\Delta_S\sigma_{xy} = [\sigma_{xy}(E_y = E) + \sigma_{xy}(E_y = -E)]/2 = \sigma_{xy}^I$, for lower in-plane magnetic field is determined by the topological component. The behavior of σ_{xy}^{II} for isotropic cubic Rashba model has been
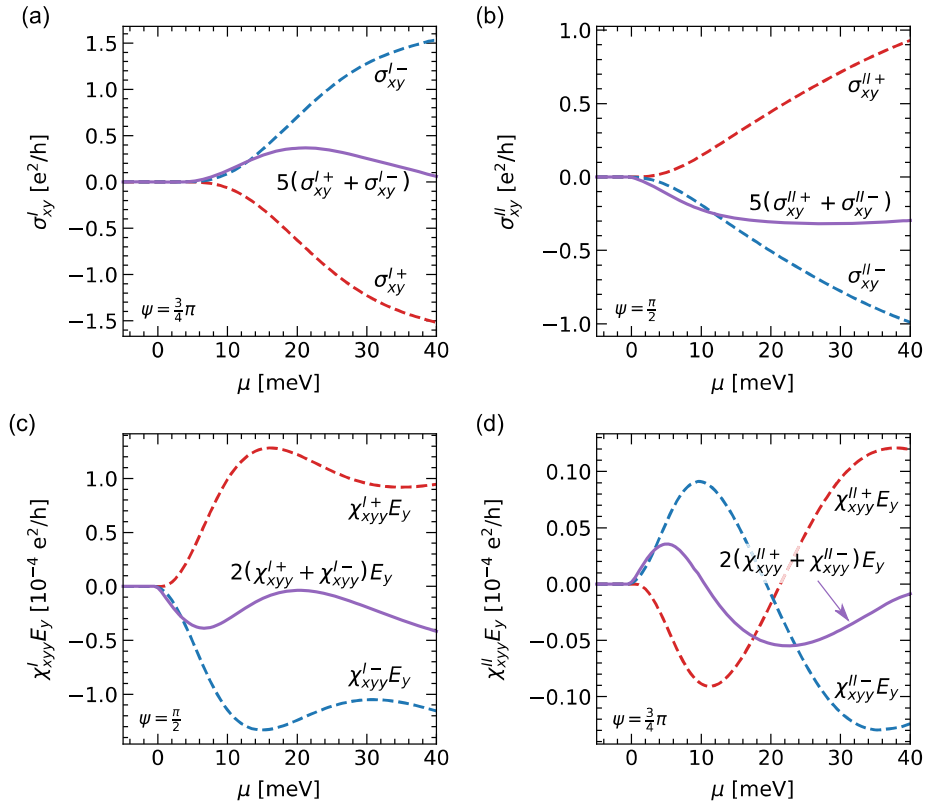
Figure 2. Four components of the Hall conductivity: a) σ^I_{xy}, b) σ^{II}_{xy}, c) $\chi^I_{xyy}E_y$, and d) $\chi^{II}_{xyy}E_y$ plotted as a function of chemical potential μ and for the indicated orientations of magnetic field (i.e., for the specific values of the angle ψ). For all components, the contributions from each of the sub-bands are presented. Here $\Delta_z = 0.4\,\text{meV}$, $B = 1.8\,\text{meV}$, $eE_y = 1\,\text{eV m}^{-1}$, $\Gamma = 5 \times 10^{-5}\,\text{eV}$, the other parameters are the same as in Figure 1.
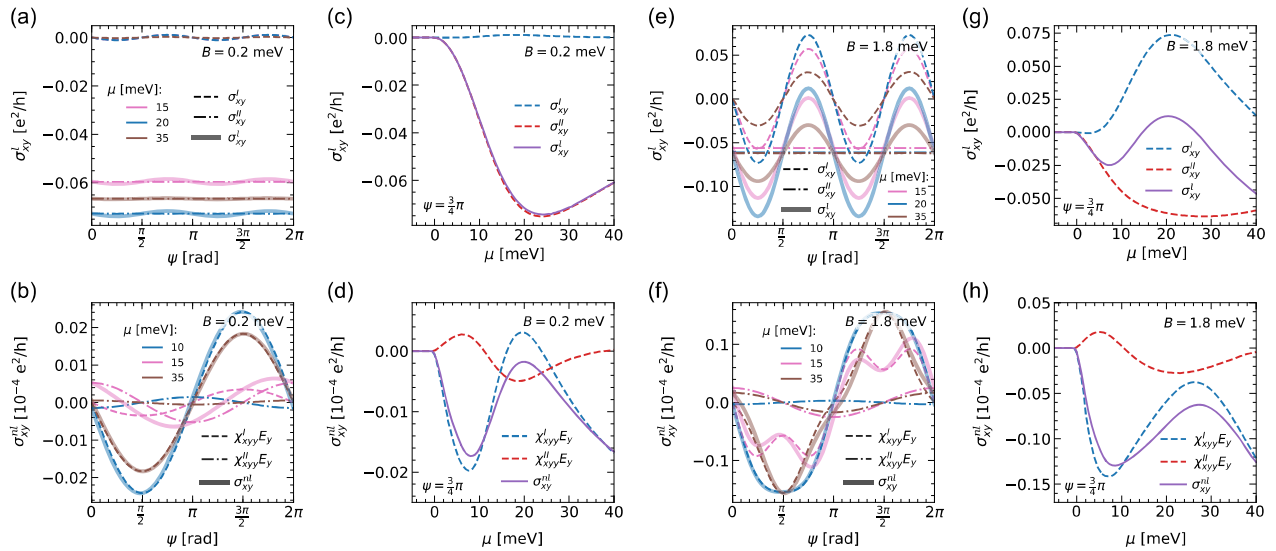
Figure 3. Linear and nonlinear Hall conductivity as a function of angle, ψ, defining the orientation of in-plane magnetic field a,b,e,f) and as a function of the chemical potential, μ c,d,g,h). The parameters are the same as in Figure 1 and 2 unless otherwise indicated on the plots.

106

discussed in detail, for example, in another work.[51]). In turn, when the amplitude of the in-plane magnetic field increases, the component σ_{xy}^{I} becomes more visible and starts to dominate.

Importantly the antisymmetric part of the Hall conductivity $\Delta_A \sigma_{xy} = [\sigma_{xy}(E_y = E) - \sigma_{xy}(E_y = -E)]/2 = \sigma_{xy}^{nl}$ can be strongly modified not only by the orientation and amplitude of in-plane magnetic field, but also by the change of chemical potential due to doping or gating. We have shown that the term related to the BCD is not sufficient to properly describe the behavior of non-linear system response, as the susceptibilities χ_{xyy}^{I} and χ_{xyy}^{II} can have opposite signs. Moreover, for larger in-plane magnetic fields, χ_{xyy}^{I} deviates from linear in **B** functional dependence.

5. Discussion and Summary

In this article, we have analyzed theoretically the linear and NLHEs in 2D systems within the isotropic k-cubed Rashba model. The analytical results are supported by numerical ones. We showed that an out-of-plane external magnetic field or magnetization leads to a nonzero Berry curvature in the system. We have also shown that the Berry curvature can be tuned by the in-plane magnetic field, and this may lead to the BCD.

We have also calculated the linear and nonlinear Hall response and have shown that in the linear response regime, the conductivity is dominated by the component due to Berry curvature. In turn, the second-order correction to the Hall conductivity is dominated by the states at the Fermi level.

Acknowledgements

Conflict of Interest

The authors declare no conflict of interest.

Data Availability Statement

The data that support the findings of this study are available from the corresponding author upon reasonable request.

Keywords

[1] Y. A. Bychkov, E. I. Rashba, *JETP Lett.* **1984**, *39*, 78.
[2] R. Winkler, *Spin—Orbit Coupling Effects in Two-Dimensional Electron and Hole Systems*, Springer, Berlin, Germany **2003**.
[3] G. Bihlmayer, O. Rader, R. Winkler, *New J. Phys.* **2015**, *17*, 050202.
[4] A. Manchon, H. C. Koo, J. Nitta, S. M. Frolov, R. A. Duine, *Nat. Mater.* **2015**, *14*, 871.
[5] G. Bihlmayer, P. Noël, D. V. Vyalikh, E. V. Chulkov, A. Manchon, *Rev. Phys.* **2022**, *4*, 642.
[6] A. Soumyanarayanan, N. Reyren, A. Fert, *Nature* **2016**, *539*, 509.
[7] Y. P. Feng, L. Shen, M. Yang, A. Wang, M. Zeng, Q. Wu, S. Chintalapati, C.-R. Chang, *WIREs Comput. Mol. Sci.* **2017**, *7*, e1313.
[8] A. Hirohata, K. Yamada, Y. Nakatani, I.-L. Prejbeanu, B. Diény, P. Pirro, B. Hillebrands, *J. Magn. Magn. Mater.* **2020**, *509*, 166711.
[9] D. Hsieh, Y. Xia, D. Qian, L. Wray, J. H. Dil, F. Meier, J. Osterwalder, L. Patthey, J. G. Checkelsky, N. P. Ong, A. V. Fedorov, H. Lin, A. Bansil, D. Grauer, Y. S. Hor, R. J. Cava, M. Z. Hasan, *Nature* **2009**, *460*, 1101.
[10] B. A. Bernevig, O. Vafek, *Phys. Rev. B* **2005**, *72*, 033203.
[11] A. Chernyshov, M. Overby, X. Liu, J. K. Furdyna, Y. Lyanda-Geller, L. P. Rokhinson, *Nat. Phys.* **2009**, *5*, 656.
[12] Y. K. Kato, R. C. Myers, A. C. Gossard, D. D. Awschalom, *Phys. Rev. Lett.* **2004**, *93*, 176601.
[13] V. Sih, R. C. Myers, Y. K. Kato, W. H. Lau, A. C. Gossard, D. D. Awschalom, *Nat. Phys.* **2005**, *1*, 31.
[14] C. H. Li, O. M. J. van 't Erve, J. T. Robinson, Y. Liu, L. Li, B. T. Jonker, *Nat. Nanotechnol.* **2014**, *9*, 24561354.
[15] J. Sinova, S. O. Valenzuela, J. Wunderlich, C. H. Back, T. Jungwirth, *Rev. Mod. Phys.* **2015**, *87*, 1213.
[16] Y. K. Kato, R. C. Myers, A. C. Gossard, D. D. Awschalom, *Science* **2004**, *306*, 1910.
[17] J. Wunderlich, B. Kaestner, J. Sinova, *Phys. Rev. Lett.* **2005**, *94*, 047204.
[18] S. O. Valenzuela, M. Tinkham, *Nature* **2006**, *442*, 176.
[19] E. Saitoh, M. Ueda, H. Miyajima, G. Tatara, *Appl. Phys. Lett.* **2006**, *88*, 182509.
[20] J. Wunderlich, B.-G. Park, A. C. Irvine, L. P. Zârbo, E. Rozkotová, P. Nemec, V. Novák, J. Sinova, T. Jungwirth, *Science* **2010**, *330*, 1801.
[21] P. He, S. S.-L. Zhang, D. Zhu, Y. Liu, Y. Wang, J. Yu, G. Vignale, H. Yang, *Nat. Phys.* **2018**, *14*, 495.
[22] A. Dyrdał, J. Barnaś, A. Fert, *Phys. Rev. Lett.* **2020**, *124*, 046802.
[23] Y. Fu, J. Li, J. Papin, P. Noël, S. Teresi, M. Cosset-Chéneau, C. Grezes, T. Guillet, C. Thomas, Y.-M. Niquet, P. Ballet, T. Meunier, J.-P. Attané, A. Fert, L. Vila, *Nano Lett.* **2022**, *22*, 7867.
[24] T. Guillet, C. Zucchetti, Q. Barbedienne, A. Marty, G. Isella, L. Cagnon, C. Vergnaud, H. Jaffrès, N. Reyren, J.-M. George, A. Fert, M. Jamet, *Phys. Rev. Lett.* **2020**, *124*, 027201.
[25] D. C. Vaz, F. Trier, A. Dyrdał, A. Johansson, K. Garcia, A. Barthélémy, I. Mertig, J. Barnaś, A. Fert, M. Bibes, *Phys. Rev. Mater.* **2020**, *4*, 071001.
[26] I. Sodemann, L. Fu, *Phys. Rev. Lett.* **2015**, *115*, 216806.
[27] Q. Ma, S.-Y. Xu, H. Shen, D. MacNeill, V. Fatemi, T.-R. Chang, A. M. Mier Valdivia, S. Wu, Z. Du, C.-H. Hsu, S. Fang, Q. D. Gibson, K. Watanabe, T. Taniguchi, R. J. Cava, E. Kaxiras, H.-Z. Lu, H. Lin, L. Fu, N. Gedik, P. Jarillo-Herrero, *Nature* **2019**, *565*, 337.
[28] K. Kang, T. Li, E. Sohn, J. Shan, K. F. Mak, *Nat. Mater.* **2019**, *18*, 324.
[29] P. He, S. S.-L. Zhang, D. Zhu, S. Shi, O. G. Heinonen, G. Vignale, H. Yang, *Phys. Rev. Lett.* **2019**, *123*, 016801.
[30] Z. Z. Du, C. M. Wang, H.-P. Sun, H.-Z. Lu, X. C. Xie, *Nat. Commun.* **2021**, *12*, 1.
[31] N. Nagaosa, J. Sinova, S. Onoda, A. H. MacDonald, N. P. Ong, *Rev. Mod. Phys.* **2010**, *82*, 1539.
[32] Z. Z. Du, C. M. Wang, S. Li, H.-Z. Lu, X. C. Xie, *Nat. Commun.* **2019**, *10*, 1.
[33] Y. Zhang, Y. Sun, B. Yan, *Phys. Rev. B* **2018**, *97*, 041101.
[34] J.-S. You, S. Fang, S.-Y. Xu, E. Kaxiras, T. Low, *Phys. Rev. B* **2018**, *98*, 121109.
[35] B. T. Zhou, C.-P. Zhang, K. T. Law, *Phys. Rev. Appl.* **2020**, *13*, 024053.

[36] S. Nandy, I. Sodemann, *Phys. Rev. B* **2019**, *100*, 195117.

[37] B. A. Bernevig, T. L. Hughes, S.-C. Zhang, *Science* **2006**, *314*, 1757.

[38] J. Schliemann, D. Loss, *Phys. Rev. B* **2005**, *71*, 085308.

[39] C.-X. Liu, B. Zhou, S.-Q. Shen, B.-F. Zhu, *Phys. Rev. B* **2008**, *77*, 125345.

[40] R. Moriya, K. Sawano, Y. Hoshi, S. Masubuchi, Y. Shiraki, A. Wild, C. Neumann, G. Abstreiter, D. Bougeard, T. Koga, T. Machida, *Phys. Rev. Lett.* **2014**, *113*, 086601.

[41] L. W. van Heeringen, A. McCollam, G. A. de Wijs, A. Fasolino, *Phys. Rev. B* **2017**, *95*, 155134.

[42] H. Nakamura, T. Koga, T. Kimura, *Phys. Rev. Lett.* **2012**, *108*, 206601.

[43] H. Liang, L. Cheng, L. Wei, Z. Luo, G. Yu, C. Zeng, Z. Zhang, *Phys. Rev. B* **2015**, *92*, 075309.

[44] A. D. Caviglia, M. Gabay, S. Gariglio, N. Reyren, C. Cancellieri, J.-M. Triscone, *Phys. Rev. Lett.* **2010**, *104*, 126803.

[45] E. Lesne, Y. Fu, S. Oyarzun, J. C. Rojas-Sanchez, D. C. Vaz, H. Naganuma, G. Sicoli, J.-P. Attané, M. Jamet, E. Jacquet, J.-M. George, A. Barthélémy, H. Jaffrès, A. Fert, M. Bibes, L. Vila, *Nat. Mater.* **2016**, *15*, 1261.

[46] F. Trier, P. Noël, J.-V. Kim, J.-P. Attané, L. Vila, M. Bibes, *Nat. Rev. Mater.* **2022**, *7*, 258.

[47] L. Karwacki, A. Dyrdał, J. Berakdar, J. Barnás, *Phys. Rev. B* **2018**, *97*, 235302.

[48] D. Xiao, M.-C. Chang, Q. Niu, *Rev. Mod. Phys.* **2010**, *82*, 1959.

[49] We do not consider here the skew-scattering and side jump processes.

[50] S. Murakami, *Phys. Rev. B* **2004**, *69*, 241202.

[51] A. Krzyzẽwska, A. Dyrdał, J. Barnás, J. Berakdar, *Phys. Status Solidi RRL* **2018**, *12*, 1800232.

Summary

The subject of this doctoral dissertation is the transport properties of a two-dimensional electron gas (2DEG) characterized by cubic forms of Rashba and Dresselhaus spin-orbit interactions. The main goal of the thesis was to theoretically investigate the intrinsic contribution to transport effects arising from the band structure of the analyzed system. The study focused on non-equilibrium spin polarization in the system, linear and nonlinear spin-orbit driven transport phenomena from the family of Hall effects, along with their thermal counterparts, such as the Nernst effect and thermally-induced spin polarization. Additionally, the interplay between spin-orbit interaction and the exchange field in magnetic systems was explored.

The cubic forms of Rashba spin-orbit interaction describe a 2D electron gas that forms at interfaces or surfaces of perovskite oxides. Recently, these materials have garnered scientific attention due to their interesting physical properties, including metallic conductivity, ferromagnetism, low-temperature superconductivity, and large spin-charge interconversion effect, making them promising for constructing spintronic devices. Additionally, the isotropic cubic Rashba model also applies to a 2D hole gas in p-doped semiconductor heterostructures. In turn, semiconductor heterostructures characterized by symmetric quantum wells exhibit the Dresselhaus type of spin-orbit interaction. Here, we consider the influence of the cubic Dresselhaus term on transport properties, particularly significant at higher chemical potentials.

The dissertation is based on six articles published in peer-reviewed journals, preceded by the introductory part. The introduction to the basic concepts utilized in the thesis provided in Chapter 1, concerns the investigated two-dimensional electron gas and the idea of spin-orbit interaction, focusing on the cubic forms of Rashba and Dresselhaus types. Chapter 2 introduces the theoretical method used in the investigations, namely Matsubara-Green's functions formalism and diagrammatic approach. Chapter 3 is dedicated to the transport phenomena considered in the dissertation, i.e., non-equilibrium spin polarization, linear anomalous, Nernst and spin Hall effects, nonlinear Hall effect, and bilinear magnetoresistance. In Chapter 4, the publications that constitute the thesis are presented along with short summaries.

The spin Hall effect in a magnetized and a nonmagnetized 2D system with an isotropic cubic

form of Rashba SOI is considered in the article A-1. It was shown that an out-of-plane oriented exchange field suppresses the spin Hall response.

Articles A-2 and A-3 were dedicated to the linear anomalous Hall and Nernst effects. The analysis of the intrinsic anomalous Hall effect in a 2D system with cubic forms of Rashba spin-orbit interaction and out-of-plane oriented magnetization field (sec. 3.2.1) indicates that the contribution from the states in the Fermi sea related to the Berry curvature dominates in a weak-scattering regime and when the impurity concentration in the system is low. The anomalous Hall effect is most pronounced when the strength of the cubic Rashba SOI and exchange interaction are comparable. Moreover, the anisotropy of the Fermi contours in wavevector-space in the considered models does not affect the results qualitatively. The examination of the intrinsic anomalous Hall effect in a 2D system with both linear and cubic forms of Dresselhaus SOI indicates the main intrinsic contribution that is robust against impurities and signifies the diminishing influence of the cubic term on the value of the anomalous Hall effect at higher chemical potentials.

Investigation of the anomalous Nernst effect in 2DEG with cubic forms of Rashba SOI (A-2 and A-3) shows that the Kubo formula is not valid at low temperature as long as the orbital magnetization current is not considered. However, using the Mott and Onsager relations one can treat the anomalous Hall effect as a thermal counterpart of the anomalous Hall effect. For higher chemical potential, experimentally observed change of the sing preceding the magnetic phase transition indicated by the Curie temperature, was found. It appears when the strength of the Rashba and saturation magnetization interactions are comparable.

The current-induced non-equilibrium spin polarization (CISP) in a symmetric quantum well growing in [001] crystallographic direction with both linear and cubic forms of Dresselhaus spin-orbit interactions was investigated in the article A-4. The study reveals that at higher chemical potential, μ, the cubic term of the Dresselhaus reduces the spin polarization in the system by 10%-30% compared to the μ-independent relation that arises when only the linear term is present. Furthermore, incorporating an out-of-plane exchange interaction, possibly originating from the magnetic substrate, introduces an additional transverse contribution to the spin polarization from the states in the Fermi sea. Additionally, the scattering processes on short-range spin-independent impurities do not affect the intrinsic contribution. However, these processes alter the dissipative component of CISP by a factor of 2 when the spin-orbit interaction dominates the exchange field.

Moreover, in the paper A-4 the analysis of thermally-induced spin polarization (TISP) in magnetized 2DEG with linear and cubic forms of Dresselhaus SOI is provided. It was found that the dissipative component of the TISP, determined by the states at the Fermi level, is linked with the current-induced spin polarization *via* Mott relation. TISP is most pronounced in the energy gap and can be tuned with a magnetization field. Thus, the cubic Dresselaus SOI term, which

influences the results at higher Fermi levels (higher carriers density), does not modify the TISP distinctly.

In the manuscript A-5, bilinear magnetoresistance in a 2DEG with an isotropic cubic form of Rashba SOI and in-plane magnetic field applied is considered. Here, using Green's functions formalism, the analytical results were obtained. The bilinear term of magnetoresistance is evoked by the non-equilibrium spin polarization in the system and is the most pronounced in a weak magnetic field regime.

In the work A-6, the role of both the intrinsic and dissipative components of the linear and nonlinear contributions to the anomalous Hall conductivity (AHC) in a magnetized 2D electron gas with isotropic cubic form of Rashba SOI is investigated. Two regimes were examined: the low in-plane magnetic field regime, where the value of the in-plane magnetic field is lower than the out-of-plane magnetization component, and the opposite situation. It was found that in the low in-plane magnetic field regime, the linear AHC is dominated by the intrinsic part, originating in the Berry curvature. In turn, for higher values of the in-plane magnetic field, the dissipative component, related to the states at the Fermi level, begins to influence the results. Interestingly, for the nonlinear component of the AHC, the dissipative component governs the transport in both regimes.

Moreover, utilizing the Zeeman-field engineering concept, it was shown that in the investigated system, the nonlinear Hall effect can be induced and tuned by the value and angle of the in-plane magnetic field. Furthermore, the intrinsic part of the linear AHC reveals a π-periodicity with respect to the angle of the in-plane magnetic field, while the nonlinear AHC, originating in the Berry curvature dipole, exhibits a 2π-periodicity with the in-plane magnetic field angle. Finally, the AHC is governed by the intrinsic part when the in-plane magnetic field is applied perpendicular to the external electric field.

The analyzed linear and nonlinear transport phenomena are known in the literature and have mostly been studied in the systems with linear form of Rashba and Dresselhaus spin-orbit interaction. In contrast, the presented thesis contributes to the field by describing these phenomena in systems where the cubic form of Rashba or Dresselhaus spin-orbit interaction exists.

The cases where the cubic form of SOC leads to different results than the linear form of SOC, as seen in the case of the spin Hall effect, have been analyzed. Here, in the presence of randomly distributed spin-independent impurities, the SHE vanishes in a 2DEG with the linear form of Rashba, but it remains unaffected when the cubic form of Rashba SOC is present (article A-1). Additionally, there are cases where the linear and different cubic forms of Rashba SOC yield similar outcomes, such as the anomalous Hall effect described in the papers A-2 and A-3. In addition, both forms of cubic Rashba SOC, isotropic and anisotropic, are analyzed, and it was

shown that both lead to similar results in the case of the anomalous Hall and Nernst effects (A-2 and A-3). Moreover, the influence of the cubic Dresselhaus SOC term on transport properties is presented in a system where the linear form of SOC also exists, see A-4.

In general, the results presented in the dissertation cover transport phenomena described by zero-temperature analytical formulas, which are important for the conceptual description of a system, as well as the numerical results for finite-temperatures. Moreover, the analytical outcomes facilitate the description of the transport properties of the system with exact expressions, where the dependencies on system parameters and external forces are directly visible. Additionally, such results allow the study of the system properties without the influence of temperature smearing. On the other hand, the numerical results in the finite-temperature regime provide the opportunity to understand how temperature affects the results, which is significant from both an experimental and an applied perspective.

However, it should be noted that the results were derived using effective Hamiltonians, describing only a part of the band structure. On the one hand, the effective Hamiltonian allows for the description of classes of structures rather than individual systems and aids in identifying the minimal set of significant parameters needed to effectively describe the physical system. However, it cannot accurately model the system at higher carrier concentration, where other bands, not covered by the effective model, influence the results. Thus, an interesting extension of the presented results could be achieved using the first-principles (*ab initio*) electronic structure methods, where the whole band structure is examined. This approach allows for observing how the other bands, at higher carrier concentrations, influence the obtained results. Moreover, the first-principles method based on density functional theory produces outcomes for specific materials, which, at low carrier concentrations, can be compared with the obtained results.

Another way to extend the presented studies is to include spin-dependent scattering processes, such as *side-jump* and *skew-scattering*, in the considered models. This extension allows for investigating how phenomena like the spin or anomalous Hall effects are modified, and for comparing the results with those known in the literature for systems with k-linear Rashba SOI [154, 236].

Recently, nonlinear effects have become a hot topic due to their sensitivity to breaking spatial symmetry, which enables potential applications in material characterization and current rectification. Moreover, the unidirectional response offers a promising platform for constructing spin-logic devices. The thesis covers the nonlinear Hall effect and bilinear magnetoresistance in systems with a cubic form of Rashba SOC. However, the study could be extended to explore the intrinsic contribution to the temperature-induced transport effects in the nonlinear regime [214, 215].

In summary, the thesis contributes to the field of two-dimensional spintronics by characterizing the transport properties of a 2DEG with cubic forms of the intrinsic spin-orbit interaction. Existing scientific research primarily addresses the linear forms of Rashba and Dresselhaus spin-orbit interaction. In contrast, the results presented in the dissertation focus on transport in systems with the cubic forms of these interactions. Combining the knowledge from the literature with the thesis outcomes may help to distinguish the form of intrinsic spin-orbit interaction based on the transport properties of the system, such as linear and nonlinear Hall effects and their thermal counterparts.

A

Permissions of the journals
to reprint the manuscripts in the thesis

- **A-2**, **A-6**: According to the Wiley Policy: *If you are the author of a published Wiley article, you have the right to reuse the full text of your published article as part of your thesis or dissertation. In this situation, you do not need to request permission from Wiley for this use.*[1]

- **A-3**, **A-4**, **A-5**: According to the Elsevier Policy: *Authors can include their articles in full or in part in a thesis or dissertation for non-commercial purposes.*

  As an Elsevier journal author, you have the right to Include the article in a thesis or dissertation (provided that this is not to be published commercially) whether in full or in part, subject to proper acknowledgment. [...] No written permission from Elsevier is necessary.

  This right extends to the posting of your thesis to your university's repository provided that if you include the published journal article, it is embedded in your thesis and not separately downloadable.[2]

---

[1]https://www.wiley.com/en-us/network/publishing/research-publishing/trending-stories/how-to-clear-permissions-for-a-thesis-or-dissertation [online access: 21.02.2024]

[2]https://www.elsevier.com/about/policies-and-standards/copyright/permissions [online access: 21.02.2024]

- **A-1**: Permission to include the entire article published in *Acta Physica Polonica A* in the doctoral thesis has been granted, and the appropriate document is attached below.

INSTITUTE OF PHYSICS
POLISH ACADEMY
OF SCIENCES

ACTA
PHYSICA
POLONICA
A
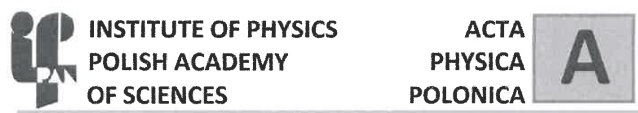
Warsaw, December 19, 2023

Dear Anna Krzyżewska,

Herewith I grant you permission to include the entire article entitled *"Temperature Dependence of Spin Hall Effect in k–Cubed Rashba Model"*, by A. Krzyżewska, A. Dyrdał, J. Berakdar — paper originally published in **Acta Physica Polonica A** Vol. 133, 558 (2018); DOI: 10.12693/APhysPolA.133.558 — in your PhD thesis, which is intended to be published in the Public Information Bulletin of Adam Mickiewicz University (https://bip.amu.edu.pl/).

A note `published with permission`, or something similar, should be added.

Prof. Jacek Kossut
The Acting Editor-in-Chief
Acta Physica Polonica A

Institute of Physics
Polish Academy of Sciences
al. Lotnikow 32/46
02-668 Warsaw, Poland

B

Statements
regarding contributions to the publications

Below both the statements of the author of the thesis as well as co-authors of the publications constituting the thesis are attached.

Poznań, 19.07.2024

Anna Krzyżewska
Faculty of Physics
Adam Mickiewicz University in Poznań
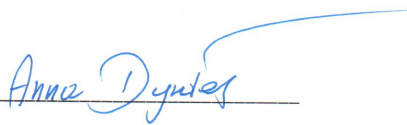anna.krzyzewska@amu.edu.pl

Statement

I hereby declare that as the author of this doctoral dissertation based on a series of published scientific articles, I am a co-author of all publications included in it, with the following contributions:

▼ A. Krzyżewska, A. Dyrdał, J. Berakdar, *Temperature Dependence of Spin Hall Effect in k–Cubed Rashba Model*, Acta Physica Polonica A **133**, 558 (2018)

In the above-mentioned work, I performed calculations, prepared the figures, and took part in data analysis.

▼ A. Krzyżewska, A. Dyrdał, J. Barnaś, J. Berakdar, *Anomalous Hall and Nernst Effects in 2D Systems: Role of Cubic Rashba Spin–Orbit Coupling*, Phys. Status Solidi RRL **12**, 1800232 (2018)

▼ A. Krzyżewska, A. Dyrdał, *Anomalous Hall and Nernst effects in a two-dimensional electron gas with an anisotropic cubic Rashba spin-orbit interaction*, J. Magn. Magn. Mater. **497**, 165919 (2020)

▼ A. Krzyżewska, A. Dyrdał, *Non-equilibrium spin polarization in magnetic two-dimensional electron gas with k-linear and k-cubed Dresselhaus spin-orbit interaction*, Physica E **135**, 114961 (2022)

▼ A. Krzyżewska, A. Dyrdał, *Bilinear magnetoresistance in 2DEG with isotropic cubic Rashba spin–orbit interaction*, J. Magn. Magn. Mater. **589**, 171615 (2024)

▼ A. Krzyżewska, A. Dyrdał, *Nonlinear Hall Effect in Isotropic k-Cubed Rashba Model: Berry-Curvature-Dipole Engineering by In-Plane Magnetic Field*, Phys. Status Solidi RRL **n/a**, 2400123 (2024)

In the above-mentioned works, I performed calculations, prepared the figures, participated in data analysis and contributed to preparing the manuscript.

_____
Supervisor

_____
Author of the doctoral dissertation

ADAM MICKIEWICZ UNIVERSITY, POZNAŃ

Faculty of Physics

Poznań, 9th August 2024

Prof. UAM dr hab. Anna Dyrdał
Head of Mesoscopic Physics Department
Institute of Spintronics and Quantum Information
Faculty of Physics, Adam Mickiewicz University in Poznań

Statement about the contribution to the publications

I hereby declare that I am aware that the following works:

1. A. Krzyżewska, A. Dyrdał, J. Berakdar, *Temperature Dependence of Spin Hall Effect in k–Cubed Rashba Model*, Acta Physica Polonica A 133, 558 (2018)
2. A. Krzyżewska, A. Dyrdał, J. Barnaś, J. Berakdar, *Anomalous Hall and Nernst Effects in 2D Systems: Role of Cubic Rashba Spin–Orbit Coupling*, Phys. Status Solidi RRL 12, 1800232 (2018)
3. A. Krzyżewska, *A. Dyrdał, Anomalous Hall and Nernst effects in a two-dimensional electron gas with an anisotropic cubic Rashba spin-orbit interaction*, J. Magn. Magn. Mater. 497, 165919 (2020)
4. A. Krzyżewska, A.Dyrdał, *Non-equilibrium spin polarization in magnetic two-dimensional electron gas with k-linear and k-cubed Dresselhaus spin-orbit interaction*, Physica E 135, 114961 (2022)
5. A. Krzyżewska, A. Dyrdał, *Bilinear magnetoresistance in 2DEG with isotropic cubic Rashba spin-orbit interaction*, J. Magn. Magn. Mater. 589, 171615 (2024)
6. A. Krzyżewska, A. Dyrdał, *Nonlinear Hall effect in isotropic k-cubed Rashba model: Berry-curvature-dipole engineering by in-plane magnetic field*, Phys. Status Solidi RRL, https://doi.org/10.1002/pssr.202400123 (2024)

of which I am a co-author, have been included in the doctoral thesis of Anna Krzyżewska.

My contribution to the above publications:

I conceived and designed the problem, proposed the theoretical approach, supervised Anna Krzyżewska, checked and corrected analytical results, analysed and interpreted the results (with contributions from other co-authors); contributed to the writing of the preliminary drafts, and wrote and edited the final versions of the manuscripts.

ul. Uniwersytetu Poznańskiego 2, 61-614 Poznań
tel. +48 61 829 52 88, e-mail: adyrdal@amu.edu.pl

Poznań, 9th August 2024

Prof. dr hab. Józef Barnaś
Mesoscopic Physics Department
Institute of Spintronics and Quantum Information
Faculty of Physics, Adam Mickiewicz University in Poznań

Statement about the contribution to the publication

I hereby declare that I am aware that the following publication:

A. Krzyżewska, A. Dyrdał, J. Barnaś, J. Berakdar, *Anomalous Hall and Nernst Effects in 2D Systems: Role of Cubic Rashba Spin–Orbit Coupling*, Phys. Status Solidi RRL 12, 1800232 (2018)

of which I am a co-author, has been included in the doctoral thesis of Anna Krzyżewska. I also declare that my contribution to this paper includes discussions of the problem at the initial stage and taking part in editing the final version of the manuscript.

Józef Barnaś

RESEARCH
UNIVERSITY
EXCELLENCE INITIATIVE   HR EXCELLENCE IN RESEARCH

Naturwissenschaftliche Fakultät II –
Chemie, Physik und Mathematik

Institut für Physik
Prof. Dr. Jamal Berakdar

Hausanschrift:
Karl-Freiherr-von-Fritsch-Str. 3
06120 Halle/Saale
Germany

Tel.   +49(0)345 55-28517
Fax   +49(0)345 55-27114
email   jamal.berakdar@physik.uni-halle.de
Internet www.physik.uni-halle.de

Martin-Luther-Universität Halle-Wittenberg, D-06099 Halle, Germany

To whom it may concern

Ihr Schreiben vom	Ihr Zeichen	Unser Zeichen	Datum
		Anna-24	18. July 2024

Concerning both papers

A. Krzyżewska, A. Dyrdał, J. Berakdar, Temperature Dependence of Spin Hall Effect in k–Cubed Rashba Model, Acta Physica Polonica A 133, 558 (2018)

A.Krzyżewska, A. Dyrdał, J. Barnaś, J. Berakdar, Anomalous Hall and Nernst Effects in 2D Systems: Role of Cubic Rashba Spin–Orbit Coupling, Phys. Status Solidi RRL 12, 1800232 (2018),

I declare herewith that my contributions are:
paricipating in discussions and editing of manuscripts.

Martin-Luther-Universität
Halle-Wittenberg
Institut für Physik
Prof. J. Berakdar
Heinrich-Damerow-Straße 4
06120 Halle (Saale)

Bibliography

1. Jacoboni, C. in *Theory of Electron Transport in Semiconductors: A Pathway from Elementary Physics to Nonequilibrium Green Functions* 363–388 (Springer, Berlin, Germany, July 2010). ISBN: 978-3-642-10586-9.

2. Galperin, Y. Quantum Transport. Lecture Notes. *Lund University Press* (Nov. 1998).

3. Akkermans, E. & Montambaux, G. *Mesoscopic Physics of Electrons and Photons* ISBN: 978-0-52185512-9 (Cambridge University Press, Cambridge, England, UK, May 2007).

4. Ihn, T. *Semiconductor Nanostructures: Quantum states and electronic transport* ISBN: 9780199534425 (Oxford University Press, Nov. 2009).

5. Ibach, H. *Fizyka ciała stałego* ISBN: 978-830112039 (PWN, Jan. 1996).

6. Kelsall, R., Hamley, I. W. & Geoghegan, M. *Nanoscale Science and Technology* ISBN: 978-0-470-85086-2 (Wiley, Hoboken, NJ, USA, Feb. 2005).

7. Lu, J. P., Yau, J. B., Shukla, S. P., Shayegan, M., Wissinger, L., Rössler, U. & Winkler, R. Tunable Spin-Splitting and Spin-Resolved Ballistic Transport in GaAs/AlGaAs Two-Dimensional Holes. *Phys. Rev. Lett.* **81,** 1282–1285. ISSN: 1079-7114 (Aug. 1998).

8. Wissinger, L., Rössler, U., Winkler, R., Jusserand, B. & Richards, D. Spin splitting in the electron subband of asymmetric $GaAs/Al_xGa_{1-x}As$ quantum wells: The multiband envelope function approach. *Phys. Rev. B* **58,** 15375–15377. ISSN: 2469-9969 (Dec. 1998).

9. Bernevig, B. A., Hughes, T. L. & Zhang, S.-C. Quantum Spin Hall Effect and Topological Phase Transition in HgTe Quantum Wells. *Science* **314,** 1757–1761. ISSN: 0036-8075 (Dec. 2006).

10. König, M., Wiedmann, S., Brüne, C., Roth, A., Buhmann, H., Molenkamp, L. W., Qi, X.-L. & Zhang, S.-C. Quantum Spin Hall Insulator State in HgTe Quantum Wells. *Science* **318,** 766–770. ISSN: 0036-8075 (Nov. 2007).

11. Mannhart, J. & Schlom, D. G. Oxide Interfaces—An Opportunity for Electronics. *Science* **327,** 1607–1611. ISSN: 0036-8075 (Mar. 2010).

12. Hwang, H. Y., Iwasa, Y., Kawasaki, M., Keimer, B., Nagaosa, N. & Tokura, Y. Emergent phenomena at oxide interfaces. *Nat. Mater.* **11,** 103–113. ISSN: 1476-4660 (Feb. 2012).

13. Sulpizio, J. A., Ilani, S., Irvin, P. & Levy, J. Nanoscale Phenomena in Oxide Heterostructures. *Annu. Rev. Mater. Res.* **44,** 117–149. ISSN: 1531-7331 (July 2014).

14. Stemmer, S. & James Allen, S. Two-Dimensional Electron Gases at Complex Oxide Interfaces. *Annu. Rev. Mater. Res.* **44,** 151–171. ISSN: 1531-7331 (July 2014).

15. Trier, F., Noël, P., Kim, J.-V., Attané, J.-P., Vila, L. & Bibes, M. Oxide spin-orbitronics: spin–charge interconversion and topological spin textures. *Nat. Rev. Mater.* **7,** 258–274. ISSN: 2058-8437 (Apr. 2022).

16. Li, C., Liu, Z., Lü, W., X. R., W., Annadi, A., Huang, Z., Zeng, S., Ariando & Venkatesan, T. Tailoring the Two Dimensional Electron Gas at Polar ABO3/SrTiO3 Interfaces for Oxide Electronics. *Sci. Rep.* **5,** 13314. ISSN: 2045-2322 (Aug. 2015).

17. Ohtomo, A. & Hwang, H. Y. A high-mobility electron gas at the LaAlO3/SrTiO3 heterointerface. *Nature* **427,** 423–426. ISSN: 1476-4687 (Jan. 2004).

18. Lesne, E., Fu, Y., Oyarzun, S., Rojas-Sánchez, J. C., Vaz, D. C., Naganuma, H., Sicoli, G., Attané, J.-P., Jamet, M., Jacquet, E., George, J.-M., Barthélémy, A., Jaffrès, H., Fert, A., Bibes, M. & Vila, L. Highly efficient and tunable spin-to-charge conversion through Rashba coupling at oxide interfaces. *Nat. Mater.* **15,** 1261–1266. ISSN: 1476-4660 (Dec. 2016).

19. Maznichenko, I. V., Ostanin, S., Ernst, A., Henk, J. & Mertig, I. Formation and Tuning of 2D Electron Gas in Perovskite Heterostructures. *Phys. Status Solidi B* **257,** 1900540. ISSN: 0370-1972 (July 2020).

20. Lorenz, M., Rao, M. S. R., Venkatesan, T., Fortunato, E., Barquinha, P., Branquinho, R., Salgueiro, D., Martins, R., Carlos, E., Liu, A., Shan, F. K., Grundmann, M., Boschker, H., Mukherjee, J., Priyadarshini, M., DasGupta, N., Rogers, D. J., Teherani, F. H., Sandana, E. V., Bove, P., Rietwyk, K., Zaban, A., Veziridis, A., Weidenkaff, A., Muralidhar, M., Murakami, M., Abel, S., Fompeyrine, J., Zuniga-Perez, J., Ramesh, R., Spaldin, N. A., Ostanin, S., Borisov, V., Mertig, I., Lazenka, V., Srinivasan, G., Prellier, W., Uchida, M., Kawasaki, M., Pentcheva, R., Gegenwart, P., Granozio, F. M., Fontcuberta, J. & Pryds, N. The 2016 oxide electronic materials and oxide interfaces roadmap. *J. Phys. D: Appl. Phys.* **49,** 433001. ISSN: 0022-3727 (Oct. 2016).

21. Nakagawa, N., Hwang, H. Y. & Muller, D. A. Why some interfaces cannot be sharp. *Nat. Mater.* **5,** 204–209. ISSN: 1476-4660 (Mar. 2006).

22. Stengel, M. First-Principles Modeling of Electrostatically Doped Perovskite Systems. *Phys. Rev. Lett.* **106,** 136803. ISSN: 1079-7114 (Mar. 2011).

23. Szewczyk, A., Wiśniewski, A., Puźniak, R. & Szymczak, H. *Magnetyzm i nadprzewodnictwo* ISBN: 978-83-01-17176-6 (Wydawnictwo naukowe PWN, 2012).

24. Manchon, A. *Spintronics Lectures* [online accessed 19. August 2024]. https://physiquemanchon.wixsite.com/research/spintronics-lectures.

25. Gerlach, W. & Stern, O. Der experimentelle Nachweis des magnetischen Moments des Silberatoms. *Z. Phys.* **8,** 110–111. ISSN: 0044-3328 (Dec. 1922).

26. Uhlenbeck, G. E. & Goudsmit, S. Spinning Electrons and the Structure of Spectra. *Nature* **117,** 264–265. ISSN: 1476-4687 (Feb. 1926).

27. *Goudsmit on the discovery of electron spin* [online accessed 25. May 2023]. Feb. 2019. https://www.lorentz.leidenuniv.nl/history/spin/goudsmit.html.

28. Dugaev, V. & Litvinov, V. *Modern Semiconductor Physics and Device Applications* ISBN: 978-0-36725082-9 (CRC Press, Boca Raton, FL, USA, Nov. 2021).

29. Sakurai, J. J. *Advanced quantum mechanics* (Addison-Wesley, 1967).

30. Manousakis, E. *Practical Quantum Mechanics* ISBN: 978-0-19874934-9 (Oxford University Press, Oxford, England, UK, Nov. 2015).

31. Winkler, R. *Spin-orbit Coupling Effects in Two-Dimensional Electron and Hole Systems* ISBN: 978-3-540-01187-3 (Springer-Verlag, Berlin, Germany, 2003).

32. Sinova, J. & MacDonald, A. H. in *Semiconductors and Semimetals* 45–87 (Elsevier, Walthm, MA, USA, Jan. 2008).

33. Crépieux, A. & Bruno, P. Theory of the anomalous Hall effect from the Kubo formula and the Dirac equation. *Phys. Rev. B* **64,** 014416. ISSN: 2469-9969 (June 2001).

34. Engel, H.-A., Rashba, E. I. & Halperin, B. I. in *Handbook of Magnetism and Advanced Magnetic Materials* (John Wiley & Sons, Ltd, Chichester, England, UK, July 2007). ISBN: 978-0-47002218-4.

35. Žutić, I., Fabian, J. & Das Sarma, S. Spintronics: Fundamentals and applications. *Rev. Mod. Phys.* **76,** 323–410. ISSN: 1539-0756 (Apr. 2004).

36. Nagaosa, N., Sinova, J., Onoda, S., MacDonald, A. H. & Ong, N. P. Anomalous Hall effect. *Rev. Mod. Phys.* **82,** 1539–1592. ISSN: 1539-0756 (May 2010).

37. Berger, L. Side-Jump Mechanism for the Hall Effect of Ferromagnets. *Phys. Rev. B* **2,** 4559–4566. ISSN: 2469-9969 (Dec. 1970).

38. Smit, J. The spontaneous Hall effect in ferromagnetics I. *Physica* **21,** 877–887 (1955).

39. Soumyanarayanan, A., Reyren, N., Fert, A. & Panagopoulos, C. Emergent phenomena induced by spin–orbit coupling at surfaces and interfaces. *Nature* **539,** 509–517. ISSN: 1476-4687 (Nov. 2016).

40. Nitta, J., Akazaki, T., Takayanagi, H. & Enoki, T. Gate Control of Spin-Orbit Interaction in an Inverted $In_{0.53}Ga_{0.47}As/In_{0.52}Al_{0.48}As$ Heterostructure. *Phys. Rev. Lett.* **78,** 1335–1338. ISSN: 1079-7114 (Feb. 1997).

41. Studer, M., Salis, G., Ensslin, K., Driscoll, D. C. & Gossard, A. C. Gate-Controlled Spin-Orbit Interaction in a Parabolic $GaAs/AlGaAs$ Quantum Well. *Phys. Rev. Lett.* **103,** 027201. ISSN: 1079-7114 (July 2009).

42. Caviglia, A. D., Gabay, M., Gariglio, S., Reyren, N., Cancellieri, C. & Triscone, J.-M. Tunable Rashba Spin-Orbit Interaction at Oxide Interfaces. *Phys. Rev. Lett.* **104,** 126803. ISSN: 1079-7114 (Mar. 2010).

43. Lechner, V., Golub, L. E., Olbrich, P., Stachel, S., Schuh, D., Wegscheider, W., Bel'kov, V. V. & Ganichev, S. D. Tuning of structure inversion asymmetry by the δ-doping position in (001)-grown GaAs quantum wells. *Appl. Phys. Lett.* **94,** 242109. ISSN: 0003-6951 (June 2009).

44. Pfeiffer, L., West, K. W., Stormer, H. L. & Baldwin, K. W. Electron mobilities exceeding 107 cm2/V s in modulation-doped GaAs. *Appl. Phys. Lett.* **55,** 1888–1890. ISSN: 0003-6951 (Oct. 1989).

45. Manfra, M. J., Pfeiffer, L. N., West, K. W., de Picciotto, R. & Baldwin, K. W. High mobility two-dimensional hole system in xn–GaAsAlGaAs-bh1f quantum wells grown on (100) GaAs substrates. *Appl. Phys. Lett.* **86,** 162106. ISSN: 0003-6951 (Apr. 2005).

46. Dingle, R., Störmer, H. L., Gossard, A. C. & Wiegmann, W. Electron mobilities in modulation-doped semiconductor heterojunction superlattices. *Appl. Phys. Lett.* **33,** 665–667. ISSN: 0003-6951 (Oct. 1978).

47. Dyakonov, M. I. & Kachorovskii, V. Y. Spin Relaxation of Two Dimensional Electrons in Noncentrosymetric Semiconductors. *Soviet Physics: Semiconductors* **20,** 110–116 (1986).

48. Walser, M. P., Siegenthaler, U., Lechner, V., Schuh, D., Ganichev, S. D., Wegscheider, W. & Salis, G. Dependence of the Dresselhaus spin-orbit interaction on the quantum well width. *Phys. Rev. B* **86,** 195309. ISSN: 2469-9969 (Nov. 2012).

49. LaShell, S., McDougall, B. A. & Jensen, E. Spin Splitting of an Au(111) Surface State Band Observed with Angle Resolved Photoelectron Spectroscopy. *Phys. Rev. Lett.* **77,** 3419–3422. ISSN: 1079-7114 (Oct. 1996).

50. Ast, C. R., Henk, J., Ernst, A., Moreschini, L., Falub, M. C., Pacilé, D., Bruno, P., Kern, K. & Grioni, M. Giant Spin Splitting through Surface Alloying. *Phys. Rev. Lett.* **98,** 186807. ISSN: 1079-7114 (May 2007).

51. Ho Park, Y., Kim, H.-j., Chang, J., Hee Han, S., Eom, J., Choi, H.-J. & Cheol Koo, H. Separation of Rashba and Dresselhaus spin-orbit interactions using crystal direction dependent transport measurements. *Appl. Phys. Lett.* **103.** ISSN: 0003-6951 (Dec. 2013).

52. Dresselhaus, P. D., Papavassiliou, C. M. A., Wheeler, R. G. & Sacks, R. N. Observation of spin precession in GaAs inversion layers using antilocalization. *Phys. Rev. Lett.* **68,** 106–109. ISSN: 1079-7114 (Jan. 1992).

53. Miller, J. B., Zumbühl, D. M., Marcus, C. M., Lyanda-Geller, Y. B., Goldhaber-Gordon, D., Campman, K. & Gossard, A. C. Gate-Controlled Spin-Orbit Quantum Interference Effects in Lateral Transport. *Phys. Rev. Lett.* **90,** 076807. ISSN: 1079-7114 (Feb. 2003).

54. Nakamura, H., Koga, T. & Kimura, T. Experimental Evidence of Cubic Rashba Effect in an Inversion-Symmetric Oxide. *Phys. Rev. Lett.* **108,** 206601. ISSN: 1079-7114 (May 2012).

55. Bychkov, Y. A. & Rashba, É. I. Properties of a 2D electron gas with lifted spectral degeneracy. *Soviet Journal of Experimental and Theoretical Physics Letters* **39,** 78. ISSN: 0021-3640 (Jan. 1984).

56. Qu, J., Han, X., Sakamoto, S., Jia, C. J., Liu, J., Li, H., Guan, D., Zeng, Y.-J., Schüler, M., Kirchmann, P. S., Moritz, B., Hussain, Z., Devereaux, T. P., Shen, Z.-X. & Sobota, J. A. Reversal of spin-polarization near the Fermi level of the Rashba semiconductor BiTeCl. *npj Quantum Mater.* **8,** 1–6. ISSN: 2397-4648 (Mar. 2023).

57. Zhong, Z., Tóth, A. & Held, K. Theory of spin-orbit coupling at LaAlO$_3$/SrTiO$_3$ interfaces and SrTiO$_3$ surfaces. *Phys. Rev. B* **87,** 161102. ISSN: 2469-9969 (Apr. 2013).

58. Khalsa, G., Lee, B. & MacDonald, A. H. Theory of t_{2g} electron-gas Rashba interactions. *Phys. Rev. B* **88,** 041302. ISSN: 2469-9969 (July 2013).

59. Kim, Y., Lutchyn, R. M. & Nayak, C. Origin and transport signatures of spin-orbit interactions in one- and two-dimensional SrTiO$_3$-based heterostructures. *Phys. Rev. B* **87,** 245121. ISSN: 2469-9969 (June 2013).

60. Shanavas, K. V. Theoretical study of the cubic Rashba effect at the SrTiO$_3$(001) surfaces. *Phys. Rev. B* **93,** 045108. ISSN: 2469-9969 (Jan. 2016).

61. Seibold, G., Caprara, S., Grilli, M. & Raimondi, R. Theory of the Spin Galvanic Effect at Oxide Interfaces. *Phys. Rev. Lett.* **119,** 256801. ISSN: 1079-7114 (Dec. 2017).

62. Liang, H., Cheng, L., Wei, L., Luo, Z., Yu, G., Zeng, C. & Zhang, Z. Nonmonotonically tunable Rashba spin-orbit coupling by multiple-band filling control in SrTiO$_3$-based interfacial d-electron gases. *Phys. Rev. B* **92,** 075309. ISSN: 2469-9969 (Aug. 2015).

63. Krzyżewska, A. & Dyrdał, A. Anomalous Hall and Nernst effects in a two-dimensional electron gas with an anisotropic cubic Rashba spin-orbit interaction. *J. Magn. Magn. Mater.* **497,** 165919. ISSN: 0304-8853 (Mar. 2020).

64. Zhou, J., Shan, W.-Y. & Xiao, D. Spin responses and effective Hamiltonian for the two-dimensional electron gas at the oxide interface $LaAlO_3/SrTiO_3$. *Phys. Rev. B* **91,** 241302. ISSN: 2469-9969 (June 2015).

65. Oguchi, T. & Shishidou, T. The surface Rashba effect: a k·p. *J. Phys.: Condens. Matter* **21,** 092001. ISSN: 0953-8984 (Jan. 2009).

66. Vajna, S., Simon, E., Szilva, A., Palotas, K., Ujfalussy, B. & Szunyogh, L. Higher-order contributions to the Rashba-Bychkov effect with application to the Bi/Ag(111) surface alloy. *Phys. Rev. B* **85,** 075404. ISSN: 2469-9969 (Feb. 2012).

67. Simon, E., Szilva, A., Ujfalussy, B., Lazarovits, B., Zarand, G. & Szunyogh, L. Anisotropic Rashba splitting of surface states from the admixture of bulk states: Relativistic ab initio calculations and $k \cdot p$ perturbation theory. *Phys. Rev. B* **81,** 235438. ISSN: 2469-9969 (June 2010).

68. Vaz, D. C., Trier, F., Dyrdał, A., Johansson, A., Garcia, K., Barthélémy, A., Mertig, I., Barnaś, J., Fert, A. & Bibes, M. Determining the Rashba parameter from the bilinear magnetoresistance response in a two-dimensional electron gas. *Phys. Rev. Mater.* **4,** 071001. ISSN: 2475-9953 (July 2020).

69. Vicente-Arche, L. M., Bréhin, J., Varotto, S., Cosset-Cheneau, M., Mallik, S., Salazar, R., Noël, P., Vaz, D. C., Trier, F., Bhattacharya, S., Sander, A., Le Fèvre, P., Bertran, F., Saiz, G., Ménard, G., Bergeal, N., Barthélémy, A., Li, H., Lin, C.-C., Nikonov, D. E., Young, I. A., Rault, J. E., Vila, L., Attané, J.-P. & Bibes, M. Spin–Charge Interconversion in KTaO3 2D Electron Gases. *Adv. Mater.* **33,** 2102102. ISSN: 0935-9648 (Oct. 2021).

70. Lin, W., Li, L., Doğan, F., Li, C., Rotella, H., Yu, X., Zhang, B., Li, Y., Lew, W. S., Wang, S., Prellier, W., Pennycook, S. J., Chen, J., Zhong, Z., Manchon, A. & Wu, T. Interface-based tuning of Rashba spin-orbit interaction in asymmetric oxide heterostructures with 3d electrons. *Nat. Commun.* **10,** 1–7. ISSN: 2041-1723 (July 2019).

71. Liu, S. Y. & Lei, X. L. Kinetic-equation approach to the anomalous Hall effect in a diffusive Rashba two-dimensional electron system with magnetization. *Phys. Rev. B* **72,** 195329. ISSN: 2469-9969 (Nov. 2005).

72. Luttinger, J. M. & Kohn, W. Motion of Electrons and Holes in Perturbed Periodic Fields. *Phys. Rev.* **97,** 869–883. ISSN: 1536-6065 (Feb. 1955).

73. Luttinger, J. M. Quantum Theory of Cyclotron Resonance in Semiconductors: General Theory. *Phys. Rev.* **102,** 1030–1041. ISSN: 1536-6065 (May 1956).

74. Karwacki, Ł., Dyrdał, A., Berakdar, J. & Barnaś, J. Current-induced spin polarization in the isotropic k-cubed Rashba model: Theoretical study of p-doped semiconductor heterostructures and perovskite-oxide interfaces. *Phys. Rev. B* **97,** 235302. ISSN: 2469-9969 (June 2018).

75. Moriya, R., Sawano, K., Hoshi, Y., Masubuchi, S., Shiraki, Y., Wild, A., Neumann, C., Abstreiter, G., Bougeard, D., Koga, T. & Machida, T. Cubic Rashba Spin-Orbit Interaction of a Two-Dimensional Hole Gas in a Strained-$Ge/SiGe$ Quantum Well. *Phys. Rev. Lett.* **113,** 086601. ISSN: 1079-7114 (Aug. 2014).

76. Van Heeringen, L. W., McCollam, A., de Wijs, G. A. & Fasolino, A. Theoretical models of Rashba spin splitting in asymmetric $SrTiO_3$-based heterostructures. *Phys. Rev. B* **95,** 155134. ISSN: 2469-9969 (Apr. 2017).

77. Dresselhaus, G. Spin-Orbit Coupling Effects in Zinc Blende Structures. *Phys. Rev.* **100,** 580–586. ISSN: 1536-6065 (Oct. 1955).

78. Eppenga, R. & Schuurmans, M. F. H. Effect of bulk inversion asymmetry on [001], [110], and [111] GaAs/AlAs quantum wells. *Phys. Rev. B* **37,** 10923–10926(R). ISSN: 2469-9969 (June 1988).

79. Bercioux, D. & Lucignano, P. Quantum transport in Rashba spin–orbit materials: a review. *Rep. Prog. Phys.* **78,** 106001. ISSN: 0034-4885 (Sept. 2015).

80. Malcher, F., Lommer, G. & Rössler, U. Electron states in GaAs/Ga1-xAlxAs heterostructures: Nonparabolicity and spin-splitting. *Superlattices Microstruct.* **2,** 267–272. ISSN: 0749-6036 (Jan. 1986).

81. Bergmann, G. Weak localization in thin films: a time-of-flight experiment with conduction electrons. *Phys. Rep.* **107,** 1–58. ISSN: 0370-1573 (May 1984).

82. Lin, J. J. & Bird, J. P. Recent experimental studies of electron dephasing in metal and semiconductor mesoscopic structures. *J. Phys.: Condens. Matter* **14,** R501. ISSN: 0953-8984 (Apr. 2002).

83. Krich, J. J. & Halperin, B. I. Cubic Dresselhaus Spin-Orbit Coupling in 2D Electron Quantum Dots. *Phys. Rev. Lett.* **98,** 226802. ISSN: 1079-7114 (May 2007).

84. Bernevig, B. A., Orenstein, J. & Zhang, S.-C. Exact SU(2) Symmetry and Persistent Spin Helix in a Spin-Orbit Coupled System. *Phys. Rev. Lett.* **97,** 236601. ISSN: 1079-7114 (Dec. 2006).

85. Weber, C. P., Orenstein, J., Bernevig, B. A., Zhang, S.-C., Stephens, J. & Awschalom, D. D. Nondiffusive Spin Dynamics in a Two-Dimensional Electron Gas. *Phys. Rev. Lett.* **98,** 076604. ISSN: 1079-7114 (Feb. 2007).

86. Meier, L., Salis, G., Shorubalko, I., Gini, E., Schön, S. & Ensslin, K. Measurement of Rashba and Dresselhaus spin–orbit magnetic fields. *Nat. Phys.* **3,** 650–654. ISSN: 1745-2481 (Sept. 2007).

87. Koralek, J. D., Weber, C. P., Orenstein, J., Bernevig, B. A., Zhang, S.-C., Mack, S. & Awschalom, D. D. Emergence of the persistent spin helix in semiconductor quantum wells. *Nature* **458,** 610–613. ISSN: 1476-4687 (Apr. 2009).

88. Ganichev, S. D. & Golub, L. E. Interplay of Rashba/Dresselhaus spin splittings probed by photogalvanic spectroscopy –A review. *Phys. Status Solidi B* **251,** 1801–1823. ISSN: 0370-1972 (Sept. 2014).

89. Kohda, M. & Salis, G. Physics and application of persistent spin helix state in semiconductor heterostructures. *Semicond. Sci. Technol.* **32,** 073002. ISSN: 0268-1242 (June 2017).

90. Mahan, G. D. *Many-Particle Physics* ISBN: 978-1-4757-5714-9 (Springer US, 2000).

91. Haug, H. & Jauho, A.-P. *Quantum Kinetics in Transport and Optics of Semiconductors* ISBN: 978-3-540-73564-9 (Springer, Berlin, Germany).

92. Fetter, A. L. & Walecka, J. D. *Quantum Theory of Many-Particle Systems* ISBN: 978-0-07020653-3 (McGraw-Hill College, June 1971).

93. Kubo, R. Statistical-Mechanical Theory of Irreversible Processes. I. General Theory and Simple Applications to Magnetic and Conduction Problems. *J. Phys. Soc. Jpn.* **12,** 570–586. ISSN: 0031-9015 (June 1957).

94. Streda, P. Theory of quantised Hall conductivity in two dimensions. *J. Phys. C: Solid State Phys.* **15,** L717. ISSN: 0022-3719 (Aug. 1982).

95. Matsubara, T. A New Approach to Quantum-Statistical Mechanics. *Prog. Theor. Phys.* **14,** 351–378. ISSN: 0033-068X (Oct. 1955).

96. Dyrdał, A., Barnaś, J. & Dugaev, V. K. Spin Hall and spin Nernst effects in a two-dimensional electron gas with Rashba spin-orbit interaction: Temperature dependence. *Phys. Rev. B* **94,** 035306. ISSN: 2469-9969 (July 2016).

97. Luttinger, J. M. Theory of Thermal Transport Coefficients. *Phys. Rev.* **135,** A1505–A1514. ISSN: 1536-6065 (Sept. 1964).

98. Dyrdał, A., Inglot, M., Dugaev, V. K. & Barnaś, J. Thermally induced spin polarization of a two-dimensional electron gas. *Phys. Rev. B* **87,** 245309. ISSN: 2469-9969 (June 2013).

99. Tatara, G. Thermal Vector Potential Theory of Transport Induced by a Temperature Gradient. *Phys. Rev. Lett.* **114,** 196601. ISSN: 1079-7114 (May 2015).

100. Anna Dyrdał's notes.

101. Dyrdał, A., Barnaś, J. & Dugaev, V. K. Current-induced spin polarization of a magnetized two-dimensional electron gas with Rashba spin-orbit interaction. *Phys. Rev. B* **95,** 245302. ISSN: 2469-9969 (June 2017).

102. Byron, F. W. & Fuller, R. W. *Mathematics of Classical and Quantum Physics (Dover Books on Physics)* ISBN: 978-0-48667164-2 (Dover Publications, Mineola, NY, USA, Aug. 1992).

103. Altland, A. & von Delft, J. *Mathematics for Physicists: Introductory Concepts and Methods* ISBN: 978-1-10855791-7 (Cambridge University Press, Cambridge, England, UK, Feb. 2019).

104. Nunner, T. S., Sinitsyn, N. A., Borunda, M. F., Dugaev, V. K., Kovalev, A. A., Abanov, A., Timm, C., Jungwirth, T., Inoue, J.-i., MacDonald, A. H. & Sinova, J. Anomalous Hall effect in a two-dimensional electron gas. *Phys. Rev. B* **76,** 235312. ISSN: 2469-9969 (Dec. 2007).

105. Economou, E. N. *Green's Functions in Quantum Physics* ISBN: 978-3-540-28841-1 (Springer, Berlin, Germany).

106. Ashcroft, N. W. & Mermin, N. D. *Solid State Physics* ISBN: 978-0-03083993-1 (Holt, Rinehart and Winston, 1976).

107. Krzyżewska, A. & Dyrdał, A. Non-equilibrium spin polarization in magnetic two-dimensional electron gas with k-linear and k-cubed Dresselhaus spin–orbit interaction. *Physica E* **135,** 114961. ISSN: 1386-9477 (Jan. 2022).

108. Dyrdał, A. & Barnaś, J. Current-induced spin polarization and spin-orbit torque in graphene. *Phys. Rev. B* **92,** 165404. ISSN: 2469-9969 (Oct. 2015).

109. Kessler, J. *Polarized Electrons* ISBN: 978-3-662-12721-6 (Springer, Berlin, Germany, 1976).

110. Kato, Y. K., Myers, R. C., Gossard, A. C. & Awschalom, D. D. Current-Induced Spin Polarization in Strained Semiconductors. *Phys. Rev. Lett.* **93,** 176601. ISSN: 1079-7114 (Oct. 2004).

111. Ganichev, S. D., Trushin, M. & Schliemann, J. in *Spintronics Handbook, Second Edition: Spin Transport and Magnetism* 317–338 (CRC Press, Boca Raton, FL, USA, May 2019). ISBN: 978-0-42943423-5.

112. Ivchenko, E. L. & Pikus, G. E. New photogalvanic effect in gyrotropic crystals. *Pis'ma Zh. Eksp. Teor. Fiz.* **27.** [JETP Lett. 27, 604 (1978)], 640–643 (June 1978).

113. Vas'ko, F. T. & Prima, N. A. Spin splitting of the spectrum of two-dimensional electrons. *Fiz. Tverd. Tela* **21.** [Sov. Phys. Solid State 21, 994 (1979)] (1979).

114. Edelstein, V. M. Spin polarization of conduction electrons induced by electric current in two-dimensional asymmetric electron systems. *Solid State Commun.* **73,** 233–235. ISSN: 0038-1098 (Jan. 1990).

115. Aronov, A. G. & Lyanda-Geller, Y. B. Nuclear electric resonance and orientation of carrier spins by an electric field. *Pis'ma Zh. Eksp. Teor. Fiz.* **50.** [JETP Lett. 50, 431 (1989)], 398–400 (Nov. 1989).

116. Averkiev, N. S., Golub, L. E. & Willander, M. Spin relaxation anisotropy in. *J. Phys.: Condens. Matter* **14,** R271. ISSN: 0953-8984 (Mar. 2002).

117. Dyakonov, M. I. & Perel, V. I. Current-induced spin orientation of electrons in semiconductors. *Phys. Lett. A* **35,** 459–460. ISSN: 0375-9601 (July 1971).

118. Sinova, J., Valenzuela, S. O., Wunderlich, J., Back, C. H. & Jungwirth, T. Spin Hall effects. *Rev. Mod. Phys.* **87,** 1213–1260. ISSN: 1539-0756 (Oct. 2015).

119. Kato, Y. K., Myers, R. C., Gossard, A. C. & Awschalom, D. D. Observation of the Spin Hall Effect in Semiconductors. *Science* **306,** 1910–1913. ISSN: 0036-8075 (Dec. 2004).

120. Wunderlich, J., Kaestner, B., Sinova, J. & Jungwirth, T. Experimental Observation of the Spin-Hall Effect in a Two-Dimensional Spin-Orbit Coupled Semiconductor System. *Phys. Rev. Lett.* **94,** 047204. ISSN: 1079-7114 (Feb. 2005).

121. Sih, V., Myers, R. C., Kato, Y. K., Lau, W. H., Gossard, A. C. & Awschalom, D. D. Spatial imaging of the spin Hall effect and current-induced polarization in two-dimensional electron gases. *Nat. Phys.* **1,** 31–35. ISSN: 1745-2481 (Oct. 2005).

122. Tarasenko, S. A. Scattering induced spin orientation and spin currents in gyrotropic structures. *JETP Lett.* **84,** 199–203. ISSN: 1090-6487 (Oct. 2006).

123. Tarasenko, S. A. Spin orientation of free carriers by dc and high-frequency electric field in quantum wells. *Physica E* **40,** 1614–1615. ISSN: 1386-9477 (Mar. 2008).

124. Norman, B. M., Trowbridge, C. J., Awschalom, D. D. & Sih, V. Current-induced spin polarization in anisotropic spin-orbit fields. *Phys. Rev. Lett.* **112,** 056601. ISSN: 1079-7114 (Feb. 2014).

125. Bernevig, B. A. & Vafek, O. Piezo-magnetoelectric effects in p-doped semiconductors. *Phys. Rev. B* **72,** 033203. ISSN: 2469-9969 (July 2005).

126. Chernyshov, A., Overby, M., Liu, X., Furdyna, J. K., Lyanda-Geller, Y. & Rokhinson, L. P. Evidence for reversible control of magnetization in a ferromagnetic material by means of spin–orbit magnetic field. *Nat. Phys.* **5,** 656–659. ISSN: 1745-2481 (Sept. 2009).

127. Mihai Miron, I., Gaudin, G., Auffret, S., Rodmacq, B., Schuhl, A., Pizzini, S., Vogel, J. & Gambardella, P. Current-driven spin torque induced by the Rashba effect in a ferromagnetic metal layer. *Nat. Mater.* **9,** 230–234. ISSN: 1476-4660 (Mar. 2010).

128. Dyrdał, A., Barnaś, J., Dugaev, V. K. & Berakdar, J. Thermally induced spin polarization in a magnetized two-dimensional electron gas with Rashba spin-orbit interaction. *Phys. Rev. B* **98,** 075307. ISSN: 2469-9969 (Aug. 2018).

129. Gorini, C., Maleki Sheikhabadi, A., Shen, K., Tokatly, I. V., Vignale, G. & Raimondi, R. Theory of current-induced spin polarization in an electron gas. *Phys. Rev. B* **95,** 205424. ISSN: 2469-9969 (May 2017).

130. Ganichev, S. D., Ivchenko, E. L., Bel'kov, V. V., Tarasenko, S. A., Sollinger, M., Weiss, D., Wegscheider, W. & Prettl, W. Spin-galvanic effect. *Nature* **417,** 153–156. ISSN: 1476-4687 (May 2002).

131. Wang, C. M. & Pang, M. Q. Thermally induced spin polarization and thermal conductivities in a spin–orbit-coupled two-dimensional electron gas. *Solid State Commun.* **150,** 1509–1513. ISSN: 0038-1098 (Sept. 2010).

132. Xiao, C., Li, D. & Ma, Z. Thermoelectric response of spin polarization in Rashba spintronic systems. *Front. Phys.* **11,** 117201–9. ISSN: 2095-0470 (Mar. 2016).

133. Hall, E. H. On a New Action of the Magnet on Electric Currents. *American Journal of Mathematics* **2,** 287–292. ISSN: 0002-9327 (Sept. 1879).

134. Doliński, J. Czujniki Halla – pomiary pola magnetycznego i detekcja położenia obiektów. *Elektronikab2b.pl* (Oct. 2017).

135. Krzyżewska, A. Dziedzictwo Edwina Halla. *Postępy Fizyki* **T. 72, z. 1.** ISSN: 0032-5430 (2021).

136. Hall, E. H. XVIII. On the "Rotational Coefficient" in nickel and cobalt. *London, Edinburgh, and Dublin Philosophical Magazine and Journal of Science* **12,** 157–172. ISSN: 1941-5982 (Sept. 1881).

137. Karplus, R. & Luttinger, J. M. Hall Effect in Ferromagnetics. *Phys. Rev.* **95,** 1154–1160. ISSN: 1536-6065 (Sept. 1954).

138. Luttinger, J. M. Theory of the Hall Effect in Ferromagnetic Substances. *Phys. Rev.* **112,** 739–751. ISSN: 1536-6065 (Nov. 1958).

139. Xu, W. J., Zhang, B., Wang, Z., Chu, S. S., Li, W., Wu, Z. B., Yu, R. H. & Zhang, X. X. Scaling law of anomalous Hall effect in Fe/Cu bilayers. *Eur. Phys. J. B* **65,** 233–237. ISSN: 1434-6036 (Sept. 2008).

140. Hou, D., Su, G., Tian, Y., Jin, X., Yang, S. A. & Niu, Q. Multivariable Scaling for the Anomalous Hall Effect. *Phys. Rev. Lett.* **114,** 217203. ISSN: 1079-7114 (May 2015).

141. Crowell, P. A. & Crooker, S. A. in *Spintronics Handbook, Second Edition: Spin Transport and Magnetism* 269–315 (CRC Press, Boca Raton, FL, USA, May 2019). ISBN: 978-0-42943423-5.

142. Berry, M. V. Quantal Phase Factors Accompanying Adiabatic Changes. *Proc. R. Soc. London A - Math. Phys. Sci.* **392,** 45–57 (Mar. 1984).

143. Jungwirth, T., Niu, Q. & MacDonald, A. H. Anomalous Hall Effect in Ferromagnetic Semiconductors. *Phys. Rev. Lett.* **88,** 207208. ISSN: 1079-7114 (May 2002).

144. Chang, M.-C. & Niu, Q. Berry phase, hyperorbits, and the Hofstadter spectrum: Semiclassical dynamics in magnetic Bloch bands. *Phys. Rev. B* **53,** 7010–7023. ISSN: 2469-9969 (Mar. 1996).

145. Sundaram, G. & Niu, Q. Wave-packet dynamics in slowly perturbed crystals: Gradient corrections and Berry-phase effects. *Phys. Rev. B* **59,** 14915–14925. ISSN: 2469-9969 (June 1999).

146. Vanderbilt, D. *Berry Phases in Electronic Structure Theory: Electric Polarization, Orbital Magnetization and Topological Insulators* ISBN: 978-1-31666220-5 (Cambridge University Press, Cambridge, England, UK, Oct. 2018).

147. Fock, V. Über die Beziehung zwischen den Integralen der quantenmechanischen Bewegungsgleichungen und der Schrödingerschen Wellengleichung. *Z. Phys.* **49,** 323–338. ISSN: 0044-3328 (May 1928).

148. Xiao, D., Chang, M.-C. & Niu, Q. Berry phase effects on electronic properties. *Rev. Mod. Phys.* **82,** 1959–2007. ISSN: 1539-0756 (July 2010).

149. Aharonov, Y. & Bohm, D. Significance of Electromagnetic Potentials in the Quantum Theory. *Phys. Rev.* **115,** 485–491. ISSN: 1536-6065 (Aug. 1959).

150. Simon, B. Holonomy, the Quantum Adiabatic Theorem, and Berry's Phase. *Phys. Rev. Lett.* **51,** 2167–2170. ISSN: 1079-7114 (Dec. 1983).

151. Thouless, D. J., Kohmoto, M., Nightingale, M. P. & Den Nijs, M. Quantized Hall Conductance in a Two-Dimensional Periodic Potential. *Phys. Rev. Lett.* **49,** 405–408. ISSN: 1079-7114 (Aug. 1982).

152. Culcer, D., MacDonald, A. & Niu, Q. Anomalous Hall effect in paramagnetic two-dimensional systems. *Phys. Rev. B* **68,** 045327. ISSN: 2469-9969 (July 2003).

153. Zhou, B., Ren, L. & Shen, S.-Q. Spin transverse force and intrinsic quantum transverse transport. *Phys. Rev. B* **73,** 165303. ISSN: 2469-9969 (Apr. 2006).

154. Dugaev, V. K., Bruno, P., Taillefumier, M., Canals, B. & Lacroix, C. Anomalous Hall effect in a two-dimensional electron gas with spin-orbit interaction. *Phys. Rev. B* **71,** 224423. ISSN: 2469-9969 (June 2005).

155. Li, R. & Yi-Ming, M. Anomalous Hall Effect in Spin-Polarized Two-Dimensional Hole Gas with Cubic-Rashbsa Spin-Orbit Interaction. *Commun. Theor. Phys.* **54,** 559. ISSN: 0253-6102 (Sept. 2010).

156. Krzyżewska, A., Dyrdał, A., Barnaś, J. & Berakdar, J. Anomalous Hall and Nernst Effects in 2D Systems: Role of Cubic Rashba Spin–Orbit Coupling. *Phys. Status Solidi RRL* **12,** 1800232. ISSN: 1862-6254 (Oct. 2018).

157. D'Yakonov, M. I. & Perel', V. I. Possibility of Orienting Electron Spins with Current. *Soviet Journal of Experimental and Theoretical Physics Letters* **13,** 467. ISSN: 0021-3640 (June 1971).

158. Hirsch, J. E. Spin Hall Effect. *Phys. Rev. Lett.* **83,** 1834–1837. ISSN: 1079-7114 (Aug. 1999).

159. Sinova, J., Culcer, D., Niu, Q., Sinitsyn, N. A., Jungwirth, T. & MacDonald, A. H. Universal Intrinsic Spin Hall Effect. *Phys. Rev. Lett.* **92,** 126603. ISSN: 1079-7114 (Mar. 2004).

160. Murakami, S., Nagaosa, N. & Zhang, S.-C. Dissipationless Quantum Spin Current at Room Temperature. *Science* **301,** 1348–1351. ISSN: 0036-8075 (Sept. 2003).

161. Balakrishnan, J., Kok Wai Koon, G., Jaiswal, M., Castro Neto, A. H. & Özyilmaz, B. Colossal enhancement of spin–orbit coupling in weakly hydrogenated graphene. *Nat. Phys.* **9,** 284–287. ISSN: 1745-2481 (May 2013).

162. Avsar, A., Tan, J. Y., Taychatanapat, T., Balakrishnan, J., Koon, G. K. W., Yeo, Y., Lahiri, J., Carvalho, A., Rodin, A. S., O'Farrell, E. C. T., Eda, G., Castro Neto, A. H. & Özyilmaz, B. Spin–orbit proximity effect in graphene. *Nat. Commun.* **5,** 1–6. ISSN: 2041-1723 (Sept. 2014).

163. Balakrishnan, J., Koon, G. K. W., Avsar, A., Ho, Y., Lee, J. H., Jaiswal, M., Baeck, S.-J., Ahn, J.-H., Ferreira, A., Cazalilla, M. A., Neto, A. H. C. & Özyilmaz, B. Giant spin Hall effect in graphene grown by chemical vapour deposition. *Nat. Commun.* **5,** 1–7. ISSN: 2041-1723 (Sept. 2014).

164. Valenzuela, S. O. & Tinkham, M. Direct electronic measurement of the spin Hall effect. *Nature* **442,** 176–179. ISSN: 1476-4687 (July 2006).

165. Saitoh, E., Ueda, M., Miyajima, H. & Tatara, G. Conversion of spin current into charge current at room temperature: Inverse spin-Hall effect. *Appl. Phys. Lett.* **88,** 182509. ISSN: 0003-6951 (May 2006).

166. Wunderlich, J., Park, B.-G., Irvine, A. C., Zârbo, L. P., Rozkotová, E., Nemec, P., Novák, V., Sinova, J. & Jungwirth, T. Spin Hall Effect Transistor. *Science* **330,** 1801–1804. ISSN: 0036-8075 (Dec. 2010).

167. Schliemann, J. & Loss, D. Spin-Hall transport of heavy holes in III-V semiconductor quantum wells. *Phys. Rev. B* **71,** 085308. ISSN: 2469-9969 (Feb. 2005).

168. Krzyżewska, A., Dyrdał, A. & Berakdar, J. Temperature Dependence of Spin Hall Effect in k–cubed Rashba Model. *Acta Physica Polonica A* **133,** 558–560 (Mar. 2018).

169. Marder, M. P. *Condensed Matter Physics* ISBN: 978-0-47061798-4 (Oct. 2010).

170. Thomson, W. Account of Experimental Investigations to answer questions roiginating int eh Mechanical Theory of Thermo-Electric Currents. *Proc. Roy. Soc. Edinburgh* **3** (1854).

171. Thomson, W. IX. On the Dynamical Theory of Heat. Part V. Thermo-electric Currents. *Earth Environ. Sci. Trans. R. Soc. Edinburgh* **21,** 123–171. ISSN: 2053-5945 (1857).

172. Thomson, W. Part VI. Thermo-Electric Currents. *Math. Phys. Papers* **1,** 232–291 (1882).

173. De Groot, S. R. & Mazur, P. *Non-equilibrium Thermodynamics* ISBN: 978-0-48664741-8 (Courier Corporation, Jan. 1984).

174. Onsager, L. Reciprocal Relations in Irreversible Processes. I. *Phys. Rev.* **37,** 405–426. ISSN: 1536-6065 (Feb. 1931).

175. Onsager, L. Reciprocal Relations in Irreversible Processes. II. *Phys. Rev.* **38,** 2265–2279. ISSN: 1536-6065 (Dec. 1931).

176. Wiedemann, G. H. & Franz, R. Über die Wärme-Leitungsfähigkeit der Metalle: Arbeiten. *Annalen der Physik u. Chemie* **89,** 497–531 (1853).

177. Ziman, J. M. in *Principles of the Theory of Solids* 2nd ed., 211–254 (Cambridge University Press, 1972).

178. Mott, N. F. & Jones, H. *The Theory of the Properties of Metals and Alloys* (Oxford University Press, 1936).

179. Chester, G. V. & Thellung, A. The Law of Wiedemann and Franz. *Proc. Phys. Soc.* **77,** 1005. ISSN: 0370-1328 (May 1961).

180. Jonson, M. & Mahan, G. D. Mott's formula for the thermopower and the Wiedemann-Franz law. *Phys. Rev. B* **21,** 4223–4229. ISSN: 2469-9969 (May 1980).

181. Smrcka, L. & Streda, P. Transport coefficients in strong magnetic fields. *J. Phys. C: Solid State Phys.* **10,** 2153. ISSN: 0022-3719 (June 1977).

182. Mott, N. F., Davis, E. A., Mott, N. F. & Davis, E. A. *Electronic Processes in Non-Crystalline Materials* ISBN: 978-0-19964533-6 (Oxford University Press, Oxford, England, UK, Feb. 2012).

183. Xiao, C., Zhu, J., Xiong, B. & Niu, Q. Conserved spin current for the Mott relation. *Phys. Rev. B* **98,** 081401. ISSN: 2469-9969 (Aug. 2018).

184. Smith, A. W. The Transverse Thermomagnetic Effect in Nickel and Cobalt. *Phys. Rev. (Series I)* **33,** 295–306. ISSN: 1536-6065 (Oct. 1911).

185. Xiao, D., Yao, Y., Fang, Z. & Niu, Q. Berry-Phase Effect in Anomalous Thermoelectric Transport. *Phys. Rev. Lett.* **97,** 026603. ISSN: 1079-7114 (July 2006).

186. Pu, Y., Chiba, D., Matsukura, F., Ohno, H. & Shi, J. Mott Relation for Anomalous Hall and Nernst Effects in $Ga_{1-x}Mn_xAs$ Ferromagnetic Semiconductors. *Phys. Rev. Lett.* **101,** 117208. ISSN: 1079-7114 (Sept. 2008).

187. Miyasato, T., Abe, N., Fujii, T., Asamitsu, A., Onoda, S., Onose, Y., Nagaosa, N. & Tokura, Y. Crossover Behavior of the Anomalous Hall Effect and Anomalous Nernst Effect in Itinerant Ferromagnets. *Phys. Rev. Lett.* **99,** 086602. ISSN: 1079-7114 (Aug. 2007).

188. Bui, C. T. & Rivadulla, F. Anomalous and planar Nernst effects in thin films of the half-metallic ferromagnet $La_{2/3}Sr_{1/3}MnO_3$. *Phys. Rev. B* **90,** 100403. ISSN: 2469-9969 (Sept. 2014).

189. Sodemann, I. & Fu, L. Quantum Nonlinear Hall Effect Induced by Berry Curvature Dipole in Time-Reversal Invariant Materials. *Phys. Rev. Lett.* **115,** 216806. ISSN: 1079-7114 (Nov. 2015).

190. Du, Z. Z., Lu, H.-Z. & Xie, X. C. Nonlinear Hall effects. *Nat. Rev. Phys.* **3,** 744–752. ISSN: 2522-5820 (Nov. 2021).

191. Zhang, C.-P., Gao, X.-J., Xie, Y.-M., Po, H. C. & Law, K. T. Higher-Order Nonlinear Anomalous Hall Effects Induced by Berry Curvature Multipoles. *arXiv* (Dec. 2020).

192. Okyay, M. S., Sato, S. A., Kim, K. W., Yan, B., Jin, H. & Park, N. Second harmonic Hall responses of insulators as a probe of Berry curvature dipole. *Commun. Phys.* **5,** 1–9. ISSN: 2399-3650 (Nov. 2022).

193. Xiang, L., Zhang, C., Wang, L. & Wang, J. Third-order intrinsic anomalous Hall effect with generalized semiclassical theory. *Phys. Rev. B* **107,** 075411. ISSN: 2469-9969 (Feb. 2023).

194. Zhang, X., Sun, K. & Meng, Z. Y. The "Sign problem" of the 3rd order anomalous Hall effect in topological magnetic materials. *arXiv* (Mar. 2023).

195. Sankar, S., Liu, R., Gao, X.-J., Li, Q.-F., Chen, C., Zhang, C.-P., Zheng, J., Lin, Y.-H., Qian, K., Yu, R.-P., Zhang, X., Meng, Z. Y., Law, K. T., Shao, Q. & Jäck, B. Observation of the Berry curvature quadrupole induced nonlinear anomalous Hall effect at room temperature. *arXiv* (Mar. 2023).

196. Xiao, D., Yao, W. & Niu, Q. Valley-Contrasting Physics in Graphene: Magnetic Moment and Topological Transport. *Phys. Rev. Lett.* **99,** 236809. ISSN: 1079-7114 (Dec. 2007).

197. Gao, Y., Yang, S. A. & Niu, Q. Field Induced Positional Shift of Bloch Electrons and Its Dynamical Implications. *Phys. Rev. Lett.* **112,** 166601. ISSN: 1079-7114 (Apr. 2014).

198. Ye, X.-G., Liu, H., Zhu, P.-F., Xu, W.-Z., Yang, S. A., Shang, N., Liu, K. & Liao, Z.-M. Control over Berry Curvature Dipole with Electric Field in WTe_2. *Phys. Rev. Lett.* **130,** 016301. ISSN: 1079-7114 (Jan. 2023).

199. Nandy, S. & Sodemann, I. Symmetry and quantum kinetics of the nonlinear Hall effect. *Phys. Rev. B* **100,** 195117. ISSN: 2469-9969 (Nov. 2019).

200. König, E. J., Dzero, M., Levchenko, A. & Pesin, D. A. Gyrotropic Hall effect in Berry-curved materials. *Phys. Rev. B* **99,** 155404. ISSN: 2469-9969 (Apr. 2019).

201. Du, Z. Z., Wang, C. M., Li, S., Lu, H.-Z. & Xie, X. C. Disorder-induced nonlinear Hall effect with time-reversal symmetry. *Nat. Commun.* **10,** 1–6. ISSN: 2041-1723 (July 2019).

202. Kang, K., Li, T., Sohn, E., Shan, J. & Mak, K. F. Nonlinear anomalous Hall effect in few-layer WTe2. *Nat. Mater.* **18,** 324–328. ISSN: 1476-4660 (Feb. 2019).

203. Du, Z. Z., Wang, C. M., Sun, H.-P., Lu, H.-Z. & Xie, X. C. Quantum theory of the nonlinear Hall effect. *Nat. Commun.* **12,** 1–7. ISSN: 2041-1723 (Aug. 2021).

204. Isobe, H., Xu, S.-Y. & Fu, L. High-frequency rectification via chiral Bloch electrons. *Sci. Adv.* **6,** eaay2497. ISSN: 2375-2548 (Mar. 2020).

205. Ma, Q., Xu, S.-Y., Shen, H., MacNeill, D., Fatemi, V., Chang, T.-R., Mier Valdivia, A. M., Wu, S., Du, Z., Hsu, C.-H., Fang, S., Gibson, Q. D., Watanabe, K., Taniguchi, T., Cava, R. J., Kaxiras, E., Lu, H.-Z., Lin, H., Fu, L., Gedik, N. & Jarillo-Herrero, P. Observation of the nonlinear Hall effect under time-reversal-symmetric conditions. *Nature* **565,** 337–342. ISSN: 1476-4687 (Dec. 2018).

206. Zhang, Y. & Fu, L. Terahertz detection based on nonlinear Hall effect without magnetic field. *Proc. Natl. Acad. Sci. U.S.A.* **118,** e2100736118 (May 2021).

207. Xiao, R.-C., Shao, D.-F., Zhang, Z.-Q. & Jiang, H. Two-Dimensional Metals for Piezoelectriclike Devices Based on Berry-Curvature Dipole. *Phys. Rev. Appl.* **13,** 044014. ISSN: 2331-7019 (Apr. 2020).

208. Facio, J. I., Efremov, D., Koepernik, K., You, J.-S., Sodemann, I. & van den Brink, J. Strongly Enhanced Berry Dipole at Topological Phase Transitions in BiTeI. *Phys. Rev. Lett.* **121,** 246403. ISSN: 1079-7114 (Dec. 2018).

209. Sinha, S., Adak, P. C., Chakraborty, A., Das, K., Debnath, K., Sangani, L. D. V., Watanabe, K., Taniguchi, T., Waghmare, U. V., Agarwal, A. & Deshmukh, M. M. Berry curvature dipole senses topological transition in a moiré superlattice. *Nat. Phys.* **18,** 765–770. ISSN: 1745-2481 (July 2022).

210. Araki, Y. Strain-induced nonlinear spin Hall effect in topological Dirac semimetal. *Sci. Rep.* **8,** 1–7. ISSN: 2045-2322 (Oct. 2018).

211. Hamamoto, K., Ezawa, M., Kim, K. W., Morimoto, T. & Nagaosa, N. Nonlinear spin current generation in noncentrosymmetric spin-orbit coupled systems. *Phys. Rev. B* **95,** 224430. ISSN: 2469-9969 (June 2017).

212. Yu, X.-Q., Zhu, Z.-G., You, J.-S., Low, T. & Su, G. Topological nonlinear anomalous Nernst effect in strained transition metal dichalcogenides. *Phys. Rev. B* **99,** 201410. ISSN: 2469-9969 (May 2019).

213. Zeng, C., Nandy, S., Taraphder, A. & Tewari, S. Nonlinear Nernst effect in bilayer WTe$_2$. *Phys. Rev. B* **100,** 245102. ISSN: 2469-9969 (Dec. 2019).

214. Zeng, C., Nandy, S. & Tewari, S. Fundamental relations for anomalous thermoelectric transport coefficients in the nonlinear regime. *Phys. Rev. Res.* **2,** 032066. ISSN: 2643-1564 (Sept. 2020).

215. Nakai, R. & Nagaosa, N. Nonreciprocal thermal and thermoelectric transport of electrons in non-centrosymmetric crystals. *Phys. Rev. B* **99,** 115201. ISSN: 2469-9969 (Mar. 2019).

216. Deyo, E., Golub, L. E., Ivchenko, E. L. & Spivak, B. Semiclassical theory of the photogalvanic effect in non-centrosymmetric systems. *arXiv* (Apr. 2009).

217. Lesne, E., Sağlam, Y. G., Battilomo, R., Mercaldo, M. T., van Thiel, T. C., Filippozzi, U., Noce, C., Cuoco, M., Steele, G. A., Ortix, C. & Caviglia, A. D. Designing spin and orbital sources of Berry curvature at oxide interfaces. *arXiv* (Jan. 2022).

218. Fu, L. Hexagonal Warping Effects in the Surface States of the Topological Insulator Bi_2Te_3. *Phys. Rev. Lett.* **103,** 266801. ISSN: 1079-7114 (Dec. 2009).

219. Johansson, A., Henk, J. & Mertig, I. Theoretical aspects of the Edelstein effect for anisotropic two-dimensional electron gas and topological insulators. *Phys. Rev. B* **93,** 195440. ISSN: 2469-9969 (May 2016).

220. Dantas, R. M. A., Legg, H. F., Bosco, S., Loss, D. & Klinovaja, J. Determination of spin-orbit interaction in semiconductor nanostructures via non-linear transport. *arXiv* (Oct. 2022).

221. Liu, C.-X., Zhou, B., Shen, S.-Q. & Zhu, B.-F. Current-induced spin polarization in a two-dimensional hole gas. *Phys. Rev. B* **77,** 125345. ISSN: 2469-9969 (Mar. 2008).

222. Campbell, L. L. *Galvanomagnetic and Thermomagnetic Effects: The Hall and Allied Phenomena* (Longmans, Green & Co., London, 1923, London, England, UK, Jan. 1923).

223. Pippard, A. B. *Magnetoresistance in Metals* ISBN: 978-0-52111880-4 (Cambridge University Press, Cambridge, England, UK, Sept. 1989).

224. Mitra, S., Kang, J. G. S., Shin, J., Ng, J. Q., Sunku, S. S., Kong, T., Canfield, P. C., Shastry, B. S., Sengupta, P. & Panagopoulos, C. Quadratic to linear magnetoresistance tuning in TmB_4. *Phys. Rev. B* **99,** 045119. ISSN: 2469-9969 (Jan. 2019).

225. Feng, Y., Wang, Y., Silevitch, D. M., Yan, J.-Q., Kobayashi, R., Hedo, M., Nakama, T., Ōnuki, Y., Suslov, A. V., Mihaila, B., Littlewood, P. B. & Rosenbaum, T. F. Linear magnetoresistance in the low-field limit in density-wave materials. *Proc. Natl. Acad. Sci. U.S.A.* **116,** 11201–11206. ISSN: 0027-8424 (June 2019).

226. He, P., Zhang, S. S.-L., Zhu, D., Liu, Y., Wang, Y., Yu, J., Vignale, G. & Yang, H. Bilinear magnetoelectric resistance as a probe of three-dimensional spin texture in topological surface states - Nature Physics. *Nat. Phys.* **14,** 495–499. ISSN: 1745-2481 (May 2018).

227. Dyrdał, A., Barnaś, J. & Fert, A. Spin-Momentum-Locking Inhomogeneities as a Source of Bilinear Magnetoresistance in Topological Insulators. *Phys. Rev. Lett.* **124,** 046802. ISSN: 1079-7114 (Jan. 2020).

228. Fu, Y., Li, J., Papin, J., Noël, P., Teresi, S., Cosset-Chéneau, M., Grezes, C., Guillet, T., Thomas, C., Niquet, Y.-M., Ballet, P., Meunier, T., Attané, J.-P., Fert, A. & Vila, L. Bilinear Magnetoresistance in HgTe Topological Insulator: Opposite Signs at Opposite Surfaces Demonstrated by Gate Control. *Nano Lett.* **22,** 7867–7873. ISSN: 1530-6984 (Oct. 2022).

229. Guillet, T., Zucchetti, C., Barbedienne, Q., Marty, A., Isella, G., Cagnon, L., Vergnaud, C., Jaffrès, H., Reyren, N., George, J.-M., Fert, A. & Jamet, M. Observation of Large Unidirectional Rashba Magnetoresistance in Ge(111). *Phys. Rev. Lett.* **124,** 027201. ISSN: 1079-7114 (Jan. 2020).

230. Zhang, S. S.-L. & Vignale, G. Theory of bilinear magneto-electric resistance from topological-insulator surface states. *arXiv* (Aug. 2018).

231. Fu, Y., Li, J., Papin, J., Noël, P., Teresi, S., Cosset-Chéneau, M., Grezes, C., Guillet, T., Thomas, C., Niquet, Y.-M., Ballet, P., Meunier, T., Attané, J.-P., Fert, A. & Vila, L. Bilinear Magnetoresistance in HgTe Topological Insulator: Opposite Signs at Opposite Surfaces Demonstrated by Gate Control. *Nano Lett.* **22,** 7867–7873. ISSN: 1530-6984 (Oct. 2022).

232. Zhang, J., Zhang, H., Chen, X., Zhang, J., Qi, S., Han, F., Chen, Y., Zhao, W., Hu, F., Shen, B. & Sun, J. Anisotropic bilinear magnetoresistance in (110) $SrTiO_3$-based two-dimensional electron gas. *Phys. Rev. B* **104,** 045114. ISSN: 2469-9969 (July 2021).

233. Murakami, S. Absence of vertex correction for the spin Hall effect in p-type semiconductors. *Phys. Rev. B* **69,** 241202. ISSN: 2469-9969 (June 2004).

234. Inoue, J.-i., Bauer, G. E. W. & Molenkamp, L. W. Suppression of the persistent spin Hall current by defect scattering. *Phys. Rev. B* **70,** 041303. ISSN: 2469-9969 (July 2004).

235. Dimitrova, O. V. Spin-Hall conductivity in a two-dimensional Rashba electron gas. *Phys. Rev. B* **71,** 245327. ISSN: 2469-9969 (June 2005).

236. Sinitsyn, N. A., MacDonald, A. H., Jungwirth, T., Dugaev, V. K. & Sinova, J. Anomalous Hall effect in a two-dimensional Dirac band: The link between the Kubo-Streda formula and the semi-classical Boltzmann equation approach. *Phys. Rev. B* **75,** 045315. ISSN: 2469-9969 (Jan. 2007).